DISCOVERY OF SHEAR- AND SIDE-DEPENDENT MICRORNAS AND MESSENGER RNAS IN AORTIC VALVULAR ENDOTHELIUM

A Dissertation
Presented to
The Academic Faculty

by

Casey J. Holliday

In Partial Fulfillment
of the Requirements for the Degree
Doctor of Philosophy in the
School of Biomedical Engineering

Georgia Institute of Technology
May 2012

DISCOVERY OF SHEAR- AND SIDE-DEPENDENT MICRORNAS AND MESSENGER RNAS IN AORTIC VALVULAR ENDOTHELIUM

Approved by:

Dr. Robert M. Nerem, Co-Advisor
Institute of Bioengineering and Bioscience
Georgia Institute of Technology

Dr. W. Robert Taylor
School of Biomedical Engineering
Georgia Institute of Technology, Emory University

Dr. Hanjoong Jo, Co-Advisor
School of Biomedical Engineering
Georgia Institute of Technology, Emory University

Dr. Ajit Yoganathan
School of Biomedical Engineering
Georgia Institute of Technology, Emory University

Dr. Suzanne Eskin
School of Biomedical Engineering
Georgia Institute of Technology

Dr. Vinod Thourani
Department of Surgery
Emory University

Date Approved: December 7, 2011

To my family and friends, especially Randy.

ACKNOWLEDGEMENTS

First, I would like to thank my parents for their continued support and emphasis on the importance of education. They showed me that hard work and perseverance are the keys to success. I would also like to thank my sister for all the long telephone calls about experiments and journal articles, even though she had no idea what I was talking about! Friends have played a big role in my thesis, whether through quick breaks during incubations, social gatherings, or help troubleshooting experiments (especially the Jo lab girls, Laura, Ashley, Fernie, Barbara, and Julia). For this and more, I thank them. Above all, I thank my wonderful fiancé/husband. Without him, this truly would not have been possible. Randy has given me unconditional support throughout the entire process. Not only has he given me emotional support, but he has helped with a lot of the experiments! We have spent late nights isolating cells and countless hours of experimental design. Through these experiences, I realized what a wonderful person he is and am so thankful we have the opportunity to spend our lives together!

I thank my co-advisors, Dr. Nerem and Dr. Jo. They have provided me the resources and support to make this thesis possible. Among many things, they taught me to conduct cutting-edge experiments and express the results in a meaningful way (through journals, grants, etc.). I thank Dr. Jo and Dr. Nerem for their investment in me and my personal development. I am better for having been in their labs. I would also like to thank many lab members for help with experiments, especially Taby and Ann for their help as I entered the lab. I would like to thank Chih-Wen for miRNA help and Haiwei for all the computer help. Last but not least, I would like to thank my committee for their support and feedback throughout this process!

TABLE OF CONTENTS

LIST OF TABLES

LIST OF FIGURES

LIST OF SYMBOLS AND ABBREVIATIONS

acLDL	acetylated low density lipoprotein
Adm	adrenomedullin
Ak2	adenylate kinase 2
Atf3	activating transcription factor 3
AV	aortic valve
Bmp	bone morphogenic protein
Camk2n1	calcium/calmodulin-dependent protein kinase II inhibitor 1
Ctdspl	CTD (carboxy-terminal domain, RNA polymerase II, polypeptide A) small phosphatase-like
Ctsk	cathepsin K
Dhh	desert hedgehog
Dnmt1	DNA (cytosine-5-)-methyltransferase 1
Dnmt3b	DNA (cytosine-5-)-methyltransferase 3 beta
EC	endothelial cell
Edn1	endothelin 1
Efna1	ephrin a1
Egr1	early growth response 1
FDR	false discovery rate
fHAVEC	fibrosa human aortic valvular endothelial cell
FL	fHAVECs exposed to laminar shear
FO	fHAVECs exposed to oscillatory shear
Fosb	FBJ murine osteosarcoma viral oncogene homolog B
HAVEC	human aortic valvular endothelial cell

Hdac1	histone deacetylase 1
HUVEC	human umbilical vein endothelial cell
Id1 protein	inhibitor of DNA binding 1, dominant negative helix-loop-helix
IFN-beta	interferon, beta
Igf5bp	insulin growth factor 5 binding protein
IkBα inhibitor, alpha	nuclear factor of kappa light polypeptide gene enhancer in B-cells
Il2	interleukin 2
Il6	interleukin 6
IPA	Ingenuity Pathway Analysis
Klf2	Kruppel-like factor 2
LNA-anti-miR	locked nucleic acid antisense microRNA
LPS	lipopolysaccharide
LS	unidirectional, steady, laminar shear
miR	micro ribonucleic acid
miRISC	multiprotein RNA-induced silencing complex
miRNA	micro ribonucleic acid
mRNA	messenger ribonucleic acid
Mylk2	myosin light chain kinase 2
Nfkbia inhibitor, alpha	nuclear factor of kappa light polypeptide gene enhancer in B cells
OS	oscillatory shear or bidirectional, steady, laminar shear
PAVEC	porcine aortic valve endothelial cell
PECAM1	platelet endothelial cell adhesion molecule
Pparg	peroxisome proliferator-activated receptor gamma

pre-miR	precursor miRNA
pre-miRNA	precursor miRNA
Prnd	prion protein
Rnf41	ring finger protein 41
Runx	runt-related transcription factor 1
RXR	Retinoid X Receptor
SAM	signficance of microarray analysis
Slco2a1	solute carrier organic anion transporter family, member 2A1
Sma	smooth muscle alpha actin
Smad homolog 1	derived from the genes Small and Mothers against decapentaplegic
Sncaip	synuclein, alpha interacting protein
Thbs1	thrombospondin 1
Tmem237	transmembrane protein 237 also known as Als2cr4
TNFα	tumor necrosis factor alpha
UTR	untranslated region
VE-Cadherin	vascular endothelial cadherin
vHAVEC	ventricularis human aortic valvular endothelial cell
VL	vHAVECs exposed to laminar shear
VO	vHAVECs exposed to oscillatory shear
vWF	von Willebrand factor

SUMMARY

Aortic valve (AV) disease is a major cause of cardiovascular-linked deaths globally. In addition, AV disease is a strong risk factor for additional cardiovascular events;[1-3] however, the mechanism by which it initiates and progresses is not well-understood and is the focus of this thesis. We hypothesize that low-magnitude and oscillatory flow is present on the fibrosa side of the AV and stimulates ECs to differentially regulate microRNA (miRNA) and mRNAs and influence AV disease progression. This hypothesis was tested employing both *in vitro* and *in vivo* approaches, high throughput microarray and pathway analyses, as well as a variety of functional assays according to the following four specific aims: 1) to isolate and characterize side-dependent, human aortic valvular endothelial cells (HAVECs), 2) to identify side- and shear-induced changes in miRNA and mRNA expression profiles in HAVECs *in vitro*, 3) to develop a method to isolate endothelial-enriched, side-dependent total RNA and to identify and validate side-dependent miRNAs in porcine aortic valvular endothelium, and finally, 4) to determine the relationship between important miRNAs (specifically miR-187 and miR-486-5p) and AV disease by modulating levels of miRNAs and performing functional assays and quantitative polymerase chain reactions (qPCR) on potential targets.

In Aim 1, we isolated side-specific HAVECs (fHAVECs and vHAVECs).[4] HAVECs were isolated from recipient hearts removed during transplantation surgeries, sorted using the functional endothelial cell marker acetylated LDL (acLDL), and characterized both phenotypically (alignment and shape index after shear) and

genotypically (through gene and protein expression analyses). More specifically, we found that fHAVECs and vHAVECs express both endothelial cells markers (PECAM1, VE-Cadherin, and vWF) as well as two smooth muscle cell markers (SMA and basic calponin) through gene expression analysis, immunocytochemistry, and flow cytometry. We found that HAVECs align in the direction of the flow, similarly to other vascular endothelial cells but in contrast to porcine aortic valvular endothelial cells.[5] Potential reasons for this difference include: 1) disease state (healthy pigs versus humans with cardiovascular disease), 2) age (young pigs versus older humans), 3) species difference (porcine versus human), and 4) sorting and purity differences (pooled, unsorted PAVECs versus side-specific, sorted HAVECs).

In Aim 2, we sheared HAVECs under the following four conditions: 1) fHAVECs under OS (FO), 2) fHAVECs under LS (FL), 3) vHAVECs under OS (VO), and 4) vHAVECs under LS (VL). Though microarray analysis, we found over 1000 shear-responsive genes in the hypothesized "most physiological" case (FO vs. VL), 30 shear-responsive miRNAs (all possible comparisons), and 3 side-dependent miRNAs.

Validation results show that 93% of genes tested with qPCR were confirmed. Further, five miRNAs were confirmed as shear-sensitive by qPCR: miR-139-3p, miR-148a, miR-187, miR-192, and miR-486-5p. We were also able to validate one side-dependent miRNA, miR-370. Through Ingenuity Pathway Analysis (IPA), we found genes that were highly connected and therefore potential master regulators: *Nfkbia*, *Thbs1*, *Pparg*, *Klf2*, and *Edn1*. We also uncovered several transcription factors including *Atf3*, *Egr1*, *Fosb, and Klf2* (mentioned previously). We found that cellular movement, death, and growth/proliferation were overrepresented cellular functions in our array

dataset. Also through IPA, we compared an existing mRNA microarray using side-specific, porcine aortic valvular endothelial RNA[6] to our HAVEC array (FO vs. VL) and found eight, connected genes that changed in the same direction, reinforcing their importance in valve biology.

miRNA analysis and literature searches further highlighted the importance of the validated miRNAs. Using a filtering process and miRWalk (a predictive program combining up to ten predictive programs), we were able to determine a short list of potential targets, many with known involvement in involved in tissue remodeling and inflammation. *In silico*, we identified overrepresented miRNA binding sequences including miR-139-3p ($p=0.035$) and miR-187 ($p=0.051$) using the DNA Intelligent Analysis Lab (Diana). We also discovered other overrepresented binding sequences for miRNAs which could be regulated by shear or involved in AV disease.

In Aim 3, we explored the following: 1) isolation of endothelial-enriched, porcine AV total RNA, 2) purity assessment of isolation technique using *Pecam1, Sma, eNos, Klf2, and vWF* as markers, 3) generation of a miRNA array using porcine endothelial-enriched total RNA to detect side-dependent miRNAs *in vivo*, 4) validation of both porcine, side-dependent and human, shear-responsive miRNAs (identified *in vivo* and *in vitro*, respectively) using qPCR , and 5) initial validation studies using fluorescent *in situ* hybridization of miR-486-5p. We were able to isolate good quality, side-specific, porcine AV endothelial RNA, identify 24 and confirm seven side-dependent miRNAs in aforementioned porcine AV endothelium, and determine side-dependency of an *in vitro,* shear-responsive miRNA, miR-486-5p (albeit in a different opposite to our hypothesis) through qPCR. Further, we established a protocol for *in situ* hybridization for miRNA

detection. Initial *in situ* hybridization experiments with miR-486-5p show a similar trend as the *in vivo*, porcine qPCR result of miR-486-5p. Finally, we categorized the *in vivo*, porcine, side-dependent miRNAs and *in vitro*, human, shear-responsive miRNAs by cellular function.

Finally, in our future work section, we 1) determined the optimal seeding and transfection conditions for shear studies with miRNA level modulation, 2) investigated eight potential targets of miR-486-5p, 3) uncovered miR-187's role in shear-mediated monocyte adhesion, and 4) determined miR-486-5p's role in migration, apoptosis, and the cell cycle. We found that HAVECs split from one dish to three dishes 48h before shear and transfected with 30nM miR-187 microRNA precursor (premiR) or 10nM miR-486-5p premiR 24h before shear are optimal experimental conditions. We also found that two of the eight potential targets of miR-486-5p show silencing after miR-486-5p overexpression (*Efna1* and *Prnd*) and have potential impact in AV disease in terms of endothelial-to-mesenchymal transition and oxidative stress, respectively. Lastly, we found that 1) miR-187 reduces monocyte adhesion under LS when compared to OS transfected with non-targeting premiR and 2) miR-486-5p increases migration and potentially decreases the number of early apoptotic cells after shear. Better investigation of these miRNAs' regulation will increase our understanding of shear's role in AV disease.

Overall, we are the first to isolate side-specific HAVECs and side-specific porcine AV endothelial-enriched total RNA to run both mRNA (HAVECs) and miRNA arrays (HAVECs and porcine). Through these arrays we uncovered *in vitro* shear-responsive (OS vs. LS) and *in vivo* side-dependent (fibrosa vs. ventricularis) miRNAs which may

serve as master regulators of AV biology and disease. Further, we have begun better understand their roles in a variety of cellular functions intimately linked to tissue remodeling and inflammation (processes important in AV disease). Moreover, we have generated a host of new hypotheses and research directions that highlight the immense potential of the field.

CHAPTER 1

INTRODUCTION

Clinical Significance of Aortic Valve Disease

Worldwide, aortic valve (AV) disease is a major cause of cardiovascular-related deaths as well as a risk factor for additional cardiovascular pathology.[1-3] Valvular degeneration, a component of AV disease, is characterized by the development of stenosis and/or regurgitation. Calcific AV stenosis alone increases the risk of myocardial infarction or death from cardiovascular causes by 50%.[7] At the time of diagnosis, prosthetic valve replacement or repair surgeries are usually the only treatment options for calcific AV stenosis.[8] Without surgery, 75% of severe aortic valve stenosis patients will die within three years.[9] Further, it is estimated that heart valve replacement surgeries will reach 850,000 in number by 2050. Studies of diseased valves reveal a wide spectrum of pathologies, including inflammation, sclerotic and calcific lesions, thrombus formations, bacterial vegetations, and fractured matrix fibers;[10, 11] however, there exists a knowledge gap regarding which genes and microRNAs (miRNAs) which change in AV endothelium, resulting in disease onset and progression.

Aortic Valve Structure and Function

As seen in Figure 1.1 and 1.2, the AV is a trileaflet valve located between the aorta and the left ventricle and acts to prevent reversing blood flow into the left ventricle during diastole.[12] Further, the AV is comprised of three layers: the fibrosa, facing the aorta; the ventricularis, facing left ventricle; and the spongiosa, the layer between the

fibrosa and ventricularis. These three layers are composed of differing amounts of collagen, elastin, and glycosaminoglycans. The fibrosa side is load-bearing and contains primarily collagen oriented circumferentially. The spongiosa contains mainly water and glycosaminoglycans; whereas the ventricularis side contains mostly elastin which acts to return the valve leaflets to an undeformed resting state.[13] The AV is composed of two main cell types: 1) interstitial cells (a mix of myofibroblasts, fibroblasts, and smooth muscle cells) which make up the majority of the valve and 2) the endothelial cells (ECs) which line the AV.[5]

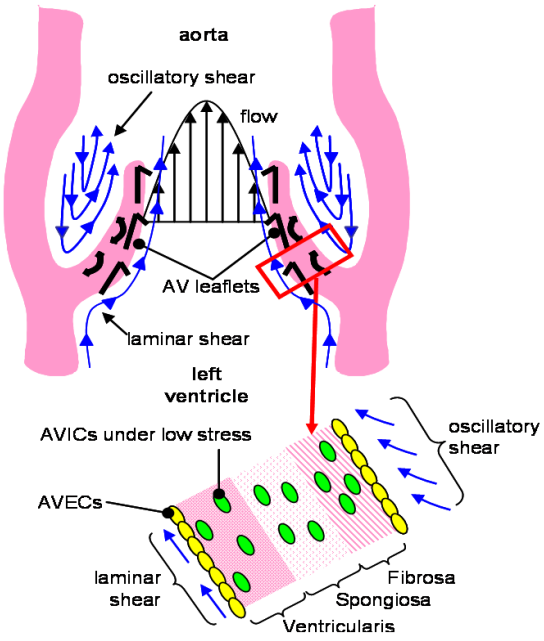

Figure 1.1: Organization of the Aortic Valve. The aortic valve is located between the aorta and the left ventricle and is comprised of three layers: the fibrosa (facing the aorta), the ventricularis (facing the left ventricle), and the spongiosa (the layer in between the fibrosa and ventricularis). (Image from Sucosky)

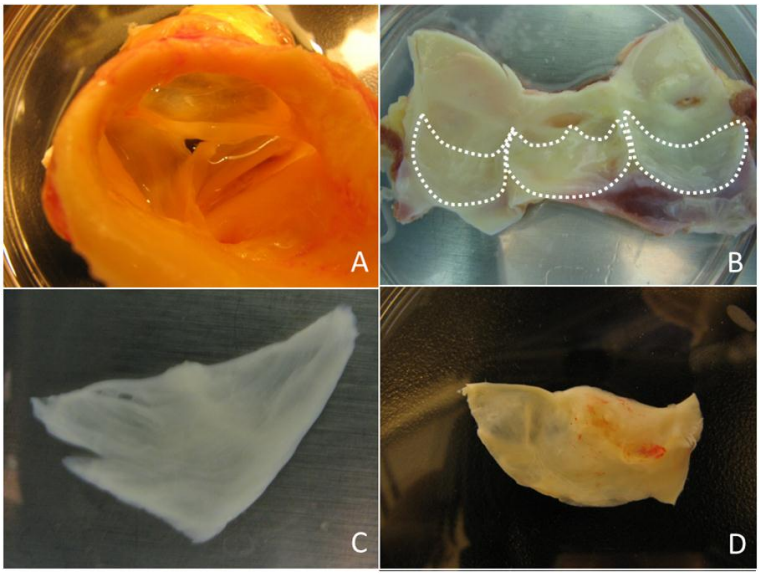

Figure 1.2: Human Aortic Valve. A) shows an intact human aortic valve, B) shows the aortic valve cusps residing in the annulus, C) shows excised a non-sclerotic leaflet, and D) shows an excised sclerotic leaflet.

Classification of Aortic Valve Disease

AV disease is characterized by inflammation, sclerotic and calcific lesions, thrombus formations, and fractured matrix fibers.[14] Further, AV disease can be classified as regurgitant, where the valve does not close completely after diastole; stenotic, where the valve does not open fully during systole; or both regurgitant and stenotic.[15] Aortic regurgitation arises as a result of retrograde flow into the left ventricle during diastole. This results in enlarging of the left ventricle and increased muscle thickening. Aortic regurgitation can be caused by an infection, an AV tear, aorta enlargement, or stenosis and symptoms include shortness of breath and chest discomfort. Conversely, as a result of decreased aortic orifice area due to leaflet stiffening, aortic stenosis causes left-ventricular pressure overload hypertrophy in an effort to preserve ejection performance. This ultimately reduces diastolic function and causes mortality.[9] Aortic stenosis is

diagnosed in late stages many times as a result of a heart murmur.[9, 16] In the developed world, 25% of patients 65 years old or older have AV sclerosis, a characteristic of AV stenosis. Aortic valve calcification is the most common cause of AV stenosis[17, 18] and is the focus of this thesis.

Valvular Disease Progression and Biology

AV disease was thought to be a "wear and tear" process.[19] Now valvular calcification is characterized by the following biological trademarks in the interstitium: 1) accumulation of extracellular matrix (ECM) proteins such as collagen[11] and 2) existence of ectopic bone and bone-related factors.[10, 20-22] Moreover, it is thought to be histologically similar to atherosclerosis, in terms of lipid deposition and macrophage and T-lymphocyte infiltration, with some differences (mineralization and small numbers of smooth muscle cells);[11, 20, 23, 24] however, it is important to note that anti-atherosclerosis therapies, such as lipid-lowering statins, are not effective at slowing AV stenosis progression according to prognostic, randomized trials.[25-27]

In AV disease, once beneath the endothelium as diagrammed in Figure 1.3, activated T-lymphocytes release cytokines including tumor necrosis factor alpha (TNFα), transforming growth factor beta 1 (TGFβ), and interleukin-1 beta (IL1β).[19, 28] These cytokines facilitate extracellular remodeling by increasing metalloprotease production.[19, 29] Infiltrating monocytes become macrophages and begin to express osteopontin, a bone-associated protein. Angiotensin converting enzyme converts Angiotensin I to Angiotensin II which works to sequester lipids in the interstitium.[19, 23, 30] Further, bone morphogenic protein signaling (as noted by side-dependent SMAD 1/5/8 activation[31])

and other osteogenic pathways are shown to be upregulated, inducing differentiation of interstitial cells into an osteogenic phenotype and calcific nodule formation composed of apoptotic cells and hydroxyapatite mineral, and surrounded by viable osteoblast-like cells that express alkaline phosphatase, BMP2 and BMP4, osteopontin, and osteocalcin[32].

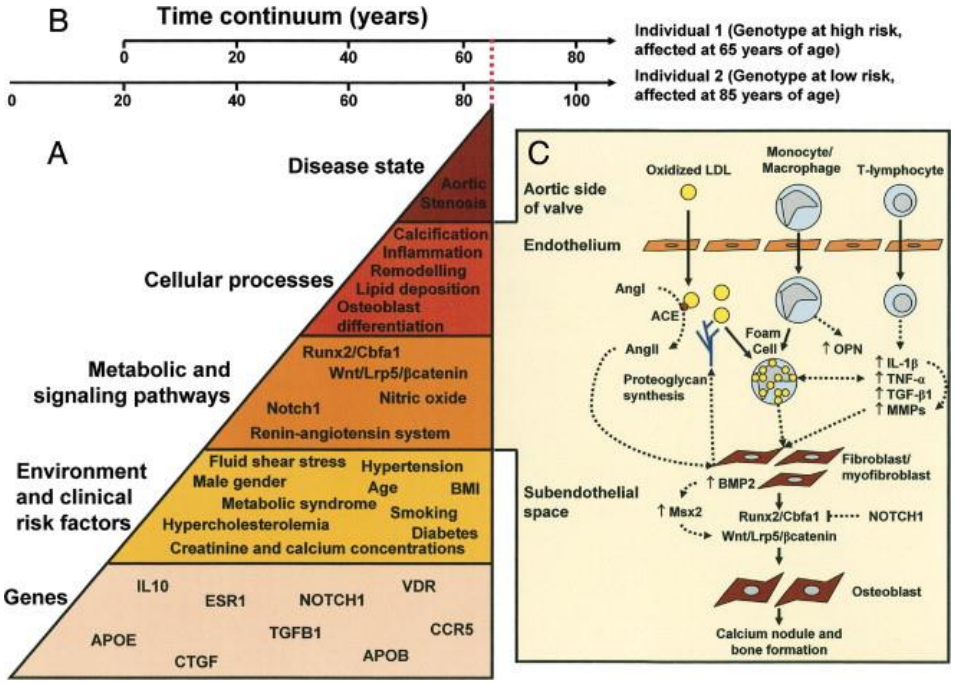

Figure 1.3: Aortic Valve Disease Progression. The above schematic highlights key processes involved in aortic valve stenosis including genes, signaling pathways, and cellular processes involved.[19]

Interestingly, AV disease is side-dependent, occurring preferentially on the fibrosa or aortic side as shown in Figure 1.4. BMP-2 and -4 expression, accumulation of inflammatory cells, and calcification occur in close proximity to each other in the fibrosa side. This suggests that factors such as BMPs produced in endothelium by the disturbed hemodynamic conditions may be a paracrine mediator, leading to side-specific lesion

development. Further supporting this, we found that human AV calcification is associated with preferential activation of SMAD1/5/8 (BMP-dependent SMADs) in the fibrosa endothelium compared to the ventricularis endothelium. Unexpectedly, however, our study showed that BMP2/4 expression was not higher in the fibrosa endothelium compared to that of ventricularis, suggesting a balance between BMPs and their antagonists. This finding indicates the complexity of the AV pathophysiology.[31] Recent microarray studies completed by Bosse, et al. elucidate differences in gene expression between stenotic and non-stenotic valves and further investigation of these differences will facilitate our understanding of the molecular mechanisms underlying AV disease.[33]

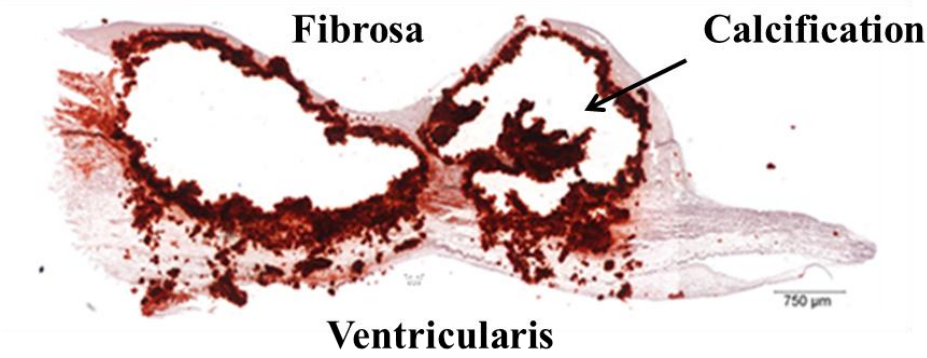

Figure 1.4: Aortic Valve Section from Sclerotic Valve. Alizarin red staining shows calcification preferentially on the fibrosa side of the valve.[34]

Valvular Endothelium, Hemodynamics and AV Disease

The endothelium is a critical mediator of humoral and hemodynamic stimuli. Typically, endothelial inflammation occurs preferentially at areas of disturbed flow[35-38] and valvular endothelial dysfunction coinciding with expression of pro-inflammatory adhesion receptors is an indication of leaflet degeneration.[39, 40] Moreover, the fibrosa and

ventricularis sides of the valve experience very different hemodynamic conditions. Although the exact hemodynamic conditions present on the fibrosa side remains unknown, several hypothesize that in the ventricularis, ECs experience pulsatile, unidirectional shear and remain relatively healthy; whereas, in the fibrosa, ECs experience low-magnitude and oscillatory flow and become diseased.[41] Our work has adopted this shear stress paradigm; however, it is important to note emerging work of Yap, et al. which suggests different shear stress waveforms. More specifically, Yap's work shows largely unidirectional, pulsatile shear stress on the ventricularis; however, there is flow reversal for a short period of time (15-25ms).[42] On the fibrosa side, Yap, et al. supports that strong unidirectional shear stress occurs during systole due to the formation of sinus vortices but that it is unlikely that the vortex will completely reverse the flow (causing oscillatory shear). Yap, et al. acknowledges that it is possible that shear stresses can reverse to small, negative values before and after the sinus vortex formation but that, according to their model, it is unlikely that the shear stresses experienced by the fibrosa endothelium is a sinusoidal wave.[43] Further investigation of the complex shear stresses experienced on the AV in the context of this thesis is necessary; however, our work begins to understand how differential hemodynamic conditions correlate with side-dependent AV calcification on the fibrosa. Lastly, it is important to note that studies in the Yoganathan lab show that both the AV endothelium from the fibrosa and ventricularis sides exposed to the same shear conditions display distinct gene transcript expression profiles, providing initial clues perhaps the mechanism behind AV disease development pattern may be a combination of both genetics and local mechanical environments.[44]

Further experiments are required to investigate additional variables such as innate differences in cell types and other mechanical stimuli.

Shear stress regulates endothelial function both acutely and chronically via mechanotransduction events. More specifically, cytoskeletal and biochemical mechanoreceptors, such as ion channels, G-protein coupled receptors, tyrosine couple receptors, and integrins, are located the endothelial surface.[45] When stimulated by different shear stress patterns, biochemical mechanoreceptors cause changes in second messengers, protein kinases, transcriptional factors, and eventually gene and protein levels. Cytoskeletal mechanoreceptors cause changes in focal adhesions and cell-cell junctions. Crosstalk occurs between many pathways affected by fluid shear stress[45, 46] and vascular and valvular ECs respond to shear stress inducing changes in gene expression profiles *in vitro* and *in vivo.* [6, 47-50]

Previously, we identified mRNA expression profiles in response to laminar shear stress (LS) using cultured porcine AVECs pooled from both fibrosa and ventricularis sides.[5] In addition, Simmons, et al. showed differential mRNA expression patterns in fibrosa and ventricularis endothelium *in vivo* using fresh porcine AVs with a frozen coverslip method.[6] However, mRNA and miRNA expression profiles under both laminar (LS) and oscillatory shear stress (OS) in human AVECs, investigated side-specifically (fibrosa vs. ventricularis), have not been determined and this is a focus of the current study.

Biogenesis of microRNAs and Gene Regulation

miRNAs are a large class of evolutionarily conserved, noncoding, small RNAs, typically 18 to 22 nucleotides in length that function post-transcriptionally by interacting with the 3' untranslated region (3' UTR) of specific target mRNAs in a sequence-specific manner. It is estimated that approximately 1,400 miRNAs exist in the human genome (mirbase.org). Also, miRNAs regulate approximately one-third of the genes in the human genome and each is thought to target multiple mRNAs, resulting in primarily mRNA degradation or translational inhibition.[51]

Several steps are involved in the biogenesis of mature miRNAs as diagrammed in Figure 1.5. Initially, pri-miRNAs are transcribed in the nucleus by RNA polymerase II. pri-miRNAs are several kilobases long and have a cap and polyadenylated tail. pri-miRNAs are then processed by Drosha (an RNase-III enzyme) and Pasha (a double-stranded RNA binding protein). After processing, pre-miRNA is formed. pre-miRNA is approximately 70 nucleotides long and is transported out of the nucleus by RanGTP and exportin. Once in the cytoplasm, Dicer (an RNase-III enzyme) cuts the pre-miRNA into double stranded segments 18-22 nucleotides in length. This double-stranded RNA is processed by the miRISC (multiprotein RNA-induced silencing complex) where it becomes single stranded. As mentioned above, mature miRNA can negatively modulate gene expression by either 1) binding to its mRNA target with complete complementarity and induce mRNA cleavage or 2) binding to its mRNA target with incomplete complementarity and block translation.[52, 53]

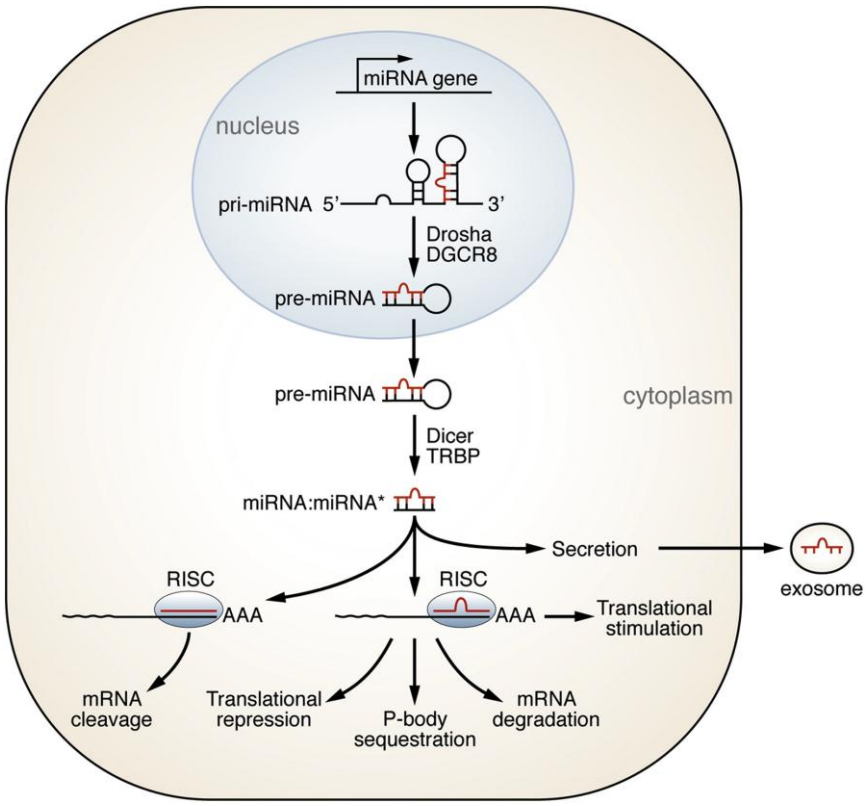

Figure 1.5: miRNA Biosynthesis. The above schematic describes processing of pri-miRNA into functional mature miRNA.[54]

Significant Roles of microRNAs in the Cardiovascular System

Further, there is an emerging role of miRNAs in various cardiovascular-related diseases.[55] Recently, miR-23b and miR-19a have been found shear-responsive in human umbilical vein ECs (HUVECs) *in vitro* and regulate cell growth and cyclin D1 expression, respectively.[48, 49] Fang, et al. showed that miR-10a regulates a pro-inflammatory state in endothelium susceptible to atherosclerosis both *in vivo* in porcine and *in vitro* in human aortic ECs.[56] Moreover, Nigam, et al. has recently identified miRNAs differentially expressed between aortic stenosis and aortic insufficiency (miRNA 26a, miRNA 30b, and miRNA 195) *in vivo* using whole, bicuspid valves and

linked them to calcification-related genes, such as *Smad1/3*, *Runx2*, and *Bmp2* in AV interstitial cells *in vitro*.[57] Since the previous study used total RNA obtained from the entire valve or interstitial cells, the role of endothelial miRNA in AV disease remains unknown.

Impact

Clinically, AV disease is diagnosed by severe symptoms and is typically treated by AV replacement or repair surgeries. For this reason, surgical treatment options and characterization of gross pathologies has been the focus of the majority of AV disease research while the molecular mechanisms (especially miRNAs' role) in aortic valve inflammation, calcification and subsequent valve dysfunction remain understudied. We hypothesize that low-magnitude and oscillatory flow thought to be present on the fibrosa side of the AV and stimulates ECs to regulate miRNAs and mRNAs to influence AV disease progression. This work reveals miRNAs that are regulated in a shear stress- (OS vs. LS) and side-dependent manner (fHAVECs vs. vHAVECs) *in vitro* in human aortic endothelial cells (HAVECs) and *in vivo* in porcine AV endothelium (fibrosa vs. ventricularis), respectively. Our functional studies begin to link the identified miRNAs to their target genes, inflammation and cellular functions involved in tissue remodeling with aspiration for future linkage to calcification and aortic valve sclerosis (AVS). Better understanding of these shear- and side-dependent miRNAs can uncover potential molecular mechanisms underlying AV disease. Further, miRNAs known to be secreted in peripheral blood may also provide potential biomarkers for AV disease.[58]

CHAPTER 2

SPECIFIC AIMS

Project Significance

AV disease is characterized by inflammation, sclerotic and calcific lesions, thrombus formations, and fractured matrix fibers.[14] Further, AV disease can be classified as either regurgitant, where the valve does not close completely after diastole; stenotic, where the valve does not open fully during systole; or both stenotic and regurgitant.[15] In the developed world, 25% of patients 65 years old or older have AV sclerosis, a characteristic of AV stenosis. Aortic valve calcification is the most common cause of AV stenosis.[17, 18]

AV disease was thought to be a "wear and tear" process[19] but is now thought to be histologically similar to atherosclerosis, in terms of lipid deposition and macrophage and T-lymphocyte infiltration, with some differences (mineralization and small numbers of smooth muscle cells).[11, 20, 23, 24] Once beneath the endothelium, activated T-lymphocytes release cytokines[19, 28] which facilitate extracellular remodeling by increasing metalloprotease production.[19, 29] Further, bone morphogenic protein (BMP) signaling and other osteogenic pathways are shown to be upregulated, inducing differentiation of interstitial cells into an osteogenic phenotype and calcific nodule formation.[32] However, it is important to note that anti-atherosclerosis therapies involving statins are not effective at slowing AV stenosis progression (although this subject remains controversial).[25-27] This further highlights the need to better understand AV disease, a disease which is currently only treatable by replacement or repair AV surgeries. As mentioned above,

microarray studies completed by Bosse, et al. have recently elucidated differences in gene expression between stenotic and non-stenotic valves and provide further understanding about the unique mechanism underlying aortic valve disease.[33]

AV disease is side-dependent[59] coinciding with different hemodynamic conditions on either side. AV calcification occurs preferentially in the fibrosa while the ventricularis is relatively unaffected. This side-dependency may be due to the different local hemodynamic conditions. Although little is known about the exact, complex shear stress patterns experienced by the AV, some support the notion that ECs on the ventricularis experience pulsatile, unidirectional shear; whereas, in the fibrosa, ECs experience low-magnitude and oscillatory flow and become diseased.[41] This work has adopted this shear stress paradigm; however, it is important to note that emerging work of Yap, et al. suggests different shear stress waveforms and is described in more detail in the introduction. Further investigation of the complex shear stresses experienced on the AV in the context of this thesis is necessary; however, this work begins to understand how differential hemodynamic conditions can correlate with side-dependent AV calcification.

Shear stress regulates endothelial function both acutely and chronically via mechanotransduction events.[45] Both vascular and valvular ECs respond to shear stress inducing changes in gene expression profiles *in vitro* and *in vivo*.[6, 47-50] Previously, we identified mRNA expression profiles in response to LS using cultured porcine AV ECs pooled from both fibrosa and ventricularis sides[5] and Simmons, et al. showed differential mRNA expression patterns in fibrosa and ventricularis endothelium *in vivo* using fresh porcine AVs[6]; however, mRNA and miRNA expression profiles under both laminar (LS)

and oscillatory shear stress (OS) in human AVECs, isolated side-specifically from the fibrosa and ventricularis sides, have not been determined and this is the focus of Aim 1.

Further, there is an emerging role of miRNAs in various cardiovascular-related diseases,[55] including shear-responsive miR-23b and miR-19a which regulate cell growth and cyclin D1 expression, respectively[48, 49] and miR-10a which regulates a proinflammatory state in endothelium susceptible to atherosclerosis both *in vivo* in porcine and *in vitro* in human aortic ECs.[56] Moreover, Nigam, et al. has recently identified miRNAs differentially expressed between aortic stenosis and aortic insufficiency (miR-26a, miR-30b, and miR-195) *in vivo* using whole, bicuspid valves and linked them to calcification-related genes, such as *Smad1/3*, *Runx2*, and *Bmp2* in AV interstitial cells *in vitro*.[57] Since the previous study used total RNA obtained from the entire valve or interstitial cells, the role of endothelial miRNA in AV disease remains unknown and that is the focus of this thesis. Identification of miRNAs and mRNAs that are shear-dependent (fHAVECs under OS vs. vHAVECs under LS) in HAVECs or side-dependent (fibrosa vs. ventricularis) in porcine AV endothelium can uncover potential molecular mechanisms underlying AV disease, including secreted, circulating miRNAs that could act as potential biomarkers for AV disease.[58]

Project Objective

The goals of this project were: 1) to isolate, purify, and characterize side-specific human aortic valvular endothelial cells from the fibrosa and ventricularis sides (fHAVECs and vHAVECs, respectively), 2) identify side- and shear-dependent miRNAs and mRNAs in HAVECs as well as modulated pathways and potential miRNA targets, 3)

identify side-dependent (fibrosa vs. ventricularis) miRNAs *in vivo* using porcine AV endothelium and confirm both shear-sensitive (FO vs. VL; Aim 2) and side-dependent (fibrosa vs. ventricularis; Aim 3) miRNAs using qPCR and *in situ* hybridization, and 4) determine the function of miR-187 and miR-486-5p by modulating their level *in vitro* and completing a variety of functional assays.

Overall Hypothesis

We hypothesize that low-magnitude and oscillatory flow is present on the fibrosa side of the AV and stimulates ECs to regulate microRNAs and mRNAs to induce AV disease progression. This hypothesis was tested according to the above four specific aims employing both *in vitro* and *in vivo* approaches, high throughput microarray and pathway analyses, and as well as a variety of functional assays.

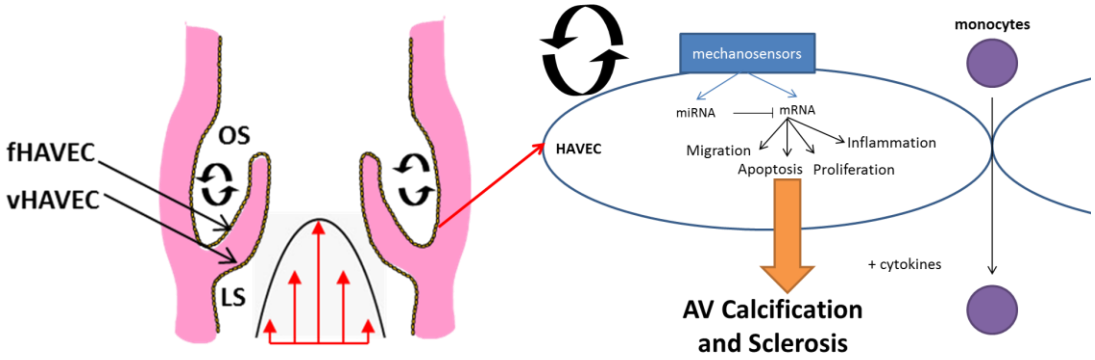

Figure 2.1: Overall Hypothesis. Low-magnitude and oscillatory flow conditions present on the fibrosa side result in differential expression of miRNAs and mRNAs. This differential expression modulates a variety of cellular functions, including migration, apoptosis, proliferation, and inflammation, ultimately resulting in aortic valve calcification and sclerosis.

Specific Aim 1

<u>Isolate</u> and <u>characterize</u> side-dependent (fHAVECs vs. vHAVECs) human aortic valvular endothelial cells (HAVECs).

This thesis describes the first isolation and characterization of human aortic valvular endothelial cells from the fibrosa and ventricularis sides (fHAVECs and vHAVECs, respectively). Non-sclerotic human aortic valves were collected from heart transplantation surgeries. HAVECs were then collected side-specifically using collagenase and a gentle scraping method.[4, 5] Following culture, fHAVECs and vHAVECs were sorted for purity using acLDL and characterized in the following manner. Laminar shear stress (LS - 20dynes/cm^2) was applied for 48h and shape index and angle of alignment were measured. Furthermore, endothelial and smooth muscle cell markers were assessed at both the gene and protein levels via qPCR and immunocytochemistry and flow cytometry respectively.

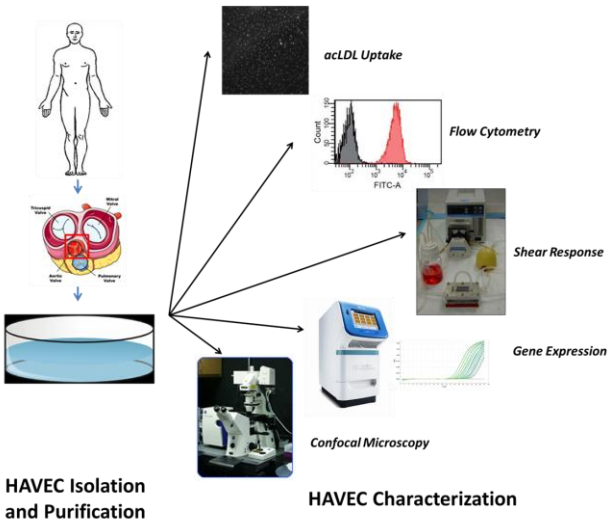

Figure 2.2: Experimental Layout for Aim 1

Specific Aim 2

To identify side- and shear-induced changes in microRNA and messenger RNA expression profiles in HAVECs *in vitro*.

Hypothesis: We hypothesize that application of shear both (steady, laminar shear and oscillatory, laminar shear) induce changes at both the microRNA and messenger RNA levels.

Using the cone-and-plate viscometer, fHAVECs and vHAVECs were exposed to both steady, laminar shear (LS) and oscillatory, laminar shear (OS) for 24h. Following shear, total RNA was collected and tested for quality and well-known mechanosensitive genes. Then, both mRNA and miRNA microarrays were generated using the following groups at the Emory Biomarker Center: 1) fHAVECs exposed to OS (FO), 2) fHAVECs exposed to LS (FL), 3) vHAVECs exposed to OS (VO), and 4) vHAVECs exposed to LS (VL). Significance of microarray analysis (SAM) was completed with all possible combinations to identify both shear- (OS vs. LS) and side-dependent (fHAVECs vs. vHAVECs) miRNAs and mRNAs. Following analysis, a subsection of both miRNAs and mRNAs were validated using qPCR and Western blot. Several *in silico* analyses were completed to better understand the large datasets. Moreover, Ingenuity Pathway Analysis (IPA) was used to determine mechanosensitive mRNA pathways as well as connections between the identified genes. Using programs such as miRWalk and a filtering technique, potential targets of shear-responsive miRNAs were identified. The program Diana was used to identify overrepresented seed sequences in the shear-applied

mRNA array to identify miRNAs potentially acting as master regulators. Identification of shear- and side-dependent miRNAs and mRNAs improves our understanding about the initiation of AV disease and may uncover potential biomarkers for early disease detection.

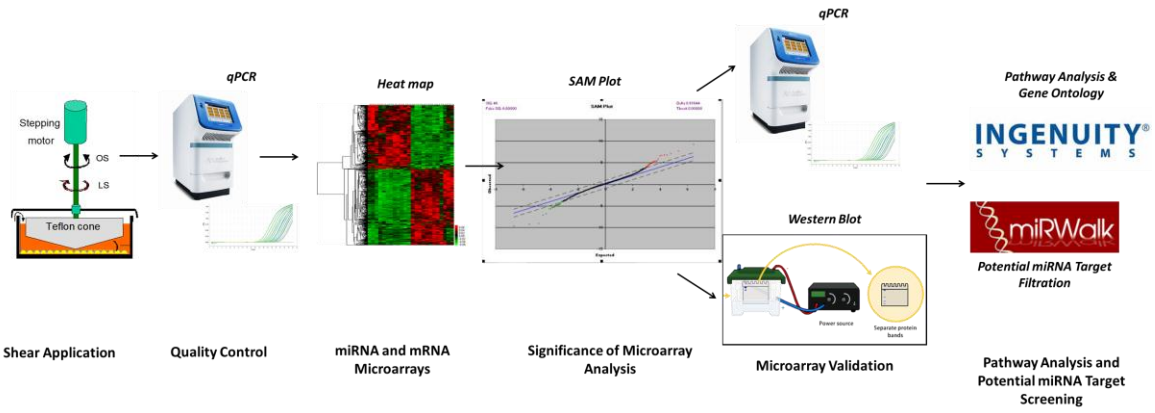

Figure 2.3: Experimental Layout for Aim 2

Specific Aim 3

To develop a method to isolate endothelial-enriched, side-dependent (fibrosa vs. ventricularis) total RNA and to identify and validate side-dependent microRNAs in porcine aortic valvular endothelium.

Hypothesis: We hypothesize that the shear-responsive microRNAs identified in our *in vitro* studies in HAVECs (Aim 2) are side-dependent *in vivo* using porcine AVs.

To date, the side-dependency of miRNA expression in the AV remains unknown. In a collaborative effort with Randall Ankeny and Zannatul Ferdous, we completed the following objectives to address our hypothesis: 1) development of technique to isolate endothelial-enriched RNA from fresh, porcine aortic valves (Holliday and Ankeny), 2) generation of miRNA microarrays from side-dependent porcine AV endothelium (Ferdous), 3) analysis and validation of array data (Ferdous and Holliday), and 4) both *en face* and cyrosection *in situ* hybridization analysis of a key miRNA (Holliday). Due to the importance of studying miRNAs that are relevant in an *in vivo* setting, the miRNAs identified *in vitro* in HAVECs were compared to those miRNAs conserved in pigs. Investigation in pigs allows for increased tissue availability in a more controlled population. Future work will use human samples as confirmation.

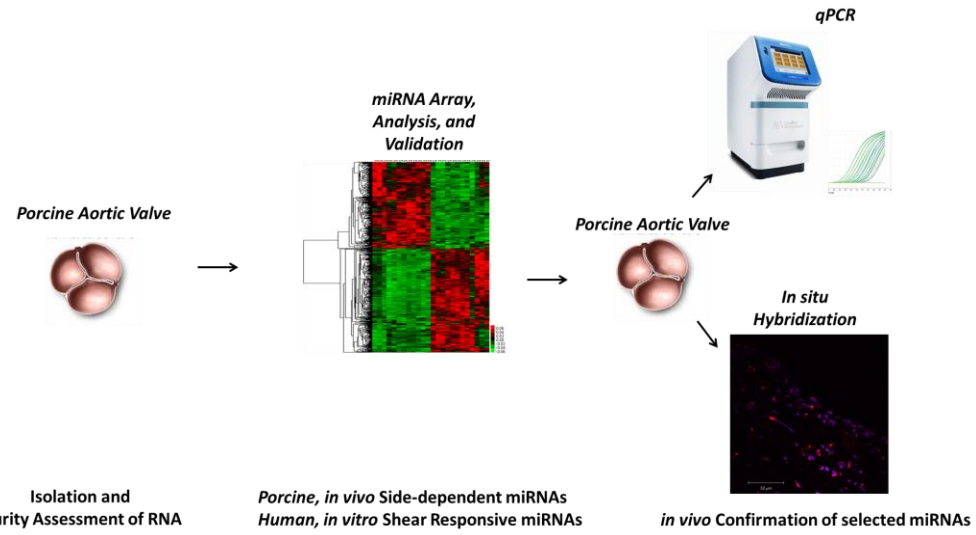

Figure 2.4: Experimental Layout for Aim 3

Future Work

To determine the relationship between important microRNAs (specifically miR-187 and miR-486-5p) and AV disease by modulating levels of microRNAs and performing functional assays and qPCR with potential targets.

Hypothesis: We hypothesize that modulation of miR-187 and miR-486-5p will induce changes in functional assays with disease implications.

Optimization of miRNA overexpression using miRNA precursors and miRNA inhibitors was completed. After selecting the optimal dose, miR-187 or miR-486-5p was overexpressed in fHAVECs and vHAVECs and the cells were sheared. After shear, miR-187's role in inflammation was investigated using a monocyte adhesion assay and miR-486-5p's involvement in migration, apoptosis, and the cell cycle was determined using the wound healing assay, Caspase-3 and Annexin-V/PI staining, and PI staining with RNase treatment respectively. Additional tests for miR-187 and inhibition studies for miR-486-5p are ongoing. By determining the role of identified and validated shear-responsive miRNAs, in particular miR-187 and miR-486-5p, helps to better understand their roles in AV disease.

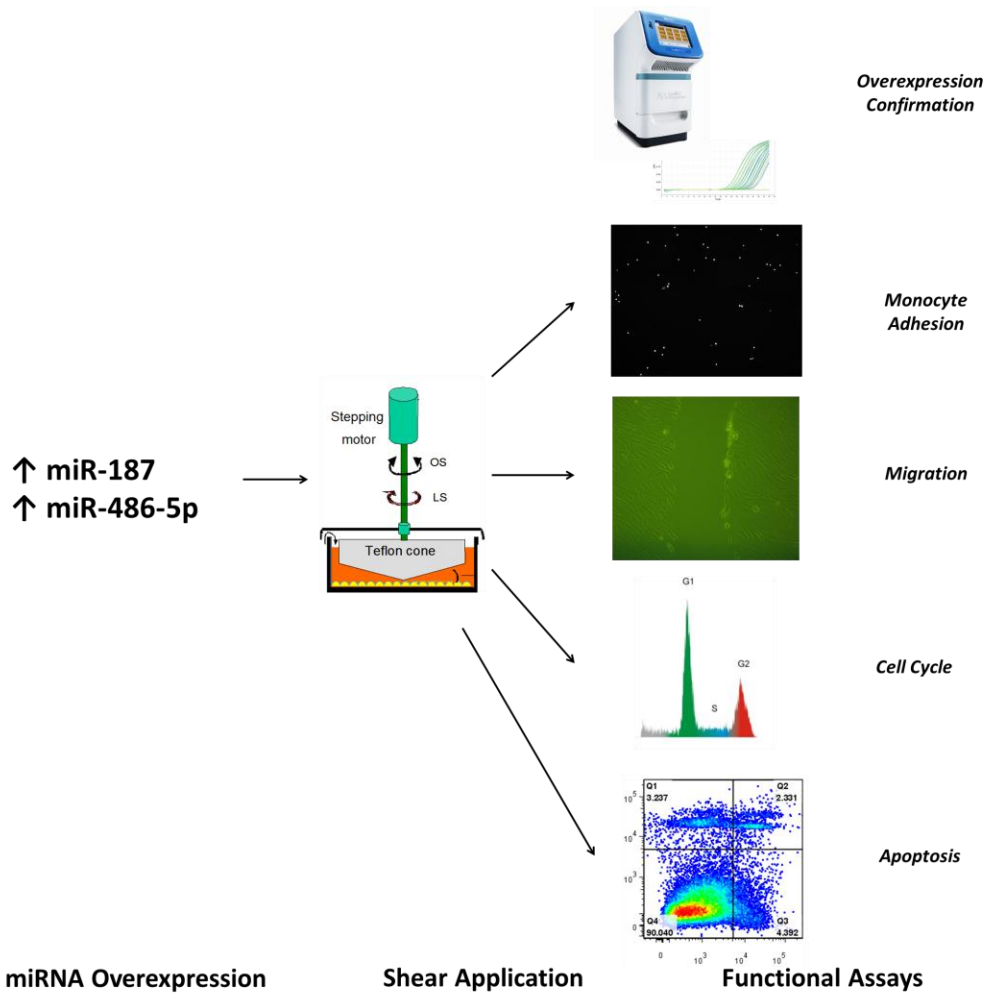

Figure 2.5: Experimental Layout for Future Work

CHAPTER 3

ISOLATION AND CHARACTERIZATION OF SIDE-SPECIFIC HUMAN AORTIC VALVULAR ENDOTHELIAL CELLS

Summary

The goal of this chapter was to isolate and characterize side-specific human aortic valvular endothelial cells (HAVECs). More specifically, side-specific HAVECs were isolated from the fibrosa (fHAVECs) and ventricularis (vHAVECs) sides using aortic valves collected from heart transplant surgeries. After isolation, HAVECs were sorted for endothelial purity using acLDL and then characterized at the gene and protein levels. Results show that both fHAVECs and vHAVECs express endothelial cells markers: PECAM1, vWF, and VE-Cadherin; however, we found that HAVECs also express SMA and basic calponin. To investigate how HAVECs respond to shear, fHAVECs and vHAVECs were exposed to unidirectional, laminar shear (20 dynes/cm^2) for 48hours. Similar to other vascular endothelial cells, HAVECs align in the direction of the flow and have the characteristic changes in shape index and angle of alignment. As far as we are aware, this is the first report of HAVECs isolated in a side-dependent manner in human AVs. Given our ultimate goal of understanding and treating human AV disease, it is important to use well-characterized, valvular ECs from human sources.

Introduction

Endothelial cells line blood vessels and the heart valves and are critical mediators of humoral and hemodynamic stimuli. More specifically, endothelial inflammation resides in diseased prone-areas in both atherosclerosis[35-38] and AV disease.[39, 40] Also, the endothelia act as mechanosensors, affecting changes in signaling cascades in response to their environmental cues.[6, 47-50] For these reasons, it is very important to understand the endothelial cell's role in AV disease.

For many decades, a variety of endothelial cell sources, including human umbilical vein endothelial cells and bovine aortic endothelial cells[60, 61], have been used as *in vitro* test systems for a variety of different research areas; however, emerging research highlights the heterogeneity in endothelial cells in different areas[62-64] and the need for a study investigating the endothelial cell's role in a particular disease using site-specific endothelial cells. In aortic valve research, a number of groups have used ovine [65] and porcine aortic valvular endothelial cells;[5, 63, 66-68] however, we are the first to isolate human aortic valvular endothelial cells (HAVECs) and study them side-specifically (fibrosa HAVECs vs. ventricularis HAVECs). Undoubtedly, experimentation with human AVECs is substantial step towards clinical significance.

In the past the isolation of side-specific human aortic valvular endothelial cells has been challenging because of the limited availability of non-calcified human aortic valves. Through collaboration with the Emory Hospital and the W. Robert Taylor lab, we have received approximately 35 non-calcified aortic valves from the recipient heart of patients undergoing heart tranplantations. The isolation, purification, and characterization (both in phenotype and genotype) of both fibrosa HAVECs (fHAVECs)

and ventricularis (vHAVECs) from these valves are the main foci of the following chapter.

Methods

Cells and Cell Culture

Side-specific human aortic valvular ECs (fHAVECs from fibrosa endothelium and vHAVECs from ventricularis endothelium) were isolated from non-calcified aortic valves (AVs) obtained from heart transplant surgeries (n=35), according to IRB-approved protocol at Emory University and Georgia Institute of Technology, using a brief collagenase digestion and gentle scraping method as previously described.[5]

Briefly, AV cusps were excised, snipped on one side to identify the fibrosa side from the ventricularis side. Next, AV cusps were rinsed in Hank's Buffered Saline Solution (HBSS), incubated in a 5x antibiotic solution on ice for 30min, and rinsed with HBSS under aseptic conditions. One mL of collagenase was incubated on the fibrosa side for ten minutes. Following collagenase incubation, the AV was scraped using sterile scalpel. Four mL of complete medium was used to wash the AV. AVs were rinsed an additional three times with HBSS and the identical isolation procedure was used to isolate endothelial cells from the ventricularis side. The collected media was centrifuged and cell pellets were resuspended in complete medium. Cells were grown to confluency in 0.1% gelatin-coated, 12-well dishes with complete medium (MCDB131 (MediaTech) supplemented with 0.002μg/ml FGF, 0.010μg/ml EGF, 0.001μg/ml VEGF, 0.002μg/ml IGF, 50μg/ml ascorbic acid, 0.001mg/ml hydrocortisone, 1% ECGS, 10%FBS, 1% L-

glutamine, and 1% penicillin-streptomycin). fHAVECs and vHAVECs were used at passage five.

Cell Sorting

Confluent cells (passage three) were sorted for endothelial purity in the following manner: fHAVECs and vHAVECs were incubated in 5µL DiI-acetylated LDL (acLDL; BTI) per mL of complete media for 4h prior to cell sorting using the FACS Aria I (BD Biosciences). Human aortic and umbilical vein ECs (HAECs and HUVECs) were used as positive controls. Human aortic smooth muscle cells (HASMCs) were used as a negative control. Before sorting, fluorescent images of cells incubated with acLDL were taken using an Axiocam MRm camera (Zeiss) and an Axiovert 200M inverted microscope (Zeiss) with a 5x (Plan-Neofluar, NA 0.15) objective lens. Axiovision 3.1 software (Zeiss) was used for image acquisition and processing. After sorting, percentage of acLDL-positive fHAVECs and vHAVECs was ascertained by flow cytometry and compared to control cells (HUVECs and HASMCs). Gates were set so that 2% of the negative population (HASMCs incubated with acLDL) were positive ($n_{patients} = 5$).

Gene Expression Analysis

After sorting, endothelial and smooth muscle marker expression was investigated at the mRNA level. Endothelial cell markers *Pecam-1*, *von Willebrand Factor* (*vWF*), and *VE-cadherin* as well as smooth muscle cell markers, *smooth muscle alpha actin (SMA)* and *basic calponin*, levels were investigated using quantitative, real-time

polymerase chain reaction (qPCR). fHAVECs and vHAVECs from five patients as well as positive (human umbilical vein endothelial cells, HUVECs) and negative (human aortic smooth muscle cells, HASMCs) control cells from three donors were investigated. qPCR was analyzed via the standard curve method to determine copy number of each target gene. 18S (Ambion) acted as an internal control. One-way Analysis of Variance (ANOVA) with a post-hoc Tukey's tests (GraphPad Prism 5) were performed to determine differences in endothelial and smooth muscle cell marker expression among cell types. The following table (Table 3.1) lists the primers used in qPCR.

Table 3.1: HAVEC Characterization Primers

Gene	Forward Primer	Reverse Primer
vWF	5' - GCA GCT CCA CTC GGC ACA T - 3'	5' -CAC CTC GAT GGA TTT CAT GCA - 3'
VE-Cadherin	5' TTT CCA GCA GCC TTT CTA CCA - 3'	5' - ACT GGT CCT GCG GAT GGA - 3'
PECAM-1	5' - GTC GGA CAG TGG GAC GTA TAT CT - 3'	5' - ACT TCG ATG GTC TGT CCT TTT ATG A - 3'
SMA	5' - GAG CGT GGC TAT TCC TTC GTT - 3'	5' - TCA GGC AAC TCG TAA CTC TTC TCA - 3'
Basic calponin	5' - TCA ATG AGT CAA CCC AAA ATT GG - 3'	5' - GTC GTT GGC CTC AAA AAT GTC - 3'

Cell Monolayer Staining

To investigate protein expression and localization of the above endothelial (vWF, VE-Cadherin, and PECAM-1) and smooth muscle cell (SMA) markers, we performed immunocytochemical staining on fHAVEC and vHAVEC monolayers. HASMCs and HUVECs were used as control cell types. Cells were seeded on 0.1% gelatin-coated glass slides at an initial, optimized seeding density of 25,000 cells/cm^2 for two days. Upon achieving confluency, fHAVECs ($n_{patients}$=4), vHAVECs ($n_{patients}$=4) were fixed with 4% formaldehyde and stained using the following antibodies at optimized dilutions: von Willebrand Factor (1:500; rabbit anti-human; Dako), PECAM1 (1:100; mouse anti-

human; Millipore), VE-cadherin (1:100; goat anti-human; Santa Cruz) and smooth muscle alpha actin (1:250; mouse anti-human; Sigma). AlexaFluor 488 (1:100), AlexaFluor 546 (1:100), or Rhodamine Red X (1:100) were used as secondary antibodies. Fluorescent images were taken using the Zeiss LSM 510 NLO META MPE confocal microscope at 40x (NA 1.3) at room temperature. Images were acquired with Zeiss's Zen software and all processing was completed using Zeiss LSM Image Browser. As a control, appropriate isotype antibodies from the same company were used at the same concentration. See Appendix A for complete staining protocol.

Flow Cytometry Analysis

To quantify immunocytochemistry staining for selected endothelial markers, flow cytometry was performed with PECAM-1 and VE-Cadherin antibodies on fHAVECs and vHAVECs with HUVECs and HASMCs as controls ($n_{patients}$=4). vWF (Dako) and SMA (Sigma) antibodies used were not suitable for flow cytometry. Isotype antibodies from the same company at the same concentration were used as a control. For both PECAM1 and VE-Cadherin staining, a dilution of 1:100 was used to calculate percent positive ECs. Fluorescence intensity was detected from 10,000 events using the BD LSR II flow cytometer and FlowJo 7.6 was used for data analysis. Gates were set so that 2% of the negative control was positive. See Appendix B for the flow cytometry protocol.

Shear Conditions

Upon confluency, HAVECs were exposed to steady, laminar shear (LS) using either the parallel plate flow chamber or the cone-and-plate viscometer as we previously

reported.[69, 70] Oscillatory, laminar shear (OS) was applied using the cone-and-plate viscometer.[69] For LS, we employed a unidirectional shear stress of 20 dynes/cm^2 and for OS, we employed a bi-directional shear stress of ± 5 dynes/cm^2 at 1 Hz to approximate the complex shear stress conditions surrounding AVECs *in vivo.*[44] The parallel plate flow chamber (Figure 3.1) and the cone-and-plate (Figure 3.2) bioreactors are explained in more detail below.

Parallel Plate Flow Chamber

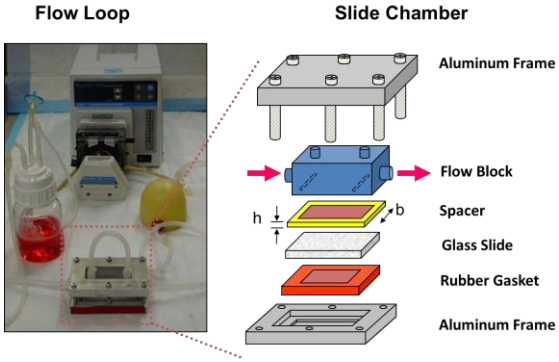

Figure 3.1: Schematic of the parallel plate flow chamber.

Shear stress in the parallel plate flow chamber may be calculated according to the following formula: $\tau = \frac{6Q\mu}{bh^2}$; where τ = shear stress (dynes/cm^2); Q = flow rate (mL/sec); μ=viscosity of media (dynes*sec/cm^2); b=channel width; h = channel height. We use the parallel plate flow chamber for morphology experiments (shape index and alignment). The constants are as follows: τ = 20 dynes/cm^2; μ=0.012 dynes*sec/cm^2; b = 2.65cm; and h=0.0495cm.

Cone and Plate Viscometer

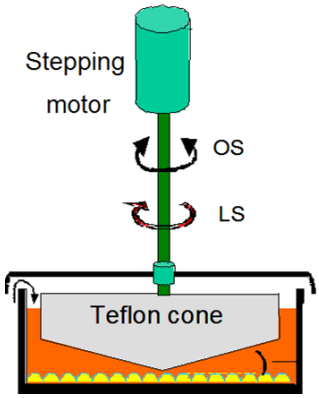

Figure 3.2: Schematic of the cone and plate viscometer.

Shear stress in the cone-and-plate viscometer may be calculated according to the following formula: $\tau = \frac{\mu\omega}{\alpha}$; where τ = shear stress (dynes/cm^2); α= cone angle (degrees); μ=viscosity of media (dynes*sec/cm^2); ω=angular velocity (degrees/sec). The constants are as follows: τ = 20 dynes/cm^2; μ=0.012 dynes*sec/cm^2; α=0.5.

Human Aortic Valvular Endothelial Cell (HAVEC) Alignment under Laminar Shear

fHAVECs and vHAVECs (n=4) were sheared under LS for 48h using the parallel plate flow chamber and shear medium 1 (MCDB131 supplemented with 5% FBS, 0.002µg/ml FGF, 0.0005µg/ml EGF, 1% L-glutamine, and 1% penicillin-streptomycin). After shearing, HAVECs were washed with phosphate-buffered saline (PBS) and fixed with 4% formaldehyde. HAVECs were then stained for F-actin using rhodamine phalloidin at a dilution of 1:40 for 30 min (Invitrogen). Slides were mounted with Fluoro-Gel (Electron Microscopy Sciences). Images were taken at 40x (NA 1.3) using a Zeiss LSM 510 UV confocal microscope. Images were acquired at room temperature

using Zeiss LSM 510 software. LSM Image Browser was used for processing. Shape index and angle of alignment were assessed as previously described.[70] Shape index (SI) ranges from zero to one where a line has a shape index of zero and a circle has a shape index of one and can be calculated according to the following relationship: Shape index = $(4\pi*\text{Area})/(\text{Perimeter}^2)$.

Results

Isolation and Purification of fHAVECs and vHAVECs

fHAVECs and vHAVECs were sorted using acLDL for purity. Post-sorting, percentage of acLDL-positive cells was compared among fHAVECs, vHAVECs, and HUVECs. Figure 3.3 shows the cobblestone morphology of HAVECs as well as acLDL uptake prior to sorting. Flow cytometry analysis after sorting revealed that 95% and 94% of vHAVEC and fHAVEC populations, respectively, are acLDL-positive compared to HUVEC with a 96% acLDL-positive population.

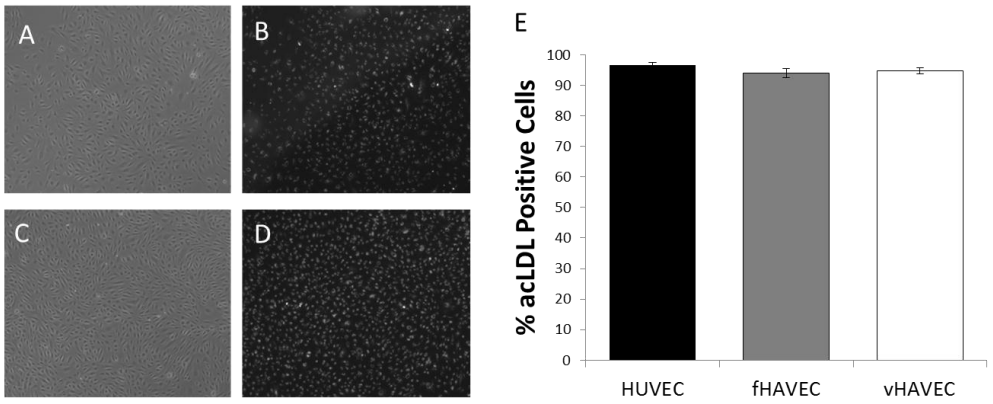

Figure 3.3: HAVEC Morphology, acLDL Uptake, and Purity Assessment. HUVECs, vHAVECs and fHAVECs were incubated with acetylated LDL for four hours to assess uptake. (A) and (B) show cobblestone morphology and acLDL uptake (respectively) prior to sorting in vHAVECs. Analogous images of fHAVECs are shown in (C) and (D). Purity was assessed post-sorting via flow cytometry and compared to a positive control for acetylated LDL uptake, HUVECs. [4] (n=5, error bars = SEM)

Characterization of Side-specific HAVECs

Gene Expression Analysis

qPCR analysis was performed using the following endothelial markers, *VE-cadherin* (Figure 3.4A), *Pecam-1* (Figure 3.4B), *vWF* (Figure 3.4C), and the smooth muscle cell markers, *Sma* (Figure 1D) and *basic calponin* (Figure 3.4E). vHAVECs and fHAVECs were compared to well-studied cells, HUVECs and HAECs as positive controls, and HASMCs as a negative control. Expression of *VE-cadherin* and *Pecam-1* in fHAVECs and vHAVECs was not significantly different from HUVECs and HAECs, while no expression was detected in HASMCs (Figure 3.4A and 3.4B). Expression of *vWF* in HAVECs tended to be lower than HUVECs and HAECs; however, there was only a significant difference between vHAVECs and HUVECs. *Sma* expression was also significantly different between vHAVECs and HUVECs. As expected, HASMCs expressed *Sma* and *basic calponin* (Figure 3.4) but surprisingly, we observed *Sma* and *basic calponin* expression in HAVECs. HUVECs and HAECs also had low but measurable mRNA levels of *Sma* and *basic calponin*. Further, fHAVECs' and vHAVECs' *Sma* expression level was approximately 24% and 41% of HASMCs, respectively and fHAVECs' and vHAVECs' *basic calponin* expression was 34% and 69% of HASMCs respectively.

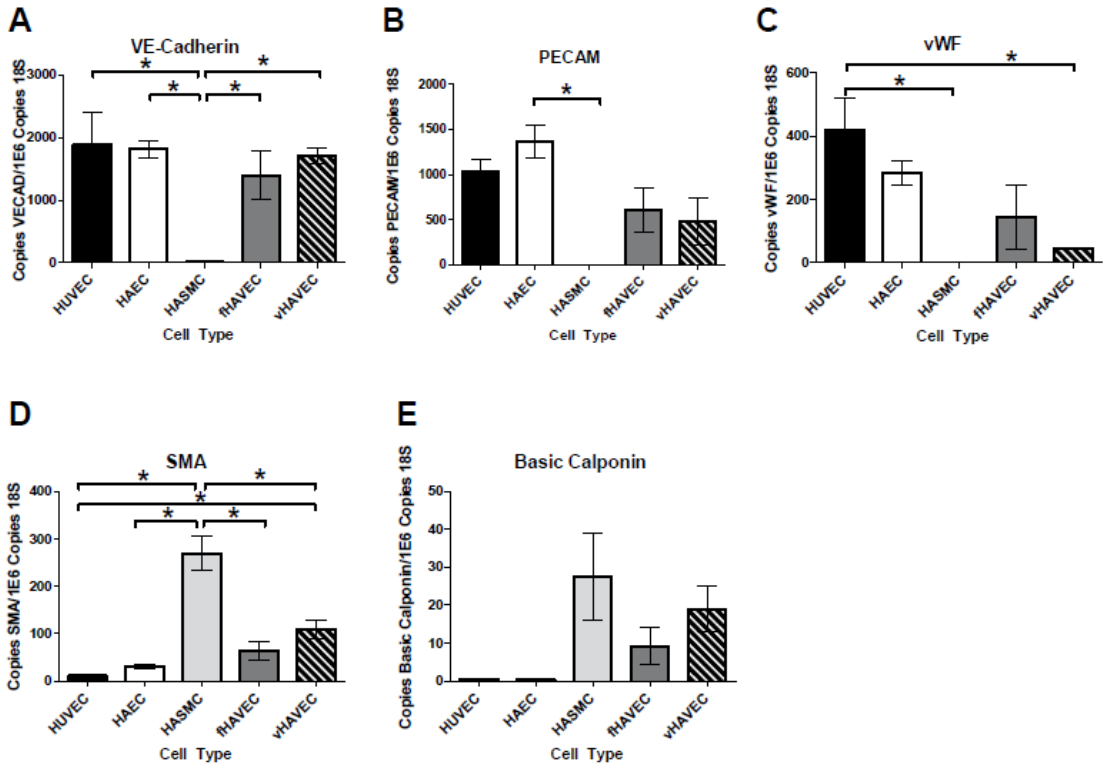

Figure 3.4: Gene Expression Analysis via qPCR. The levels of various endothelial cell markers (A-C) and two smooth muscle markers: smooth muscle alpha actin (D) and basic calponin (E) were investigated in fHAVECs and vHAVECs. HUVECs acted as positive controls for endothelial cells and HASMCs acted as positive control for *Sma*.

Protein Analysis: Immunocytochemistry

Next, we examined the above cell markers at the protein level using immunocytochemistry in HAVECs. Similar to mRNA results, we observed expression and expected localization of PECAM1, vWF, and VE-cadherin as shown in Figure 3.5A-F. As expected, SMA staining was intense and well-organized into filaments in HASMCs (Figure 3.5G); however, fHAVECs and vHAVECs also showed SMA staining although it was not well-organized (Figure 3.5E-F and 3.5I-J). To confirm that SMA

staining in our cultured HAVECs was not due to a contaminating subpopulation of interstitial cells and, in fact, HAVECs expressed both SMA and EC markers, we co-stained HAVECs with both SMA and VE-cadherin and, indeed, found that most SMA-positive cells also expressed VE-cadherin, suggesting that HAVECs indeed coexpressed both endothelial markers and a smooth muscle marker. To determine if this *in vitro* finding was also observed *in vivo*, we co-stained human AV frozen sections with vWF and SMA. As shown in Figure 3.5K-L, some HAVECs expressed both vWF and SMA. This result is consistent with a previous report by Paranya, et al. in ovine AV endothelium.[65]

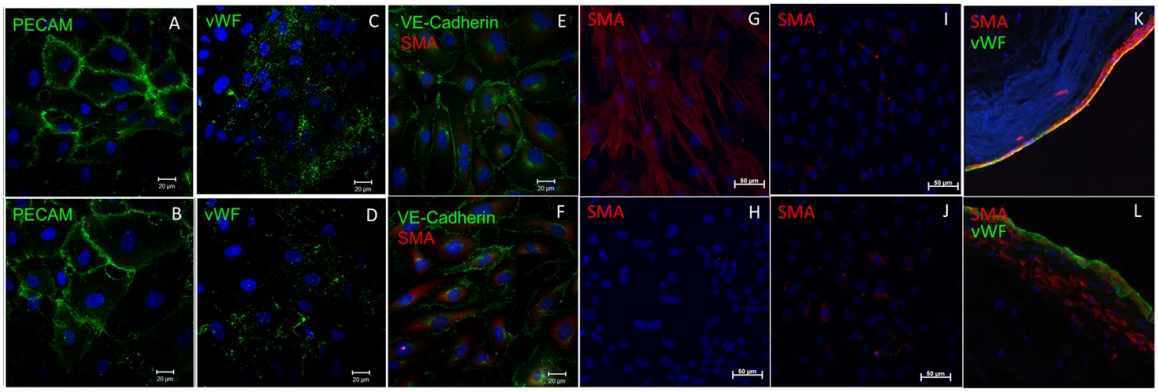

Figure 3.5: HAVEC Characterization. To assess EC markers and a SMC marker, we performed immunocytochemical staining on fHAVECs and vHAVECs. (A), (C), and (E) show PECAM1, vWF, and co-staining of VE-cadherin and SMA in fHAVECs taken with a confocal microscope (scale bar = 20μm) respectively. (B), (D), and (F) show analogous staining in vHAVECs (n=4). Images (G)-(J) show images of SMA staining taken with traditional fluorescence (n=4; scale bar = 50μm). (G) shows SMA staining in HASMC whereas (H) shows staining in HUVEC. (I) and (J) are representative images of SMA staining in fHAVECs and vHAVECs respectively. Shown in (K) and (L) are images of frozen sections from human AV co-stained with vWF and SMA. Original Magnifications of (K) and (L) are x10 and x40, respectively.[4] (Green signifies EC marker staining; Red signifies SMA; Blue is a Hoechst counterstain.)

Protein Analysis: Flow Cytometry

To further confirm the purity of isolated ECs, we investigated the percentage of cells expressing two EC markers, PECAM1 and VE-Cadherin, by flow cytometry. When compared to its isotype or cell type controls, 91-93% of all isolated HAVECs expressed PECAM1, similar to a positive control, HAECs (Figure 3.6A-D; Table 3.2). In contrast, HASMCs did not express the endothelial marker, PECAM1, at the mRNA (qPCR; Figure 3.4B) and protein (flow cytometry; Figure 3.6B and D) levels. When investigating VE-Cadherin, only a subsection of fHAVECs (~41%) and vHAVECs (~38%) were positive for the marker (when gates were set on HASMC expression); however, this expression was comparable to other ECs (HUVECs, ~51% and HAECs, ~45%) as shown in Table 3.2. Further, more immunocytochemistry supports the flow cytometry analysis suggesting that not all ECs express VE-Cadherin.

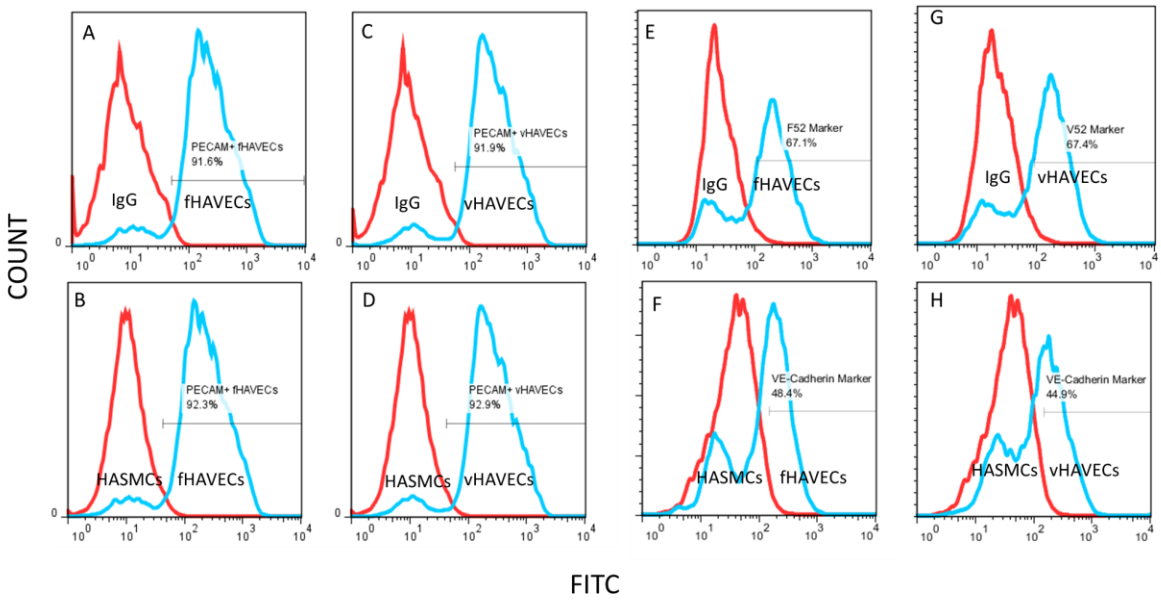

Figure 3.6: Flow Cytometry Analysis of PECAM1 and VE-Cadherin. (A)-(H) show PECAM1 and VE-Cadherin expression via flow cytometry. (A) and (B) show representative histograms of fHAVECs and vHAVECs staining of PECAM1 compared to the isotype control, respectively. (B) and (D) show representative histograms of fHAVECs and vHAVECs PECAM1 staining to HASMCs, respective. (E) - (H) show an analogous comparison for VE-Cadherin (n=4).

Table 3.2: Percentages of PECAM1 and VE-Cadherin Positive Cells

	% PECAM + (versus IgG)	% VE-Cadherin + (versus IgG)	% PECAM + (versus HASMCs)	% VE-Cadherin + (versus HASMCs)
HAECs	92.8	48.5	98.05	45.15
HASMCs	0.134	14.75	1.9	2.01
HUVECs	94.05	76	98.1	50.5
fHAVECs	91.15	47.525	93.325	40.775
vHAVECs	92.525	47.6	93.075	38.075

Shear-response of Side-specific HAVECs

To examine how HAVECs isolated separately from both the fibrosa and ventricularis respond to shear stress, we studied shear-induced cell alignment and shape. After shearing for 48h, both fHAVECs and vHAVECs aligned in the direction of the flow as seen in Figure 3.7B and 3.7D. This shear-induced shape change was further confirmed by quantitative analysis of shape index and angle of alignment (Figure 3.7E-F). fHAVECs showed small, but statistically significant, increased alignment over vHAVECs ($p<0.05$). Also, LS increased both basal expression of *eNOS* as seen in Figure 4.2 in the following chapter as well as phosphorylation of eNOS over static and oscillatory shear samples as shown in Figure 3.7G. It is important to note that when phosphorylated eNOS is normalized to total eNOS the shear response is blunted.

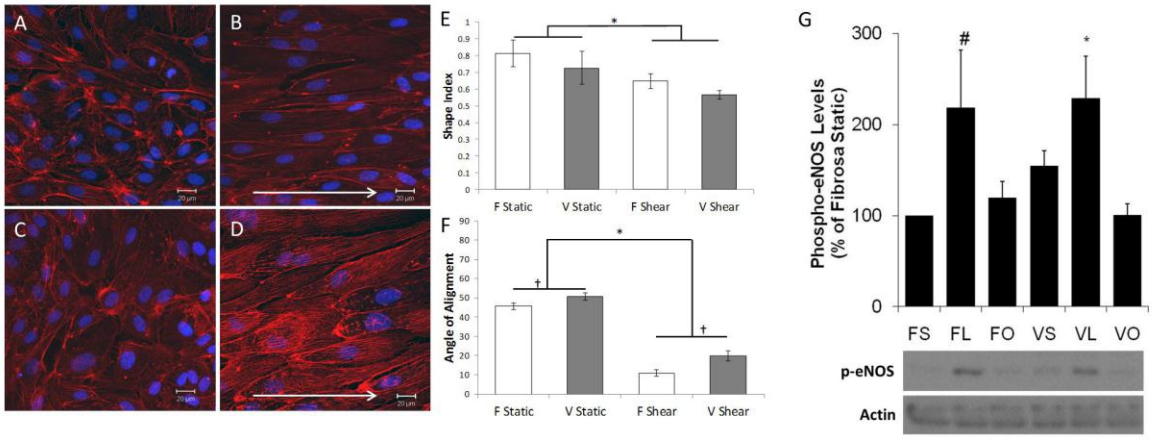

Figure 3.7: Side-specific HAVECs' Response to Laminar Shear. fHAVECs (B) and vHAVECs (D) were sheared under laminar shear (20 dynes/cm^2) for 48h and compared to static controls ((A) fHAVEC and (C) vHAVEC, respectively). Shape index (E) and angle of alignment (F) were compared between sides and conditions (n=4; $p<0.05$). (*) denotes differences in shear condition and (†) denotes difference in side. G) LS increased phosphorylation of eNOS over static and oscillatory shear samples (n=4; * represents $p<0.05$ when compared to FS and VO ; # represents $p=0.06$ when compared to FS and # represents $p=0.12$ when compared to FO).[4]

Discussion

Here, we have been able to isolate, culture, and characterize side-specific HAVECs. As far as we are aware, this is the first report of HAVECs isolated in a side-dependent manner in human AVs. Given our ultimate goal of understanding and treating human AV disease, it is important to use valvular ECs from human sources. Our isolated HAVECs retain many molecular markers (vWF, VE-cadherin, and PECAM1), functions (phosphorylation of eNOS in LS), and phenotypes (alignment and shape index) characteristic of vascular endothelial cells.

Although HAVECs are ECs, they are a unique class of ECs. To our initial surprise, we found that HAVECs express SMA and basic calponin (smooth muscle cell

markers). One potential explanation was that our HAVECs were contaminated with HAVICs, expressing smooth muscle cell markers. Although we cannot completely rule out the possibility of a small contamination, our flow cytometry and immunocytochemistry (Figure 3.5 and 3.6) data strongly support that most of the cells were endothelial. Smooth muscle marker expression in ECs was also reported by others previously both *in vivo* and *in vitro*. Porcine coronary microvascular ECs expressed SMA whereas porcine aortic ECs did not.[71] Also, vascular ECs express SMA and basic calponin as they undergo endothelial-to-mesenchymal transdifferentiation (EMT).[72, 73] Moreover, ovine AV endothelium expressing SMA were shown to undergo EMT *in vivo.*[65] Further statistical analysis between fHAVECs and vHAVECs showed that there was an increase in SMA ($p=0.0243$) and basic calponin ($p=0.0676$) expression in vHAVECs as compared to fHAVECs. Therefore, it is possible that some of our HAVECs, especially vHAVECs, that express SMA may be undergoing EMT. This EMT could have been exacerbated since we isolated HAVECs from patients undergoing heart transplantation. However, currently we do not have access to healthy AVs, and future studies using healthy animal or human AVs are necessary.

Our functional studies showed that HAVECs aligned in the direction of the flow using approximately 35 HAVEC isolations. While this is consistent to that of vascular ECs, it is different from porcine AV ECs which aligned perpendicular to flow.[5] Potential explanations include: 1) a species difference (human versus porcine), 2) side-dependency (fHAVECs and vHAVECs versus pooled PAVEC), and 3) sorting and purity (sorted HAVECs and unsorted PAVECs). Future studies will be critical for a thorough understanding of valvular biology in human disease and in animal models of disease.

CHAPTER 4

IDENTIFICATION OF SHEAR- AND SIDE-DEPENDENT MICRORNAS AND MESSENGER RNAS IN HUMAN AORTIC VALVULAR ENDOTHELIAL CELLS

Summary

We hypothesize oscillatory shear (OS) thought to be present on the fibrosa stimulates ECs to modify mRNAs and miRNAs inducing disease. Our goal was to identify mRNAs and miRNAs differentially regulated by OS and laminar shear (LS) in AVECs from the fibrosa (fHAVECs) and ventricularis (vHAVECs). HAVECs were exposed to OS and LS for 24h, checked for characteristic shear response, and then total RNA was analyzed by mRNA and miRNA microarrays. We found over 700 and 300 mRNAs down- and upregulated, respectively, by OS; however, there was no side-dependency. mRNA microarray results were validated for 26 out of 28 tested genes. Ingenuity Pathway Analysis revealed *Thbs1* and *Nfkbia* as highly-connected, shear-sensitive genes. miRNA array analysis yielded 30 shear-sensitive miRNAs and three side-specific miRNAs. miRNA validation confirmed four of 17 shear-sensitive and one of three side-dependent (FL vs. VL) miRNAs. qPCR of additional miRNAs yielded miR-148a as shear-sensitive. Using miRWalk and several filtering steps, we identified shear-sensitive mRNAs potentially targeted by shear-sensitive miRNAs. These genes and signaling pathways could act as therapeutic targets of AV disease.

Introduction

AV disease is side-dependent[59] which coincides with different, complex hemodynamic conditions on either side. AV calcification occurs preferentially in the fibrosa while the ventricularis is relatively unaffected. This side-dependency may be due to the different local hemodynamic conditions. For these studies, we have adopted the following paradigm for shear stress conditions;[41] however, it is important to note that different paradigms are emerging.[42, 43] We hypothesize that on the ventricularis, ECs experience pulsatile, unidirectional shear; whereas, in the fibrosa, ECs experience low-magnitude and oscillatory flow and become diseased.[41] However, if differential hemodynamic conditions correlate with side-dependent AV calcification remains unknown.

Shear stress regulates endothelial function both acutely and chronically via mechanotransduction events.[45] Both vascular and valvular ECs respond to shear stress inducing changes in gene and protein expression profiles *in vitro* and *in vivo.*[6, 47-50] Previously, we identified mRNA expression profiles in response to LS using cultured porcine AVECs pooled from both fibrosa and ventricularis sides.[5] In addition, Simmons, et al. showed differential mRNA expression patterns in fibrosa and ventricularis endothelium *in vivo* using fresh porcine AVs with a frozen coverslip method.[6] However, mRNA and miRNA expression profiles under both laminar (LS) and oscillatory shear stress (OS) in human AV ECs, in a side-dependent manner, have not been determined and are the focus of this chapter.

As described earlier, miRNAs are now known to play a role in various cardiovascular-related diseases as well as respond to different hemodynamic conditions.[55]

miRNAs are short nucleotide sequences which bind to the 3'UTR of mRNA thereby regulating protein expression mainly by degradation of mRNA targets or by suppression of translation.[51] miR-23b and miR-19a have been found shear-responsive in HUVECs *in vitro* and regulate cell growth and cyclin D1 expression, respectively.[48, 49] Fang, et al. showed that miR-10a regulates a proinflammatory state in endothelium susceptible to atherosclerosis both *in vivo* in porcine and *in vitro* in human aortic ECs.[56] Nigam, et al. has recently identified miRNAs differentially expressed between aortic stenosis and aortic insufficiency (microRNA 26a, microRNA 30b, and microRNA 195) *in vivo* using whole, bicuspid valves and linked them to calcification-related genes, such as *Smad1/3*, *Runx2*, and *Bmp2* in AV interstitial cells *in vitro*.[57] Since the previous study used total RNA obtained from the entire valve or interstitial cells, the role of endothelial miRNA in AV disease remains unknown.

We hypothesize that low-magnitude and oscillatory flow is present on the fibrosa side of the AV and stimulates ECs to regulate miRNAs and mRNAs to induce AV disease progression. Identification of miRNAs and mRNAs that respond to shear stress (shear-sensitive) in HAVECs can uncover potential molecular mechanisms underlying AV disease and circulating genes may also provide potential biomarkers for AV disease.[58] Here, we carried out microarrays to identify shear- (OS vs. LS) and side-dependent (fHAVECs vs. vHAVECs) mRNAs and miRNAs in HAVECs *in vitro*.

Methods

Isolation of Total RNA and Messenger RNA and microRNA Microarrays

HAVECs were sheared under either LS or OS for 24h in shear medium (MCDB131 supplemented with 2.5% FBS, 1% L-glutamine, 1% penicillin-streptomycin). Total RNAs were generated from the following conditions: 1) fHAVECs exposed to OS (FO), 2) fHAVECs exposed to LS (FL), 3) vHAVECs exposed to OS (VO), and 4) vHAVECs exposed to LS (VL). Following shear exposure, cell alignment was verified by phase contrast microscopy (n=6). Cells were washed three times with ice-cold PBS and scraped in Qiazol (Qiagen) to isolate total RNA following the miRNeasy kit (Qiagen). Then, Kruppel-like factor 2 (*Klf2*) and endothelial nitric oxide synthase (*eNOS*), well-known shear-responsive genes, were analyzed by qPCR to determine whether HAVECs responded as anticipated. Next, samples from six different HAVEC isolations were selected based on quality-control analysis using Agilent Bioanalyzer and Taqman Assay for RNU24. Full coverage miRNA (Illumina Human microRNA BeadChips) and mRNA arrays (Illumina Human HT-12 Expression BeadChips) were completed (n=6 each). 24 mRNA microarrays and 24 miRNA microarrays (four groups; n=6 each) were run by the Emory Biomarker Center from total RNA samples. After hybridization, BeadChips were scanned on the Illumina BeadArray Reader to determine the probe fluorescence intensity of 47,231 probes on the mRNA array and 1,145 probes on the miRNA array. Non-normalized, raw probe intensities were used for analysis. Microarray data have been uploaded to GEO (GSE26953).

Microarray Analysis and Heat Map Generation

Significance of microarray analyses (SAM 3.0) was completed to determine shear- and side-dependent differences in HAVEC miRNA and mRNA arrays. Paired comparisons were made among all four groups. Significance was assessed with a false discovery rate of <6% for mRNA arrays and <25% for miRNA arrays. Heat maps of shear-responsive miRNAs and mRNAs were created using Cluster 3.0 for clustering and Java Treeview for visualizing as previously described.[47]

Validation by Quantitative Polymerase Chain Reaction Analysis

qPCR with the same RNA preparations used in microarray studies was used to validate selected shear- (OS vs. LS) and side-dependent miRNAs (fHAVECs vs. vHAVECs) and mRNAs. Significance testing was performed using Student's T-tests with $p<0.05$. mRNAs were validated for those changed in the most physiologically relevant condition, mimicking the hypothesized *in vivo* shear conditions: fibrosa endothelium exposed to OS and ventricularis endothelium exposed to LS (FO compared to VL). From this group, we selected genes which 1) showed a large fold change, 2) were transcription regulators, 3) were well-known, shear -sensitive genes, or 4) were novel targets that may be involved in AV disease. All miRNAs changed in FO versus VL, side-dependent miRNAs, and those miRNAs previously found to be shear-sensitive in HUVEC (miR-192) were validated.[74] qPCR using Taqman assays with pre-designed primers and probes from Applied Biosystems were used for validation. All values were normalized to internal controls: 18S for mRNA arrays or RNU6B for miRNA arrays. Fold changes were calculated using the $\Delta\Delta$Ct method. An additional panel of 15

miRNAs not identified by the SAM analysis but which were interesting based fold change and potential importance in other datasets were investigated by qPCR in the same manner as described above.

Results

Messenger RNA Microarray of Sheared, Side-specific HAVECs

Both fHAVECs and vHAVECs were exposed to LS (20 dynes/cm^2) and OS (± 5 dynes/cm^2) for 24h. Total RNA was prepared for mRNA and miRNA microarray analyses of the following four groups: fHAVECs exposed to OS (FO), fHAVECs exposed to LS (FL), vHAVECs exposed to OS (VO), and vHAVECs exposed to LS (VL). Our results confirmed that our HAVECs responded to shear as expected for some of the well-known mechanoresponses. HAVECs aligned in the direction to the flow as shown in Figure 4.1 and laminar shear increased both endothelial nitric oxide synthase (*eNOS*) and Kruppel-like factor 2 (*Klf2*) expression at the gene level as shown in Figure 4.2. Therefore, we carried out genome-wide microarray studies using these quality-controlled HAVEC samples to determine expression profiles of both mRNAs and miRNAs in response to shear stress.

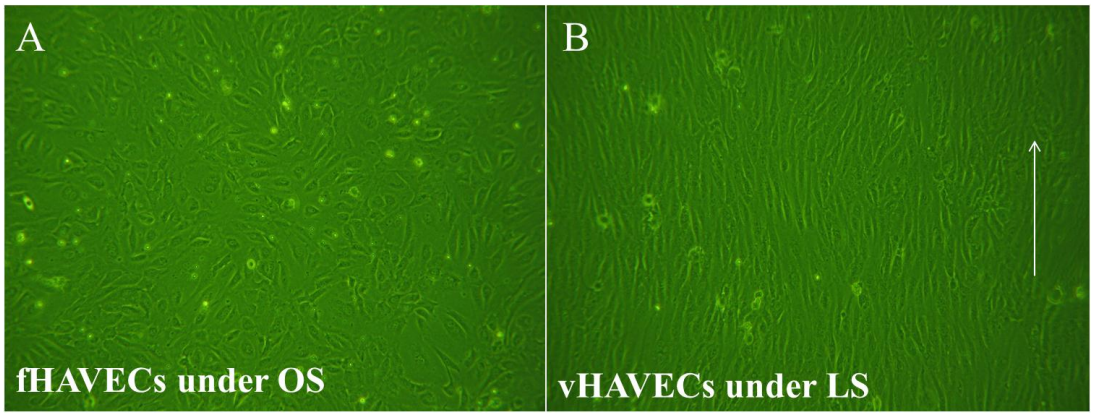

Figure 4.1: Confirmation of LS-Alignment. After 24h shear, HAVECs were inspected under the phase contrast microscope to ensure proper alignment. (A) fHAVECs exposed to OS did not align. (B) vHAVECs exposed to LS align in the direction of the flow (n=6).

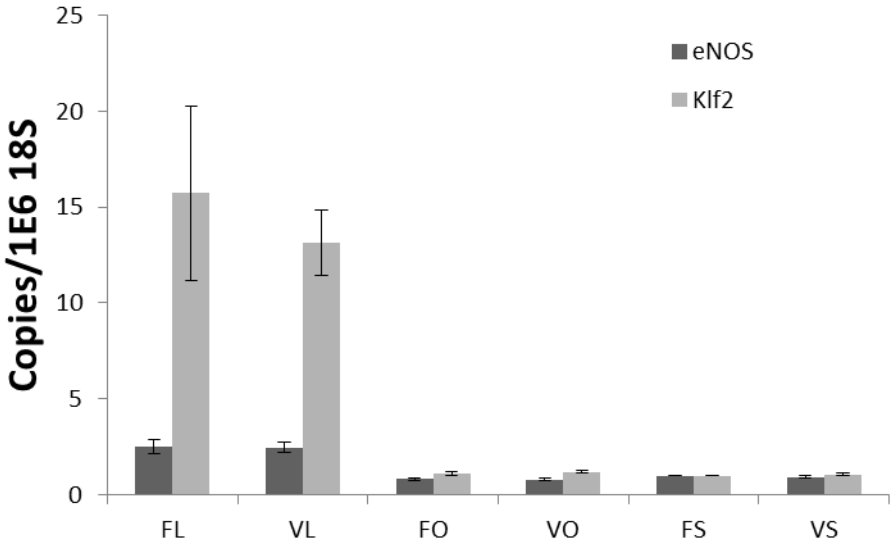

Figure 4.2: Gene Expression Analysis of Mechanosensitive *eNOS* and *Klf2*. Laminar shear (L) upregulated two well-known mechanosensitive genes, *eNOS* and *Klf2*, in fHAVECs (F) and vHAVECs (V) as compared to oscillatory (O) and static conditions (error bars = standard error; n=6).

Results from the mRNA microarray using Illumina Human HT-12 BeadChips (47,231 human probes) were analyzed using significance of microarray analysis

(Stanford excel plug-in). Because of their hypothesized physiological relevance, we focused only three out of possible four comparisons: 1) FO vs. VL, 2) FO vs. FL, and 3) VO vs. VL. The first comparison is the hypothesized most physiologically relevant comparison and the latter two comparisons investigate shear dependency when controlled for cell type. In all comparisons, it appears that there are few cell-dependent differences (as shown in Figure 4.3D and discussed below). In the hypothesized "most physiological case", significance of microarray analysis revealed that over 1,000 genes were differentially regulated by OS compared to LS (>700 downregulated genes in OS and >300 upregulated genes in OS; FDR<6%) as shown in Table C.1 in Appendix C.

Significantly altered gene probes were analyzed by hierarchical clustering to investigate intragroup and intergroup variation as represented in the heat map (Figure 4.3A-C). These three heat maps show low variability within groups, showing the reproducibility of the data. Venn diagrams (Figure 4D) were also used to investigate differences and overlaps in shear-responsive genes among these three groups. The majority of shear-sensitive genes identified were common to all three groups (53% for FO versus VL, 67% for VO versus VL, and 69% for FO versus FL). The Venn diagram suggested minimal side-specific differences in gene expression. Interestingly, significance of microarray analysis also did not detect any side-dependent differences between fHAVECs and vHAVECs at the mRNA level, confirming the Venn diagram analysis.

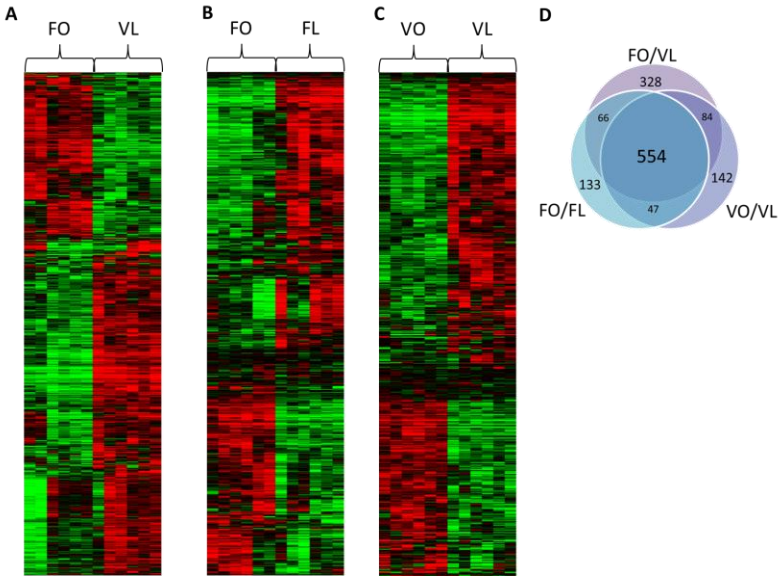

Figure 4.3: Shear-responsive mRNA Heat Maps. (A)-(C) show a visual representation of the three following comparisons: (A) fHAVECs exposed to OS vs. vHAVECs exposed to LS, (B) fHAVECs exposed to OS vs. fHAVECs exposed to LS, (C) vHAVECs exposed to OS vs. vHAVECs exposed to LS where red = upregulated and green = downregulated. (D) shows the overlap of shear-sensitive genes in these three comparisons.

Validation of Shear-sensitive Messenger RNAs in HAVECs by Quantitative Polymerase Chain Reaction

To validate the mRNA microarray data, we carried out qPCR for 28 genes selected based on the following criteria: 1) top changers in both directions (*Slco2a1*, *Igf5bp*, *Sncaip,* and *Adm*), 2) known shear-sensitive genes (*Klf2, Nos3*, and *Bmp4*), 3) well-known targets in cardiovascular disease (*Ctsk*), 4) novel targets that may be related to AV disease (*Hdac1*, *Id1*, and *Dhh*), 5) transcription factors that have the potential to regulate many genes (*Atf3, Egr1*, *Fosb,and Klf2*), and 6) those that showed many relationships with other genes in Ingenuity Pathway Analysis (*Thbs1* and *Nfkbia*). We found that the mRNA array data was highly accurate with 26 out of 28 genes (93%) confirmed (Figure 4.4A and Table D.1). We further confirmed mRNA microarray results

using cell lysates obtained from fHAVECs and vHAVECs exposed to LS, OS, or static conditions for 24h. Western blot (Figure 4.4B-D) results showed that OS increased BMP4 protein expression while decreasing IκBα and eNOS protein expression when compared to LS, which agreed with the mRNA results ($p<0.05$).

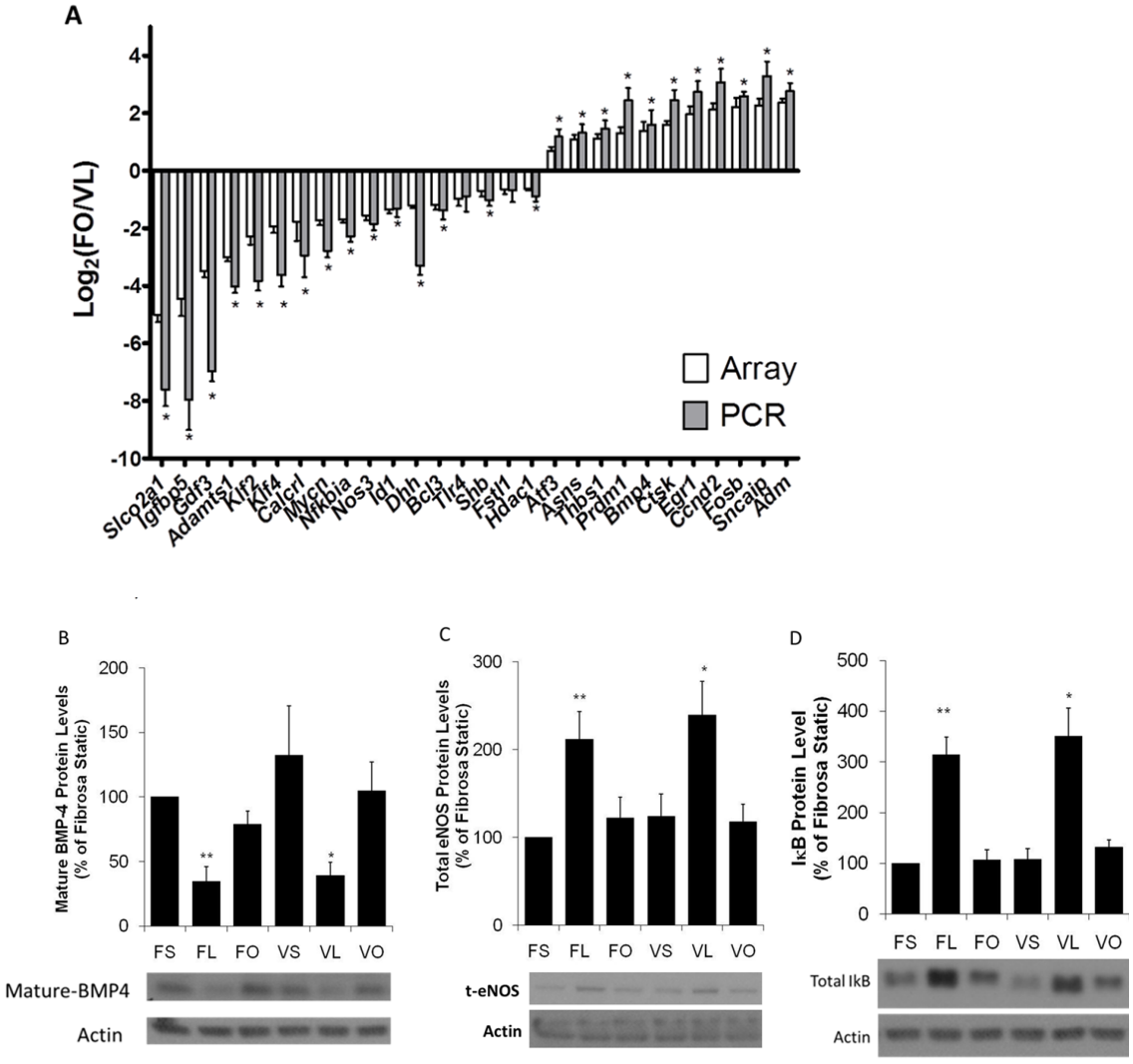

Figure 4.4: HAVEC mRNA Validation. Of the 28 shear-sensitive mRNAs changed in the most physiological conditions (fHAVECs under OS conditions (FO) and vHAVECs under LS conditions (VL)) according to microarray analysis, 26 were confirmed with qPCR (n=6; * = $p<0.05$). For validation at the protein level, protein lysate was used for Western Blots using antibodies against (A) BMP-4, (B) total eNOS, and (C) IκB. FS: fHAVECs under static conditions, FL: fHAVECs under LS, FO: fHAVECs under OS, VS: vHAVECs under static conditions, VL: vHAVECs under LS, VO: vHAVECs under

OS. Representative blots for each antibody including an internal control, β-actin are shown. Bar graphs quantify the blots. For BMP4, n=5; * = $p<0.05$ when compared to FS, VS, and VO and ** = $p<0.05$ when compared to FS and FO. For IκB, n=3; * = $p<0.05$ when compared to FS, VS, VO and ** = $p<0.05$ when compared to FS, VS, and FO. For total eNOS, n=5; * = $p<0.05$ when compared to FS, FO, VS, VO and ** = $p<0.05$ when compared to FS, FO, VS, and VO.[4]

Functional Annotation and Categorization of Mechanosensitive Genes

To better understand the mRNA microarray data set as well as demonstrate possible areas of research stemming from this work, we employed Ingenuity Pathway Analysis (IPA) to investigate the top pathways and functions changed in FO compared to VL, the hypothesized "most physiologically" relevant condition *in vivo* as shown in Table 4.1. The top molecular and cellular functions based on number of genes and p-value were cell movement, cell death, cellular growth and proliferation. While genes involved in the cardiovascular system constituted the top physiological system related to development and function.

Table 4.1: Overrepresented gene ontology categories regulated by shear stress in HAVECs

24h after Shear	*Number of Genes*
Molecular and Cellular Functions	
Cell Movement	175
Cell Death	264
Cellular Growth and Proliferation	257
Cellular Development	221
Cellular Compromise	28
Physiological System Development and Function	
Cardiovascular System Development and Function	118
Organismal Development	136
Organismal Survival	124
Tissue Development	157
Skeletal and Muscular System Development and Function	92
Top Canonical Pathways	
LPS/IL-1 Mediated Inhibition of RXR Function	
Sulfur Metabolism	
Hepatic Fibrosis/Hepatic Stellate Cell Activation	
Keratan Sulfate Biosynthesis	
Neuregulin Signaling	

To further our understanding of AV physiology and disease, we used the pathway builder to uncover known relationships between shear-sensitive genes as shown by Figure 4.5. This analysis highlights the following highly connected nodes: *Nfkbia, Thbs1, Pparg, Klf2,* and *Edn1*. Next, we used the comparison function of IPA to compare our mRNA microarray data set to other shear- and valve-related data sets. About 45% of the shear-sensitive genes (466 of 1041 genes) identified in our HAVEC

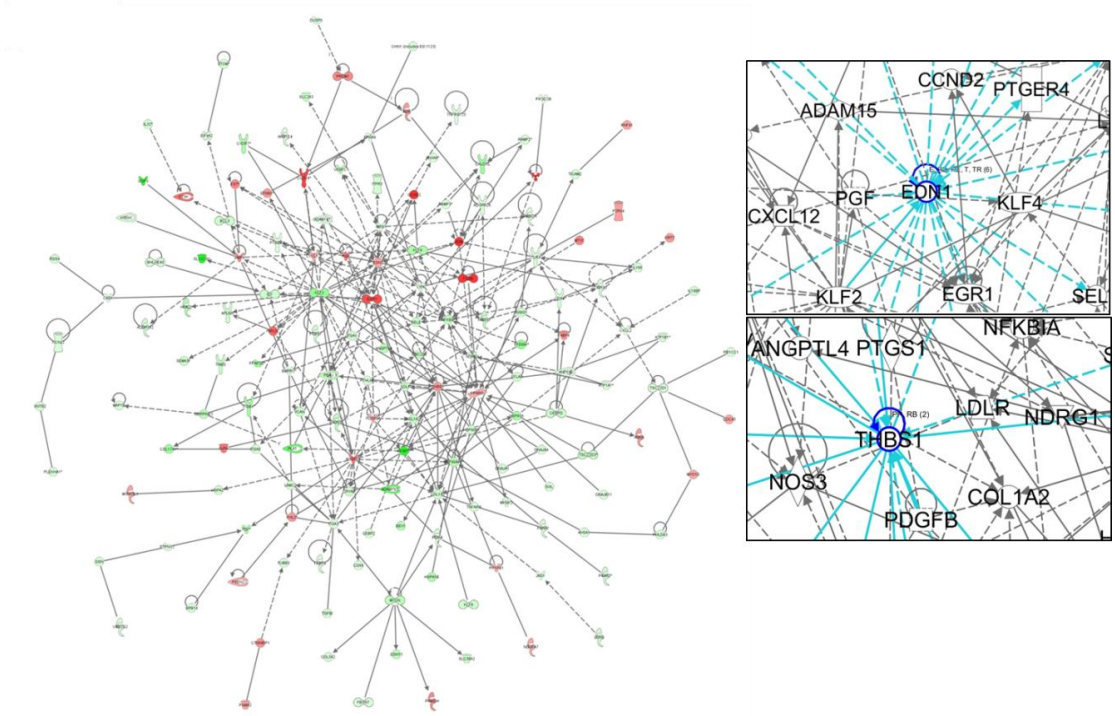

Figure 4.5: Known Relationships between Shear-sensitive Genes. The network shows a subsection (Fold change > $|1.7175|$) of shear-sensitive genes with known connections. Red and green denote those genes that were upregulated and downregulated in FO compared to VL, respectively. Zoomed images show heavily connected nodes *Edn1* and *Thbs1*.

mRNA microarray (FO versus VL) were also reported in HUVECs.[74] We then compared our HAVEC microarray result (FO versus VL) to that of *in vivo* porcine AV endothelium (fibrosa versus ventricularis) reported by Simmons, et al.[6] This comparison revealed 24 genes that changed in the same direction (FO versus VL compared to fibrosa versus ventricularis porcine endothelium). Of those 24 genes, eight genes have known relationships as shown in Figure 4.6. This analysis highlights that some mechanosensitive genes are conserved *in vitro* compared to *in vivo* across species.

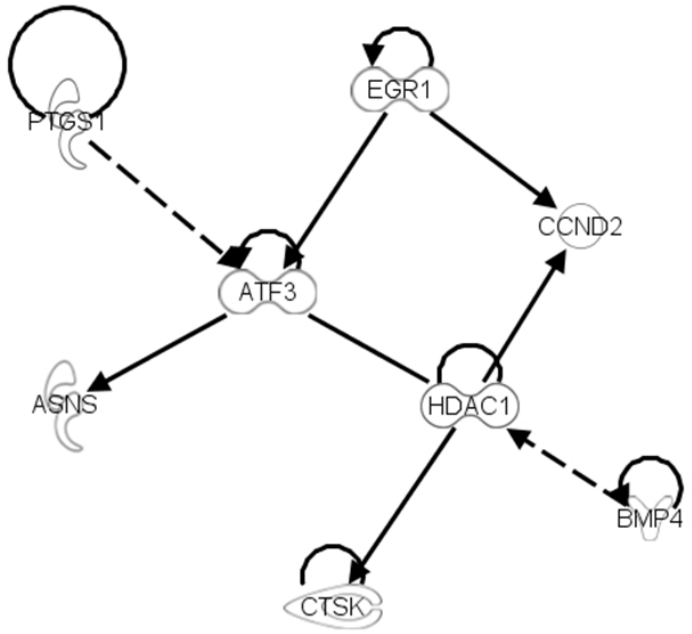

Downregulated gene probes			Upregulated gene probes	
Gene ID	**Gene Name**		**Gene ID**	**Gene Name**
Asns	Asparagine Synthetase		Hdac1	Histone Deacetylase 1
Atf3	Activating Transcription Factor 3		Ptgs1	Prostagladin Endoperoxidase Synthase 1
Bmp4	Bone Morphogenic Protein 4			
Ccnd2	Cyclin D2			
Ctsk	Cathepsin K			
Egr1	Early Growth Response 1			

Figure 4.6: Comparison of Flow-sensitive Genes in HAVECs *in vitro* to Pig Aortic Valve Endothelium *in vivo*. This figure shows a network of connected genes common and similarly modulated to the following two groups: 1) FO versus VL and 2) mRNA isolated from the fibrosa side of pig AVs compared to mRNA from ventricularis side.

Identification of Shear-sensitive and Side-dependent microRNAs in HAVECs

To discover shear-sensitive (OS vs. LS) and side-dependent (fHAVECs vs. vHAVECs) miRNAs in HAVECs, we carried out miRNA microarrays using Illumina Human microRNA BeadChips (1,145 human probes) using total RNA as described above for mRNA microarray. Analyses were conducted using the following four groups: FO,

FL, VO, and VL. Comparisons were made among three groups: 1) FO versus VL, 2) FO versus FL, and 3) VO versus VL to investigate the differential responses of HAVECs to OS versus LS. We did not include the comparison between VO and FL because of its hypothesized lack of physiological relevance *in vivo*. To investigate side-dependent miRNAs in HAVECs, we compared 1) FL versus VL and 2) FO versus VO.

Among all comparisons, SAM analysis of miRNA microarray data showed 30 shear-responsive miRNAs and three side-dependent changes as shown in Table E.1. Heat map analysis, shown in Figure 4.7, showed more intragroup and intergroup variation compared to the mRNA microarray (Figure 4.3).

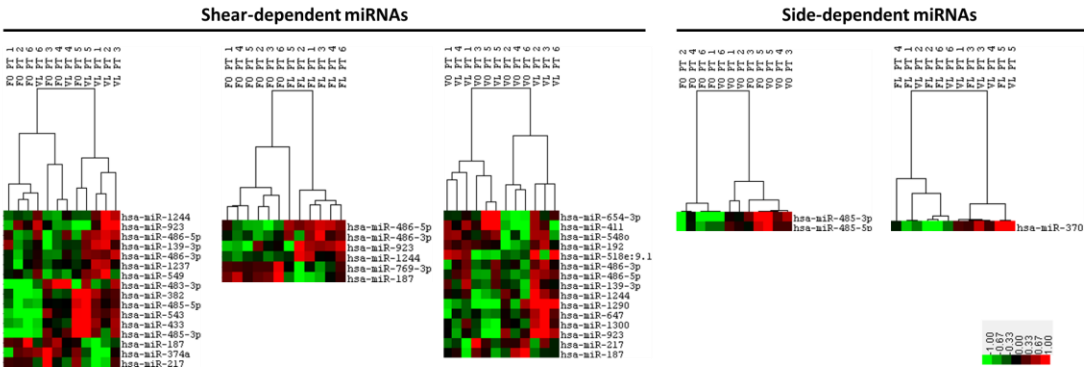

Figure 4.7: Shear-responsive miRNA Heat Maps. The above heat maps show miRNA expression profiles for the following shear-response comparisons: (A) FO versus VL, (B) FO versus FL, and (C) VO versus VL. (D) and (E) show side-dependent differences between the following groups: 1) FO versus VO and 2) FL versus VL (FDR<25%; n=6).[4]

Validation of Shear-sensitive and Side-dependent microRNAs in HAVECs by qPCR

We validated shear-sensitive and side-dependent miRNAs using qPCR (Table D.1). For validation, we chose all 16 miRNAs identified in the FO versus VL group

(Figure 4.8A), as well as all side-dependent miRNAs (FL versus VL and FO versus VO; Figure 4.8C-D). We also selected miR-192 identified in VO versus VL (Figure 4.8B)

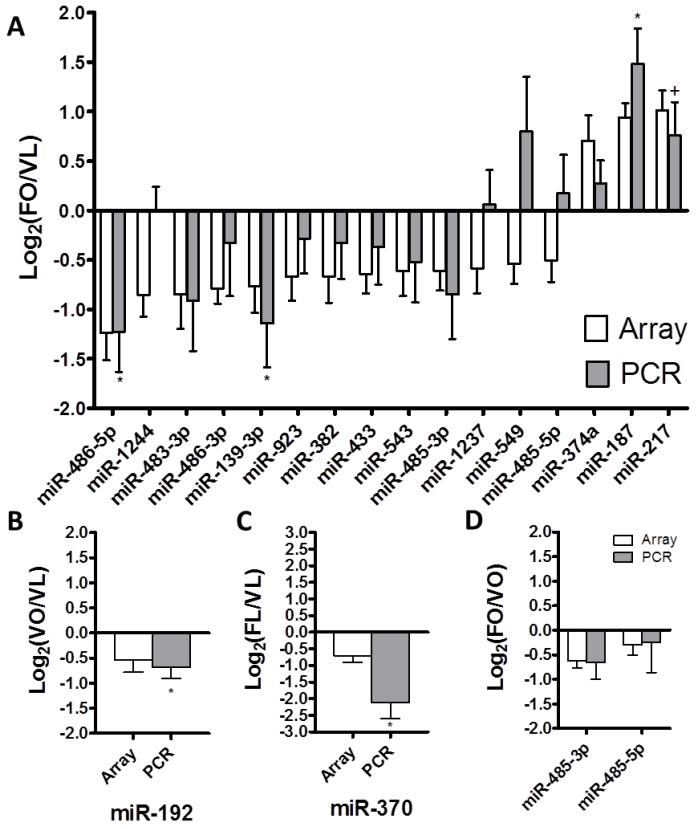

Figure 4.8: Shear-responsive miRNA Validation. (A) Of the 16 miRNAs that were found to be shear-responsive in the most physiological conditions (fHAVECs under oscillatory shear conditions (FO) and vHAVECs under laminar shear conditions (VL)) through microarray analysis, three were confirmed with qPCR. (B) miR-192 found to be shear-sensitive in vHAVECs was confirmed. (C) Side-dependent miR-370 was confirmed. (D) Side-dependent miRNAs 485-3p and 485-5p were not confirmed (* = $p<0.05$ and + = $p<0.1$; n=6).[4]

since it was previously found as a shear-sensitive miRNA.[74] Three out of 16 (miR-139-3p, miR-187, miR-486-5p) miRNAs identified in FO versus VL were validated. Also, there is a trend showing increased expression of miR-217 in FO versus VL ($p<0.1$).

Moreover, miR-192 was also confirmed. Interestingly, we validated one side-dependent miRNA, miR-370 (FL versus VL). As mentioned above, 15 additional miRNAs, chosen based on fold change and importance in other data sets,[56, 74] were investigated in the hypothesized most physiological case (FO vs. VL). Figure 4.9 shows these results. miR-148a was found to shear-responsive ($p<0.05$) and there is trend suggesting that miR-424 ($p<0.1$) is also shear-responsive. The following chapter outlines progress made towards validating shear- (OS vs. LS) and side-dependent (fHAVECs vs. vHAVECs) miRNAs *in vivo* using fluorescent *in situ* hybridization.

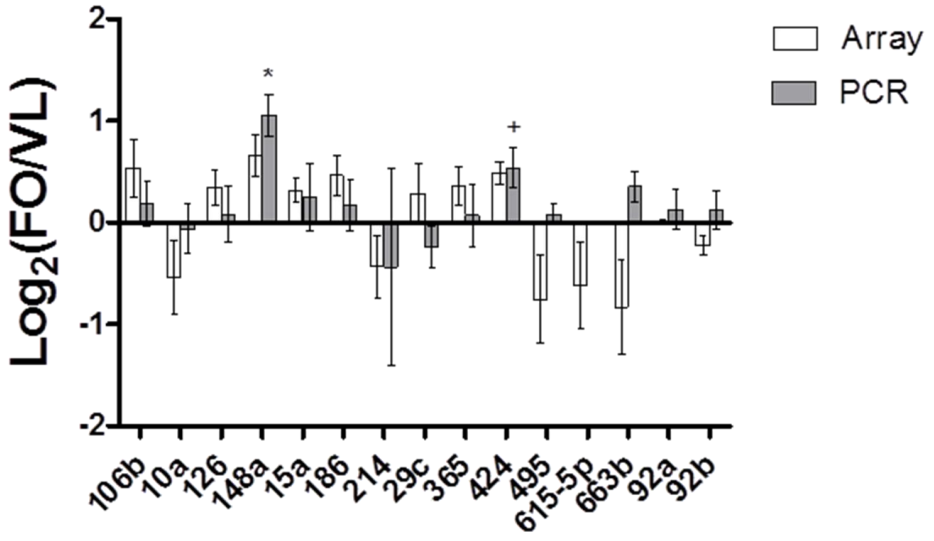

Figure 4.9: qPCR Validation of 15 Additional miRNAs in HAVECs. Out of the 15 miRNAs investigated in FO vs. VL, one additional miRNA was found to be shear-dependent: miR-148a. There is trend of an increase of miR-424 (* = $p<0.05$ and + = $p<0.1$; n=6).

Identification of Potential Gene Targets of Shear-sensitive microRNAs

Our goal was to discover potential, shear-sensitive mRNAs that are regulated by shear-sensitive miRNAs. To achieve our goal, the miRWalk program, which combines

ten web-based gene target prediction programs, was used to initially identify potential miRNA targets. Of those targets, we selected genes identified by more than three prediction programs. These selected genes were further filtered for those identified as shear-sensitive in our mRNA microarray. Lastly, we selected shear-sensitive mRNAs that showed an inverse relationship compared to the miRNA. An example of this filtering process is shown in Figure 4.10. From this filtering process, we identified two

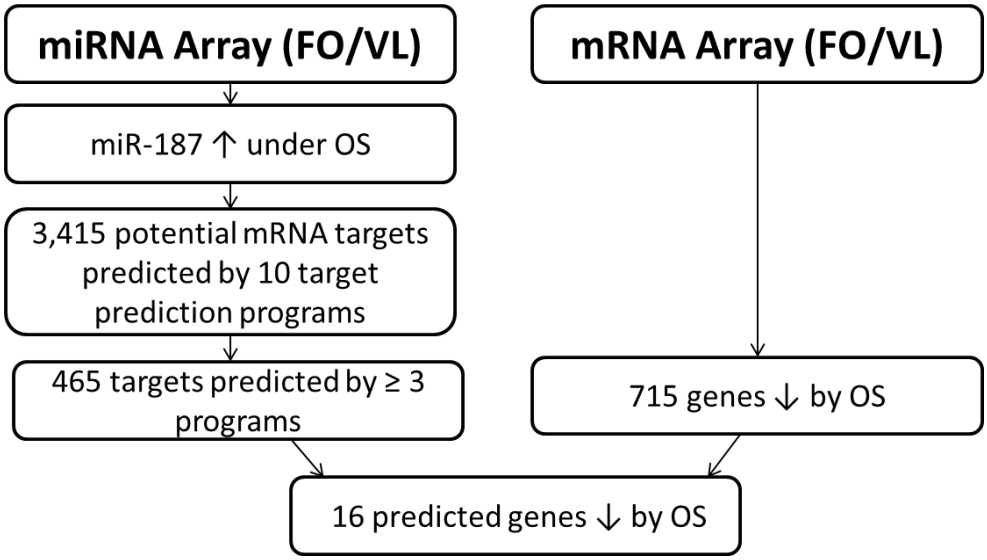

Figure 4.10: Identification of Potential mRNA Targets for Shear-responsive miRNAs. This filtering process reduces the number of potential mRNA targets using 10 predictive programs as well as sheared mRNA microarray dataset.

potential targets for miR-139-3p, 16 potential targets for miR-187, 22 potential targets for miR-192, 8 potential targets for miR-486-5p, and an impressive 147 potential targets for miR-148a listed in Table F.1. The four originally identified miRNAs are categorized by cellular function in Figure 4.11. Because of the large number of targets in each category, miR-148a's targets were not included in Figure 4.11; however, briefly, there were 30 inversely-regulated, predicted genes that were involved in cell death, 41 in cell

movement, 22 in the cell cycle, 46 in inflammation, 2 in calcification (*Bmpr2* and *Cd276*), and 50 in proliferation. Interestingly, miR-139-3p identifies the transcription factor *Fosb* as a putative target while miR-192 potentially targets the transcription factors *Atf3*, *Egr1*, and *Fosb*. miR-148a's potential targets include members of the bone morphogenic protein (BMP) pathway, *Bmpr2* and *Smad5*; a handful of transcription factors, *Ets1* and *Id1*; *Ctsl* which is known to play a role in atherosclerosis, as well as *Cd276* which has a role in calcification.

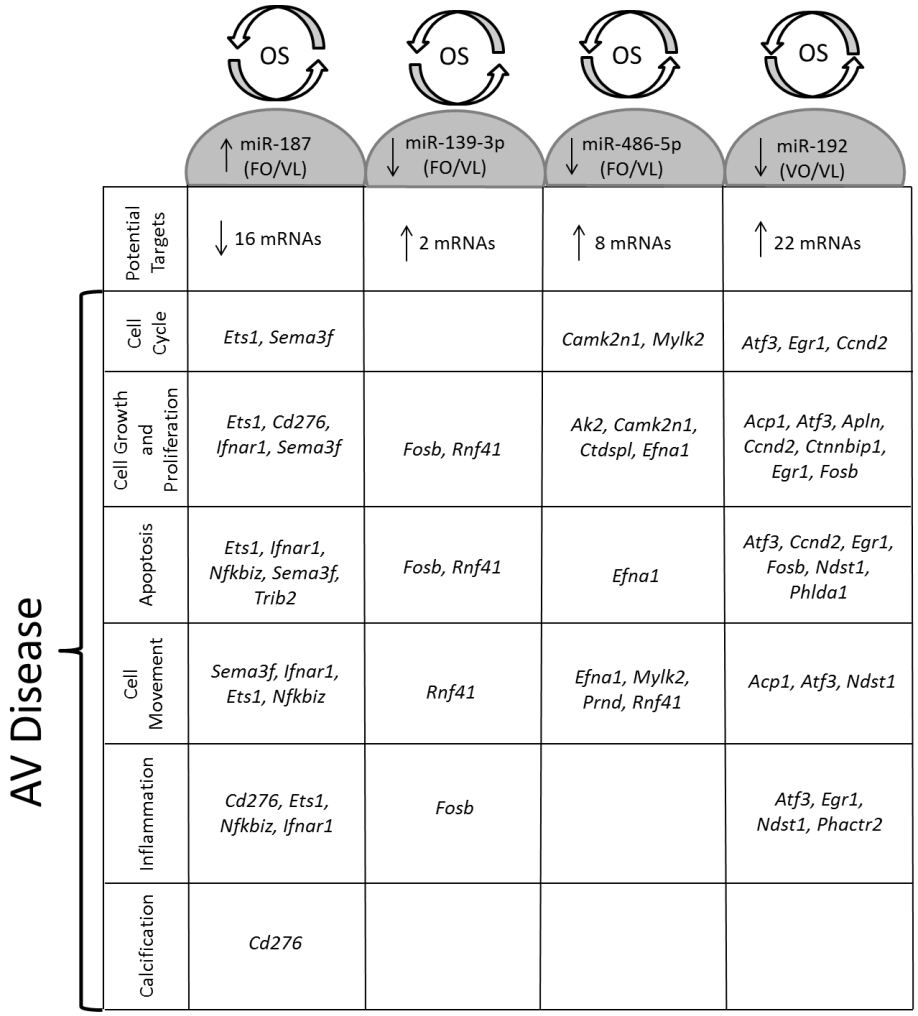

Figure 4.11. Predicted Targets in Aortic Valve Disease. This chart organizes predicted targets from Table F.1 (without miR-148a) by cellular functions important in aortic valve disease using Ingenuity Pathway Analysis and AmiGO.

Identification of Additional Potentially Important microRNAs using Diana Analysis

In order to determine overrepresented miRNA binding sequences in our shear-sensitive mRNA data set, we used DIANA-mirExTra (http://diana.cslab.ece.ntua.gr/). This program determines which hexamers or partial seed sequences are overrepresented in a given data set and therefore which miRNAs may serve as master regulators over a dataset. Here, we use our shear-sensitive dataset comparing FO versus VL. Analysis yielded binding sequences for approximately 280 unique miRNAs, including those validated in the human, *in vitro* miRNA microarray: miR-139-3p, miR-148a, and miR-187 as well as those validated in the porcine, *in vivo* miRNA microarray (described in the following chapter): miR-130a, miR-181a, miR-181b, and miR-214. The full list may be found in Appendix G.

Discussion

Using fHAVECs and vHAVECs, we carried out gene microarray studies to identify shear-sensitive (OS vs. LS) and side-dependent (fHAVECs vs. vHAVECs) mRNAs and miRNAs. The samples used for microarray analysis were selected based on the following critieria: 1) LS-induced alignment (Figure 4.1), 2) *eNOS* and *Klf2* upregulation by LS (Figure 4.2), and 3) total RNA quality (assessed by the Emory Biomarker Center). We chose to focus on comparisons made between FO and VL because we hypothesize that these conditions mimic *in vivo* hemodynamic conditions for each side of the AV.

When comparing FO versus VL, over 300 genes were upregulated and over 700 genes were downregulated by OS (Table C.1 and Figure 4.3). The mRNA microarray data is remarkably accurate as we were able to validated 26 out of 28 genes tested (93% validated). As described in the results, we validated some of the most well-known shear-sensitive genes, *Klf2*, *Nos3*, and *Bmp4*, providing further confidence in our microarray results. In addition, we identified expected targets such as *Ctsk* as well as interesting targets that may be related to AV disease, including *Hdac1*, *Id1*, and *Dhh*. Moreover, we identified shear-sensitive transcription factors such as *Atf3*, *Egr1*, and *Fosb* that may serve as master regulators.

Interestingly, SAM analysis did not detect any side-dependent (fHAVECs vs. vHAVECs) differences. The absence of side-dependent differences in mRNA expression suggests that microenvironment (i.e., shear stress patterns, etc.) could be responsible for differences between fHAVECs and vHAVECs seen *in vivo* rather than them being inherently different cell types. Further investigation is required to address this question.

To better understand shear-sensitive changes in gene expression profiles, Ingenuity Pathway Analysis (IPA) was completed and showed that *Thbs1* and *Nfkbia* were genes with the most connections to other flow-sensitive genes. Interestingly, *Thbs1*, which plays a role in blocking angiogenesis and has a pro-apoptotic role,[75] was found to be increased under FO versus VL. Likewise, NFκBIA (IκKα), which plays an anti-apoptotic role by sequestering inactive NFκB,[76] was found to be decreased under FO versus VL. Strikingly, the data suggest that *Thbs1* and *Nfkbia* are highly-connected, shear-regulated genes which promote a pro-apoptotic environment under oscillatory shear

in HAVECs; however, their role in AV disease has not yet been reported and their potential as therapeutic targets of AV disease has not been fully realized.

Further gene ontology analysis, using IPA, shows that the top canonical pathway (Table 4.1) regulated by shear (OS/LS) was lipopolysaccharide (LPS)/interleukin-1 mediated inhibition of retinoid X receptor (RXR) function. RXR inhibition has been recently hypothesized to induce a pro-atherogenic environment by decreasing macrophages' ability to efflux cholesterol.[77] Although atherosclerosis and AV disease are mechanistically different as evident by statin therapy, further research is warranted to determine the EC's role in RXR function in AV disease. Another top pathway related to shear in HAVECs was sulfur metabolism. Recent research highlights the importance of sulfur metabolism, particularly hydrogen sulfide, in cardiac protection;[78] however the role of sulfur metabolism in AV's has yet to be well-described. Investigation into the roles of these mechanosensitive genes and pathways in AV disease is required in the future.

This is the first study comparing AV endothelial cells under LS and OS *in vitro*; however, Simmons, et al. showed side-dependent (fibrosa vs. ventricularis) expression profiles of porcine AV endothelium *in vivo.* When comparing HAVECs (FO versus VL) to porcine AV endothelium *in vivo* (fibrosa versus ventricularis endothelium), we found 24 genes out of 48 common genes that changed in the same direction. Eight out of the 24 common genes have known relationships according to IPA (Figure 4.6), including *Bmp4*, *Ctsk*, *Hdac1*, and *Atf3*. In an effort to determine if the porcine mRNA dataset would match better if we adopted shear paradigms more similar to those suggested by Yap, et al., we compared fHAVECs exposed to LS and vHAVECs are exposed to OS (FL vs. VO). Through this analysis, we see 20 genes that are conserved between the two datasets

and changed in the same direction (including *Smad6*, *eNOS*, and *Klf4*); however, Ingenuity Pathway Analysis shows few relationships between the genes (a maximum of one connection between two genes). It appears that the FO vs. VL comparison fairs slightly better than the FL vs. VO comparison; however, much more research is required to understand the complex shear conditions of the AV. Experimental differences between the two datasets in either comparison may explain the relatively low number of common genes: 1) varied donor health history (diseased human AVs versus healthy, young pigs), 2) species difference (human versus porcine), 3) *in vitro* versus *in vivo*, and 4) different array platforms with different probes (Illumina versus Affymetrix). Interestingly, we found over 450 shear-responsive genes conserved between our HAVEC shear dataset and HUVECs sheared in the same cone-and-plate system using the same array platform,[74] providing additional confidence in our data.

Our miRNA microarray data showed 30 shear-sensitive miRNAs and 3 side-dependent miRNAs. We validated three out of 16 miRNAs tested in FO versus VL (miR-139-3p, miR-187, and miR-486-5p). Further, miR-192 was validated in VO versus VL. Lastly, side-dependent miR-370 was validated in FL versus VL. As demonstrated in heat map analysis (Figure 4.7) and qPCR validation (Figure 4.8), miRNA microarray data was less reproducible and accurate than the mRNA microarray. This may be due to a low quality miRNA microarray platform, given its relative infancy. In fact, miR-148a was found to be shear-sensitive through qPCR but was not found to be significant in the miRNA array.

The identified shear-responsive miRNAs are reportedly involved in several cell functions which may provide insight into the miRNAs' role in aortic valve disease and

stenosis (Figure 4.10). For instance, it is known that proliferation, apoptosis, and migration all play a role in tissue remodeling in aortic valve disease and that aortic valve disease is characterized by increased monocyte and T-cell binding and invasion into the interstitial space, hallmarks of inflammation.[19] Here, we hypothesized that OS modulates these shear-responsive miRNAs to induce disease. Several studies implicate these miRNAs' role in aortic valve disease, either directly or in a paracrine manner. Notably, OS-induced miR-187 was also found to be increased in thyroid tumors compared to hyperplastic nodules[79] and increased with LPS in the mouse lung.[80] Moreover, a reduction of miR-187 caused a decrease in cell growth in HeLa cells.[81] These studies suggest OS-induced miR-187's role in promoting tissue remodeling and inflammation in aortic valve disease.

Additionally, we found miR-486-5p to be reduced under OS in HAVECs. Another study found that miR-486-5p was decreased in eight types of cancer suggesting that a reduction of miR-486-5p supports tissue remodeling as characterized by increased proliferation,[82] an important component of aortic valve disease. Moreover, OS-diminished miR-192 was also found to be decreased in mice whose mothers were fed a high fat diet.[83] This suggests a potential role for miR-192 in atherogenesis. Further, OS-diminished miR-192 has been linked to cellular proliferation and is thought to be a tumor suppressor decreased in primary cancers.[84] Lastly, studies showed that a decrease in miR-192 correlates with a decrease in cell growth.[85] These studies support that the OS-dependent loss of miR-192 promotes proliferation and an atherogenic environment. Research regarding OS-diminished miR-139-3p is limited and unclear; however, one study shows miR-139-3p down regulation in malignant adrenocortical carcinomas when

compared to benign adrenocortical adenomas, suggesting miR-139-3p's role in migration suppression.[86-88]

The relationship between OS-induced miR-148a and its potential role in AV disease is unclear. For instance, many reports show a decrease of miR-148a in gastric and colorectal cancers, suggesting that miR-148a does not play a clear role in tissue remodeling associated with AV disease;[89] whereas, proponent studies link miR-148a to growth and apoptosis (functions known to be important in tissue remodeling).[90, 91] Moreover, miR-148a has been shown to decrease inflammatory cytokines such as IL-12, IL-6, TNF-alpha, and IFN-beta.[92] There are conflicting reports of miR-148a's role in osteoblast-like cells; where some reports show miR-148a is overexpressed[93] and others state that miR-148a is underexpressed.[94] Further, there are inconsistent reports about miR-148a's role in proliferation and migration. [95-97] Interestingly, as mentioned above in the context of gastric cancer, miR-148a has been shown to be silenced in a variety of cancers and is known to target two important methylators: *Dnmt1* and *Dnmt3b*.[98-102] The role of methylation in atherosclerosis and AV disease is not well understood; however, modulation of the methylation status of several atherogenic genes could have a profound effect on disease initiation and progression. Lastly, through Ingenuity Pathway Analysis of miR-148a's inversely-regulated potential targets, we found that one of the top canonical pathways was the *Notch* signaling pathway (*Furin, Hey2,* and *Numb*). The *Notch* signaling pathway is well-known to be involved in AV disease and therefore increases the potential significance of miR-148a.[71] In summary, although the specific role of these shear-sensitive miRNAs in AV ECs must be established, these findings raise interesting hypotheses regarding their potential role in AV disease.

Interestingly, some shear-responsive miRNAs identified in this study were not shared by other shear-response studies in endothelial cells. Though miR-192 is common to both our HAVEC dataset and Ni's HUVEC dataset, the identification of miR-139-3p, miR-187, and miR-486-5p as shear-sensitive in ECs is a first to our knowledge. Conversely, shear-responsive miR-23b and miR-19a, previously identified as shear-sensitive in HUVECs, are not present in our data set further supporting the idea that shear regulation of miRNAs in HAVECs is unique from other ECs.[48, 49] Additional contributing factors may include cell source (young, relatively healthy versus heart transplant patients), shear conditions (LS/static versus OS/LS), and the infancy of miRNA platforms in general.

Through the miRWalk analysis as described in Figure 4.9, we have identified shear-sensitive potential mRNA targets regulated by shear-sensitive miRNAs. This analysis involved several filtering steps to reduce the number of predicted mRNA targets. Validation of these relationships is required in the future. More specifically, we must perform dual luciferase assays with the 3'UTR of potential miRNA targets.

Diana analysis of overrepresented miRNA binding sequences in the shear-sensitive mRNA microarray yielded several interesting miRNAs including two of our validated miRNAs found in the HAVEC miRNA microarray: miR-139-3p and miR-187. Interestingly, four miRNAs discovered in the miRNA microarray from porcine aortic valve endothelium (discussed in the following chapter) where detected as well: miR-130a, miR-214, miR-181a, and miR-181b. Repeated identification of these miRNAs increases confidence in further exploration. In future experiments, these miRNAs will be targeted. Interestingly, Diana analysis also yielded overrepresented miRNA binding sites

important in other datasets. For instance, miR-10a and miR-10b, modulated in athero-susceptible areas, were identified.[56] Further, miR-19a, found to be shear-sensitive in HUVECs, has an overrepresented binding sequence in the HAVEC mRNA array suggesting its potential to regulate many mRNAs in response to shear in HAVECs.[48] Although miR-19a was not found to be shear-sensitive in the HAVEC mRNA array, it should be validated and investigated via qPCR in the future.

In summary, we found shear-sensitive miRNA and mRNA in side-specific human AV endothelial cells by microarray analysis. Using IPA, we also found shear-sensitive signaling nodes and pathways. These genes and signaling pathways identified in this study as well as the miRNAs that regulate them could be used as therapeutic targets of AV disease.

CHAPTER 5

SIDE-DEPENDENT MICRORNAS IN PORCINE AORTIC VALVULAR ENDOTHELIUM

Summary

miRNAs have the potential to be master regulators; however, to date, differential expression of miRNAs on the fibrosa and ventricularis sides of the aortic valve remain unknown. In this chapter, we will address the following objectives: 1) isolation of endothelial-enriched porcine AV total RNA (both mRNA and miRNA), 2) validation of endothelial-enriched, side-specific RNA isolation technique using the following markers: *Pecam1, Sma, Klf2, and vWF*, 3) generation of a miRNA array using aforementioned porcine endothelial total RNA to detect side-dependent (fibrosa vs. ventricularis) miRNAs, 4) validation of both porcine, side-dependent (Figure 5.4) and human, shear-responsive miRNAs (Figure 5.5) using qPCR , and 5) initial validation studies using *in situ* hybridization of miR-486-5p. We found that we were able to develop a technique to isolate good quality, side-specific, porcine AV endothelial RNA, identify 24 and confirm 7 side-dependent miRNAs in aforementioned porcine AV endothelium, and confirm a side-dependency of an *in vitro* shear-responsive miRNA, miR-486-5p (albeit in the opposite direction) through qPCR. Further, we were able to establish a protocol for *in situ* hybridization which shows a trend to confirm the qPCR result of miR-486-5p. Lastly, we were able to categorize the *in vivo*, porcine, side-dependent (fibrosa vs. ventricularis) miRNAs and *in vitro*, human, shear-responsive (FO vs. VL) miRNAs by cellular function.

Introduction

Previous investigations of the AV have yielded side-specific mRNA expression profiles in pigs, differential expression profiles between atherosusceptible and atheroprotected areas of the porcine vasculature, as well as differential expression between human valves with either aortic stenosis or aortic insufficiency. More specifically, Simmons, et al. showed differential mRNA expression patterns in fibrosa and ventricularis endothelium *in vivo* using fresh porcine AVs with a frozen coverslip method.[6] Fang, et al. showed that miR-10a regulates a proinflammatory state in endothelium susceptible to atherosclerosis both *in vivo* in porcine and *in vitro* in human aortic ECs.[56] Moreover, Nigam, et al. has recently identified miRNAs differentially expressed between aortic stenosis and aortic insufficiency (miRNA 26a, miRNA 30b, and miRNA 195) *in vivo* using whole, bicuspid valves and linked them to calcification-related genes, such as *Smad1/3*, *Runx2*, and *Bmp2* in AV interstitial cells *in vitro.*[57] None of the previous studies have used endothelial-enriched, side-specific porcine AV endothelium to detect differential expression of miRNAs. Further, no study has determined and validated shear-sensitive miRNAs from side-specific, human AV endothelial cells. The goal of this chapter is to investigate these two objectives: 1) determination of side-specific (fibrosa vs. ventricularis) miRNAs in porcine AVs and 2) validate aforementioned miRNAs as well as shear-sensitive (FO vs. VL) miRNAs identified in Aim 2. We hypothesize that shear-sensitive (FO vs. VL) miRNAs identified *in vitro* using HAVECs will also be side-dependent (fibrosa vs. ventricularis) miRNAs *in vivo* using endothelial-enriched pig AV RNA and *in situ* hybridization.

Methods

Isolation of Endothelial-enriched Total RNA from Porcine Aortic Valves

Holliday, CJ and RF Ankeny

An adaptation of a Qiazol-based isolation method to extract RNA from mouse carotid arteries was used here.[103] Porcine aortic valves were excised immediately following slaughter (Holifield Farms) and either placed in nuclease-free PBS (for initial RNA quality studies) or RNAlater (Qiagen; for generation of miRNA array samples). Valves were placed on ice and transported back to the laboratory. The valves were then arranged on thin pieces of plastic so that the fibrosa (or ventricularis) sides were facing up. The plastic was cupped slightly and then 200µL of Qiazol was poured over one side of the leaflet into a microcentrifuge tube. The leaflet was then washed well with nuclease-free PBS three times and the same method was repeated using a new piece of plastic on the opposite side of the valvular leaflet. Total RNA from three leaflets was pooled side-specifically and the Qiagen protocol was used for RNA isolation. (For initial purity assessment, both sides were pooled.)

Purity Assessment of Endothelial-enriched Total RNA from Porcine Aortic Valves

CJ Holliday, and RF Ankeny

To assess purity of the total RNA as well as our ability to isolate both miRNA and mRNA, we investigated three markers: *Pecam1,* an endothelial cell marker (n=5); *Sma*, a smooth muscle cell marker (n=5); and let-7c, an abundant miRNA (n=1). Porcine aortic endothelial cells (PAECs; n=1) were used as a positive control for *Pecam1* and porcine

aortic smooth muscle cells (PASMCs; n=1) were used as a positive control for *Sma*. HAVECs (n=1) were used as a positive control for let-7c.

Ferdous, Z

After establishing a general protocol for endothelial-enriched total RNA isolation from AVs, Ferdous refined this technique to isolate RNA from the fibrosa and ventricularis sides separately. She then assessed her isolation technique for purity and quality using *Klf2*, *eNOS*, and *vWF*, three endothelial markers, as well as *Sma*, a marker of smooth muscle cells found in the interstitum. Samples for miRNA array analysis were isolated in an analogous manner and pooled to increase RNA amount ($n_{samples}$=3; 3 valves pooled). Because of low RNA amount, only a subsection of the RNA isolations (n=2 leaflets) was assessed for purity to conserve the sample for array analysis. Additional quality control to investigate the integrity of the RNA samples was completed by the Emory Biomarker Center, including Taqman analysis for RNU24, an abundant small nucleolar RNA, and Bioanalyzer analysis.

<u>Generation, Analysis, and Validation of microRNA Arrays from the Side-specific Endothelial-enriched Total RNA</u>

Ferdous, Z

Similarly to described above, endothelial-enriched total RNA from AV leaflets was collected in a side-specific manner (fibrosa vs. ventricularis) and assessed for purity (*vWF*, *Klf2*, and *Sma;* n=2 leaflets) and integrity (RNU24 and Bioanalyzer through

Emory Biomarker Center; n=3 pooled). Total RNA was then hybridized on Affymetrix Multispecies Microarray Gene Chips and intensity values were recorded for analysis.

Ferdous, Z and CJ Holliday

The side-specific miRNA microarray data was then analyzed using Significance of Microarray Analysis (Stanford; Holliday and Ferdous). A false discovery rate (FDR) of 25% was observed; however, additional validation is required. A heat map was then generated using Cluster 3.0 and Treeview (Holliday). Selected miRNAs (miR-100, miR-130a, miR-181a/b, miR-199a-3p, miR-199a-5p, and miR-214) were validated via qPCR (Invitrogen's Ncode kit and Applied Biosystem's SYBR green; Ferdous).

Validation of *in vitro*, Shear-responsive microRNAs from HAVEC microRNA Microarray

Holliday, CJ

To determine the *in vivo* significance of miRNAs identified and validated in the HAVEC microarray, we investigated their homology as well as expression levels in side-specific porcine aortic valve endothelium samples prepared by Ferdous as described above using qPCR and custom designed primers. Three of the validated, shear-sensitive, human miRNAs are homologous in porcine: miR-192, miR-486-5p, and miR-148a. (This analysis does not focus on the shear-dependency of miR-148a as it was just discovered. Further investigation is needed to understand its role in porcine AV endothelium. It was not the target of our preliminary studies.) Moreover, we investigated the expression and localization of a shear-sensitive miRNA identified in HAVECs *in vitro*, miR-486-5p,

using fluorescence *in situ* hybridization (FISH). FISH was conducted in both cryosections (n=14 slides from 4 different pigs; prepared at the slaughterhouse) as well as *en face* (n=4 pigs; 2-3 leaflets per pig). Briefly, anti-digoxigenin-POD probes (Exiqon) against miR-486-5p, RNU6B (a positive control), and a non-targeting probe (negative control) were hybridized to tissue/tissue sections at a concentration of 60nM for cryosections and 40nM for tissue at a hybridization temperature of 60 degrees Celsius. Probes were detected using TSA-Cy3 Fluorescence System (Perkin Elmer). A custom quantification program for endothelial intensity developed by Choon Yap of the Yoganathan lab was used to compare fibrosa versus ventricularis staining intensities within the same slide. For *en face in situ* hybridization, the tissue was mounted between two coverslips to permit imaging on both the fibrosa and ventricularis sides of the same tissue section. Detailed protocols for both cryosection and *en face* FISH maybe found in Appendix H.

Results

Isolation and Assessment of Endothelial-enriched Total RNA from Porcine Aortic Valves

Holliday, CJ and Ankeny, RF

During isolation technique development, three markers were used to assess purity and ability to isolate miRNAs: *Pecam1*, an endothelial cell marker; *Sma*, a smooth muscle cell marker, and let-7c, an abundant miRNA. Figure 5.1 shows the expression of these three markers with respects to their positive and/or negative controls. *Pecam1* expression of the endothelial-enriched total RNA for porcine AV endothelium (labeled Tissue Sample) was roughly twice the levels of cultured PAECs. Also similar to PAECs,

the porcine AV endothelium expresses little to no *Sma*. When comparing Ct values, both vHAVECs and porcine AV endothelium had similar levels of let-7c. These results show clean preparation of endothelial-enriched porcine AV total RNA.

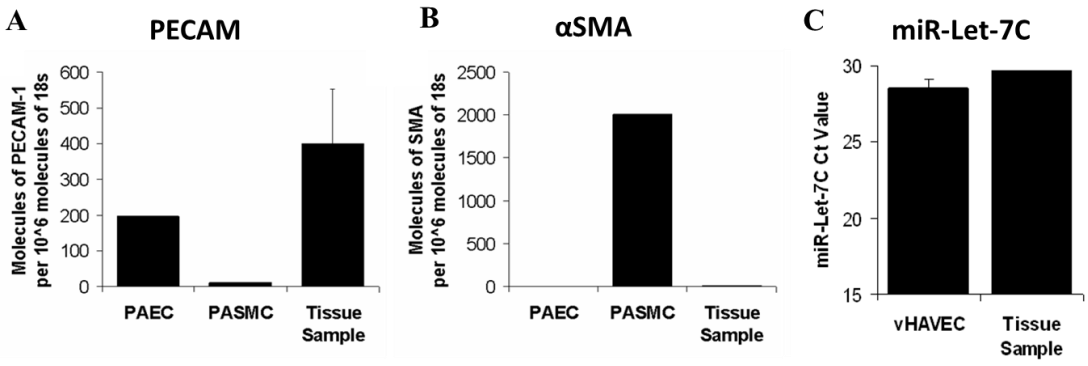

Figure 5.1: Purity and miRNA Isolation Assessment from Pig AVs. (A) Endothelial-enriched RNA tissue samples express *Pecam1* at levels roughly twice that of PAECs. (B) Endothelial-enriched RNA tissue samples do not express smooth muscles alpha actin similarly to PAECs; whereas, PASMCs do. (C) Both vHAVECs and endothelial-enriched RNA tissue samples express similar levels of let-7c. ($n_{\text{tissue samples}} = 5$; $n_{\text{PAECs}}=1$; $n_{\text{PASMCs}}=1$; $n_{\text{vHAVECs}}=1$; Holliday and Ankeny, unpublished)

RNA Isolation Technique and Sample Generation and Purity Assessment for microRNA Microarray

Ferdous, Z

Ferdous refined the established endothelial-enriched total RNA isolation method such that RNA from the fibrosa and ventricularis sides was collected separately. To show purity and reproducibility of the isolation technique the following markers were investigated in four separate isolations: *vWF*, *eNOS*, *Klf2*, and *Sma* as shown in Figure 5.2A. Results show expression of the endothelial cell markers (*vWF*, *eNOS*, and *Klf2*) with minimal *Sma* contamination (less than 25 copies of *Sma* /1E6 copies 18S). Samples to be used for microarray analysis were collected using the above validated isolation

technique. Because of the low RNA yield, a subsection of the RNA to be used for the array was assessed for endothelial purity (n=2 leaflets). Figure 5.2B shows that RNA to be used in miRNA array expressed *vWF* and *Klf2* abundantly. Similarly, endothelial-enriched, porcine aortic valve samples showed less than 75 copies of *Sma* per million copies 18S.

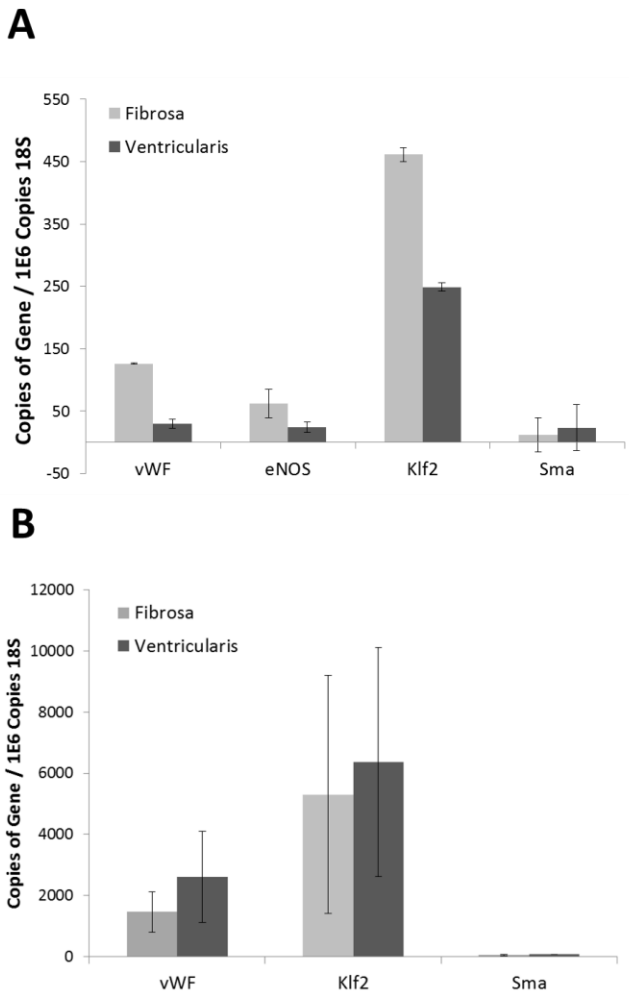

Figure 5.2: Side-specific Purity Assessment of Porcine Endothelial-enriched Total RNA. Total RNA isolated from both the fibrosa and ventricularis endothelium express *vWF* and *Klf2* but not *Sma*. (A) shows validation of the isolation technique (n=4) and (B) shows purity assessment in a subsection of samples to be used for array (n=2 leaflets).

Generation, Analysis, and Validation of microRNA Arrays from the Side-specific, Endothelial-enriched Total RNA

Ferdous, Z and CJ Holliday

Endothelial-enriched, side-specific porcine aortic valve RNA was used to generate miRNA microarrays through the Emory Biomarker Center (Ferdous). From Significance of Microarray Analysis, we found 24 unique side-specific miRNAs (Ferdous and Holliday). Thirteen of the 24 miRNAs were detected by multiple species probes and thereby increased our confidence in their true side-specificity. Figure 5.3 shows a heat map representation of the side-dependent (fibrosa vs. ventricularis) miRNAs (Holliday). It is important to note each miRNA is represented in this heat map once in order to prevent visual bias. Further, analysis shows that all side-specific miRNAs detected were increased on the fibrosa side as compared to the ventricularis side. A complete list of changed miRNAs may be found in Appendix I.

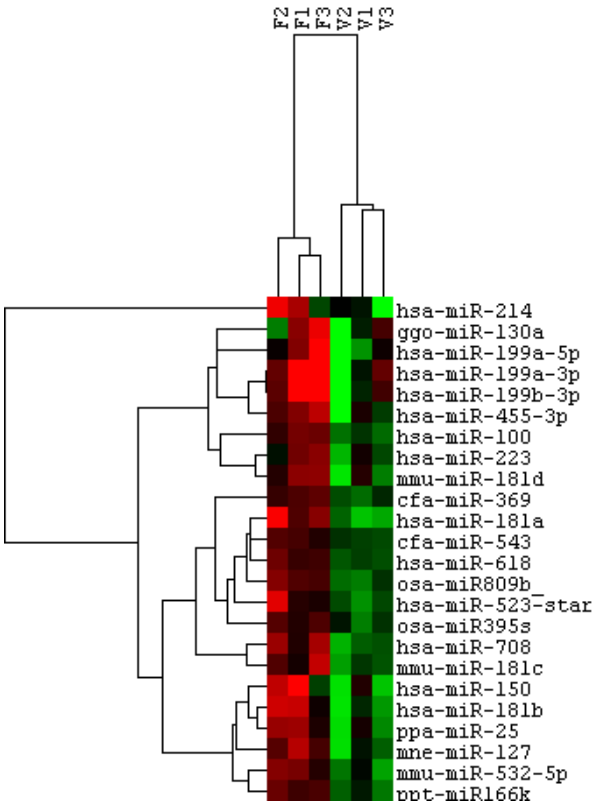

Figure 5.3: Heat Map of Side-specific miRNAs from Porcine AV Endothelium. Through Significance of Microarray Analysis, 24 miRNAs were found to be side-dependent (n=3 pooled samples; FDR < 25%; red=upregulated and green = downregulated; Ferdous and Holliday, unpublished).

Following Significance of Microarray Analysis, selected miRNAs were validated through qPCR based on detection level as well as multiple detections on the array. Figure 5.4 shows the validation of seven miRNAs by qPCR. All miRNAs were confirmed including the miRNA cluster members, miR-214 and miR-199a.

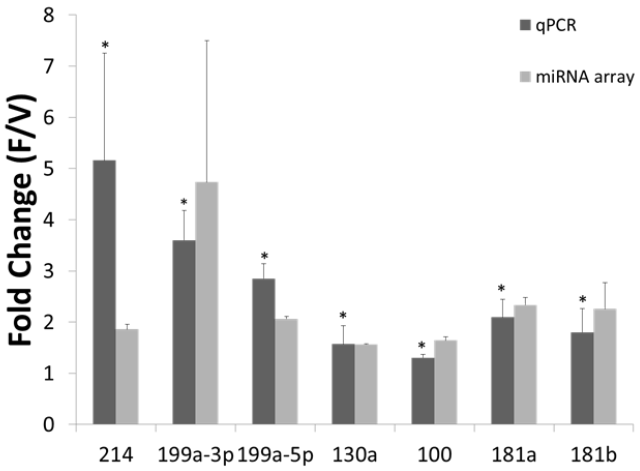

Figure 5.4: miRNA Validation of Side-specific Porcine AV Endothelial Arrays. All seven potentially side-specific miRNAs were validated by qPCR (n=5; Ferdous, unpublished).

Validation of *in vitro*, Shear-responsive microRNAs from HAVEC microRNA Microarray

Holliday, CJ

To validate *in vivo* significance of the shear-sensitive HAVEC miRNAs determined in Aim 2, we performed qPCR with side-specific, endothelial-enriched porcine AV RNA (isolated by Ferdous). Porcine AVs were used instead of human AVs because of availability and absence of disease. Figure 5.5 shows validation of the two *in vitro* shear-dependent miRNAs homologous in porcine.

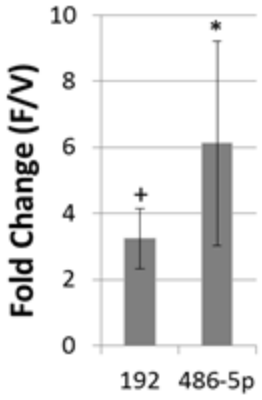

Figure 5.5: Validation of miR-192 and miR-486-5p in Porcine AV Endothelium. qPCR results show an upregulation of miR-486-5p on the fibrosa side (p=0.0347) and a trend of an increase of miR-192 on the fibrosa side (p=0.1233) (n=9 leaflets, ±SEM).

In order to further validate the shear-responsiveness *in vitro* using human AV endothelial cells (Aim 2) or the side-dependency using side-specific porcine AV endothelium (Aim 3), we have devised a protocol for performing *in situ* hybridization on aortic valve leaflets, using both cryosections and whole tissue sections. Previous attempts of *in situ* hybridization on human AV sections provided an unacceptable level of background (data not shown). For this reason as well as the issue of availability, we have performed all *in situ* experiments in porcine aortic valves.

Initial experiments were performed using cryosections. Both probe concentration and hybridization temperature was optimized for RNU6B, a housekeeping miRNA and miR-486-5p, a shear-sensitive miRNA validated in Aim 2 (data not shown). After performing *in situ* hybridization and imaging, images were analyzed using a custom program written by Choon Yap of the Yoganathan lab. This program allows for quantification of staining intensity on the endothelial layer, allowing for an internal comparison within the same section. Figure 5.6 shows representative images of miR-

486-5p, RNU6B, and non-targeting probes on fibrosa and ventricularis sides of porcine AV cryosections.

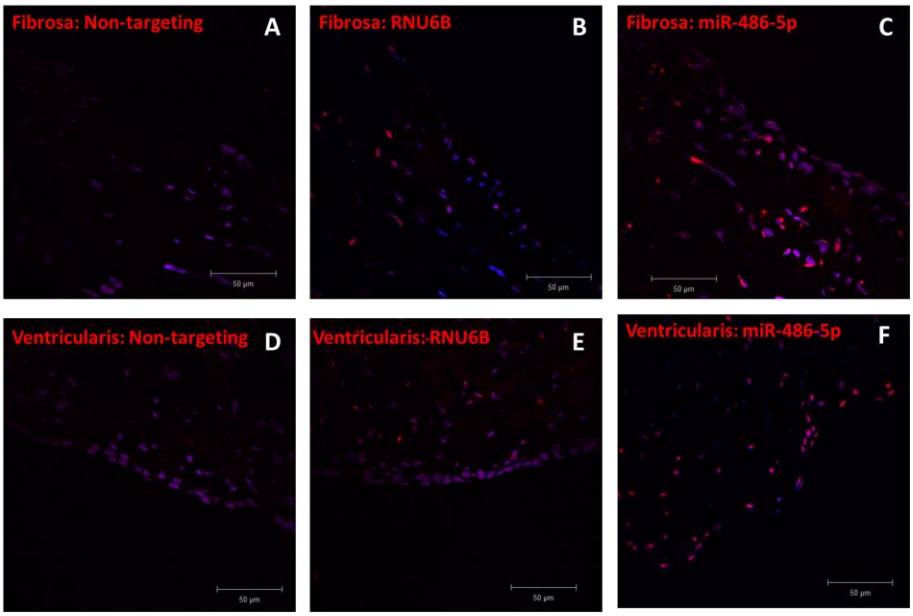

Figure 5.6: Representative *in situ* hybridization Images for miR-486-5p and Controls. (A)-(C) shows representative images for non-targeting, RNU6B, and miR-486-5p probes, respectively, for the fibrosa side of the AV. (D)-(F) show analogous images for the ventricularis side. (n=14 slides from 4 different pigs; red = probe and blue = nuclei; Holliday, unpublished).

Quantification of miR-486-5p staining on the fibrosa and ventricularis sides is shown in Figure 5.7. Due to the small sampling array of endothelium in each section, there is much variation in intensity; however, there is a trend for increased staining on the fibrosa side as compared to the ventricularis side. This is consistent with the qPCR results for miR-486-5p as described above.

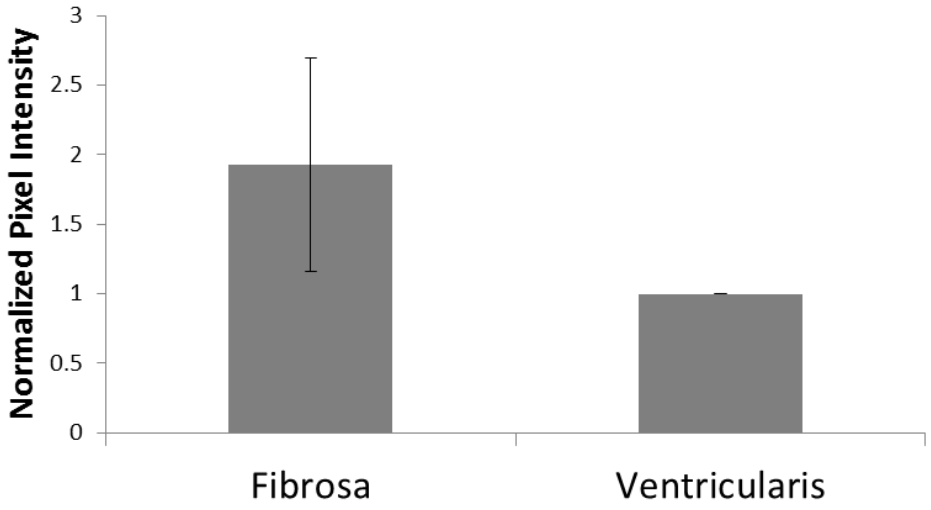

Figure 5.7: Normalized Pixel Intensity for miR-486-5p in Porcine AV Cryosections. Although not statistically significant, there is a trend for increased miR-486-5p on the fibrosa side (p=0.25; n=14 slides from 4 pigs) consistent with the qPCR data from side-specific, porcine AV endothelium (Holliday and Yap, unpublished).

In an effort to increase the sampling of endothelial expression of miR-486-5p, we attempted *en face in situ* hybridization where the entire endothelial layer is stained and both sides of the tissue are imaged. Sample images from *en face* staining are in Figure 5.8. It is important to note that there was some non-specific binding of the TSA-Cy3 on the collagen and elastin fibers which has been reported by others.[104] Initial studies suggest that miR-486-5p is increased on the fibrosa side; however, improved signal detection methods are required for definitive assessment. Future work will explore colorimetric detection methods.

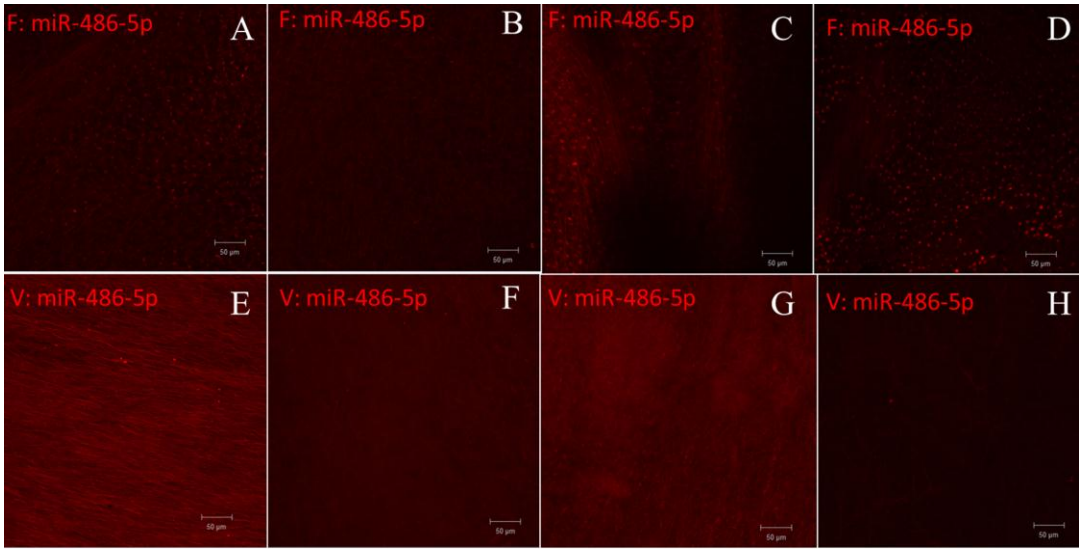

Figure 5.8: *en face, in situ* Hybridization of miR-486-5p in Porcine AV Endothelium. (A)-(D) show representative images of miR-486-5p expression and localization from the fibrosa side and (E)-(H) show representative images from the ventricularis side (n=4 pigs; 2-3 leaflets per pig; Holliday, unpublished).

Categorization of *in vitro*, human, shear-dependent microRNAs and *in vivo*, porcine, side-dependent microRNAs

Holliday, CJ

In order to determine the potential role of the identified shear-dependent (FO vs. VL; Aim 2) or side-dependent (fibrosa vs. ventricularis; Aim 3) miRNAs, similar to the strategy taken in Figure 4.10 with predicted mRNA targets of the *in vitro* miRNAs, we categorized these miRNAs based known cellular functions. The cellular functions focused in this filtering were those known to play a role in tissue remodeling such as migration, proliferation, apoptosis, and cell cycle changes, as well as inflammation and calcification. It is important to note that the functions of these miRNAs have not been studied in endothelial cells but were mostly studied in cancer cells. Also, certain studies highlight miRNA regulation of mRNAs known to play a role in these mentioned cellular functions but did not investigate the miRNA function directly. For our purposes, we

categorized these cases to the associated cellular function as shown in Figure 5.9. Briefly, miR-214 was found to play a role in proliferation,[105, 106] cell death,[107-109] cell cycle,[105] migration,[107, 110] and inflammation.[106, 108, 109] miR-199a played a role in growth,[111] proliferation,[112] apoptosis,[113] cell cycle,[113] migration,[111, 112] inflammation,[109] and calcification (BMP2/SMAD1).[114] miR-100 played a role in cell cycle,[115] apoptosis,[116] and proliferation;[117] whereas, miR-181a played a role in growth,[118] proliferation,[119] calcification (osteopontin),[119] apoptosis,[118, 120, 121] endothelial-to-mesenchymal transition,[122] and cell cycle (p27).[123] Moreover, miR-181b contributes to apoptosis and growth changes as well.[118]

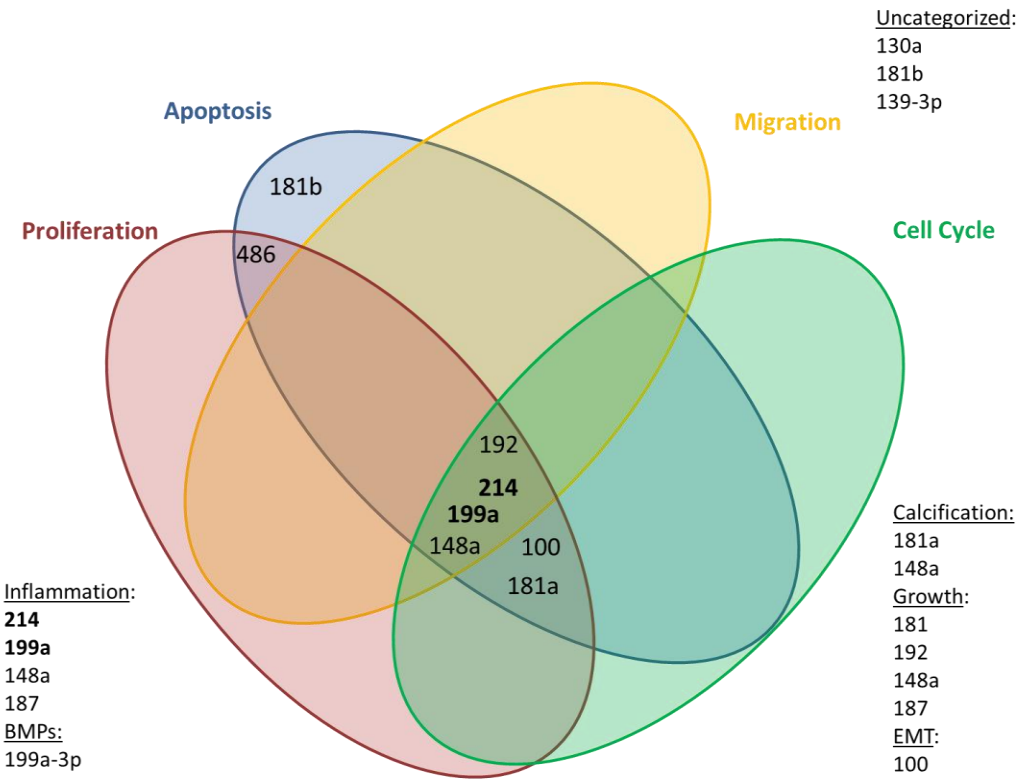

Figure 5.9: Organization of Key Shear-sensitive and Side-dependent miRNAs. Previous studies show that many of the miRNAs highlighted in this study are involved in cellular functions important in heart valve disease (Holliday).

For the *in vitro* studies, we were able to definitively categorize four of the five shear-sensitive miRNAs with the exception of miR-139-3p. A more detailed explanation of what is known about these miRNAs resides in Chapter 3. A brief summary is provided here. Studies have shown that miR-486-5p plays a role in proliferation[124, 125] and apoptosis.[124, 126, 127] miR-187 plays a role in inflammation[79, 80] and growth[81] whereas miR-148a plays a role in migration,[95, 97] apoptosis,[90] proliferation,[95, 96] inflammation,[92, 102] growth,[91] cell cycle,[96] and calcification.[93, 94] Lastly, miR-192 is important in growth (TGFβ),[128] migration,[128, 129] cell cycle,[85, 130, 131] apoptosis,[132] and proliferation.[132] In summary, these miRNAs have a large potential impact of AV disease (especially through tissue remodeling, inflammation, and calcification); however, their importance in heart valve biology and disease has yet to be realized.

Discussion

In this chapter we have discussed 1) isolation of endothelial-enriched, side-specific porcine AV total RNA (both mRNA and miRNA), 2) purity assessment via the following markers: *Pecam1, Sma, Klf2, and vWF,* 3) generation a miRNA array using aforementioned porcine endothelial total RNA to detect 24 side-dependent miRNAs, 4) validation of both porcine, side-dependent (Figure 5.4) and human, shear-responsive miRNAs (Figure 5.5) using qPCR , and 5) initial validation studies using *in situ* hybridization of miR-486-5p.

We were able to successfully isolate side-dependent RNA from porcine aortic valves which expressed endothelial cell markers and very little *Sma*. As described earlier, it may be possible for the source of this *Sma* to be from the endothelial cells

themselves.[4] Previous research has shown that other markers initially that to be absent from endothelial cells such as basic calponin are also found in valvular endothelial cells.[4] Another issue with the isolation technique is the low amount of RNA isolated, requiring only a subsection of the RNA to be assessed for purity before array generation. Moreover, each pooled sample is roughly on the order of tens of nanograms and amplification was required for miRNA microarray generation. For this reason, selected miRNAs will be rigorously validated as well as improved isolation techniques will be explored.

Of the 24 miRNAs detected by the side-specific porcine AV endothelial array, seven were chosen for validation and seven were confirmed. This high validation rate is in contrast to the *in vitro*, shear-responsive miRNAs in HAVECs for several reasons. First, the *in vitro*, shear-responsive miRNAs in HAVECs were detected on the Illumina platform which was subsequently discontinued due to variation in results. Further, the pig population sampled was much tighter in terms of age, health, diet, and gender compared to the human samples. Lastly, the fact that *in vivo* samples have higher amounts of miRNAs than *in vitro* samples per the same unit of total RNA may have improved the results. (Even though we had less miRNA in the pig arrays, the ratio of miRNA to total RNA was higher. After amplification, this ratio could have continued to be higher than the *in vitro* array.) Another interesting observation is that all side-dependent miRNAs detected were higher on the fibrosa side. Further investigation into the epigenetic regulation (potential silencing by methylation) of genes and miRNAs on the fibrosa versus ventricularis sides would be interesting.

Another interesting result is that validation of miR-192 and miR-486-5p in porcine AV endothelium provided opposite results to the array performed on *in vitro* sheared human AV endothelium. We had hypothesized that disturbed flow conditions are present on the fibrosa side and induce disease whereas the ventricularis side remains relatively healthy due to the unidirectional, laminar shear stress. A model supporting this paradigm has recently been published;[41] however, emerging research by Yap, et al suggests different waveform patterns.[42, 43] As these complex waveforms become better understood, we may be better able to interpret this "discrepancy" between *in vivo* and *in vitro* results. Also, further investigation into the spatial differences in shear stress within a leaflet side will be important in interpreting *in vitro* results in an i*n vivo* context. Moreover, complexity present *in vivo* but not accounted for *in vitro* include: additional mechanical forces besides shear stress such as stretch, a complex extracellular matrix, as well as a sophisticated three-dimensional environment. Additional experiments are necessary to understand the aforementioned factors' role in miRNA regulation.

Of the miRNAs validated, several had been studied in other context such as cancer and play an important role in cellular functions also known to be important in AV disease including apoptosis, migration, proliferation, endothelial-to-mesenchymal transition, inflammation, and calcification as discussed above in Figure 5.9. To date, the importance of these miRNAs has not been determined in AV disease and will be the focus of future research. However, from this classification strategy, we have been able to devise a hypothesis as shown below in Figure 5.10. Recent research shows that TWIST1, a transcription factor, has the ability to regulate the miRNA cluster 199a/214. Moreover, it is known that TWIST1 has a role in apoptosis and inflammation, functions both

important in AV disease.[109] Interestingly, we have found both miR-199a and miR-214 to be upregulated on the fibrosa side of porcine AVs. Therefore, we hypothesize that TWIST1 is increased on the fibrosa side of the AV and acts as a master regulator to increase miR-199a2/214 cluster expression and affect changes in a variety of cellular functions involved in AV biology and disease. Further, our results show that miR-199a and miR-214 are increased on the fibrosa side and that much research has implicated these two miRNAs in a variety of cellular functions as described in Figure 5.9. Through collaboration with the Yoganathan lab, we plan to confirm the differential expression of TWIST1 in AV leaflets as well as how miR-199a and miR-214 modulates cellular function *in vitro* and *ex vivo*. Finally, our *in vitro* and *ex vivo* findings will be confirmed *in vivo* using a mouse model of AV disease.

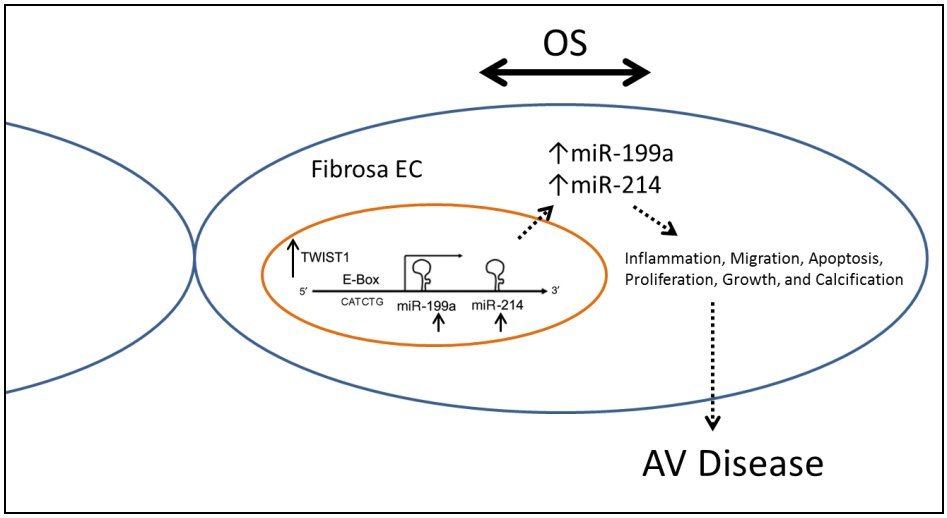

Figure 5.10: A Proposed Mechanism of AV Disease. Modified from Lee, et al.[133]

CHAPTER 6

MODULATION OF MIR-187 AND MIR-486-5P AND INVESTIGATION OF POTENTIAL TARGETS

Summary

We have identified both shear-sensitive miRNAs in HAVECs *in vitro* (miR-139-3p, miR-148a, miR-187, miR-192, and miR-486-5p) as well as side-dependent miRNAs in porcine AV endothelium *in vivo* (miR-100, miR-130a, miR-181a, miR-181b, miR199a-3p, miR-199a-5p, and miR-214). While there has been some work to uncover the function of these miRNAs, their role in AV disease remains unclear. The objectives of this chapter include: 1) determining the optimal seeding and transfection conditions for shear studies, 2) investigating eight potential targets of miR-486-5p, 3) uncovering the role of miR-187 in monocyte adhesion post-shear, and 4) determining the role of miR-486-5p in migration, apoptosis, and the cell cycle. Further we found that two of the eight potential targets of miR-486-5p experienced knockdown after miR-486-5p overexpression (*Efna1* and *Prnd*) and have potential impact in AV disease development in terms of endothelial-to-mesenchymal transition and oxidative stress. Lastly, we found that miR-187 reduces monocyte adhesion under LS when compared to OS transfected with the non-targeting premiR and that miR-486-5p increases migration and potentially decreases the number of early apoptotic cells after shear. Better understanding of these miRNAs will have profound effects of better understanding shear and AV disease.

Introduction

In Aims 2 and 3, we identified both shear-dependent (OS vs. LS) and side-dependent (fibrosa vs. ventricularis) miRNAs *in vitro* using HAVECs and *in vivo* using porcine AV endothelium, respectively. Further, the role of some of these miRNAs has been investigated in other fields. Briefly, OS-induced miR-187 was also found to be increased in thyroid tumors compared to hyperplastic nodules[79] and increased with LPS in the mouse lung.[80] A reduction of miR-187 caused a decrease in cell growth in HeLa cells.[81] This work suggests miR-187's may have a role in promoting tissue remodeling and inflammation in aortic valve disease. Additionally, we found miR-486-5p to be reduced under OS in HAVECs. Another study found that miR-486-5p was decreased in eight types of cancer suggesting that a reduction of miR-486-5p supports tissue remodeling as characterized by increased proliferation,[82] an important component of aortic valve disease. However, it remains unknown the role of these shear-dependent and side-dependent miRNAs in AV disease.

The objective of this chapter is to begin to uncover the role of two identified, shear-dependent miRNAs: miR-187 and miR-486-5p. We will adopt an approach similar to other groups involving gain-of-function and loss-of-function studies in conjunction with a variety of cellular assays.[124] More specifically, the approach is to overexpress these two miRNAs in HAVECs, apply shear (OS vs. LS), and then perform a variety of the following functional assays to determine their potential role in AV disease: monocyte adhesion for inflammation, Caspase-3 and Annexin-V/PI staining for apoptosis, PI staining for cell cycle analysis, and a scratch assay for migration. We will also further

explore inhibition of these miRNAs as well. Future work is required to better understand their function as well as explore the function of the remaining identified miRNAs.

Methods

Optimization of Cell Splitting Ratio for Transfection Studies

In order achieve proper confluency after transfection of either a miRNA precursor (pre-miR) or a miRNA inhibitor (LNA-anti-miR), an optimization study investigating different splitting ratios (one to two, one to three, and one to four) was completed using fHAVECs and vHAVECs (passage five). The adopted experimental scheme is shown in Figure 6.1. HAVECs (passage four) were grown to confluency and then split at one of three aforementioned ratios (n=3-4 for each condition). The following day, HAVECs were transfected with one dose (30nM) of non-targeting pre-miR tagged with FITC for visualization purposes. On day 3, HAVECs were changed to flow media (formulation in Aim 2) and confluency was assessed. On day 4, fluorescent images were taken to determine transfection efficiency.

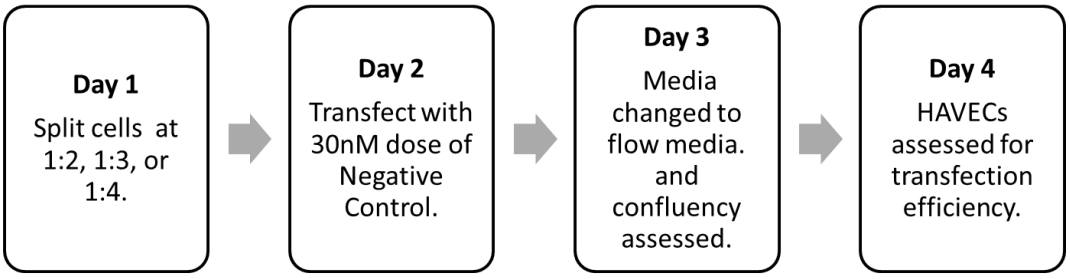

Figure 6.1: Optimization of HAVEC Splitting Ratio Prior to Transfection.

Optimization of microRNA Precursor Overexpression

HAVECs were transfected at three doses of pre-miR (10nM, 30nM, and 100nM; Ambion) with non-targeting pre-miR at the same doses as a control (Ambion; $n_{patient}$=1; $n_{replicates}$ = 3. HAVECs were transfected using Oligofectamine (Invitrogen) according to manufacturer's suggestions one day before shear in 80% confluent HAVECs. A detailed protocol can be found in Appendix J. A similar regime was followed as Figure 6.1 but instead of varying the HAVEC splitting ratio, the dose of the pre-miR was varied. Four different targeting pre-miRs were used corresponding to the validated, shear-dependent miRNAs identified in HAVECs *in vitro*: miR-139-3p, miR-187, miR-192, and miR-486-5p. (Due to the recent discovery of this shear-dependent miRNA, modulation of miR-148a's levels will be performed for future studies.) For this experiment, three wells were used per condition. qPCR (Applied Biosystems) with SYBR green (Stratagene) was used to assess the fold increases of miR-486-5p for dose-dependency (n=3 wells). All samples were normalized to RNU6B.

Optimization of microRNA Inhibition

Similarly to the optimization of the pre-miR, optimization studies were carried out using LNA-anti-miRs at 3 different doses: 10nM, 50nM, and 100nM using the same protocol found in Appendix J ($n_{experimental}$ = 3; $n_{replicates}$ = 3). Also, the same four miRNAs were optimized: miR-139-3p, miR-187, miR-192, and miR-486-5p. Briefly, HAVECs were transfected using Oligofectamine (Invitrogen) according to the manufacturer's specifications one day before shear in 80% confluent cells. qPCR (Applied Biosystems) with SYBR green (Stratagene) was used to assess the fold increases of miR-486-5p for

dose-dependency ($n_{experimental}$ = 3; $n_{replicates}$ = 3; each replicate had 3 technical replicates). All samples were normalized to RNU6B.

Modulation of Potential Targets by microRNA Precursor Overexpression of miR-486-5p

HAVECs were transfected with four doses of pre-miR 486-5p (0.1nM, 1nM, 10nM, and 100nM) to investigate potential targets found in Figure 4.10: *Ak2, Als2cr4 (Tmem237), Camk2n1*, *Ctdspl*, *Efna1*, *Mylk2, Prnd*, and *Rnf41* ($n_{patient}$=1; 3 wells per conditions). More specifically, qPCR (Applied Biosystems) with SYBR green (Stratagene) was run for the aforementioned markers to look for dose-dependent modulation of predicted targets of miR-486-5p. All samples were normalized internally to 18S and then compared to their respective non-targeting control. After analyzing preliminary results, two additional targets, *Efna1* and *Prnd*, were investigated in multiple patients (n=4) at one overexpression level, 10nM.

Monocyte Adhesion Analysis after Overexpression of miR-187

Because of miR-187's role in inflammation,[80] we investigated monocyte adhesion in HAVECs overexpressing miR-187 ($n_{patients}$=3; each endpoint has 2-4 dishes with 8 pictures per dish). Further, because of the known conserved similarities between fHAVECs and vHAVECs described in Aim 2, this preliminary study was conducted in only vHAVECs. vHAVECs were transfected with 30nM miR-187 pre-miR and sheared for 24h (LS: 20dynes/cm^2 and OS: ±5 dynes/cm^2). (It is also important to note that in all future shear experiments that 5% hyskon was used to reduce the revolutions per minute while maintaining adequate shear levels.) This change decreased the amount of heat

generated in the incubator. qPCR was performed to confirm overexpression in samples as compared to non-targeting controls. After shear, vHAVECs were incubated with 6 BCECF-AM fluorescently-labeled monocytes for 30min. Unbound monocytes were gently rinsed away. Cells were then fixed and imaged. Eight images were taken per dish and monocytes were counted. Comparisons were made among the four groups: 1) vHAVECs overexpressing miR-187 exposed to OS, 2) vHAVECs overexpressing miR-187 exposed to LS, 3) vHAVECs with non-targeting pre-miR exposed to OS, and 4) vHAVECs with non-targeting pre-miRs exposed to LS. A two-way ANOVA was used to assess for differences between shear condition and overexpression of miR-187. A more detailed protocol for monocyte adhesion may be found in Appendix K.

Cellular Function Analysis after Overexpression of miR-486-5p

From the previous study, we determined that a dose of 10nM miR-486-5p pre-miR was optimal. We then followed the same experimental regime as set forth earlier. Briefly, we adopted our hypothesized most physiological shear stress conditions where fHAVECs are exposed to OS (FO) and vHAVECs are exposed to LS (VL). We overexpressed miR-486-5p one day before shear in 80% confluent HAVECs. We then sheared for 24h and performed the three different functional assays: a wound healing assay for migration, caspase-3 and Annexin-V/PI staining for apoptosis, and PI staining after RNA digestion for cell cycle analysis. Overexpression was confirmed in all samples. Unlike the monocyte adhesion assay above to determine miR-187's role using only vHAVECs, we used both fHAVECs and vHAVECs in all studies with miR-486-5p.

Migration

After shear, four scratches were made on each 10cm dish and imaged at 0h. At 4h ($n_{patients}$ = 3) and 8h ($n_{patients}$ = 2), we retook the pictures. Analysis was performed by determining the area of the wound using ImageJ. The results were displayed as percentage of the original wound. A two-way ANOVA was used to determine if there were any statistically significant differences in shear and overexpression of miR-486-5p.

Apoptosis

Two different apoptosis assays were used to assess miR-486-5p's role: Caspase-3 assay (early apoptosis) and the Annexin-V/PI staining (early and later apoptosis). For the Caspase-3 assay, a kit from BD Pharmingen was used. fHAVECs under OS and vHAVECs under LS were sheared for 24h. The cell lysate was collected and incubated with a substrate of Caspase-3, Ac-DEVD-AMC. Caspase-3 acts to release the fluorescent AMC which is detected by a fluorescent plate reader. The more Caspase-3 in the sample, the more it will fluoresce. The appropriate controls were used for comparison and normalization (negative controls = no cell lysate or no substrate). Also, a protein assay (BCA; Pierce) was used to normalize Caspase-3 activity to total protein. Differences in shear condition and miR-486-5p overexpression were investigated using a two-way ANOVA. Further, Caspase-3 activity was assessed in four different patients (2-3 dishes per condition per patient).

The Annexin-V/PI staining for apoptosis is a flow cytometry-based assay which allows for detection of four different populations: 1) live cells, 2) cells undergoing early apoptosis, 3) cells undergoing late apoptosis, and 4) necrotic cells. Annexin-V detects

phosphatidylserine only available when the cell membrane begins to lose its integrity, a hallmark of apoptosis. Further, as the cells undergo late apoptosis and necrosis, the nuclear membrane is damaged allowing propidium iodide (PI) staining. With identical conditions as the previous Caspase-3 assay, miR-486-5p was overexpressed in HAVECs and HAVECs were sheared. Following shear, HAVECs were trypsinized into a single cell suspension. Half of the cells were reserved for the cell cycle analysis. A detailed protocol of this procedure may be found in Appendix L but briefly, 5µL or 1 test of Annexin-V solution was added to 500 µL of Annexin-V Binding Buffer. HAVECs were incubated for 15min at room temperature. After washing, HAVECs were incubated with PI and the samples were run on the flow cytometer (BD LSR II). For single color controls, one dish of HAVECs were incubated with 1µM staurosporin, an apoptosis-inducing agent, as a positive control for Annexin-V-APC and heat-killed cells incubated with only PI served as the PI or FITC control. Non-staining HAVECs acted as a negative control and the quadrant gate was set to this sample. The percentage of cells in each quadrant was then used to compare between groups using a two-way ANOVA ($n_{patients}$=2; 2-3 dishes per condition).

Cell Cycle

Using the remaining half of the samples from the Annexin-V/PI staining, cell cycle analysis was completed. The detailed protocol can be found in Appendix L but briefly, HAVECs were treated concurrently with 200µL of 2mg/mL RNAse solution and 200 µL of 40µg/mL PI staining solution in order to remove all RNA and stain the DNA for 30min. Immediately following, samples were run on the flow cytometer (BD LSR II;

$n_{patients}$=3; 2-3 dishes per condition). First, the HAVEC population was gated to remove debris and aggregates and then the cell cycle model (Dean-Jett-Fox) was used to fit the data in FlowJo. Percentages of the G0/G1 (quiescent/growth phases, 1 set of DNA), S (DNA replication), and G2/M (mitotic phase, 2 sets of DNA) were gathered. Statistical differences G0/G1, S, and G2/M were investigated using a two-way ANOVA comparing overexpression of miR-486-5p and shear condition.

Results

Optimization of Cell Splitting Ratio for Transfection Studies

Briefly, the HAVEC splitting ratio was optimized using the following three ratios: one to two (1:2), one to three (1:3), and one to four (1:4). Figure 6.2 shows the confluency of HAVECs prior to shear period on day 3. Cultures split both 1:3 and 1:2 were confluent at the time shear would commence. Figure 6.3 show confluency as well as the transfection efficiency on day 4. From this optimization study, it was determined that the optimal splitting ratio was 1:3 and that most of the HAVECs in culture express pre-miR-FITC by day 4 (or the end of the proposed study).

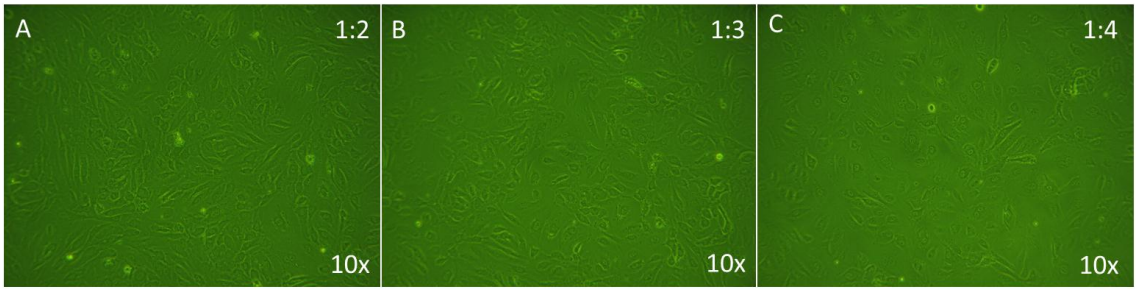

Figure 6.2: Confluency before Shear. (A) shows the confluency before the shear period of cells split 1:2 24h. (B) and (C) show 1:3 and 1:4 splits (n=3-4 each).

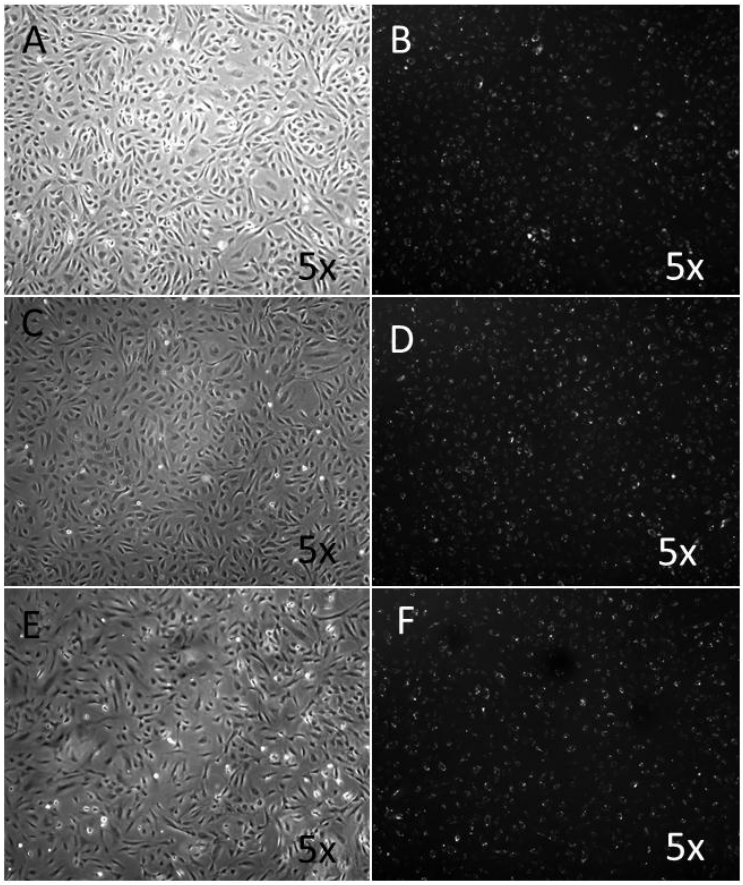

Figure 6.3: Transfection Efficiency after Shear Period. (A), (C), and (E) show the confluency of HAVECs on day 4; whereas, (B), (D), and (F) show the transfection efficiency of pre-miR-FITC on day 4 (n=3).

Optimization of microRNA Precursor Overexpression

Briefly, HAVECs were transfected with three doses of pre-miR: 10nM, 30nM, and 100nM (n=3) corresponding to four of the five validated, shear-responsive miRNAs identified *in vitro* in HAVECs compared to the non-targeting control. (miR-148a will be investigated in the future.) Generally doses of 10nM, 30nM, and 100nM yielded overexpression in the range of 10s, 100-1000s, and 10000s respectively. In an effort to adequately overexpress each miRNA without becoming physiologically irrelevant, we

selected the 30nM dose for miR-187 and the 10nM dose for miR-486-5p. It was our aim to overexpress around 100-1000 fold higher than the endogenous level.

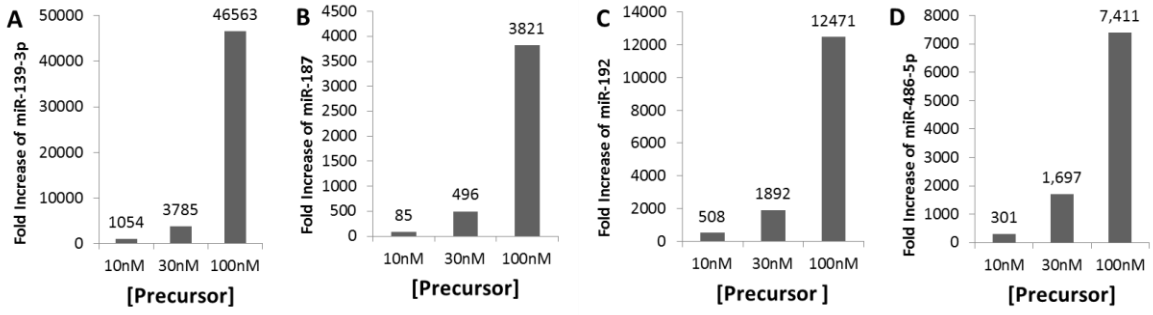

Figure 6.4: pre-miR Optimization Test. (A)-(D) shows dose optimization of miR-139-3p, miR-187, miR-192, and miR-486-5p respectively. The fold change compared to the corresponding non-targeting control is above each bar ($n_{experimental} = 1$; $n_{replicates} = 3$).

Optimization of microRNA Inhibition

Similarly to the pre-miR optimization study, three doses (10nM, 50nM, and 100nM) were used to access LNA-anti-miR inhibition of miR-139-3p, miR-187, miR-192, and miR-486-5p. However, results show that there was unreliable inhibition most likely, due to low basal levels of these miRNAs. It is interesting to note that LNA-anti-miR for miR-192 seems to have silenced the miRNA in each dosage but not in a dose-dependent manner. Further experiments using higher doses (200nM-400nM) are currently underway.

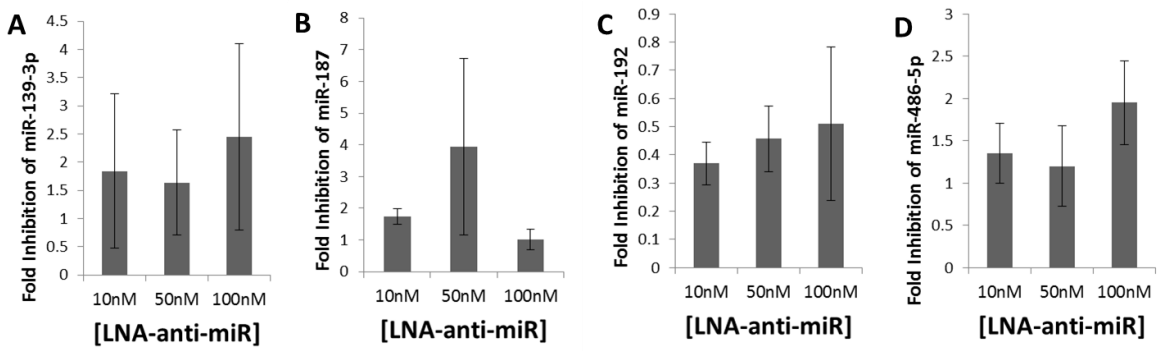

Figure 6.5: LNA-anti-miR Optimization Studies. (A)-(D) show the results of the inhibition study of miR-139-3p, miR-187, miR-192, and miR-486-5p ($n_{experimental}$ =3 and $n_{replicates}$ = 3).

Modulation of Potential Targets by microRNA Precursor Overexpression of miR-486-5p

A preliminary study using fHAVECs transfected with four doses of pre-miR 486-5p (0.1nM, 1nM, 10nM, and 100nM) was used to investigate potential targets found in Figure 4.10: *Ak2*, *Als2cr4 (Tmem237)*, *Camk2n1*, *Ctdspl*, *Efna1*, *Mylk2*, *Prnd*, and *Rnf41* ($n_{patient}$=1; $n_{replicates}$ = 3 wells; technical replicates of each replicate =3). Figure 6.6 confirms overexpression of the miR-486-5p in the samples used for potential target investigation. Figure 6.7 shows the fold change of each gene compared between miR-486-5p overexpressing samples and non-targeting samples. Results highlight two interesting potential targets that required further investigation: *Prnd* and *Efna1*. In both of these cases, three out of four of the doses of the miR-486-5p precursor showed a trend to reduce *Prnd* and *Efna1* expression.

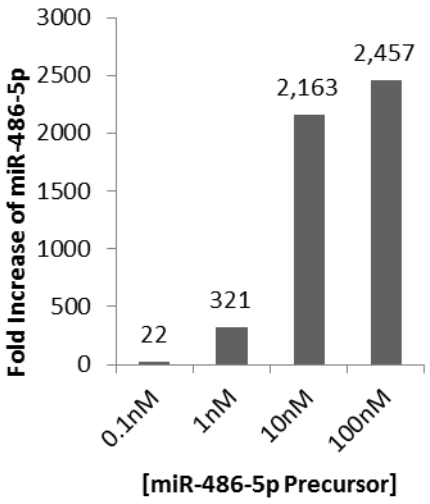

Figure 6.6: Confirmation of miR-486-5p Overexpression. fHAVECs transfected with four doses of miR-486-5p precursor showed overexpression of miR-486-5p ($n_{patient}$=1; $n_{replicates}$ = 3; technical replicates of each replicate =3).

Figure 6.8 shows an expanded investigation of the two best potential targets of miR-486-5p: *Prnd* and *Efna1*. Figure 6.8A shows the *Efna1* expression in fHAVECs (n=4) and vHAVECs (n=4) after overexpression of miR-486-5p (10nM) graphed individually. miR-486-5p overexpression was confirmed in all samples and not shown. When averaged together (Figure 6.8B), there is a small but statistically significant (p=0.0399) decrease in *Efna1* expression after miR-486-5p overexpression. Figure 6.8C shows the *Prnd* expression in fHAVECs (n=4) and vHAVECs (n=4) overexpressing miR-486-5p (10nM) graphed individually. When the fHAVECs and vHAVECs are pooled by side, there is a trend of *Prnd* reduction after miR-486-5p overexpression in fHAVECs shown in Figure 6.8D. A dual luciferase assay with the 3' UTR of each target is necessary to confirm the interaction between miR-486-5p and *Enfa1* and *Prnd*.

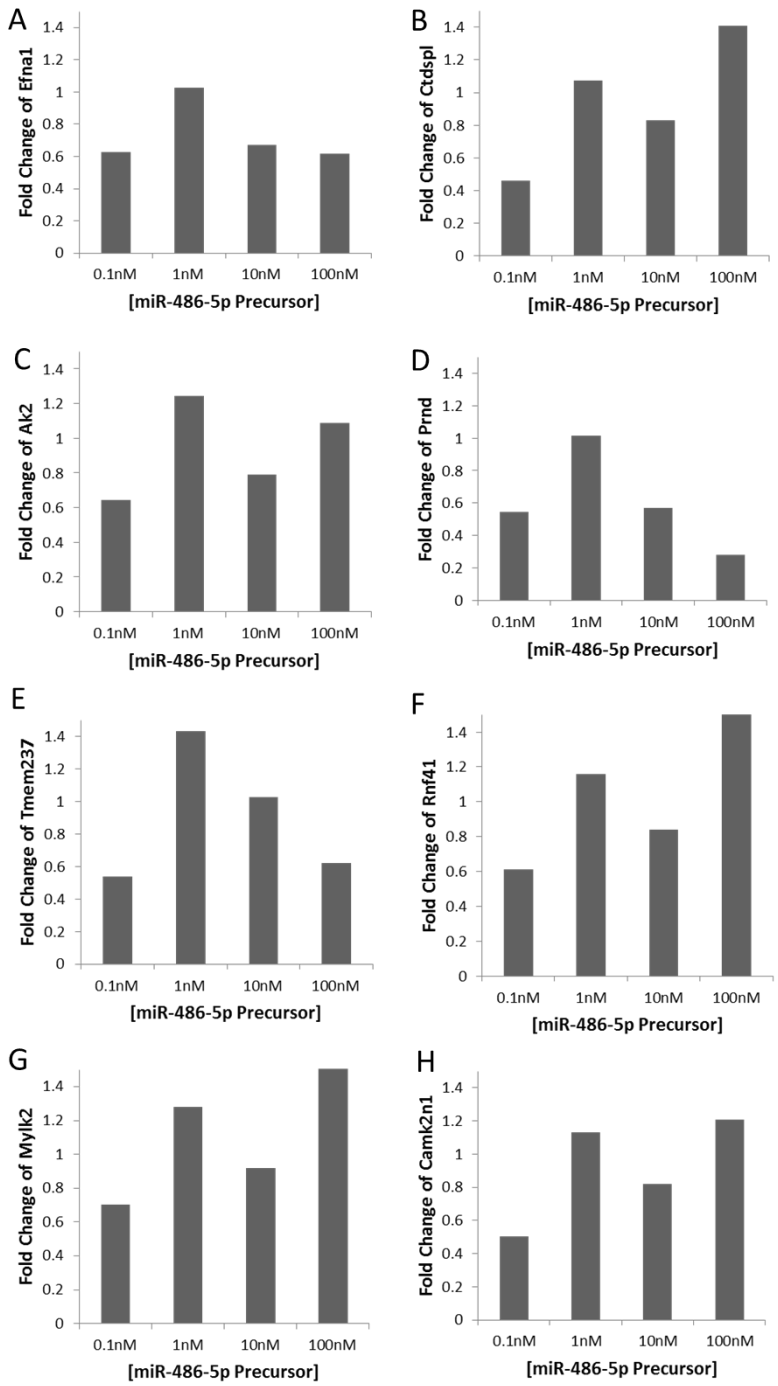

Figure 6.7: Preliminary Study of miR-486-5p's Potential Targets. (A)-(H) show gene expression levels in fHAVECs overexpressing miR-486-5p as compared to the fHAVECs with the same dose of non-targeting control. (A) and (D) show the most promise as three out of four are decreased ($n_{patient}$=1; $n_{replicates}$ = 3; technical replicates of each replicate =3).

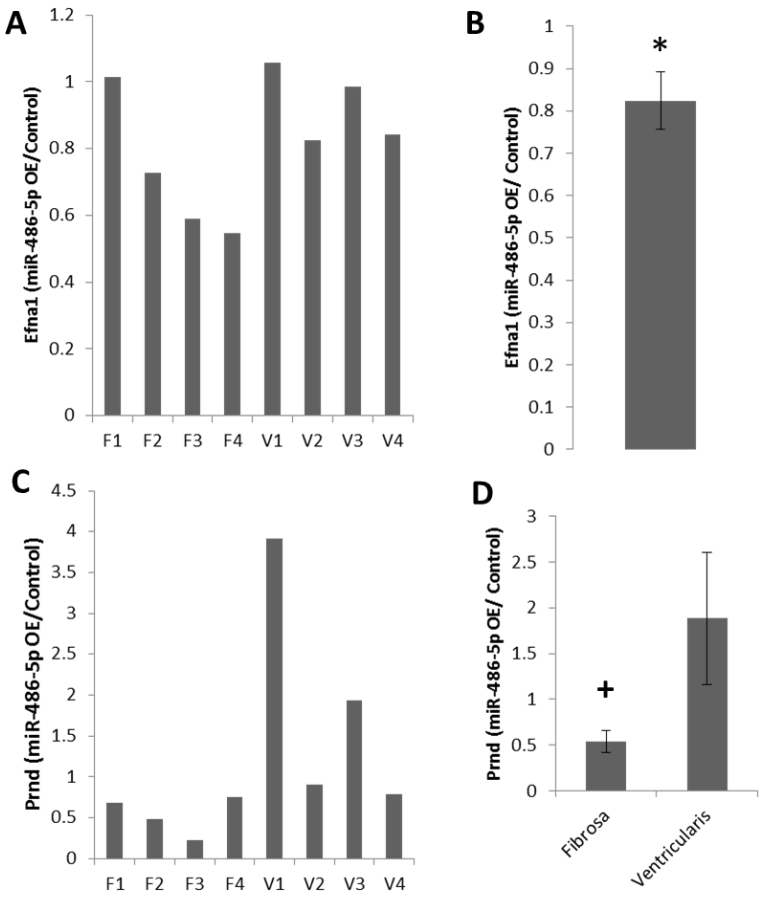

Figure 6.8: Investigation of Two Potential Targets of miR-486-5p. (A) shows *Efna1* expression after miR-486-5p overexpression (10nM) in fHAVECs and vHAVECs graphed individually. (B) shows a significant reduction in *Efna1* expression after miR-486-5p overexpression with the same samples are pooled (n=4; ±SEM). (C) and (D) are analogous graphs for *Prnd1* except that in (D) HAVECs are pooled by sides (n=4; ±SEM).

Monocyte Adhesion Analysis after Overexpression of miR-187

As mentioned above, vHAVECs were transfected with miR-187, sheared under OS and LS, and then a monocyte adhesion test was performed. qPCR showed that miR-187 was overexpressed in all experiments similarly to Figure 6.4 (data not shown). Figure 6.9 shows the monocyte adhesion results from three different patients. In the vHAVECs expressing the non-targeting pre-miR, we see the characteristic increase in

monocyte adhesion in OS as seen previously by the Jo Lab (1.5-1.8 OS/LS). With miR-187 overexpression, the magnitude of OS and LS appears to decrease compared to the negative controls under OS and LS. After statistical testing, we found that there is a statistically significant difference between vHAVECs under OS expressing the non-targeting control and vHAVECs under LS expressing miR-187. From these results, it appears that overexpression of miR-187 may decrease monocyte adhesion which is contrary to our hypothesis formed on the basis that miR-187 has been shown to be pro-inflammatory.

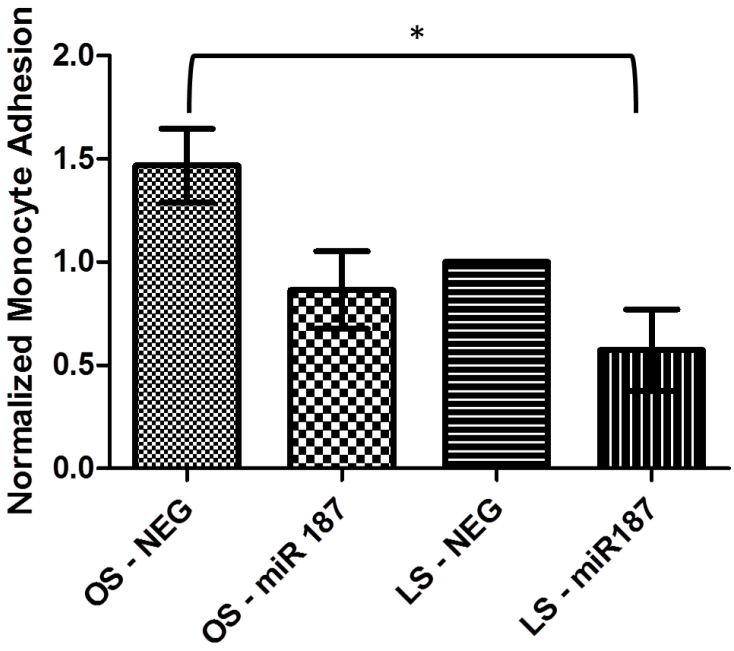

Figure 6.9: Monocyte Adhesion after miR-187 Overexpression in HAVECs. The leftmost two bars are vHAVECs expressing the non-targeting and miR-187 pre-miR under OS respectively. The rightmost two bars show the analogous graphs for vHAVECs under LS. ($n_{patients}$ =3; 2-3 dishes per condition per patient; 8 images per dish; * = $p<0.05$).

Cellular Function Analysis after Overexpression of miR-486-5p

Migration

Briefly, HAVECs were sheared and a scratch assay was performed. Images were taken at 0h, 4h, and 8h. As expected, HAVECs exposed to OS (FO) closed the wound faster than those exposed to LS (VL) as seen in Figure 6.10 ($p=0.0043$; $n_{patients} = 3$). Further, the results at 4h show that there is a slight but statistically significant increase in wound healing in samples overexpressing miR-486-5p ($p=0.0447$; $n_{patients} = 3$). At 8h, there is no longer a statistically significant differences due to shear ($p=0.0990$; $n_{patients} = 2$) or overexpression ($p=0.0820$; $n_{patients} = 2$); however, there is still a trend similar to that seen at 4h. Figure 6.11 shows representative images of the comparison between samples overexpressing miR-486-5p and those with the non-targeting control as well as quantitation of these results at both the 4h and 8h time points.

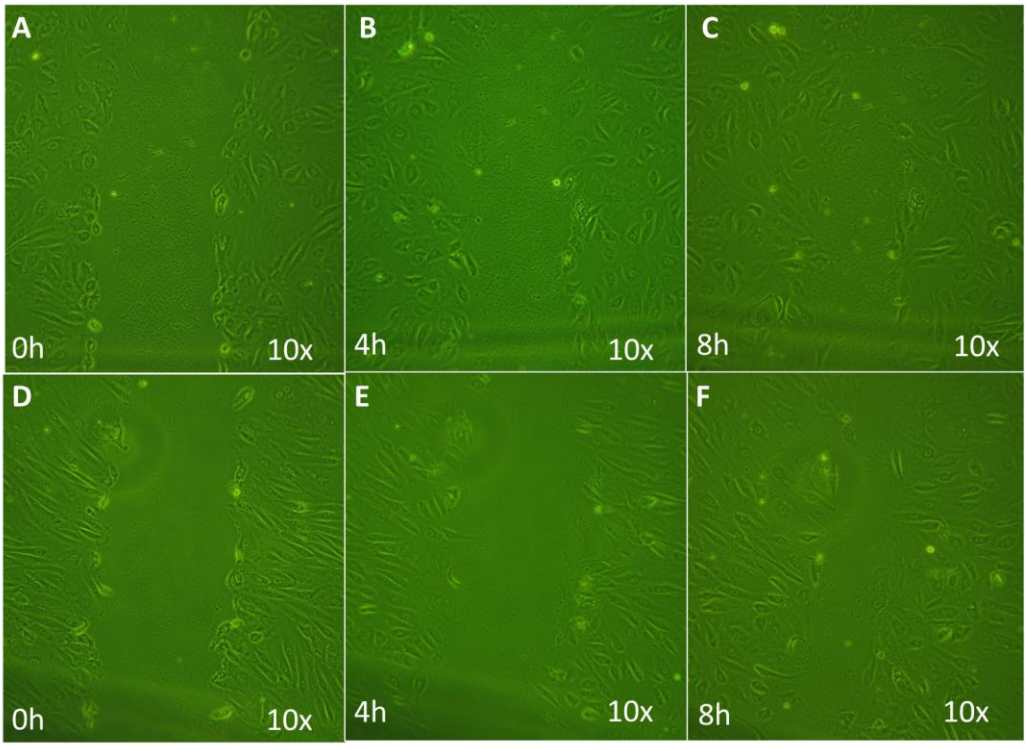

Figure 6.10: Wound Healing in HAVECs. The above pictures show a scratch assay in both fHAVECs exposed to OS (A-C) and vHAVECs exposed to LS (D-F) at 0h, 4h, and 8h post-scratch ($n_{patients}$=2-3; 2-3 dishes, 4 scratches per dish). HAVECs are overexpressing the non-targeting control.

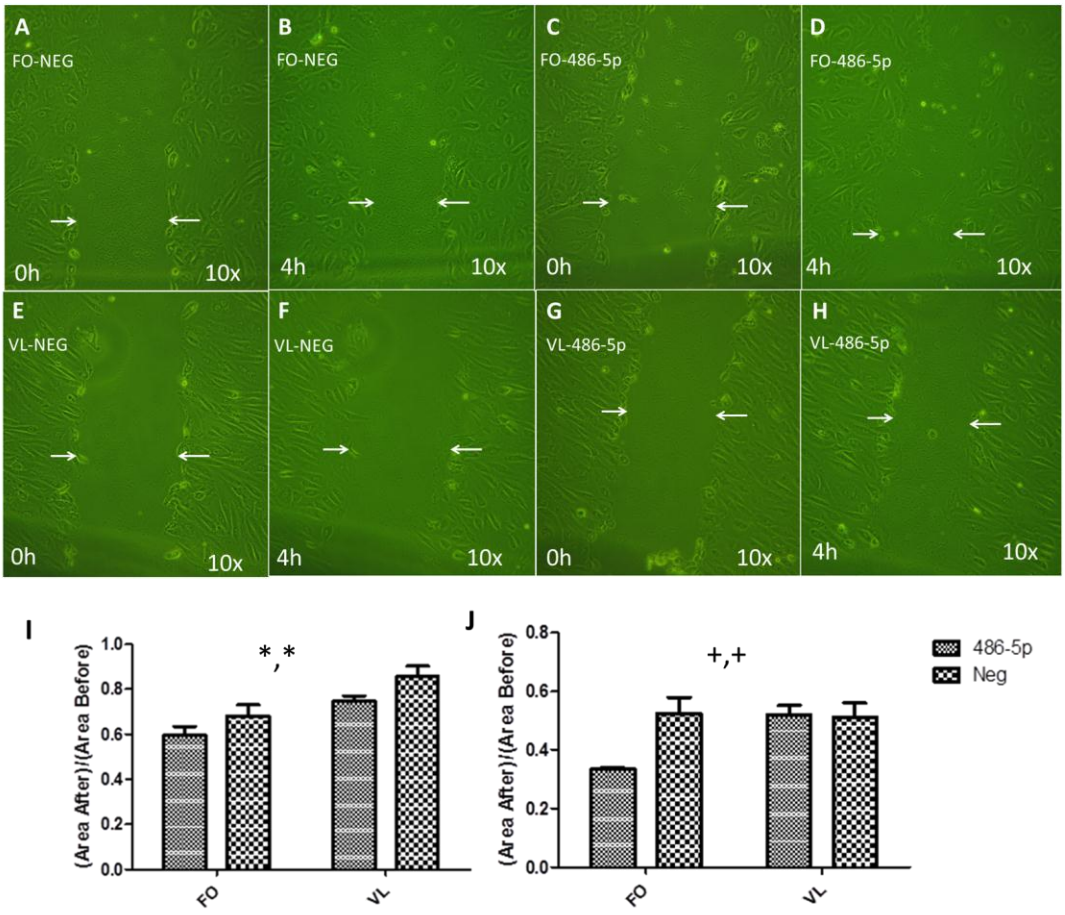

Figure 6.11: Comparison between miR-486-5p Samples and Non-targeting Control. (A-D) represent fHAVECs exposed to OS both overexpressing non-targeting (A-B) and miR-486-5p (C-D) precursors at 0h and 4h. (E-H) show analogous pictures for vHAVECs exposed to LS ($n_{patients}$=2-3; 2-3 dishes, 4 scratches per dish; FO =fHAVECs exposed to OS and VL = vHAVECs exposed to LS). (I) shows a slight but statistically significant increase in wound healing in samples overexpressing miR-486-5p as compared to control (* = p=0.0447) as well as a statistically significant increase in wound healing in OS vs. LS (* = p=0.0043). (J) shows a similar trend at 8h but is not statistically significant for either variable (+ = p_{shear}=0.0990 and + = $p_{overexpression}$=0.0820; FO =fHAVECs exposed to OS and VL = vHAVECs exposed to LS).

Apoptosis

Briefly, two different assays were used to assess apoptosis in HAVECs overexpressing miR-486-5p as compared to their non-targeting controls: Caspase-3 and Annexin-V/PI staining. As anticipated, LS decreases Caspase-3 activity when compared to OS ($p=0.0027$; $n_{patients}=4$) as shown in Figure 6.12; however, there was no statistically significant difference between samples overexpressing miR-486-5p and non-targeting precursors ($p=0.1736$; $n_{patients}=4$).

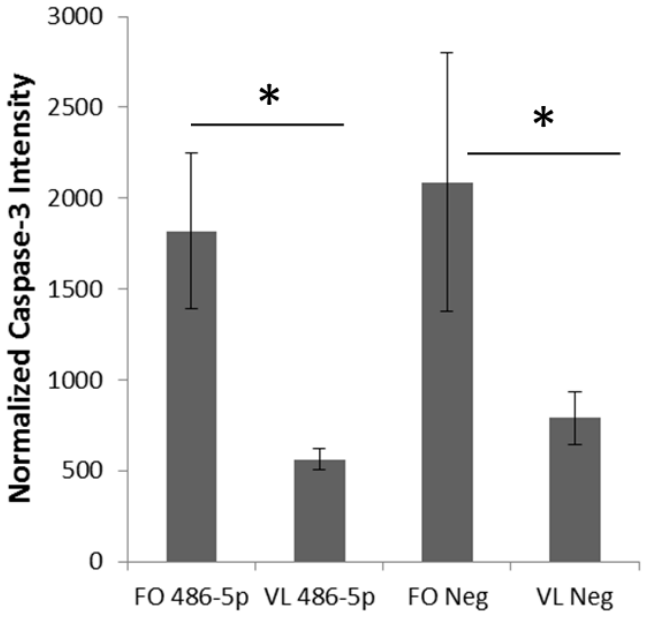

Figure 6.12: Caspase-3 Activity after miR-486-5p Overexpression and Shear. The leftmost portion of the graph shows normalized Caspase-3 intensity of HAVECs overexpressing miR-486-5p after shear. The rightmost portion shows HAVECs under the same shear conditions but overexpressing the non-targeting control ($p_{shear}=0.0027$ and $p_{overexpression}=0.1736$; $n_{patients}=4$).

According to the Annexin-V/PI staining, there are no statistically significant differences in shear or overexpression state of miR-486-5p; however, there is a trend for

decrease in early apoptotic HAVECs in both fHAVECs under OS (FO) and vHAVECs under LS (VL) as seen in representative graphs and quantitation in Figure 6.13. Further experiments are required to increase the endpoint ($n_{patients}$=2).

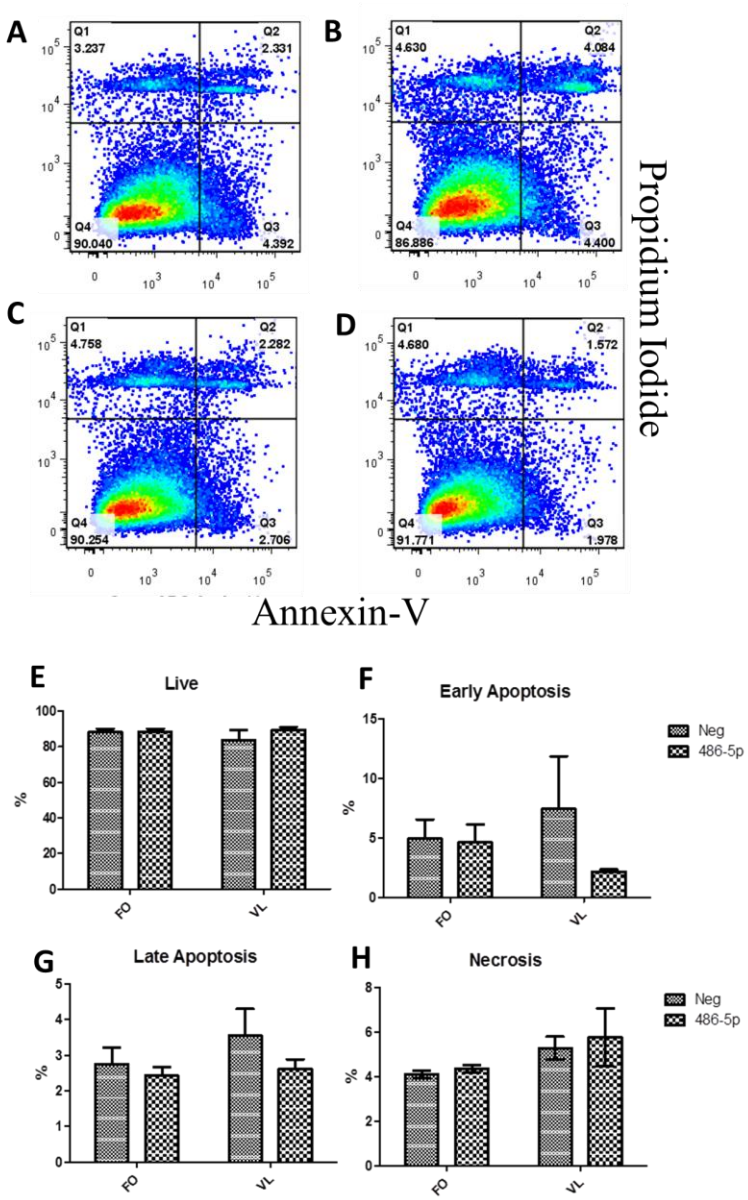

Figure 6.13: Apoptosis and Necrosis Analysis in HAVECs after Shear and miR-486-5p Overexpression. (A) shows fHAVECs overexpressing the non-targeting pre-miR exposed to OS and (B) shows vHAVECs overexpressing the non-targeting pre-miR exposed to LS. (C) shows fHAVECs overexpressing miR-486-5p exposed to OS, and

(D) shows vHAVECs overexpressing miR-486-5p exposed to LS ($n_{patients}$ = 2; 2-4 dishes per condition per patient; Q1 = necrosis, Q2 = late apoptosis, Q3 = early apoptosis, and Q4 = live cells). (E) shows the percentage of live cells (Annexin-V - and PI -), (F) shows the percentage of HAVECs undergoing early apoptosis (Annexin-V + and PI -), (G) shows the percentage of HAVECs undergoing late apoptosis (Annexin-V + and PI +), and (H) shows the percentage of HAVECs undergoing necrosis (Annexin-V – and PI +). After two-way ANOVA, there are no statistical differences between shear and overexpression (FO = fHAVECs exposed to OS and VL = vHAVECs exposed to LS; Neg = non-targeting premiR and 486-5p = miR-486-5p premiR).

Cell Cycle

Briefly, HAVECs overexpressing either miR-486-5p or non-targeting premiRs were sheared for 24h and collected for cell cycle analysis. The cell cycle model Dean-Jett-Fox was applied and percentages of G0/G1, S, and G2/M were determined. Representative histograms of the four groups are shown in Figure 6.14A-D: FO with non-targeting premiR (FO-NEG), FO with miR-486-5p premiR (FO-486-5p), VL with non-targeting premiR (VL-NEG), and VL with miR-486-5p premiR (VL-486-5p). There are no statistically significant differences in terms of overexpression or shear according to the two-way ANOVA ($n_{patients}$ = 3) as shown in Figure 6.14E.

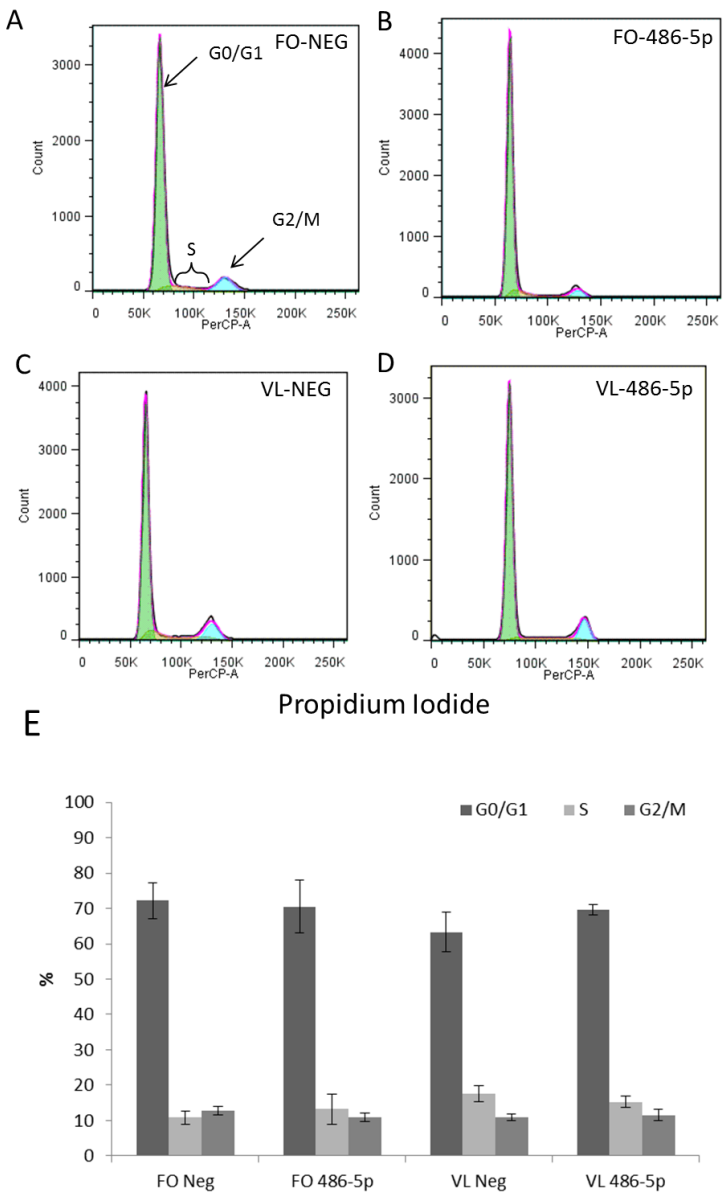

Figure 6.14: miR-486-5p Overexpression, Shear, and the Cell Cycle. (A-D) show the following groups: fHAVECs exposed to OS (FO) with the non-targeting premiR (NEG), FO with miR-486-5p premiR (486-5p), vHAVECs exposed to LS (VL) with NEG, and VL with 486-5p ($n_{patients}$ =3). (E) The above bar graph shows percentages of G0/G1, S, and G2/M for the following groups: fHAVECs exposed to OS (FO) with the non-targeting premiR (Neg), FO with miR-486-5p premiR (486-5p), vHAVECs exposed to LS (VL) with Neg, and VL with 486-5p ($n_{patients}$ =3).

Discussion

In this chapter, we have performed the following tasks in an effort to better understand the role of miR-187 and miR-486-5p in AV disease: 1) optimized the shear experiment with miRNA level modulation (both splitting ratio and concentration of premiRs and LNA-anti-miRs), 2) investigated two potential targets of miR-486-5p (*Efna1* and *Prnd1*), 3) assessed monocyte adhesion after shear and overexpression of OS-induced miR-187, and 4) investigated three cellular functions (migration, apoptosis, and cell cycle) in HAVECs overexpressing miR-486-5p.

In these experiments, we used the following shear strategy: split the cells 48h before shear, transfected 24h before shear, sheared for 24h, and then performed a variety of cellular functions. Optimization of ratio splitting showed that HAVECs should be split one to three instead of one to four as done in previous studies. This suggests that the transfection may cause cell death and that this phenomenon could be exasperated by the transfected material. In this case, certain pre-miRs could affect cell growth. These changes are controlled by including a non-targeting pre-miR or LNA-anti-miR. Further, we found that the optimal overexpression conditions for miR-187 and miR-486-5p were 30nM and 10nM respectively. We chose these conditions based on the concentrations that would cause roughly 1000-fold increases; however, further investigation (assessing cellular function at various doses) is required to ensure that these levels do not cause various feedback loops or responses based on concentration. Further, results contradictory to our hypothesis may be explained by the selected dose.

miRNA inhibition studies with LNA-anti-miR were insufficient to select the optimal dose. In most cases, we did not see reliable, dose-dependent inhibition of

miRNAs with the partial exception of miR-192. One potential explanation could be that *in vitro* miRNA expression levels are already low and the aim to further decrease these miRNA levels is problematic. Further, it is also possible that miR-192 LNA-anti-miR is a more efficient probe than the others investigated since the basal levels of all miRNAs investigated are similar. In the future, we will transfect HAVECs at higher doses (200nM-400nM) proven to be effective in other arenas. Furthermore, we will increase the amount of RNA assessed by qPCR in an effort to cause signal detection above the noise level. Lastly, future experiments should be completed in tissue where the endogenous levels of the identified miRNAs are much higher. Lastly, optimization of the recently discovered shear-responsive miR-148a should be completed. miR-148a's potential targets include members of the bone morphogenic protein (BMP) pathway, *Bmpr2* and *Smad5;* a handful of transcription factors, *Ets1* and *Id1*; *Ctsl* which is known to play a role in atherosclerosis, as well as *Cd276* which has a role in calcification.

Through filtering methods described in Figure 4.10, we were able to identify eight potential targets of miR-486-5p. Two of these eight targets showed some inhibition in samples overexpressing miR-486-5p: *Efna1* and *Prnd*. The additional six targets will be explored in additional patients but it is important to note that targets are predicted by miRWalk based on sequence alone. miRNAs do not have a one-to-one relationship, meaning one miRNA does not bind to one mRNA. Because of these complex interactions, there are many false positives with this approach. Further investigation, including a luciferase assay, is required to confirm the relationship between miR-486-5p and *Efna1* and *Prnd*; however, these two targets could play an important role in AV disease. First, through Ingenuity Pathway Analysis, both *Efna1* and *Prnd* were found to

play important roles in various cellular functions associated with AV disease. Categorization of these cellular functions may be found in Figure 4.11. *Prnd* is related to cell movement; whereas, *Efna1* is known to play a role in cell movement, cell growth and proliferation, and apoptosis. Further, *Efna1* is upregulated in cancers, similar to the upregulation of *Efna1* in OS.[134] Through our initial cellular function studies described in this chapter, we were able to note a statistically significant change in cell movement ($p=0.0447$) and a trend for change in apoptosis when HAVECs overexpressed miR-486-5p, the potential regulator of these targets. Moreover, one study shows that if *Enfa1* or Ephrin-A1 is overexpressed in development that endothelial-to-mesenchymal transition (EMT) is inhibited.[135] EMT is known to replenish the valvular interstitial cells and is normal, reparative and developmental process.[136] We hypothesize that OS-diminished miR-486-5p would cause an increase in *Efna1* leading to an inhibition of EMT and eventually contribute to AV disease onset. Further experimentation is required to investigate this hypothesis. Research has also shown that prion protein (or *Prnd*) plays a role similar to superoxide dismutase[137] and is seen to be upregulated in cardiac hypertrophy. Similar to what is hypothesized in cardiac hypertrophy,[138] *Prnd* could be increased through a miR-486-5p-dependent mechanism in response to oxidative stress involved in AV disease initiation/progression and act as a compensatory, protective response. Further investigation into the relationship between miR-486-5p, *Prnd*, shear stress's regulation of oxidative stress, as well as AV disease is warranted. Undoubtedly, these two potential targets of miR-486-5p could have impact in AV disease. Additional potential targets of miR-486-5p will be investigated through microarray or proteomic analysis with HAVECs stably overexpressing miR-486-5p.

Also in this chapter, we overexpressed miR-187 and miR-486-5p and performed a variety of cellular functions, including monocyte adhesion for inflammation, scratch assay for migration, Caspase-3 and Annexin-V/PI staining for apoptosis, and PI staining after RNAse treatment for cell cycle analysis. More specifically, when we overexpressed miR-187 in vHAVECs, we found that there was a statistically significant decrease in monocyte adhesion in samples submitted to both LS and miR-187 overexpression when compared to vHAVECs exposed to OS with the non-targeting pre-miR. This result contradicted our hypothesis because other researchers found the miR-187 increased with LPS in the mouse lung,[80] suggesting that miR-187 is pro-inflammatory. Two potential explanations for this result are that miR-187 plays a different role in a different context or that the concentration of miR-187 pre-miR used in these studies is supraphysiological and therefore is inducing some feedback response. In order to eliminate the latter possibility, this experiment should be performed using LNA-anti-miR and should also be investigated using miRNA manipulation in tissues *ex vivo*. Also, as further support, we will investigate possible protein mediators of monocyte adhesion including ICAM and VCAM to confirm miR-187's effect on monocyte adhesion.

When HAVECs overexpressing miR-486-5p were exposed to both LS and OS, we found that 1) there was a small but statistically significant increase in wound healing in samples overexpressing miR-486-5p, 2) there was trend for a decrease in HAVECs undergoing early apoptosis in samples overexpressing miR-486-5p, and 3) there was no change in the percentage of HAVECs in G0/G1, S, G2/M in cell cycle analysis. Because miR-486-5p is found to be downregulated in cancer and decrease proliferation, migration, and apoptosis,[124-126] our original hypothesis stated that overexpressing miR-486-5p would

result in a decrease in migration and apoptosis. While our apoptosis finding shows a trend in reduction of early apoptosis in samples overexpressing miR-486-5p and thereby fitting with our hypothesis, our migration assay result shows the opposite of our anticipated effect. As an alternative explanation, this increase in migration could be caused by an upregulation of miR-486-5p-dependent *Efna1*, known to increase migration in some contexts.[139] Further investigation is required to test this hypothesis. To better understand if this is the true phenomenon in our system or possibly a result of using a supraphysiological dose of pre-miR, we will investigate this cellular function in response to a variety of other doses and investigate in tissue samples using an *ex vivo* system. Lastly, while we anticipated that there would be changes in the cell cycle (decrease in S and G2/M) due to previous reports that miR-486-5p decreases proliferation, we saw no changes as a result of pre-miR overexpression. Interestingly, we also saw no difference in shear. Classically, LS causes a reduction in proliferation or S and G2/M phases. Three possible reasons could explain this result. First, because of the total confluency of cells required for shear, any differences due to miR-486-5p may be hard to detect. Moreover, we have only performed this assay in two different patients. Further experimentation is required to increase the endpoints. Lastly, there could be some differences in the environments of the OS- and LS-sheared samples. For example, because of the high rotations per minute in the LS case, media evaporates in the LS dishes and changes the concentration of the media. Further, there is slight scraping in the center of the LS dish causing some cell death and lastly, we noted that HAVECs adhered more to the dish in the LS case and it was difficult to remove all cells in a timely manner. The above reasons could explain why we did not see the characteristic change in LS. In

the future, we will explore options to reduce media evaporation (using a Servo motor instead of a Stepper motor and higher percentages of hyskon to reduce revolutions per minute) as well as use higher concentrations of trypsin to dislodge all cells more quickly.

This work provides the foundation for exploring a variety of cellular functions in conjunction with miRNA level modulation. From our work, we have discovered that miR-187 reduces monocyte adhesion (FO with non-targeting premiR vs. VL with miR-187 premiR), suggesting its role in providing a less inflammatory environment in HAVECs. Further, we found that miR-486-5p causes an increase in migration, shows a trend to decrease the number of HAVECs undergoing early apoptosis, and has no apparent effects on cell cycle. Future work using LNA-anti-miR is required to look for inverse responses of the pre-miR experiments and provide additional confidence in our findings. Lastly, this work must be translated to an *ex vivo* tissue system. With this additional insight, we will be better able to determine the role of the identified shear-sensitive and side-dependent miRNAs and learn their potential role in AV disease.

CHAPTER 7

DISCUSSION

Summary

Globally, Aortic valve (AV) disease is a major cause of cardiovascular-related deaths, as well as a risk factor for additional cardiovascular pathologies;[1-3] however, the mechanism by which it initiates and progresses is not well-understood and is the focus of this thesis. We hypothesize that low-magnitude and oscillatory flow is present on the fibrosa side of the AV and stimulates ECs to regulate miRNAs and mRNAs to induce AV disease progression. This hypothesis was tested according to four specific aims employing both *in vitro* and *in vivo* approaches, high throughput microarray and pathway analyses, and as well as a variety of functional assays: Aim 1) To isolate and characterize side-dependent human aortic valvular endothelial cells (HAVECs), Aim 2) To identify side- and shear-induced changes in miRNA and mRNA expression profiles in HAVECs *in vitro,* Aim 3) To develop a method to isolate endothelial-enriched, side-dependent total RNA and to identify and validate side-dependent miRNAs in porcine aortic valvular endothelium, and Future Work) To determine the relationship between important miRNAs (specifically miR-187 and miR-486-5p) and AV biology and disease by modulating levels of miRNAs and performing functional assays and qPCR with potential targets.

In Aim 1, we were the first to isolate side-specific HAVECs (fHAVECs and vHAVECs).[4] HAVECs were isolated from hearts removed during transplantation surgeries, sorted using the functional endothelial cell marker acLDL, and characterized

both phenotypically and genotypically. More specifically, we found that fHAVECs and vHAVECs express both endothelial cells markers (*Pecam1*, *VE-cadherin*, and *vWF*) as well as two smooth muscle cell markers (*Sma* and basic calponin) through gene expression analysis, immunocytochemistry, and flow cytometry. We found that HAVECs align in the direction of the flow, similarly to other vascular endothelial cells but in contrast to porcine aortic valvular endothelial cells.[5] Potential reasons for this difference include: 1) disease state (healthy pigs versus humans with cardiovascular disease), 2) age (young pigs versus older humans), 3) species difference (porcine versus human), and 4) sorting and purity differences (pooled, unsorted PAVECs versus side-specific, sorted HAVECs).

In Aim 2, we sheared HAVECs under the following four conditions: 1) fHAVECs under OS (FO), 2) fHAVECs under LS (FL), 3) vHAVECs under OS (VO), and 4) vHAVECs under LS (VL). Though microarray analysis, we found over 1000 shear-responsive genes (FO vs. VL), 30 shear-responsive miRNAs, and 3 side-dependent miRNAs.

Validation results show that 93% of genes tested with qPCR were confirmed. Further, five miRNAs were confirmed to be shear-sensitive by qPCR: miR-139-3p, miR-148a (not found in SAM), miR-187, miR-192, and miR-486-5p. We were also able to validate one side-dependent miRNA, miR-370 (FL vs. VL). Through Ingenuity Pathway Analysis (IPA), we found genes that were highly connected and therefore potential master regulators: *Nfkbia*, *Thbs1*, *Pparg*, *Klf2*, and *Edn1* as well as transcription factors: *Atf3*, *Egr1*, *Fosb*, and *Klf2*. We found that cellular movement, death, and growth/proliferation were overrepresented cellular functions in our array dataset. Also

through IPA, we compared an existing microarray using side-specific porcine aortic valvular endothelium[6] to our HAVEC array (FO vs. VL) and found eight genes that were both related and changed in the same direction, reinforcing their importance in valve biology.

miRNA analysis and literature search further explored the importance of the validated miRNAs. Using a filtering process and miRWalk, we were able to determine a short list of potential targets, many with known involvement in a variety of cellular functions involved in tissue remodeling and inflammation. Through Diana analysis, we identified overrepresented miRNA binding sequences including miR-139-3p and miR-187 as well as miRNAs to investigate in the future as potential players in AV disease.

In Aim 3, we explored the following: 1) isolation of endothelial-enriched porcine AV total RNA, 2) validation of a side-specific, endothelial-enriched RNA isolation technique using the following markers: *Pecam1, Sma, Klf2, and vWF* , 3) generation a miRNA array using porcine AV endothelial total RNA to detect side-dependent miRNAs, 4) validation of both porcine, side-dependent (Figure 5.4) and human, shear-responsive miRNAs (Figure 5.5) using qPCR, and 5) initial validation studies using *in situ* hybridization of miR-486-5p. We found that were able to isolate good quality, side-specific, porcine AV endothelial RNA, identify 24 and confirm seven side-dependent miRNAs in aforementioned porcine AV endothelium. Further, we were able to confirm a side-dependency of an *in vitro* shear-responsive miRNA, miR-486-5p (albeit in the opposite direction) through qPCR. Further, we established a protocol for *in situ* hybridization (both cryosection and *en face*) for miRNA detection and initial *in situ* hybridization experiments with miR-486-5p show a similar trend as the qPCR result of

miR-486-5p. Finally, we categorized the *in vivo*, porcine, side-dependent (fibrosa vs. ventricularis) miRNAs and *in vitro*, human, shear-responsive (FO vs. VL) miRNAs by cellular function.

Lastly, in the future work section, we have 1) determined the optimal seeding and transfection conditions for shear studies, 2) investigated eight potential targets of miR-486-5p, 3) uncovered the role of miR-187 in monocyte adhesion after 24h shear, and 4) determined the role of miR-486-5p in migration, apoptosis, and the cell cycle. We found that HAVECs split 1:4 48h before shear and transfected with 30nM miR-187 pre-miR or 10nM miR-486-5p pre-miR 24h before shear are optimal experimental conditions. We also found that two of the eight potential targets of miR-486-5p show silencing after miR-486-5p overexpression (*Efna1* and *Prnd*) and have potential impact in AV disease in terms of endothelial-to-mesenchymal transition and oxidative stress. Lastly, we found that miR-187 reduces monocyte adhesion under LS when compared to OS transfected with the non-targeting pre-miR and that miR-486-5p increases migration and potentially decreases the number of early apoptotic cells after shear. Better understanding of these miRNAs will have profound effects of better understanding shear and AV disease.

Overall, we are the first to isolate side-specific HAVECs and side-specific porcine AV endothelial-enriched RNA and run both mRNA (HAVECs only) and miRNA arrays to uncover *in vitro* shear-responsive and *in vivo* side-dependent miRNAs. These miRNAs may serve as master regulators of AV biology and disease. Further, we have begun to better understand their roles in a variety of cellular functions that are intimately linked to tissue remodeling and inflammation known to be involved in AV disease.

Moreover, we have generated a host of new hypotheses and research directions that highlight the immense potential of the field.

Limitations

In Aim 1, we isolated HAVECs from AVs of hearts removed during transplantation surgeries. We must acknowledge that the tissue comes from patients with cardiovascular disease. Further, we do not have identifying information about the donors, including any potential medications, gender, race, or age. We have included all valves in this study due to the limited availability and subsequent low endpoint number.

Further, we detect smooth muscle alpha actin and basic calponin, markers of endothelial-to-mesenchymal transition (EMT), in the isolated HAVECs. Although this is a phenomenon that is seen *in vivo* and is thought to be restorative,[136] we cannot eliminate the possibility that culture conditions cause phenotypic drift.

Potential limitations to Aim 2 include under-defined shear conditions. As mentioned above, the complex shear conditions on either side of the AV are not well-known. While most hypothesize that the fibrosa side is exposed to low-magnitude and oscillatory shear while the ventricularis side is exposed to pulsatile, laminar shear, there are emerging reports suggesting different waveforms that should be further explored.[42, 43] It is important to note that because of the lack of understanding of these complex flow patterns, we are all working in a model system and that the ultimate test of a gene's or miRNA's significance will be through *in vivo* studies.

Another limitation of Aim 2 is that the studies were completed in only six patients due to availability and cost. For this reason, we have samples with varied health histories, ages, and races. In the future, we must increase the endpoint number to

adequately sample the population as well as find a source of AVs that does not have a history of cardiovascular disease (a tissue bank, for example). For this reason among others (species, matrix, *in vivo* vs. *in vitro*, etc.), we find that there are few similarities between genes identified in side-dependent porcine AV endothelium and our HAVEC (FO vs. VL) array.

Lastly, because of the low validation rate of the miRNA array, we are unable to rely on the results before extensive validation. It is widely known that miRNA array platforms are in their infancy and since our project, the Illumina miRNA array was discontinued. In the future, additional miRNA studies on more sophisticated platforms are required.

In Aim 3, we must acknowledge limitations in our isolation of side-specific, porcine AV endothelium. First, we had low RNA concentration, ranging on the nanogram level requiring purity assessment in only a subsection of the array samples as well as amplification in the array study. Future improvement of this technique such that amplification is no longer needed will be useful during further experimentation (arrays with different treatments). Also, rigorous validation of identified miRNAs is required. Secondly, we must discuss the issue of using smooth muscle alpha actin as purity marker for our *in vivo* RNA isolation technique. Although our HAVECs have been shown to express smooth muscle alpha actin, previous reports show that porcine AVECs do not express smooth muscle alpha actin.[5] Further, our qPCR shows very low expression of smooth muscle alpha actin in these samples. In the future, we must also include markers of monocytes such as *Cd11b*; however, because RNA was collected from healthy, porcine AVs, we hypothesize that monocyte infiltration is minimal. Thirdly, *in vivo* in

porcine AV endothelium, we see opposite regulation of miR-486-5p as compared to *in vitro* HAVECs. Although it is undeniable that shear plays an important part in the regulation of miR-486-5p, we must acknowledge that other forces (mechanical and chemical) may also be modulating its levels. Further, as we better understand the exact shear stress waveforms seen *in vivo*, we may be better able to interpret this discrepancy.

Although extensive optimization involving five adaptations of a well-received fluorescence *in situ* hybridization protocol[140] was completed, we still have a significant amount of background staining, especially in the *en face in situ* hybridization due to non-specific binding of the TSA-Cy3 fluorophore. Future work will investigate colorimetric detection methods.

One potential limitation of our studies involving pre-miRs and LNA-anti-miRs includes the possibility of modulating the miRNAs levels to the point of creating non-physiological feedback loops, thereby studying an artifact. In order to circumvent this potential limitation, we will perform a dose-dependent study to look for changes in cellular function for a select number of miRNAs. Also, current work to optimize LNA-anti-miR silencing has not revealed dose-dependent, reliable silencing. Future work will include higher doses of LNA-anti-miR (200nM-400nM) that have worked well in other contexts. Further, we do not see perfect dose-dependent knockdown of miR-486-5p's potential targets: *Efna1* and *Prnd*. A dual luciferase assay is required to confirm them as targets. Lastly, after 24h shear, vHAVECs exposed to LS (VL) are not easily removed from the dish, thereby creating unequal handling of fHAVECs exposed to OS compared to VL. There is also some degree of media evaporation and scraping in a small portion of

the dish's center. These reasons may explain why the characteristic increase in apoptosis in OS versus LS was not observed.

Overall, we have identified limitations of our study that will be addressed in the future; however, as described above, we have made several important strides in understanding shear-dependent and side-dependent miRNAs in AV biology.

Conclusions

In Aim 1, we conclude that it is possible to isolate side-specific fHAVECs and vHAVECs which express endothelial cell markers and respond to shear. We conclude that HAVECs are different from other vascular endothelial cells in terms of smooth muscle alpha actin and basic calponin expression and therefore should be studied for additional differences to facilitate better understanding of AV biology, disease, and tissue engineering design criteria.

In Aim 2, we discovered many shear-responsive genes and miRNAs which are intimately linked, unique from other shear datasets (e.g. HUVECs), and could act as potential master regulators of AV biology and disease. Our *in vitro* studies support that fHAVECs and vHAVECs are different because of their microenvironment as suggested by the absence of side-dependent genes. We did, however, find one side-dependent miRNA-370 (FL vs. VL) linked to EMT which requires further analysis. Future work will also look at shear-related differences in miRNAs along the various stages of miRNA biogenesis (pri-miRNA, pre-miRNA, and mature miRNA).

In Aim 3, we may conclude that we have developed an appropriate method to isolate side-specific, porcine AV endothelial-enriched RNA and yielded highly validated

miRNA data using the Agilent platform (as compared to the Illumina platform of Aim 2). Further, we were the first to identify side-dependent miRNAs in porcine AV endothelium. We also found that shear-responsive miR-486-5p identified *in vitro* in HAVECs was also side-dependent (fibrosa vs. ventricularis) *in vivo* in porcine AV endothelium although in the opposite direction as anticipated. This increases confidence in miR-486-5p's role in AV disease.

In the future work section, we concluded that miR-187 plays a role in inflammation by decreasing monocyte adhesion in vHAVECs exposed to LS (VL) compared to fHAVECs exposed to OS (FO) expressing the negative control. Further, we found that miR-486-5p increases wound healing, shows a trend to decrease early apoptosis, and has no effect (to date) on cell cycle progression. Lastly, we identified two novel potential targets of miR-486-5p, *Efna1* and *Prnd*, which could have profound effects on EMT and oxidative stress which are both important processes in AV biology and disease. By better understanding these identified miRNAs' cellular functions, we will better understand their role in AV biology and disease.

Future Directions

Future work for Aim 1 includes isolating side-specific, endothelial-enriched human aortic valve RNA for microarray studies. Comparison of these *in vivo* results with our *in vitro* results will further support the fact that HAVECs express both endothelial cell markers as well as smooth muscle cell markers. Also, future studies would benefit from collecting identifiers from human aortic valves. With this information, comparisons between diabetics and non-diabetics, etc. will be made possible. Lastly, because of the

statistically significant increase in smooth muscle alpha actin and basic calponin (and subsequently revealed increase in EMT-related miR-370[72]) in vHAVECs over fHAVECs, it would be interesting to investigate EMT differences in these two cell populations by using EMT-based qPCR arrays. From this finding, we hypothesize that fHAVECs are unable to undergo reparative EMT, resulting in a disease-preference on the fibrosa side; however, further experimentation is required.

Future work for Aim 2 includes testing more complex shear stress waveforms and comparing identified genes and miRNAs to our existing dataset. We will also focus on understanding the role of the highly-connected nodes identified through IPA: *Nfkbia*, *Thbs1*, *Pparg*, *Klf2*, and *Edn1*. We are especially interested in the role of *Nfkbia* (an anti-apoptotic factor decreased in OS) and *Thbs1* (a pro-apoptotic factor increased in OS) in OS-induced apoptosis in AV disease. Further investigation of three top pathways identified through IPA is required. First, we will investigate a potential role of the endothelial cell in LPS/IL1 mediated inhibition of RXR function in AV disease because of its linkage to atherosclerosis, while being cautious about the known differences between atherosclerosis and AV disease.[77] We would also like to investigate sulfur metabolism in our system as it has been linked to cardiac protection.[78] Lastly, IPA found that the NOTCH signaling pathway is overrepresented (*Hey2*, *Furin*, and *Numb*). Although it is known that NOTCH1 knockout mice have increased AV calcification,[141] the study of this pathway in valvular endothelial cells is lacking and could play an instrumental role in AV disease as well. We will continue to test for potential cellular targets for the identified miRNAs identified in Figure 4.11 as well as explore the overrepresented miRNAs discovered through Diana analysis. We are particularly

interested in miR-19a as it has been found in other shear-responsive datasets.[48] Another future priority includes testing the remainder of identified shear-responsive miRNAs for their cellular function using pre-miRs and LNA-anti-miRs. Another interesting project would be to investigate shear-responsive miR-148a's role in epigenetics since it includes *Dnmt1* and *Dnmt3b* as known targets.[98-102]

Future work for Aim 3 includes discovering the cellular function of the identified miRNAs in collaboration with Swetha Rathan of the Yoganathan lab. We will work to optimize protocols for overexpressing and silencing key miRNAs in porcine AV tissue and apply physiological shear waveforms using an *ex vivo* system.[44] We will investigate similar cellular functions as described in Aim 2 (migration, inflammation, apoptosis, etc.) and will include markers of calcification such as phospho SMADs, RUNX2, osteopontin and osteocalcin, among others. Also, we will confirm the shear-responsiveness of the identified side-dependent (fibrosa vs. ventricularis) miRNAs using HAVECs *in vitro*. Our primary focus will be on those validated both *in vivo* and *in vitro*. Further, because of the interesting observation that all identified side-dependent miRNAs were upregulated on the fibrosa side, we will investigate potential epigenetic mechanisms regulated by shear that could be responsible for this phenomenon. Epigenetic changes act as powerful master regulators and how shear affects them has not been studied to date. We will also test the hypothesis highlighted in Figure 5.10. Here, we hypothesize that *Twist1* which is known to modulate apoptosis, inflammation, and miRNA cluster 199a/214,[109] is differentially expressed on the fibrosa and ventricularis sides of the AV, causing side-dependent AV disease through the modulation of various cellular functions, namely apoptosis and inflammation. Lastly, we will improve our current *in situ*

hybridization protocol by using colorimetric detection methods instead of fluorescence to reduce background signal.

In the future work section, we would like to continue identifying the associated cellular function of key miRNAs and include a variety of pre-miR and LNA-anti-miR doses to ensure we are studying responses in a physiologically relevant way. Further, we would like to increase the dose of LNA-anti-miR to 200-400nM as a reliable, dose-dependent responses were not observed at lower doses. Also, in an effort to ensure efficient removal of LS-exposed HAVECs for flow-based studies, we will increase the trypsin concentration by 5-fold. After *in vitro* assessment of these miRNAs' cellular function, investigation in porcine AV tissue in an *ex vivo* system is warranted. Lastly, if *Efna1* and *Prnd* are confirmed as targets of miR-486-5p, we will investigate their role in EMT and oxidative stress, respectively, as both are thought to play a role in AV disease and have not been studied to date.

Undoubtedly, as we begin to answer questions about these shear-dependent and side-dependent miRNAs, we uncover new and promising avenues of future research. Pursuit of these avenues will provide important information about AV biology and disease and hopefully great therapies, including tissue-engineered AVs.

APPENDIX A

IMMUNOCYTOCHEMISTRY PROTOCOL

modified from Adele Doyle

Supplies

- PBS with Calcium and Magnesium
- 4% ice cold formaldehyde (dilute in PBS with calcium and magnesium as needed)
- Permeabilizing Solution
    - 0.05% Triton X (dilute in PBS). *I usually use 0.1% solution. Adele uses 0.05% solution. Best to make a more concentrated solution (1%) and dilute down after fully incorporated.*
- Blocking Solution
    - 5% serum in PBS
- Pap Pen
- Primary and Secondary Antibodies
- Isotype controls
- DI water or PBS without calcium and magnesium
- Razor
- Coverslips (1 or 1.5 variety)
- Fingernail polish

Protocol

1. **Wash** slides with PBS (3 x 5' in excess PBS). *Note: I have only washed 1x in the past for less than 5 minutes with no problem.*
2. **Fix** the slides/dishes for 10' at RT. Best to use ice cold 4% formaldehyde. *Dispose of waste in special container and use in chemical hood.*

3. **Wash** well with PBS (3 x 5' in excess PBS). Dispose of diluted formaldehyde in same special container. *Note: I have only washed 1x in the past for less than 5 minutes with no problem.*
4. **Permeabilize** for 15' at RT if staining for an intracellular marker.
5. **Wash** well with PBS (3 x 5' in excess PBS).
6. Use a **hydrophobic marker** around the staining section. *Note: By doing this, you can use the same dish to stain for more than one marker/control and reduce the amount of reagents. You can do this step after blocking if you'd prefer. I do.*
7. **Block** with serum from the species in which your secondary antibody was made for 30-60minutes. *If double staining, can use just one serum usually. For example, if you have a goat and donkey secondary, it is ok to just block with donkey serum.*
8. Incubate with **primary antibody** or **isotype control** (diluted in blocking solution) at appropriate dilution for 2 hours at RT or overnight at 4deg C. Use a humidifying chamber.
9. **Wash** well with PBS (3 x 5' in excess PBS).
10. Incubate with **secondary antibody** and **nuclear stain** (diluted in blocking solution) for 1 hour at RT.
11. **Wash** well with PBS (3 x 5' in excess PBS). Rinse with DI water or PBS without calcium and magnesium before coverslipping to avoid salt crystal formation.
12. **Remove** pap pen with a razor.
13. **Coverslip** (use 1 or 1.5 coverslips), let dry, and then put fingernail polish around edges. Allow for mounting media to dry overnight before imaging.
14. **Store** at 4deg C in light-protective box.

APPENDIX B

FLOW CYTOMETRY PROTOCOL

modified from Adele Doyle

Materials

Reagents

- Antibodies: specific to each run.
- Phosphate Buffered Saline solution (PBS): w/o Ca/Mg (1X) Invitrogen (Gibco) Cat # 14190-144; http://www.invitrogen.com/; store room temp
- Fetal Bovine Serum (FBS): heat inactivated; Cellgro Cat # MT35-011-CV; http://www.cellgro.com/; store frozen
- Bovine Serum Albumim
    - Formaldehyde: 10%, methanol free, Ultra Pure[50-00-0]; Polysciences Cat # 04018-1

Working Solutions

- **Working buffer solution (0.3% BSA, 0.001% Tween):** Add 0.3 g BSA to 100 ml PBS. Add 1ul Tween 20 per 100ml WBS (or appropriate amount from a diluted Tween solution). Filter-sterilize.
- **Blocking solution (Serum of secondary antibody donor species)** Add 1:10 of serum to working buffer solution. Most of our antibodies are made in donkey; AlexaFluor 546 anti-rabbit is made in goat.
- **Permeabilizing solution (0.5% Triton)**: Add 1 ml of 100% Triton to 200 mls sterile water. Store at 4°C.

- **Fixing solution (4% Formaldehyde)**: Dilute 20 mls of 10% formaldehyde with 30 mls sterile filtered PBS with Calcium and Magnesium for 50 ml final volume of 4% formaldehyde. Store at 4˚C (up to ~1 week).

Methods

1.0 PREPARE CELLS: Wash, trypsinize, and quench cells as normal.

2.0 PELLET: Spin 5' at 1000rpm. Aspirate supernatant.

3.0 FIX: Add 4 mls 4% formaldehyde for 15 min at 4ºC.

4.0 PELLET: Dilute w/ working buffer solution, centrifuge and aspirate.

5.0 PERMEABILIZE: (For intracellular markers only!) Add ~2 mls of permeabilizing solution for 30 min (vortex every 15 min to prevent cell settling) at 4°C.

5.1 PELLET: (Intracellular markers only.) Dilute w/ working buffer solution, centrifuge and aspirate.

6.0 BLOCK: Add 1 ml of blocking solution for 1 hr (vortex every 15 min to prevent cell settling).

7.0 PELLET: Dilute w/ working buffer solution, centrifuge and aspirate.

8.0 STAINING PREPARATION: Add 400 µl of working buffer solution and split tubes if appropriate.

9.0 PRIMARY STAINING: To all tubes, except controls, add primary antibody in 400ul (optimized dilution amount). Incubate at 4°C for 30 min.

10.0 PELLET: Dilute w/ working buffer solution, centrifuge and aspirate.

11.0 SECONDAY STAINING: To all tubes, except appropriate controls, add secondary antibody (optimized dilution amount). Incubate at 4°C for 30 min.

12.0 PELLET: Dilute w/ working buffer solution, centrifuge, and aspirate.

13.0 WASH: Add 1 ml working buffer solution, centrifuge and aspirate.

14.0 FINAL SAMPLE PREPARATION: Reconstitute all tubes to 0.5 ml w/ working buffer solution. Filter to remove particles >0.5 microns using blue-capped filter sterilizing test tubes.

15.0 Run samples on BD LSR. Normalize FSC and SSC voltages to ensure the cell population falls within the scale. Normalize fluorochrome voltage to ensure signal is distributed across the range of standard bead intensities. Record voltage settings. Measure all samples.

APPENDIX C

SHEAR-RESPONSIVE GENE PROBES FROM MICROARRAYS

Table C.1 Shear-responsive Gene Probes from Microarrays

Downregulated gene probes (FO/VL) (703)			Upregulated gene probes (FO/VL) (338)		
Gene Name	**Fold Change**	**q-value (%)**	**Gene Name**	**Fold Change**	**q-value (%)**
GJC2	-5.99	0.00	DHRS3	3.76	0.00
UBN1	-1.84	0.00	CCDC106	1.88	0.00
HEG1	-3.26	0.00	SLC7A7	2.84	0.00
ATP8B2	-1.86	0.00	TMEM14C	1.67	0.00
PODXL	-6.44	0.00	CIRBP	3.64	0.00
PPIC	-1.66	0.00	RALGDS	2.01	0.00
MOBP	-1.81	0.00	TMEM88	2.50	0.00
CSRP2	-2.05	0.00	ADM	5.01	0.00
THBD	-3.10	0.00	CERK	1.97	0.00
BCAR3	-2.31	0.00	GADD45B	1.64	0.00
ITGB4	-4.73	0.00	NDUFA7	1.72	0.00
NFKBIA	-3.29	0.00	DDX19B	1.62	0.00
TPST2	-2.78	0.00	FHL2	2.03	0.00
ATP1A1	-1.79	0.00	APLN	3.07	0.00
SYTL4	-2.34	0.00	CAMK2B	3.55	2.00
SULT1A4	-2.61	0.00	FHL2	1.77	0.00
ENDOD1	-1.54	0.00	ALKBH3	1.50	0.00
OBFC1	-2.21	0.00	GTF2IRD2B	1.54	0.00
TSC22D3	-2.45	0.00	MYO1D	1.78	0.00
TEK	-4.94	0.00	PMM2	1.75	0.00
TEK	-4.92	0.00	THBS1	2.10	0.00
TSC22D1	-1.81	0.00	PPP1R16B	2.39	0.00
CDH11	-3.37	0.00	CTSK	2.96	0.00
MTMR11	-2.40	0.00	EWSR1	1.53	0.00
PLAU	-3.71	0.00	RNF41	1.82	0.00
VGLL4	-1.70	0.00	SH3GLB2	1.59	0.00
HIST1H2BK	-3.84	0.00	LTB	2.24	0.00
PPAP2B	-3.64	0.00	PDGFB	1.75	0.00
TPST2	-2.90	0.00	STK32B	1.89	0.00
MGC10997	-1.70	0.00	CRYL1	1.59	0.00
LYN	-2.26	0.00	MGC4172	1.92	0.00
PIK3C2B	-1.73	0.00	C10orf10	11.39	0.00
RPS29	-1.71	0.00	MEF2D	1.52	0.00

NR2F2	-1.64	0.00	EFEMP1	1.57	0.00
KLF2	-5.35	0.00	TCF25	1.64	0.00
LFNG	-2.19	0.00	SEC14L1	1.61	0.00
ZNFX1	-1.64	0.00	ATP5S	1.52	0.00
CDR2L	-2.66	0.00	MT1E	1.96	0.00
ADAMTS1	-8.18	0.00	LOC730534	1.84	0.00
CD59	-1.98	0.00	NAV1	1.80	0.00
HIST2H2BE	-1.91	0.00	KIT	3.95	0.00
ITGA10	-2.43	0.00	LOC148915	1.70	0.00
DNASE1L1	-2.60	0.00	MT1F	2.42	0.00
ITGB4	-2.31	0.00	TMEM185A	1.84	0.00
HIST1H2BD	-4.52	0.00	NANOS3	1.71	0.00
GSN	-2.06	0.00	COQ3	1.55	0.00
JAG1	-1.85	0.00	SLC25A15	1.53	0.00
CDC25B	-3.10	0.00	FAM89A	2.57	0.00
NDST2	-1.85	0.00	MTMR14	1.66	0.00
ZNF467	-2.86	0.00	EFNA1	2.12	0.00
STOM	-1.61	0.00	CXCL12	1.58	0.00
ABI3	-2.74	0.00	EIF2B2	1.97	0.00
C20orf160	-3.11	0.00	C20orf100	1.99	0.00
CD59	-3.37	0.00	NSFL1C	1.90	0.00
CTSL1	-1.54	0.00	FAM43A	1.95	0.00
ITPR3	-2.20	0.00	PDGFRL	2.14	0.00
UBE2F	-2.26	0.00	KIT	2.93	0.00
SLCO2A1	-34.74	0.00	DKFZp761P0423	2.25	0.00
GNA14	-2.29	0.00	CAMK2N1	1.73	0.00
TMEM173	-2.31	0.00	ASNS	2.06	0.00
HSPA12B	-9.03	0.00	GRK5	1.90	0.00
IL18BP	-2.14	0.00	CD2BP2	1.53	0.00
ANKS1A	-1.73	0.00	RASSF2	2.08	0.00
CARHSP1	-2.05	0.00	SNORD13	3.08	0.00
SVIL	-1.98	0.00	FAM89A	2.12	0.00
PLVAP	-1.99	0.00	GATS	1.79	0.00
HSPE1	-1.99	0.00	CMTM7	1.51	0.00
DHH	-2.32	0.00	NPEPL1	1.57	0.00
HDAC1	-1.54	0.00	SPC24	1.91	0.00
GPR162	-2.61	0.00	GSTZ1	1.76	0.00
PPP1R3C	-2.91	0.00	CSTF3	1.52	0.00
CLDN15	-6.90	0.00	TGFBRAP1	1.92	0.00
PODXL	-4.19	0.00	FAM89A	2.65	0.00
MN1	-1.76	0.00	GABARAPL1	1.69	0.00
SULT1A1	-1.62	0.00	TNFRSF4	3.93	0.00
KIAA1522	-2.62	0.00	NIT2	1.53	0.00

RNASE1	-2.31	0.00	ABCB9	1.83	0.00
FUK	-2.56	0.00	ME3	1.65	0.00
KIAA1754	-2.28	0.00	CERK	1.67	0.00
HS3ST1	-7.70	0.00	ECHDC2	1.55	0.00
PHYH	-1.50	0.00	HBEGF	1.53	0.00
OAF	-3.66	0.00	C11orf80	1.60	0.00
ID1	-2.61	0.00	C22orf29	1.60	0.00
SH3PXD2A	-1.52	0.00	TMEM178	1.67	0.00
PMP22	-3.43	0.00	PGF	2.64	0.00
LUZP1	-1.68	0.00	CXCR4	3.80	0.00
TICAM2	-2.02	0.00	ARFGAP2	1.54	0.00
TSC22D3	-2.69	0.00	AK2	1.54	0.00
ST3GAL1	-1.69	0.00	ASMTL	2.09	0.00
APOL2	-1.56	0.00	TMEM14B	1.81	0.00
DNAJC3	-1.50	0.00	RNF144	3.01	0.00
COL13A1	-1.81	0.00	GPX1	1.51	0.00
PPAP2B	-5.08	0.00	MPP4	1.92	0.00
HIST1H2BD	-2.16	0.00	BST1	1.56	0.00
ATP1B1	-2.00	0.00	PDGFB	1.68	0.00
BCL3	-2.37	0.00	RASSF2	1.98	0.00
COL13A1	-1.52	0.00	C1orf102	1.89	0.00
TMEM171	-1.98	0.00	MOV10L1	1.83	0.00
TRIB2	-1.66	0.00	DYNLT1	1.69	0.00
NOS3	-3.04	0.00	SLC35C2	1.60	0.00
GNGT2	-2.27	0.00	LOC441408	1.63	0.00
TTYH3	-1.90	0.00	C20orf127	1.95	0.00
MAP4K2	-1.59	0.00	OSBPL10	1.98	0.00
HCCA2	-1.67	0.00	SHMT1	1.79	0.00
ITGA6	-2.06	0.00	EXOSC6	1.67	0.00
KLF4	-4.06	0.00	CDC45L	1.80	0.00
SFT2D1	-1.57	0.00	GJA4	2.75	0.00
PAPSS1	-1.55	0.00	C6orf108	2.14	0.00
ZNF589	-1.68	0.00	SNCAIP	4.43	0.00
MPZL2	-3.38	0.00	EGR1	3.54	0.00
PEA15	-1.63	0.00	PRKAB1	1.76	0.00
ABCC5	-1.55	0.00	CD99L2	1.53	0.00
STARD8	-2.53	0.00	WFS1	2.52	0.00
MKNK2	-2.47	0.00	FEN1	1.58	0.00
LDLR	-2.46	0.00	CYTL1	1.87	0.00
DDIT4	-2.11	0.00	FTSJ1	1.64	0.00
MSN	-1.55	0.00	MRPS16	1.56	0.00
C14orf139	-1.95	0.00	RANGAP1	1.56	0.00
C14orf78	-2.31	0.00	PTTG1	1.54	0.00

STOM	-2.00	0.00	ASMTL	2.04	0.00
IER5	-1.83	0.00	MAST4	2.55	0.00
PPIC	-1.57	0.00	C7orf47	1.75	0.00
SLC27A3	-2.36	0.00	CPT2	1.54	0.00
C10orf78	-1.95	0.00	C19orf48	1.52	0.00
MALL	-5.10	0.00	CHMP4B	1.51	0.00
ZCCHC24	-1.75	0.00	MGC61598	1.88	0.00
P4HA2	-2.43	0.00	ZNF395	2.31	0.00
MRAS	-1.54	0.00	PTTG1	1.56	0.00
DUSP3	-1.92	0.00	PSEN2	1.73	0.00
RECK	-1.71	0.00	TCF7L1	2.12	0.00
HYAL2	-3.75	0.00	GALNAC4S-6ST	1.77	0.00
CTSL1	-1.53	0.00	C7orf50	1.62	0.00
GRB14	-1.92	0.00	TRMT5	1.87	0.00
ATP1B1	-2.03	0.00	NSFL1C	1.78	0.00
SLC29A1	-2.27	0.00	ALDH7A1	1.64	0.00
CXXC5	-2.03	0.00	TIGA1	1.66	0.00
RBMS1	-1.78	0.00	STX11	1.62	0.00
MYCT1	-2.40	0.00	P2RX4	1.87	0.00
PI16	-30.61	0.00	MPP1	1.82	0.00
NDRG1	-2.52	0.00	LRIG1	1.83	0.00
PANK1	-1.58	0.00	BMP4	2.35	0.00
FAM167B	-3.07	0.00	CXCR4	3.04	0.00
DRAM	-2.02	0.00	MAGED1	1.58	0.00
INSIG1	-2.43	0.00	AP1B1	1.51	0.00
ENTPD1	-2.79	0.00	PPM1H	1.72	0.00
SLC24A6	-2.21	0.00	PDE4B	2.24	0.00
COPS8	-1.94	0.00	HINT2	1.53	0.00
LIMS2	-1.82	0.00	CLDN5	1.94	0.00
HIST1H4H	-1.57	0.00	LOC440895	1.63	0.00
HSPE1	-1.54	0.00	RASD1	2.62	0.00
LOC57228	-2.66	0.00	SLC35E3	1.54	0.00
ARHGEF3	-2.53	0.00	TCEA2	1.57	0.00
UBFD1	-1.79	0.00	MUM1	1.64	0.00
EML1	-1.54	0.00	PXMP2	1.54	0.00
HTATIP2	-1.63	0.00	FOS	1.66	0.00
MYCN	-3.40	0.00	CHRNA1	2.17	0.00
C13orf33	-1.82	0.00	PICK1	1.56	0.00
ADCY4	-1.69	0.00	CTHRC1	1.61	0.00
FGR	-1.71	0.00	C1orf97	1.79	0.00
RHOJ	-1.52	0.00	GIMAP8	2.08	0.00
COPS8	-1.80	0.00	FOSB	4.08	0.00

ITGA3	-1.75	0.00	PSAT1	1.61	0.00
MAFB	-1.63	0.00	C17orf58	2.08	0.00
LY96	-1.74	0.00	PHGDH	2.35	0.00
TMEM2	-2.94	0.00	SLC37A4	1.71	0.00
MRPS6	-2.56	0.00	CENPM	1.84	0.00
CNTNAP1	-1.63	0.00	WDR68	1.71	0.00
DAG1	-1.52	0.00	C3orf21	1.52	0.00
SLC29A1	-2.35	0.00	C1orf97	1.53	0.00
TRAK1	-1.91	0.00	LIG1	1.65	0.00
ODZ3	-1.80	0.00	C17orf58	2.21	0.00
SULT1A3	-2.64	0.00	CHRNA1	2.50	0.00
DNAJB11	-1.73	0.00	FJX1	1.76	0.00
AQP1	-1.93	0.00	LOXL4	1.65	0.00
GPER	-2.71	0.00	PHLDA1	1.63	0.00
C6orf128	-2.07	0.00	MGC70857	1.76	0.00
PPAP2A	-3.08	0.00	PNMA2	1.83	0.00
PARP9	-1.52	0.00	ECHDC3	1.76	0.00
ZFP36L1	-2.09	0.00	FST	2.02	0.00
DNAJA1	-2.17	0.00	COMMD4	1.65	0.00
NDRG4	-1.72	0.00	CTNNBIP1	2.10	0.00
IFI27	-1.97	0.00	CD99L2	1.56	0.00
CCDC69	-1.68	0.00	MAGED1	1.81	0.00
DNAJA4	-2.00	0.00	MTE	1.76	0.00
GLDC	-2.76	0.00	NRIP3	1.55	0.00
ZMIZ2	-1.55	0.00	LOC644033	1.81	0.00
S100P	-2.00	0.00	C6orf85	1.80	0.00
KLF11	-2.49	0.00	NASP	1.59	0.00
ZBTB46	-1.72	0.00	TMEM177	1.58	0.00
C1orf225	-2.88	0.00	TMEM118	1.55	0.00
SYT11	-1.74	0.00	IL11RA	1.76	0.00
TMBIM1	-2.48	0.00	ADA	2.06	0.00
PAPSS1	-1.84	0.00	DHRS1	1.51	0.00
GOLM1	-1.52	0.00	EDN1	1.78	0.00
COL17A1	-4.76	0.00	LOC728014	1.61	0.00
S100A3	-4.41	0.00	FOXRED1	1.61	0.00
SNHG3-RCC1	-1.52	0.00	LOC642477	1.50	0.00
ORAI1	-1.63	0.00	TNFAIP8L1	1.67	0.00
SEMA4B	-3.55	0.00	FAM64A	1.89	0.00
CPNE8	-1.96	0.00	CCNA1	2.32	0.00
EPHA4	-1.78	0.00	ERCC2	1.57	0.00
ADAM15	-1.68	0.00	PSMD9	1.54	0.00
LCN6	-11.25	0.00	CCL23	1.85	0.00

SLCO4A1	-2.17	0.00	RPS6KB2	1.53	0.00
CRYBA4	-1.74	0.00	ATOH8	1.60	0.00
PTPRE	-1.66	0.00	DDHD2	1.55	0.14
PRCP	-1.55	0.00	RNF144B	1.58	0.14
CGN	-1.74	0.00	ATF3	1.57	0.14
RGS4	-2.09	0.00	GPR146	1.69	0.14
HSPH1	-3.75	0.00	C17orf58	2.13	0.14
NFKBIZ	-3.44	0.00	LOC400879	1.53	0.14
NUMB	-1.58	0.00	LOC653071	1.57	0.14
VEGFC	-3.88	0.00	LOC728014	1.62	0.14
CEBPD	-2.42	0.00	ATP9A	1.51	0.14
PLAT	-7.97	0.00	TTC32	1.52	0.14
APOL3	-2.23	0.00	HLX	1.86	0.14
COL5A2	-1.98	0.00	GPIHBP1	3.52	0.14
RHOJ	-1.52	0.00	CTPS	1.52	0.14
PRCP	-1.94	0.00	GINS2	1.79	0.14
SNX27	-1.51	0.00	CCND2	4.13	0.14
PPFIBP1	-1.50	0.00	SNX8	1.63	0.14
GDF3	-11.91	0.00	PFKP	1.57	0.14
BCL2L1	-1.64	0.00	OSAP	2.34	0.14
PRICKLE1	-1.99	0.00	ACOX2	1.87	0.14
LOC401720	-2.47	0.00	TGFB1I1	1.51	0.14
ADAMTS9	-2.48	0.00	CMTM7	1.59	0.14
RNASE1	-2.06	0.00	RBP1	1.89	0.14
MEIS2	-1.89	0.00	IFT122	1.66	0.14
SLC5A3	-1.93	0.00	GMFG	1.59	0.14
ASS1	-2.20	0.00	LOX	1.71	0.14
IKBKB	-1.61	0.00	PIM3	2.15	0.14
S100A4	-5.20	0.00	PAQR4	1.54	0.14
NPC1	-2.19	0.00	MTMR14	1.55	0.14
SASH1	-1.67	0.00	CHST7	1.72	0.14
LOC57228	-2.34	0.00	DPYSL4	1.61	0.14
RECK	-1.67	0.00	CTDSPL	1.53	0.14
ANPEP	-2.04	0.00	PRND	2.91	0.14
UBR4	-3.51	0.00	EFNA1	1.60	0.14
CLDN14	-2.61	0.00	MTUS1	2.12	0.14
ADAMTSL1	-1.61	0.00	MRPL23	1.60	0.14
CFLAR	-2.24	0.00	ALDH1A3	1.94	0.14
AKR1B1	-2.32	0.00	ALDH1A3	1.96	0.14
HYAL1	-4.77	0.00	RAD51C	1.74	0.14
FSTL1	-1.62	0.00	CCL15	2.99	0.14
GPER	-2.85	0.00	IL17D	1.62	0.14
IRAK2	-1.65	0.00	PRMT1	1.56	0.14

PLCD3	-1.55	0.00	APOA1BP	1.60	0.14
HSPD1	-1.70	0.00	FABP5	1.63	0.14
FCN3	-6.78	0.00	ATPAF1	1.57	0.14
TPP1	-1.68	0.00	PRDM1	2.37	0.14
PLAC9	-3.07	0.00	ABLIM1	1.70	0.14
ZNF185	-3.09	0.00	C13orf15	1.70	0.14
PCYOX1	-1.54	0.00	RAB11FIP1	1.89	0.14
ZFHX3	-1.54	0.00	LOC388588	1.67	0.14
EPHB4	-2.15	0.00	VASH1	2.46	0.14
LYPD5	-2.86	0.00	ABCB9	1.53	0.14
IFNAR1	-1.93	0.00	ASF1B	1.64	0.14
ANTXR2	-1.56	0.00	ALS2CR4	1.50	0.14
ZDHHC6	-1.50	0.00	C9orf103	1.53	0.14
LMAN2L	-2.01	0.00	CLEC1A	1.65	0.14
PTGS1	-2.16	0.00	CYP26B1	1.70	0.14
ATXN7L1	-1.53	0.00	MYH10	1.65	0.14
SNTB2	-1.81	0.00	SYT15	1.51	0.14
ADORA2A	-1.90	0.00	FRAS1	1.59	0.14
CXCR7	-2.68	0.00	PPFIBP2	1.59	0.14
TBXA2R	-1.57	0.00	KRT80	1.52	0.14
MAP1B	-1.73	0.00	TMEM163	1.92	0.14
C12orf34	-1.78	0.00	OSAP	2.16	0.14
HYAL1	-1.85	0.00	LXN	2.28	0.14
CPNE8	-1.84	0.00	INHBB	1.63	0.14
SULT1A3	-2.03	0.00	MAPKAPK3	1.55	0.14
C21orf63	-1.67	0.00	DACT3	1.85	0.14
ATP1A1	-1.65	0.00	HCP5	1.74	0.14
SQLE	-1.76	0.00	C18orf34	2.58	0.14
CASK	-1.91	0.00	ATP5D	1.57	0.14
AKR1C3	-2.02	0.00	PC-3	1.95	0.14
RAMP2	-1.88	0.00	PRR6	1.53	0.14
COL17A1	-1.84	0.00	FST	2.34	0.14
P4HA2	-2.15	0.00	GIMAP5	2.50	0.14
TEAD4	-2.09	0.00	N4BP3	1.52	0.14
FAM24B	-2.95	0.00	BMP2	1.58	0.14
CXCR7	-4.20	0.00	FAM101B	1.51	0.14
SLC20A1	-1.89	0.00	PFAS	1.52	0.14
EMP3	-2.10	0.00	RGL1	1.52	0.14
FAM107A	-1.94	0.00	KCNF1	1.81	0.14
HIST1H3D	-1.66	0.00	TRO	1.56	0.14
ITGB1BP1	-1.60	0.00	PDE7B	2.43	0.14
HSPA2	-2.30	0.00	GCDH	1.52	0.14
SERTAD2	-1.59	0.00	ANGPT2	2.79	0.31

TRIMP1	-2.43	0.00	FKBP11	1.52	0.31
PMEPA1	-1.79	0.00	FABP4	2.29	0.31
LPAR5	-1.73	0.00	GIMAP4	2.03	0.31
CRELD1	-1.83	0.00	TXNRD2	1.63	0.31
TMEM50B	-1.73	0.00	LOC642342	1.68	0.31
S100A4	-5.61	0.00	CHST1	1.95	0.31
TNFRSF25	-1.81	0.00	MTUS1	1.79	0.31
PLTP	-2.12	0.00	LOC440160	1.56	0.31
GLS	-3.73	0.00	HNMT	1.60	0.31
MOBP	-1.64	0.11	CNTNAP3	1.86	0.31
C9orf3	-1.68	0.11	PRMT1	1.54	0.31
PPAP2A	-1.67	0.11	GAMT	1.51	0.31
GFPT2	-3.01	0.11	CXCL12	1.81	0.31
UBTD2	-1.50	0.11	PCK2	1.68	0.31
HIST2H2AA3	-2.22	0.11	LOC653355	1.98	0.31
INTS3	-1.76	0.11	ATAD3A	1.53	0.40
SLC9A3R2	-1.93	0.11	SFRS5	1.63	0.40
PTPRB	-1.53	0.11	CXADR	2.27	0.40
CCND3	-1.55	0.11	MYO5C	2.55	0.40
CYP1A1	-1.85	0.11	LIMCH1	1.99	0.40
SERPINE2	-3.33	0.11	NTN4	1.54	0.40
TRIM5	-1.66	0.11	ASH2L	1.55	0.40
SDCBP	-2.19	0.11	DDIT4L	2.24	0.40
NEK6	-1.57	0.11	MYRIP	1.68	0.40
HIST1H2BK	-1.64	0.11	ANGPTL2	1.50	0.40
MPZL2	-2.40	0.11	ACSS1	1.94	0.40
PPP2R2B	-2.78	0.11	ITM2C	1.54	0.40
KIAA0363	-1.66	0.11	NMT2	1.91	0.40
QPCT	-1.90	0.11	MYO1B	1.60	0.48
SLC2A3	-2.68	0.11	FLJ39632	1.63	0.48
CYBRD1	-1.76	0.11	PPARG	1.74	0.48
CROT	-2.26	0.11	TCF4	1.55	0.48
SULT1A2	-1.68	0.11	MAOA	1.52	0.48
ABCC3	-1.69	0.11	FNDC5	2.97	0.55
SDCBP	-1.88	0.11	DACH1	1.51	0.55
NSDHL	-1.95	0.11	FAM107B	1.63	0.55
PALLD	-2.60	0.11	TK1	1.71	0.55
TMEM184B	-1.74	0.11	TOMM20	1.50	0.55
HSPA2	-1.92	0.11	C12orf26	1.52	0.55
CDC42EP4	-1.66	0.11	LOC440157	1.58	0.55
LMCD1	-1.58	0.11	SPHK1	1.58	0.71
C15orf52	-1.74	0.11	MGC16121	1.53	0.71
BTBD14A	-1.52	0.11	SFRS5	1.51	0.91

AGPS	-1.51	0.11	KRT7	1.99	0.91
SC4MOL	-2.47	0.11	KIAA0494	1.51	0.91
HYAL3	-2.04	0.11	IL8	1.57	0.91
HSP90AA1	-2.95	0.11	MYLK2	1.50	1.11
SLC38A9	-1.51	0.11	IL8	1.51	1.11
KLF11	-1.52	0.11	CLEC1B	1.61	1.34
SASH1	-1.79	0.11	CPA4	1.55	2.41
FAM70B	-1.73	0.11			
PPP1R14A	-1.54	0.11			
HECA	-1.61	0.11			
GRRP1	-1.72	0.11			
TSKU	-1.80	0.11			
SHB	-1.70	0.11			
PTPLB	-1.63	0.11			
PTGER4	-1.83	0.11			
PLOD3	-1.88	0.11			
C8orf4	-2.87	0.11			
ATP6V1D	-2.10	0.11			
TNFAIP8L3	-1.91	0.11			
CLDN15	-1.87	0.11			
LRRC8A	-1.69	0.11			
PPP1R3F	-1.54	0.11			
CALU	-1.61	0.11			
FLJ20489	-1.78	0.11			
RAMP2	-1.63	0.11			
TLR4	-2.11	0.11			
PDLIM4	-1.74	0.11			
NKIRAS1	-1.59	0.11			
PTPRE	-1.72	0.11			
PDIA4	-1.82	0.11			
BANP	-1.50	0.11			
ASAP3	-1.55	0.11			
DUSP5	-1.85	0.11			
LPHN2	-2.57	0.11			
LOC731895	-1.66	0.11			
SEMA3F	-2.60	0.11			
ANXA6	-1.86	0.11			
HSPB8	-1.66	0.11			
TNS1	-1.71	0.11			
HECW2	-2.72	0.11			
MLKL	-1.77	0.11			
PTPLB	-1.72	0.11			
VCAN	-2.65	0.11			

LHX6	-1.76	0.11
E2F7	-1.84	0.11
CHN1	-2.05	0.11
ATP1A1	-1.52	0.11
HSP90B1	-2.44	0.11
MRPL9	-1.59	0.11
P2RY2	-1.58	0.11
CACYBP	-1.56	0.11
MYCT1	-1.77	0.11
FILIP1L	-2.22	0.11
SLFN11	-1.57	0.11
C1QTNF6	-1.91	0.11
VAMP8	-1.65	0.11
AKR1C4	-1.85	0.11
HSPA1B	-4.02	0.11
SRGN	-2.10	0.11
APLNR	-2.52	0.11
SPCS3	-1.76	0.11
HSPA1A	-4.40	0.11
SYNC1	-1.77	0.11
FILIP1L	-2.76	0.11
GUK1	-1.61	0.11
ACSL5	-1.63	0.11
TMEM189	-1.65	0.11
BANP	-1.69	0.11
BEX1	-3.64	0.11
CLIC3	-3.96	0.11
MPZL2	-2.06	0.11
PTMS	-1.69	0.11
REP15	-1.52	0.11
RAB23	-1.66	0.11
HIST2H2AA3	-3.50	0.11
NRGN	-1.73	0.11
CRELD2	-1.64	0.11
SELE	-2.73	0.31
HSP90AA1	-3.67	0.31
DNASE1L1	-1.58	0.31
RAC2	-1.58	0.31
ANKRD55	-2.18	0.31
CD68	-1.72	0.31
PRIC285	-1.51	0.31
LDB2	-1.61	0.31
CXCL2	-1.75	0.31

ZMIZ1	-1.50	0.31
FLJ11795	-2.21	0.31
TPD52L1	-1.58	0.31
OGT	-1.74	0.31
RAB17	-2.83	0.31
EFNB1	-1.60	0.31
FILIP1L	-2.43	0.31
SSH2	-1.94	0.31
CYLN2	-1.60	0.31
MAMLD1	-1.58	0.31
FAM38B	-2.04	0.31
LAMC2	-2.03	0.31
SCD	-1.61	0.31
ITM2A	-1.96	0.31
CYBRD1	-1.66	0.31
HTRA1	-2.20	0.31
PNPLA6	-1.55	0.31
S100A11	-1.65	0.40
ITGB8	-1.53	0.40
ARSA	-1.53	0.40
FURIN	-1.65	0.40
PLEK2	-2.27	0.40
KTELC1	-1.57	0.40
PRKCH	-1.51	0.40
ADRB2	-1.51	0.40
KCNJ2	-1.85	0.40
IRF9	-1.62	0.40
SP100	-1.55	0.40
ASPHD2	-1.63	0.40
PHLDA3	-2.08	0.40
P4HA1	-2.01	0.40
H19	-1.89	0.40
ITPKA	-1.71	0.40
LAMA5	-1.57	0.40
KLHL5	-1.76	0.40
CAPN11	-1.60	0.40
SPOCK1	-2.00	0.40
CLIP2	-1.55	0.40
IL6	-1.56	0.40
PHF15	-1.55	0.40
KITLG	-1.50	0.48
AEBP1	-1.60	0.48
LIMA1	-1.52	0.48

IL32	-2.14	0.48
RAB21	-1.50	0.48
TMEM126B	-1.87	0.48
CD58	-1.54	0.48
HEY2	-1.56	0.48
LOC346887	-2.77	0.48
TBC1D2	-2.06	0.48
C1orf71	-1.74	0.48
SMAD6	-1.60	0.48
DUSP1	-1.51	0.48
CLDN1	-1.73	0.48
EPB49	-1.64	0.48
OSBPL8	-1.55	0.48
SULT1B1	-1.70	0.48
SLC38A2	-2.77	0.48
COL5A1	-1.60	0.48
MORG1	-1.51	0.48
NNMT	-1.72	0.48
HIST2H2AC	-2.33	0.48
LRRC32	-1.66	0.55
HSD17B12	-1.68	0.55
BUB3	-1.60	0.55
IGFBP5	-15.88	0.55
PLEKHB2	-1.67	0.55
CANX	-1.60	0.55
ZMPSTE24	-1.90	0.55
CYYR1	-1.88	0.55
LARP6	-1.70	0.55
CALCRL	-4.86	0.55
IL32	-1.92	0.55
SH3BGRL3	-1.83	0.55
PLA2G4C	-1.55	0.55
LOC650263	-1.66	0.55
NQO1	-1.54	0.55
HMGCR	-1.85	0.55
KIAA0746	-1.55	0.55
FNDC4	-1.71	0.55
SRGN	-2.16	0.55
CRYAB	-2.31	0.55
FES	-1.60	0.55
ATG4A	-1.60	0.55
PRSS35	-1.55	0.55
OAS1	-1.75	0.55

IGFBP5	-31.99	0.55
ADAM15	-1.90	0.55
KIF1B	-1.50	0.71
NTHL1	-1.56	0.71
FOXO3	-1.53	0.71
PTHLH	-1.98	0.71
TMEM100	-2.81	0.71
PHTF1	-1.65	0.71
MVP	-1.60	0.71
HSD17B12	-1.65	0.71
ZDHHC17	-1.63	0.71
TBC1D9	-1.60	0.71
RYBP	-1.79	0.71
CDKN2B	-1.56	0.71
KAT2A	-1.63	0.71
RUSC1	-1.57	0.71
CD14	-2.31	0.71
KTELC1	-1.83	0.71
ELMOD1	-1.57	0.71
PTHLH	-1.97	0.71
ETS1	-1.56	0.71
CALHM2	-1.90	0.71
SULT1E1	-1.68	0.71
IFIT1	-1.83	0.71
DNAJB9	-1.92	0.71
ANXA6	-1.75	0.71
AKR1C2	-2.34	0.71
RRAS	-1.74	0.71
FGFR3	-1.59	0.71
KLF9	-2.46	0.91
C19orf33	-1.77	0.91
AHSA1	-1.73	0.91
ADAM15	-1.96	0.91
ADAMTS6	-1.89	0.91
ANO6	-1.53	0.91
IMPAD1	-1.55	0.91
CRK	-1.52	0.91
CLCN3	-1.52	0.91
CNKSR3	-1.58	0.91
MFAP2	-1.63	0.91
EIF4A2	-1.85	0.91
BIN1	-1.55	1.11
C1QTNF1	-1.81	1.11

PRRX1	-1.81	1.11
MLLT11	-1.53	1.11
SULF1	-2.04	1.11
TUBA4A	-1.64	1.11
ATP11C	-1.82	1.11
BHLHB2	-1.79	1.11
PTPN12	-1.86	1.11
ACTA2	-1.53	1.11
FAM110A	-1.57	1.11
ZBTB20	-1.75	1.11
FBXW7	-1.86	1.11
DNAJB1	-1.64	1.11
TRIML2	-1.62	1.34
PGM2L1	-1.56	1.34
FLNC	-1.79	1.34
TGFBR2	-1.54	1.34
MSRB3	-1.58	1.34
C6orf15	-1.50	1.34
RDH14	-1.51	1.34
LOC88523	-2.14	1.34
HSPD1	-1.55	1.34
BMPR2	-1.79	1.34
PLEKHG4	-1.55	1.34
LYPD1	-1.50	1.34
PC	-1.54	1.34
UGDH	-1.51	1.69
CD46	-1.67	1.69
SC5DL	-1.60	1.69
CDC42EP2	-1.58	1.69
PICALM	-1.50	1.69
TMEM126B	-1.94	1.69
ACAD11	-1.76	1.69
DHCR7	-1.62	1.69
CPXM2	-1.71	1.69
DKK2	-1.62	1.69
ALDH3A1	-3.08	1.69
PLEKHA1	-1.89	1.69
C7orf36	-1.51	1.69
SLK	-1.64	1.69
ATP13A2	-1.65	1.69
TCF15	-1.80	1.69
FKBP4	-1.80	1.69
TNFAIP6	-1.78	1.69

BAZ1A	-1.62	1.69
MEG3	-1.51	1.90
MMRN2	-1.59	1.90
TRIM47	-1.53	1.90
LPCAT4	-1.51	1.90
BIN1	-1.59	1.90
VIP	-1.65	1.90
ABI3BP	-2.02	1.90
KRAS	-1.51	1.90
SLC12A2	-1.69	1.90
ANGPTL4	-3.53	1.90
UGP2	-1.51	1.90
ALDH1A2	-2.41	1.90
TUBB3	-1.95	1.90
ISG20	-1.97	1.90
TUBB2A	-1.61	1.90
SLC16A5	-1.52	1.90
SLC35A1	-1.70	1.90
OPTN	-1.51	2.41
DCBLD2	-1.67	2.41
DHCR7	-1.72	2.41
FBXO11	-1.56	2.41
SERPINH1	-1.53	2.41
RAB11A	-1.55	2.41
ITGAV	-2.13	2.41
SRPK1	-1.55	2.41
ARHGAP21	-1.52	2.41
HMOX1	-3.13	2.41
ARMC7	-1.53	2.41
SLC38A10	-1.58	2.41
PDLIM7	-1.97	2.41
LIPG	-2.04	2.41
REEP5	-1.70	2.41
IFNGR1	-1.52	2.41
ASS1	-1.65	2.41
HMGCS1	-2.10	2.41
CD276	-1.63	2.77
FLRT3	-1.63	2.77
TGFBI	-2.14	2.77
BMPR2	-2.05	2.77
CROP	-1.57	2.77
KRT19	-1.65	2.77
ATXN3	-1.59	2.77

INTS6	-1.52	2.77
ATP1B3	-1.53	2.77
RAB3GAP1	-1.56	2.77
F2RL1	-1.61	2.77
TUBAL3	-1.53	2.77
TRIM13	-1.64	2.77
C12orf48	-1.72	2.77
EMCN	-1.74	2.77
SUCLA2	-1.64	3.16
IPO11	-1.53	3.16
PRKRIR	-1.70	3.16
AMD1	-1.61	3.16
FTHL3P	-1.53	3.16
SLC44A1	-1.51	3.16
COL1A2	-2.76	3.16
TXNDC1	-1.57	3.51
COL1A2	-2.94	3.51
MAP2K1IP1	-1.53	3.51
CGGBP1	-1.86	3.51
TMEM158	-1.55	3.51
FEM1C	-1.58	3.51
GPX3	-1.58	3.51
DYNC1LI2	-1.50	3.51
LPXN	-1.56	3.51
UBE2Q2	-1.72	3.51
GLCE	-1.85	3.51
PCOLCE2	-1.52	3.92
IGFBP6	-1.59	3.92
CRIP1	-1.93	3.92
WNK4	-1.65	3.92
CEBPZ	-1.94	3.92
COL6A3	-3.05	3.92
CPD	-1.63	3.92
ACSL4	-1.53	3.92
RN7SK	-1.52	3.92
PLEKHA1	-1.58	3.92
TRAM1	-1.70	3.92
CRYZ	-1.65	4.29
KTN1	-1.51	4.29
THOC1	-1.52	4.29
XPO1	-1.60	4.29
BIRC2	-1.63	4.29
RAMP3	-1.59	4.29

LIPG	-1.59	4.29
SMAD5	-1.70	4.29
PAPOLA	-1.78	4.29
SPATA7	-1.52	4.29
MBNL2	-1.73	4.41
CHD9	-1.79	4.41
RAMP3	-1.75	4.41
PDGFRB	-1.53	4.41
NKTR	-1.73	4.41
BCL6B	-1.62	4.76
CRBN	-1.92	4.76
TMEM123	-1.78	4.76
AP1S2	-1.57	4.76
COL6A3	-1.95	4.76
NDUFS2	-1.95	4.76
RB1CC1	-1.75	5.14
VASN	-1.63	5.14
PSMC6	-1.62	5.14
ZNF277	-1.51	5.14
COL1A1	-2.37	5.14
RAB8B	-1.55	5.14
DDX3X	-1.55	5.51
TROVE2	-1.58	5.51
MATR3	-1.73	5.51
THBS2	-1.66	5.54
DCN	-1.68	5.85
EIF3E	-1.67	5.92

Downregulated gene probes (FO/FL) (474)

Gene Name	Fold Change	q-value (%)
DNASE1L1	-2.30	0.00
KLF2	-4.97	0.00
BCL2L1	-1.66	0.00
BCAR3	-2.16	0.00
DRAM	-1.68	0.00
LOC57228	-2.56	0.00
INTS3	-1.66	0.00
KIAA1754	-2.02	0.00
ID1	-2.44	0.00
OAS1	-1.59	0.00
ADAMTS1	-6.80	0.00

Upregulated gene probes (FO/FL) (332)

Gene Name	Fold Change	q-value (%)
PSEN2	1.64	0.00
DHRS3	4.09	0.00
CPT2	1.63	0.00
CDH2	1.64	0.00
BCAP29	1.53	0.00
SLC7A7	2.68	0.00
ARFGAP2	1.54	0.00
TMEM88	2.51	0.00
MYO1D	1.79	0.00
FAM89A	2.11	0.00
MGC70857	1.57	0.00

NDRG1	-2.65	0.00	THBS1	2.16	0.00
KLF11	-2.16	0.00	MTMR14	1.60	0.00
DUSP3	-1.67	0.00	CERK	1.77	0.00
ATP8B2	-1.65	0.00	CTSK	3.40	0.00
PLOD3	-1.68	0.00	ADM	4.77	0.00
CDH11	-2.87	0.00	CAMK2B	3.69	0.00
UBE2F	-2.13	0.00	FAM101B	1.66	0.00
CCDC69	-1.58	0.00	MEF2D	1.66	0.00
NKIRAS1	-1.54	0.00	MAPKAPK3	1.58	0.00
PPAP2B	-3.54	0.00	DYNLT1	1.55	0.00
ATP1A1	-1.69	0.00	PPP1R16B	2.38	0.00
ZNF467	-3.09	0.00	GSTZ1	1.68	0.00
ZCCHC24	-1.72	0.00	TIGA1	1.73	0.00
NFKBIA	-3.16	0.00	HDDC2	1.53	0.00
HEY2	-1.63	0.00	CHMP4B	1.52	0.00
OAF	-3.13	0.00	NANOS3	1.55	0.00
PPAP2B	-4.88	0.00	DDX19B	1.51	0.00
MALL	-4.37	0.00	CIRBP	3.87	0.00
PEA15	-1.55	0.00	RPAIN	1.57	0.00
UBR4	-2.50	0.00	APLN	2.91	0.00
SNTB2	-1.63	0.00	FHL2	1.78	0.00
OBFC1	-1.98	0.00	SEC14L1	1.73	0.00
ABI3	-2.49	0.00	ATPAF1	1.63	0.00
COPS8	-1.70	0.00	C7orf47	1.69	0.00
SYTL4	-2.28	0.00	BMP4	2.17	0.00
TTYH3	-1.74	0.00	C20orf100	2.14	0.00
TEAD4	-1.96	0.00	TCEA2	1.51	0.00
SVIL	-1.87	0.00	C22orf29	1.70	0.00
HYAL2	-3.00	0.00	FHL2	2.02	0.00
SLC31A2	-1.50	0.00	MT1F	2.42	0.00
LUZP1	-1.61	0.00	CTHRC1	1.68	0.00
C14orf78	-1.93	0.00	TMEM14C	1.51	0.00
CD68	-1.61	0.00	NAV1	2.03	0.00
IRAK2	-1.54	0.00	CRYL1	1.61	0.00
HCCA2	-1.70	0.00	NDUFA7	1.56	0.00
HEG1	-2.68	0.00	NDST1	1.67	0.00
GOSR2	-1.59	0.00	C10orf10	11.11	0.00
AKR1C3	-1.89	0.00	HLX	1.86	0.00
SDCBP	-1.87	0.00	PRMT1	1.54	0.00
GUK1	-1.61	0.00	HGS	1.67	0.00
CDR2L	-2.55	0.00	ATP5D	1.52	0.00
CGN	-1.95	0.00	ASNS	2.15	0.00
NOS3	-2.43	0.00	MUM1	1.67	0.00

LOC57228	-2.03	0.00	TTC32	1.52	0.00
PHF15	-1.53	0.00	VWF	1.50	0.00
RECK	-1.63	0.00	FAM89A	2.22	0.00
GJC2	-5.17	0.00	TNFAIP8L1	1.97	0.00
SFT2D1	-1.64	0.00	ASMTL	2.06	0.00
IER5	-1.71	0.00	PRKAB1	1.79	0.00
S100A10	-1.50	0.00	DKFZp761P0423	2.24	0.00
TSC22D1	-1.69	0.00	TRMT5	1.76	0.00
TICAM2	-1.83	0.00	ME3	1.52	0.00
CXXC5	-1.93	0.00	ABCB9	1.61	0.00
SLC2A3	-2.45	0.00	FJX1	1.84	0.00
CD59	-2.80	0.00	CSTF3	1.58	0.00
GPR162	-2.43	0.00	LRIG1	1.87	0.00
MTMR11	-2.21	0.00	RASD1	3.02	0.00
C14orf139	-1.79	0.00	TNFRSF4	3.83	0.00
EPHA4	-1.66	0.00	CLDN5	2.03	0.00
C20orf160	-3.00	0.00	GADD45B	1.60	0.00
ARHGEF3	-2.14	0.00	PMM2	1.59	0.00
DNAJA4	-1.75	0.00	RASSF2	1.97	0.00
PLEK2	-2.06	0.00	CD99L2	1.54	0.00
PDLIM4	-1.55	0.00	RNF41	1.66	0.00
KIAA1522	-2.54	0.00	MT1G	1.56	0.00
TPD52L1	-1.52	0.00	EFNA1	1.99	0.00
COLEC11	-1.66	0.00	GINS2	1.58	0.00
GLDC	-2.50	0.00	C20orf127	1.82	0.00
C10orf78	-1.84	0.00	PDGFRL	1.99	0.00
RBMS1	-1.53	0.00	LOC148915	1.64	0.00
PLAU	-2.76	0.00	EXOSC6	1.54	0.00
SLC29A1	-2.32	0.00	LOC91561	1.62	0.00
PMP22	-2.87	0.00	EIF2B2	1.75	0.00
RPS29	-1.64	0.00	CYTL1	2.05	0.00
TMEM189	-1.55	0.00	KIT	3.45	0.00
KAT2A	-1.58	0.00	WFS1	2.67	0.00
HSPB8	-1.62	0.00	MPP4	2.02	0.00
HSPA12B	-7.43	0.00	CCDC106	1.57	0.00
STARD8	-2.72	0.00	EGR1	5.13	0.00
CD59	-1.80	0.00	MYH10	1.62	0.00
HECW2	-2.22	0.00	TCF7L1	1.88	0.00
C1orf225	-2.42	0.00	C1orf97	1.87	0.00
PPP2R2B	-2.31	0.00	ALDH7A1	1.62	0.00
NDST2	-1.81	0.00	LTB	2.16	0.00
SEMA4B	-2.77	0.00	GRK5	2.05	0.00
LYN	-1.91	0.00	PHGDH	2.15	0.00

HIST1H2BK	-3.50	0.00	EWSR1	1.55	0.00
P4HA2	-2.04	0.00	ACOX2	1.80	0.00
THBD	-2.86	0.00	SNX8	1.54	0.00
HYAL1	-4.58	0.00	MGC4172	1.72	0.00
CDC25B	-2.86	0.00	MAGED1	1.56	0.00
NSDHL	-1.94	0.00	ATF3	1.76	0.00
ANXA6	-1.72	0.00	LOC441408	1.50	0.00
EIF4A2	-1.57	0.00	LARP6	1.70	0.00
SEMA3F	-2.12	0.00	RALGDS	1.86	0.00
TRIM5	-1.77	0.00	SPOCD1	1.74	0.00
RAB17	-3.10	0.00	ATP5S	1.60	0.00
UBN1	-1.73	0.00	CERK	1.52	0.00
LIMS2	-1.69	0.00	KIT	2.88	0.00
PROCR	-1.53	0.00	ASMTL	1.80	0.00
OGT	-1.55	0.00	SNORD13	3.08	0.00
STOM	-1.81	0.00	RPS6KB2	1.57	0.00
HSP90B1	-1.94	0.00	GABARAPL1	1.63	0.00
GNA14	-2.16	0.00	P2RX4	1.81	0.00
C9orf3	-1.75	0.00	RNF10	1.55	0.00
ANXA6	-1.70	0.00	CENPM	1.62	0.00
DHH	-2.07	0.00	FAM89A	1.83	0.00
CLDN14	-2.07	0.00	ECHDC2	1.56	0.00
SLC24A6	-1.79	0.00	SMARCC1	1.58	0.00
MRPL9	-1.56	0.00	NSFL1C	1.84	0.00
ZNF589	-1.59	0.00	MOV10L1	1.80	0.00
CHN1	-1.73	0.00	C1orf102	1.75	0.00
ITPR3	-1.93	0.00	CDK5RAP3	1.52	0.00
TEK	-4.18	0.00	C6orf108	1.83	0.00
PPIC	-1.65	0.00	ENC1	1.52	0.00
HIST1H2BD	-4.33	0.00	MGC61598	1.90	0.00
SLC9A3R2	-1.80	0.00	NASP	1.56	0.00
PTMS	-1.67	0.00	EFEMP1	1.85	0.00
C21orf63	-1.64	0.00	FAM43A	2.10	0.00
FLOT1	-1.50	0.00	DTD1	1.55	0.00
GNGT2	-2.42	0.00	GATS	1.82	0.00
S100A13	-1.57	0.00	PRMT1	1.61	0.00
PODXL	-5.77	0.00	SEMA6B	1.70	0.00
C6orf128	-1.83	0.00	SNCAIP	3.93	0.00
P4HA2	-1.75	0.00	RASSF2	2.03	0.00
COL17A1	-4.59	0.00	C13orf15	2.21	0.00
SLC29A1	-2.27	0.00	TMEM185A	1.74	0.00
HCFC1R1	-1.51	0.00	HLA-B	1.70	0.00
C12orf34	-1.62	0.00	FST	2.06	0.00

HSPA1A	-3.21	0.00	CXCR4	3.42	0.00
LPHN2	-2.35	0.00	PDE4B	2.07	0.00
TEK	-4.30	0.00	ABLIM1	1.66	0.00
LFNG	-2.19	0.00	FAM107B	1.91	0.00
TSC22D3	-2.39	0.00	TGFBRAP1	1.75	0.00
P2RY2	-1.61	0.00	MT1E	1.81	0.00
HIST1H2BD	-2.06	0.00	LTB	1.57	0.00
LMAN2L	-1.86	0.00	GIMAP8	2.30	0.00
TSC22D3	-2.31	0.00	PGF	2.51	0.00
ARRB1	-1.58	0.00	C3orf21	1.60	0.00
PRICKLE1	-1.75	0.00	MAGED1	1.73	0.00
PTPLB	-1.53	0.00	STK32B	1.79	0.00
PPAP2A	-2.49	0.00	HNRPK	1.55	0.00
NPC1	-1.78	0.00	NSFL1C	1.72	0.00
C13orf33	-1.62	0.00	SLC35E3	1.56	0.00
GLS	-2.83	0.00	RHOT2	1.55	0.00
MN1	-1.65	0.00	LOC440895	1.57	0.00
LDLR	-2.24	0.00	EDN1	1.65	0.00
FAM70B	-1.85	0.00	STX11	1.61	0.00
BANP	-1.71	0.00	GIMAP6	1.53	0.00
SH3BGRL3	-1.63	0.00	RGL1	1.64	0.00
SP100	-1.54	0.00	MAST4	2.55	0.00
ANXA5	-1.50	0.00	LHFPL2	1.63	0.00
MAP4K2	-1.56	0.00	ADA	2.01	0.00
ZFP36L1	-1.99	0.00	BTF3L4	1.52	0.00
SRGN	-1.67	0.00	RBM24	1.54	0.00
ATP1B1	-1.85	0.00	TCF25	1.54	0.00
LCN6	-10.77	0.00	PPM1H	1.56	0.00
MKNK2	-2.07	0.00	RNF144	2.76	0.00
CALHM2	-1.86	0.00	FKBP11	1.63	0.00
TRIMP1	-2.80	0.00	L3MBTL3	1.54	0.00
IL18BP	-1.92	0.00	TGFB1I1	1.54	0.00
HYAL1	-1.79	0.00	C17orf58	2.16	0.00
SULT1B1	-1.52	0.00	WDR68	1.54	0.00
ADRB2	-1.65	0.00	TMEM14B	1.66	0.00
APOL3	-2.05	0.00	IFT122	1.69	0.00
TNFAIP8L3	-1.93	0.00	LOC644033	1.78	0.00
TBC1D2	-1.56	0.00	FAM64A	1.76	0.00
HS3ST1	-7.34	0.00	NIT2	1.61	0.00
EMP3	-1.96	0.00	GALNAC4S-6ST	1.59	0.00
NFKBIZ	-2.59	0.00	RNF19A	1.62	0.00
COPS8	-1.86	0.00	PHLDA1	1.76	0.00

HEBP1	-1.67	0.00	CAMK2N1	1.50	0.00
ZBTB46	-1.72	0.00	FOSB	5.36	0.00
CARHSP1	-1.97	0.00	SHMT1	1.65	0.00
C10orf114	-1.53	0.00	MCM2	1.59	0.00
SDCBP	-1.58	0.00	CDCA4	1.54	0.00
SULT1A3	-2.75	0.00	MTUS1	2.38	0.00
TMEM2	-2.41	0.00	ZNF395	2.25	0.00
SERPINE2	-3.12	0.00	VASH1	2.86	0.00
ITGA6	-1.72	0.00	C1orf97	1.51	0.00
LOC401720	-2.80	0.00	PIM3	2.36	0.00
PODXL	-3.75	0.00	BCKDHB	1.51	0.00
SLCO2A1	-30.21	0.00	CHRNA1	2.74	0.00
SHB	-1.62	0.00	CXCL12	1.52	0.00
TMBIM1	-2.48	0.00	PCK2	2.02	0.00
INSIG1	-2.17	0.00	PDGFB	1.62	0.00
PLAT	-4.69	0.00	GADD45A	1.63	0.00
FLJ20489	-1.96	0.00	CHST7	1.90	0.00
KLF4	-3.63	0.00	HCP5	1.85	0.00
NDRG4	-1.69	0.00	CTDSPL	1.65	0.00
SULT1A1	-1.80	0.00	RAB11FIP1	1.60	0.00
SULT1A4	-2.76	0.00	MT1A	1.56	0.00
NQO1	-1.52	0.00	SLC35C2	1.51	0.00
LPCAT2	-1.65	0.00	OSAP	2.50	0.00
ZNF185	-2.94	0.00	CTNNBIP1	2.05	0.00
COL13A1	-1.56	0.00	TOMM20	1.67	0.00
SLC27A3	-2.09	0.00	RBBP9	1.59	0.00
UBFD1	-1.88	0.00	C6orf85	1.66	0.00
ZBTB20	-1.82	0.00	DHRS1	1.58	0.00
MPZL2	-1.95	0.00	CXCR4	2.77	0.00
HIST1H3D	-1.58	0.00	C19orf22	1.81	0.00
HYAL3	-1.88	0.00	LIG1	1.53	0.00
ATP1B1	-1.77	0.00	GPR116	1.66	0.00
PHTF1	-1.52	0.00	MPP1	1.66	0.00
FTHL12	-1.51	0.00	C17orf58	2.18	0.00
BANP	-1.51	0.00	RNF144B	1.59	0.00
ISG20	-1.80	0.00	LOC730534	1.65	0.00
FUK	-2.45	0.00	FOXO1	1.62	0.00
SYT11	-1.66	0.00	LXN	3.50	0.00
GSDMB	-1.50	0.00	FST	2.32	0.00
SRGN	-1.73	0.00	RAD51C	1.70	0.00
LARP6	-1.52	0.00	N4BP3	1.58	0.00
H2AFJ	-1.51	0.00	PDGFB	1.72	0.00
ATP6V1D	-1.54	0.00	SYT15	1.52	0.00

PIK3C2B	-1.71	0.00	ALDH1A3	2.00	0.00
MORG1	-1.80	0.00	FOS	1.80	0.00
MGC10997	-1.55	0.00	LOX	2.04	0.00
DAPP1	-1.52	0.00	TCF4	1.69	0.00
QPCT	-1.64	0.00	ROBO4	1.63	0.00
AKR1B1	-2.43	0.00	BMX	1.56	0.00
CLDN15	-7.09	0.00	ENDOGL1	1.52	0.00
CROT	-2.28	0.00	LOC642342	1.76	0.00
C15orf52	-1.53	0.00	OSAP	2.38	0.00
PLVAP	-1.89	0.00	IL11RA	1.56	0.00
KLF9	-1.70	0.00	LIMCH1	2.36	0.00
SC4MOL	-2.02	0.00	SDPR	2.02	0.00
TMEM184B	-1.56	0.00	CBS	1.69	0.00
VEGFC	-2.62	0.00	CMTM7	1.60	0.00
PLAC9	-3.44	0.00	ALDH1A3	2.23	0.00
VGLL4	-1.54	0.00	EFNA1	1.56	0.00
MAFB	-1.67	0.00	HMGN2	1.54	0.00
FTHL8	-1.51	0.00	C17orf58	2.30	0.00
APOL2	-1.60	0.00	HNMT	1.69	0.00
CLDN15	-1.90	0.00	BMP2	1.60	0.00
C1QTNF6	-1.78	0.00	HNRPA1P4	1.51	0.00
FILIP1L	-2.46	0.00	GJA4	1.99	0.00
FTHL11	-1.75	0.00	PDE7B	2.83	0.00
FKBP4	-1.81	0.00	CHRNA1	2.04	0.00
SSH2	-1.67	0.00	CCNA1	2.22	0.00
PDIA4	-1.55	0.00	KIAA0494	1.71	0.00
BCL3	-1.96	0.00	ESM1	1.95	0.00
GFPT2	-2.04	0.00	MTE	1.63	0.00
FILIP1L	-2.02	0.00	SSBP4	1.83	0.00
TPP1	-1.51	0.00	LOC642817	1.55	0.00
EPHB4	-1.92	0.00	FBP1	1.53	0.00
TMEM173	-2.27	0.00	BTF3L4	1.54	0.00
TSKU	-1.55	0.00	NMT2	2.11	0.00
PAPSS1	-1.89	0.00	VWCE	1.50	0.00
MATR3	-1.63	0.00	GPIHBP1	3.83	0.00
AKR1C4	-2.01	0.00	FRMD6	1.58	0.00
P4HA1	-1.52	0.00	C12orf26	1.69	0.00
RAMP2	-1.70	0.00	OSBPL10	1.96	0.00
CFLAR	-1.82	0.00	SNRK	1.76	0.00
SEC61A2	-1.54	0.00	SNRK	1.80	0.00
PPP1R3C	-2.45	0.00	DPYSL4	1.53	0.00
MYCN	-2.92	0.00	PRDM1	2.48	0.00
ADAMTSL1	-1.61	0.00	IL8	3.25	0.00

CYBRD1	-1.54	0.00	RBP1	1.59	0.00
LYPD5	-2.47	0.00	TNFSF10	1.55	0.00
LY96	-1.61	0.00	SPHK1	1.72	0.00
TMEM50B	-1.51	0.00	C18orf34	2.17	0.00
LAMC2	-1.66	0.00	ESM1	1.83	0.00
CACYBP	-1.55	0.00	UBTD1	1.63	0.00
MRPS6	-2.36	0.00	TXNRD1	1.59	0.00
RRAS	-1.58	0.00	IL8	2.61	0.00
MAP1B	-1.51	0.00	SFRS5	1.61	0.00
GBGT1	-1.68	0.00	PC-3	1.67	0.00
HIST2H2BE	-1.83	0.00	MYRIP	1.84	0.00
CASK	-1.92	0.00	PRND	2.84	0.00
MYCT1	-2.20	0.00	PSAT1	1.66	0.00
HTATIP2	-1.60	0.00	SLC7A5	1.68	0.00
MAMLD1	-1.67	0.00	CCND2	3.76	0.00
S100A3	-3.78	0.00	EVI1	1.58	0.00
PLEKHB2	-1.81	0.00	GIMAP4	2.06	0.00
SULT1A3	-2.26	0.00	TXNRD1	1.51	0.00
ADAM15	-1.50	0.00	ANGPTL2	1.67	0.00
IFNAR1	-1.76	0.00	CYP26B1	1.77	0.00
KTELC1	-1.51	0.00	PNMA2	1.81	0.00
CYP1A1	-2.13	0.00	DACH1	1.55	0.00
TRIB2	-1.52	0.00	MTUS1	1.77	0.00
GDF3	-12.01	0.00	MYO1B	1.61	0.00
ITGB4	-2.07	0.00	CHST1	1.97	0.00
E2F7	-1.63	0.00	LOC648210	1.52	0.00
ASS1	-1.55	0.00	CLEC1A	1.69	0.00
CNPY4	-1.53	0.00	GIMAP5	2.31	0.00
AXL	-1.52	0.00	FABP4	2.11	0.00
CRIP1	-1.78	0.00	NTN4	1.69	0.00
IFI27	-1.82	0.00	DACT3	1.84	0.00
ITGA10	-2.40	0.00	TMEM163	1.92	0.00
RNASE1	-2.37	0.00	MYO5C	2.75	0.00
RAMP2	-2.18	0.00	C1orf24	1.55	0.00
HSPE1	-1.61	0.00	CCL15	2.71	0.00
ADORA2A	-1.89	0.00	DDIT4L	1.88	0.00
FAM107A	-1.92	0.00	IL17D	1.59	0.10
TMEM100	-2.36	0.00	LOC653355	2.22	0.10
MPZL2	-1.68	0.00	CCND2	1.50	0.10
HMOX1	-2.84	0.00	SFRS5	1.56	0.10
ITGB4	-4.10	0.00	SCHIP1	1.50	0.10
GPER	-3.35	0.00	CCL23	1.51	0.10
GPER	-3.02	0.00	KCNF1	1.79	0.10

C8orf4	-2.65	0.00	CNTNAP3	2.02	0.10
ORAI1	-1.67	0.00	CXADR	2.36	0.10
TRAK1	-1.74	0.00	GMFB	1.55	0.10
ATP11C	-1.71	0.00	GIMAP7	1.61	0.10
GPX3	-1.57	0.00	FAM116B	1.52	0.10
ABCC3	-1.70	0.00	TK1	1.55	0.10
NRGN	-1.65	0.00	KRT7	2.31	0.10
HSPA2	-2.95	0.00	SLITRK4	1.55	0.27
TMEM171	-1.68	0.00	IGFBP3	2.03	0.27
ITGA9	-1.58	0.00	ACSS1	1.96	0.27
FILIP1L	-2.32	0.00	INHBB	1.55	0.27
SLC20A1	-1.54	0.00	PPARG	1.60	0.27
RNASE1	-1.95	0.00	STC2	1.96	0.27
ENTPD1	-2.77	0.00	ANGPT2	2.55	0.34
HMGCR	-1.55	0.00	FNDC5	2.98	0.34
ADAMTS9	-1.94	0.00	CXCL12	1.63	0.34
C12orf57	-1.50	0.00	LYVE1	1.67	0.54
HIST2H2AC	-2.27	0.00	MGC16121	1.52	0.54
C1QTNF1	-1.50	0.00	CLEC4GP1	1.51	0.78
PRCP	-1.74	0.00	CLEC1B	1.60	0.78
PTPLB	-1.51	0.00	IGFBP3	1.71	1.01
FBXW7	-1.55	0.00	CPA4	1.79	1.17
ITPKA	-1.59	0.00			
LIPG	-1.55	0.00			
ZMPSTE24	-1.56	0.00			
TUBA4A	-1.74	0.00			
SAP30L	-1.67	0.00			
PHLDA3	-1.74	0.00			
FAM70B	-1.51	0.00			
TLR4	-1.85	0.00			
FGR	-1.53	0.00			
TPST2	-2.75	0.00			
RGS3	-1.51	0.00			
GRB14	-1.84	0.00			
DNAJA1	-1.60	0.00			
CRELD1	-1.70	0.00			
FNDC4	-1.54	0.00			
COL17A1	-1.73	0.00			
CPNE8	-1.60	0.09			
TFF3	-1.67	0.09			
SLC38A2	-2.17	0.09			
HIST2H2AA3	-3.42	0.09			
CPNE8	-1.74	0.09			

CALCRL	-3.43	0.09
ACSS2	-1.54	0.09
MPZL2	-2.37	0.09
HSP90AA1	-1.94	0.09
PPP1R3F	-1.64	0.09
HSPH1	-3.19	0.09
MRAS	-1.65	0.09
NTHL1	-1.66	0.09
S100A4	-5.41	0.09
TBXA2R	-1.61	0.09
MEIS2	-1.70	0.09
PAPSS1	-1.59	0.09
HIST1H2BK	-1.64	0.09
CLIP2	-1.51	0.09
FCN3	-6.95	0.09
SULT1A2	-1.77	0.09
HSPD1	-1.54	0.09
AQP1	-1.94	0.09
HSPA1B	-2.70	0.09
GRRP1	-1.80	0.09
LOC88523	-1.72	0.09
EMCN	-1.58	0.09
IGFBP5	-10.66	0.09
GSN	-1.96	0.09
OSBPL8	-1.61	0.09
CLDN1	-1.62	0.09
ADAMTS6	-1.79	0.09
FAM167B	-3.25	0.09
TNFRSF25	-1.69	0.09
OPRL1	-1.52	0.09
DDIT4	-1.81	0.09
ITM2A	-1.61	0.09
LOC650263	-1.70	0.09
PPP1R14A	-1.78	0.09
SLCO4A1	-2.16	0.09
S100A4	-5.69	0.09
SPCS3	-1.69	0.09
CLIC3	-2.69	0.09
IGFBP5	-18.66	0.09
GLCE	-1.50	0.09
MLKL	-1.58	0.09
SYNC1	-1.55	0.09
PMEPA1	-1.85	0.09

ADAM15	-1.72	0.09
TCF15	-1.72	0.09
TPST2	-2.63	0.09
SASH1	-1.52	0.27
FLJ11795	-1.85	0.27
ATP1B3	-1.59	0.27
IL32	-1.57	0.27
PLTP	-1.95	0.27
LPAR5	-1.82	0.27
CSRP2	-2.36	0.27
PALLD	-2.30	0.27
CHORDC1	-1.58	0.27
AKR1C2	-3.41	0.27
ANPEP	-1.67	0.27
ANKRD55	-1.92	0.27
HSP90AA1	-2.36	0.27
S100P	-1.91	0.27
HSPA2	-2.76	0.27
VIP	-1.77	0.27
ATP11C	-1.51	0.27
PTHLH	-1.57	0.27
IFIT1	-1.55	0.27
ZDHHC17	-1.56	0.27
SLC5A3	-1.68	0.27
MYCT1	-1.96	0.27
CXCR7	-2.27	0.34
FLRT3	-1.55	0.34
ACAD11	-1.68	0.34
BMPR2	-1.62	0.34
ITGAV	-1.58	0.34
PDLIM7	-1.76	0.34
CRYBA4	-2.06	0.34
HIST2H2AA3	-2.26	0.34
FAM24B	-2.56	0.34
CD14	-1.72	0.34
JAG1	-1.73	0.34
ADAM15	-1.71	0.34
TM7SF2	-1.68	0.34
KCNJ2	-1.67	0.34
LOC346887	-2.09	0.34
CTSH	-1.53	0.34
HTRA1	-1.80	0.34
CXCR7	-3.25	0.34

H19	-1.81	0.38
STARD10	-1.55	0.38
ABCB6	-1.51	0.38
CEBPD	-1.87	0.38
APLNR	-2.27	0.38
KIAA0363	-1.80	0.38
TUBB3	-1.73	0.38
LOC731895	-1.58	0.38
PI16	-30.35	0.38
PTGIS	-1.55	0.38
C6orf15	-1.66	0.38
FAM38B	-1.52	0.38
PTGS1	-1.83	0.38
PTHLH	-1.71	0.38
PRRX1	-1.62	0.38
C12orf48	-1.81	0.38
ALDH3A1	-3.52	0.54
COL5A2	-1.58	0.54
HIST1H1C	-1.69	0.54
FTHL3P	-1.72	0.54
PRSS35	-1.51	0.54
IL32	-1.73	0.54
ALDH1A2	-1.56	0.54
VCAN	-2.20	0.54
HAPLN1	-1.52	0.54
CAPN11	-1.67	0.78
CHP	-1.60	0.78
SELE	-1.67	0.78
ASS1	-2.48	0.78
ADCY4	-1.60	0.78
ANGPTL4	-2.11	1.01
SLC16A5	-1.51	1.01
BEX1	-4.02	1.17
CRYAB	-3.57	3.03
COL1A2	-1.53	3.39

Downregulated gene probes (VO/VL) (486)			**Upregulated gene probes (VO/VL) (316)**		
Gene Name	**Fold Change**	**q-value (%)**	**Gene Name**	**Fold Change**	**q-value (%)**
GJC2	-5.90	0.00	MTUS1	2.26	0.00
GSN	-2.01	0.00	DHRS3	3.42	0.00
LIMS2	-1.91	0.00	GALNAC4S-	1.88	0.00

			6ST		
LFNG	-2.52	0.00	ASB1	1.58	0.00
ABI3	-3.10	0.00	SPOCD1	1.63	0.00
RNASE1	-2.47	0.00	C17orf58	2.22	0.00
SOX13	-1.59	0.00	EWSR1	1.57	0.00
CXXC5	-2.37	0.00	RALGDS	1.85	0.00
CARHSP1	-2.36	0.00	C6orf108	1.99	0.00
IL18BP	-2.11	0.00	PMM2	1.79	0.00
ATP1A1	-1.59	0.00	C17orf58	2.09	0.00
HEG1	-3.32	0.00	GIMAP8	2.44	0.00
CD59	-1.95	0.00	NAV1	1.96	0.00
SULT1A4	-2.91	0.00	FAM89A	1.82	0.00
ITGB4	-4.54	0.00	RAD51C	2.03	0.00
TSC22D3	-2.48	0.00	FJX1	1.90	0.00
ZNFX1	-1.56	0.00	OSBPL10	2.13	0.00
CSRP2	-2.03	0.00	PGF	2.68	0.00
NDRG1	-2.37	0.00	ASH2L	1.67	0.00
PLAU	-2.68	0.00	MAGED1	1.79	0.00
PODXL	-5.96	0.00	ASMTL	1.76	0.00
C20orf160	-3.37	0.00	DYNLT1	1.74	0.00
KLF2	-5.07	0.00	AK2	1.57	0.00
CDH11	-2.88	0.00	ADM	5.01	0.00
UBN1	-1.80	0.00	LOC730534	1.73	0.00
SLC29A1	-2.33	0.00	MTUS1	1.98	0.00
PPIC	-1.57	0.00	WFS1	2.57	0.00
CDR2L	-2.66	0.00	CDCA7L	1.55	0.00
SLC29A1	-2.03	0.00	ENC1	1.64	0.00
NFKBIA	-3.01	0.00	TOMM20	1.87	0.00
VGLL4	-1.67	0.00	ACBD6	1.51	0.00
ITPR3	-2.12	0.00	IL17D	1.55	0.00
TSC22D1	-1.64	0.00	RPS6KB2	1.50	0.00
LDLR	-2.31	0.00	CTHRC1	1.69	0.00
SYTL4	-2.22	0.00	HBEGF	1.58	0.00
APOL2	-1.57	0.00	SNCAIP	4.33	0.00
GPR162	-2.79	0.00	MAGED1	1.53	0.00
CDC25B	-3.12	0.00	CIRBP	3.43	0.00
GNA14	-2.21	0.00	SLC35C2	1.52	0.00
OBFC1	-2.23	0.00	DDX19B	1.54	0.00
FUK	-2.55	0.00	ZNF395	2.09	0.00
THBD	-3.11	0.00	C10orf10	10.50	0.00
KIAA1522	-2.52	0.00	LHFPL2	1.61	0.00
HIST1H2BD	-4.31	0.00	FAM43A	1.90	0.00
PPAP2B	-3.20	0.00	C17orf58	2.19	0.00

SLC24A6	-2.15	0.00	C20orf100	1.99	0.00
TEK	-4.49	0.00	CERK	1.97	0.00
TEK	-4.54	0.00	DKFZp761P0423	2.12	0.00
HIST1H2AC	-1.52	0.00	CYR61	1.52	0.00
COPS8	-1.80	0.00	SLC35E3	1.71	0.00
RNASE1	-2.31	0.00	SH3BP4	1.51	0.00
BCL3	-2.16	0.00	MGC70857	1.67	0.00
OAF	-3.12	0.00	ATPAF1	1.65	0.00
DNASE1L1	-2.35	0.00	NSFL1C	1.78	0.00
HYAL2	-3.16	0.00	BTF3L4	1.53	0.00
ZFP36L1	-1.83	0.00	GIMAP7	1.80	0.00
BCAR3	-2.22	0.00	EDN1	1.92	0.00
ATP8B2	-2.04	0.00	TGFBRAP1	2.09	0.00
MTMR11	-2.19	0.00	FTSJ1	1.67	0.00
ZNF467	-3.45	0.00	SFRS2	1.52	0.00
HIST1H2BK	-3.40	0.00	FHL2	2.01	0.00
GNGT2	-2.48	0.00	ALS2CR4	1.65	0.00
CTSL1	-1.50	0.00	KIAA0101	1.56	0.00
HSPB8	-1.81	0.00	NDUFA7	1.56	0.00
MN1	-1.81	0.00	MAPKAPK3	1.57	0.00
PIK3C2B	-1.80	0.00	CXCR4	3.02	0.00
ITGB4	-2.18	0.00	MPP1	1.65	0.00
ZCCHC24	-1.77	0.00	FHL2	1.70	0.00
EPHB4	-2.04	0.00	CXCR4	3.53	0.00
MKNK2	-2.35	0.00	TMEM185A	1.57	0.00
CD59	-2.74	0.00	SPRY2	1.53	0.00
SAMD14	-1.57	0.00	STX11	1.63	0.00
SLC16A5	-1.60	0.00	TCF7L1	1.85	0.00
HCCA2	-1.74	0.00	SPC24	1.61	0.00
IKBKB	-1.66	0.00	TMEM88	1.98	0.00
MGC10997	-1.58	0.00	SMARCC1	1.67	0.00
HSPA12B	-7.82	0.00	TCF25	1.52	0.00
C14orf78	-2.11	0.00	CDH2	1.63	0.00
ANKS1A	-1.54	0.00	MGC4172	1.76	0.00
LY96	-1.70	0.00	GATS	1.88	0.00
PAPSS1	-1.66	0.00	RASSF2	2.38	0.00
PEA15	-1.56	0.00	EGR1	3.96	0.00
TMEM184B	-1.68	0.00	KRT7	2.33	0.00
RAMP2	-2.14	0.00	C19orf48	1.51	0.00
TTYH3	-1.76	0.00	MPP4	2.08	0.00
HSPD1	-1.51	0.00	CAMK2N1	1.82	0.00
RPS29	-1.81	0.00	PSEN2	1.64	0.00
ZBTB46	-1.95	0.00	STK32B	2.02	0.00

HIST1H2BD	-2.16	0.00	LIG1	1.52	0.00
SLCO2A1	-32.25	0.00	PDGFRL	2.13	0.00
ORAI1	-1.71	0.00	NSFL1C	1.76	0.00
TSC22D3	-2.96	0.00	NRIP3	1.66	0.00
ODZ3	-1.55	0.00	THBS1	2.30	0.00
LMCD1	-1.90	0.00	CRYL1	1.57	0.00
TMEM173	-2.32	0.00	C3orf26	1.69	0.00
ADAMTS1	-6.59	0.00	TMEM14B	1.73	0.00
UBE2F	-2.32	0.00	CPT2	1.55	0.00
NOS3	-3.28	0.00	C6orf85	1.61	0.00
CLDN15	-6.76	0.00	SLC7A7	2.70	0.00
SULT1A4	-1.53	0.00	NIT2	1.61	0.00
TSKU	-1.57	0.00	PRKAB1	1.63	0.00
TPST2	-2.82	0.00	INHBB	1.55	0.00
ID1	-2.61	0.00	CSTF3	1.50	0.00
DHH	-2.61	0.00	BMP4	2.26	0.00
IFI27	-1.78	0.00	EWSR1	1.57	0.00
ADAM15	-1.78	0.00	TCF4	1.87	0.00
TPST2	-2.95	0.00	MT1E	2.00	0.00
GUK1	-1.69	0.00	P2RX4	1.75	0.00
RAMP2	-1.77	0.00	APLN	3.10	0.00
PPP1R3C	-3.01	0.00	KIAA0494	1.78	0.00
SLC27A3	-2.63	0.00	MGC16121	1.54	0.00
LYN	-1.92	0.00	RNF144B	1.74	0.00
DDIT4	-2.06	0.00	CAMK2B	3.28	0.00
MAP4K2	-1.73	0.00	MT1F	2.22	0.00
KIAA1754	-1.96	0.00	CHST1	2.00	0.00
HIST2H2BE	-1.88	0.00	KIT	2.83	0.00
MOBP	-1.68	0.00	PIM3	2.11	0.00
PPAP2B	-4.92	0.00	GIMAP4	2.27	0.00
RRAS	-1.68	0.00	C13orf15	1.97	0.00
HS3ST1	-6.93	0.00	GSTZ1	1.52	0.00
ABCC5	-1.50	0.00	HDDC2	1.71	0.00
PMP22	-3.15	0.00	LXN	3.29	0.00
TNFAIP8L3	-1.77	0.00	CTPS	1.68	0.00
STARD8	-2.34	0.00	EIF2B2	1.90	0.00
NDST2	-1.92	0.00	ASMTL	1.77	0.00
STOM	-1.68	0.00	HNMT	1.65	0.00
MALL	-4.55	0.00	GJA4	1.93	0.00
IER5	-1.73	0.00	LIMCH1	2.24	0.00
ACSS2	-1.57	0.00	ACP1	1.63	0.00
NDRG4	-1.76	0.00	PDE7B	3.11	0.00
FAM167B	-3.27	0.00	GABARAPL1	1.75	0.00

P4HA2	-1.98	0.00	C18orf34	2.44	0.00
PNPLA6	-1.53	0.00	PDE4B	2.52	0.00
PLOD3	-1.85	0.00	MYO1D	1.71	0.00
PODXL	-3.95	0.00	LOC728014	1.56	0.00
MAFB	-1.78	0.00	RASSF2	1.98	0.00
TPP1	-1.55	0.00	NASP	1.61	0.00
SULT1A1	-1.57	0.00	CHRNB1	1.51	0.00
AKR1C3	-1.88	0.00	PPP1R16B	2.23	0.00
KLF4	-3.85	0.00	LRIG1	1.84	0.00
ITGA6	-2.27	0.00	IFT122	1.57	0.00
PLVAP	-1.88	0.00	ESM1	1.87	0.00
PPAP2A	-2.62	0.00	RBM24	1.59	0.00
CRYBA4	-1.73	0.00	ABLIM1	1.60	0.00
EMP3	-2.04	0.00	CCDC106	1.68	0.00
C10orf78	-1.93	0.00	HNRPK	1.74	0.00
ARIH1	-1.51	0.00	LOC644033	1.94	0.00
ARRB1	-1.52	0.00	DDHD2	1.58	0.00
TRAK1	-1.83	0.00	CTDSPL	1.51	0.00
SHB	-1.71	0.00	NOX4	1.75	0.00
TMBIM1	-2.25	0.00	LTB	2.47	0.00
JAG1	-1.73	0.00	GPIHBP1	2.64	0.00
TNS1	-1.64	0.00	CLDN5	1.87	0.00
P4HA2	-1.95	0.00	C1orf102	1.61	0.00
P2RY2	-1.75	0.00	CERK	1.64	0.00
CLDN14	-2.84	0.00	MAST4	2.12	0.00
RBMS1	-1.66	0.00	MOV10L1	1.77	0.00
PRRG2	-1.59	0.00	GMFB	2.12	0.00
PRICKLE1	-2.15	0.00	PTTG1	1.52	0.00
GRB14	-1.79	0.00	TTC32	1.56	0.00
ASAP3	-1.63	0.00	NTN4	1.79	0.00
TNFAIP1	-1.60	0.00	MTE	1.95	0.00
TMEM2	-2.68	0.00	DDIT4L	2.29	0.00
ENTPD1	-2.83	0.00	LOC642197	1.57	0.00
STAT6	-1.52	0.00	GADD45A	1.57	0.00
ST3GAL1	-1.67	0.00	FAM89A	2.21	0.00
COPS8	-1.70	0.00	FABP5	1.61	0.00
ACSS2	-1.56	0.00	RBBP9	1.51	0.00
ADAMTSL1	-1.53	0.00	CHST7	1.75	0.00
PI16	-28.84	0.00	BST1	1.60	0.00
KIAA0363	-1.79	0.00	SNRK	1.74	0.00
C14orf139	-1.88	0.00	C12orf26	1.55	0.00
KLF11	-2.38	0.00	MUM1	1.58	0.00
FURIN	-1.66	0.00	SLC25A15	1.58	0.00

SEMA4B	-3.03	0.00	RGL1	1.59	0.00
AQP1	-2.03	0.00	FST	2.46	0.00
RNF11	-1.53	0.00	LOC148915	1.68	0.00
HTATIP2	-1.66	0.00	PC-3	1.91	0.00
ZMIZ2	-1.52	0.00	CYP26B1	1.97	0.00
ANPEP	-1.92	0.00	ITGB3BP	1.56	0.00
LOC57228	-2.49	0.00	PRDM1	2.68	0.00
LMAN2L	-1.93	0.00	TNFAIP8L1	1.62	0.00
ASS1	-2.36	0.00	CTNNBIP1	2.15	0.00
LOC652968	-1.56	0.00	KCNMB4	1.51	0.00
S100A3	-4.28	0.00	C1orf97	1.92	0.00
PLAC9	-2.79	0.00	GPR116	1.68	0.00
PPAP2A	-1.64	0.00	MYRIP	1.97	0.00
PLAT	-3.76	0.00	ABCB9	1.61	0.00
CHST3	-1.54	0.00	ALDH1A3	1.93	0.00
DNAJB2	-1.56	0.00	MYH10	1.73	0.00
SULT1A3	-2.65	0.00	CYTL1	2.11	0.00
PTMS	-1.82	0.00	RNF144	2.71	0.00
MYCT1	-1.70	0.00	C1orf97	1.53	0.00
RECK	-1.63	0.00	RASD1	2.24	0.00
HYAL3	-2.08	0.00	ABCE1	1.58	0.00
NPC1	-1.94	0.00	VASH1	2.11	0.00
CGN	-1.80	0.00	PFAS	1.62	0.00
MPZL2	-2.58	0.00	C1orf24	1.52	0.00
APOL3	-2.02	0.00	C20orf127	1.94	0.00
MAMLD1	-1.61	0.00	SPHK1	1.68	0.00
MRPS6	-2.80	0.00	ACOX2	1.80	0.00
TLR4	-1.95	0.00	MGC61598	1.95	0.00
C1QTNF6	-2.07	0.00	TXNRD1	1.61	0.00
COL17A1	-4.70	0.00	KIT	3.67	0.00
C1orf225	-2.52	0.00	RNF19A	1.64	0.00
FAM24B	-2.81	0.00	IL8	2.21	0.00
FGR	-1.66	0.00	TRMT5	1.65	0.00
FAM70B	-1.80	0.00	ALDH1A3	2.15	0.00
VEGFC	-3.03	0.00	LOC642342	1.85	0.00
TEAD4	-1.95	0.00	MCM6	1.65	0.00
SLC5A3	-1.87	0.00	SFRS5	1.69	0.00
GLDC	-2.56	0.00	OSAP	2.61	0.00
DUSP3	-1.75	0.00	SLC37A4	1.58	0.00
GFPT2	-2.51	0.00	EFNA1	1.82	0.00
UBR4	-3.26	0.00	TIGA1	1.60	0.00
NKIRAS1	-1.50	0.00	PPM1H	1.66	0.00
SH3BGRL3	-1.98	0.00	CTSK	3.13	0.00

SLC9A3R2	-2.01	0.00	SHMT1	1.59	0.00
TICAM2	-1.74	0.00	MYO5C	2.72	0.00
IRAK2	-1.60	0.00	NOL5A	1.52	0.00
SULT1A3	-2.15	0.00	IL8	2.40	0.00
SVIL	-1.69	0.00	SNORD13	2.64	0.00
NRGN	-1.62	0.00	FABP4	1.97	0.00
C6orf128	-1.74	0.00	L3MBTL3	1.58	0.00
S100P	-2.21	0.00	GADD45B	1.57	0.00
ATP6V1D	-1.57	0.00	HCLS1	1.55	0.00
LCN6	-10.38	0.00	FEN1	1.57	0.00
MYCN	-3.20	0.00	C7orf47	1.65	0.00
LOC57228	-2.43	0.00	PNMA2	1.83	0.00
LOC401720	-2.83	0.00	TFIP11	1.52	0.00
ASPHD2	-1.79	0.00	CHRNA1	2.50	0.00
TRIM5	-1.69	0.00	DACH1	1.65	0.00
SULT1A2	-1.56	0.00	IGFBP3	1.95	0.00
S100A4	-5.03	0.00	FST	1.85	0.00
AKR1B1	-2.48	0.00	FAM64A	1.74	0.00
PHLDA3	-1.76	0.00	EFEMP1	1.60	0.00
HIST1H4H	-1.62	0.00	CNOT1	1.57	0.00
ARHGEF3	-2.21	0.00	ALDH7A1	1.59	0.00
DRAM	-1.64	0.00	LOX	1.87	0.00
ATP1B1	-1.85	0.00	LOXL4	1.76	0.00
DHCR7	-1.65	0.00	EVI1	1.68	0.00
ATP1A1	-1.63	0.00	SDPR	1.80	0.00
SDCBP	-1.72	0.00	PDGFB	1.60	0.00
FAM107A	-1.79	0.00	ZNF280D	1.51	0.00
HYAL1	-4.73	0.00	CDC45L	1.64	0.00
ITGA10	-2.38	0.00	CTHRC1	1.76	0.00
SYT11	-1.57	0.00	ANGPT2	3.73	0.00
CROT	-2.17	0.00	MYO1B	1.81	0.00
UBFD1	-1.78	0.00	FBXO32	1.65	0.00
GPER	-2.98	0.00	CXADR	2.44	0.00
CD68	-1.60	0.00	PSAT1	1.59	0.00
LARP6	-1.59	0.00	OSAP	2.48	0.00
SLCO4A1	-2.07	0.00	PHLDA1	1.58	0.00
NSDHL	-1.95	0.00	TNFRSF4	3.23	0.00
PPP2R2B	-2.47	0.00	C3orf21	1.51	0.00
NFKBIZ	-2.83	0.00	C9orf103	1.51	0.00
CASK	-1.79	0.00	FAM107B	1.77	0.00
ZNF185	-2.77	0.00	FRMD6	1.69	0.00
NNMT	-1.68	0.00	FOSB	3.82	0.00
CCDC69	-1.77	0.00	FRMD6	1.64	0.00

PMEPA1	-1.74	0.00	DPYSL4	1.63	0.00
ADORA2A	-1.77	0.00	FAM89A	2.32	0.00
GDF3	-11.08	0.00	RAI14	1.57	0.00
DHCR7	-1.63	0.00	LOC493869	1.63	0.00
HIST2H2AA3	-2.36	0.00	RAB11FIP1	1.82	0.00
CLIP2	-1.56	0.00	BMP2	1.74	0.00
PDLIM7	-1.86	0.00	ACSS1	1.75	0.00
ADAMTS9	-2.25	0.00	SSBP4	1.54	0.00
RECK	-1.55	0.00	CXCL12	1.66	0.00
SEMA3F	-2.40	0.00	CLEC1A	1.64	0.00
CCND3	-1.51	0.00	PCK2	1.68	0.00
SFT2D1	-1.52	0.00	GRK5	1.70	0.00
ACSL5	-1.63	0.00	AKTIP	1.50	0.00
SDCBP	-1.94	0.00	ESM1	1.79	0.00
MOBP	-1.60	0.00	ATF3	1.71	0.00
PLCD3	-1.57	0.00	ASNS	1.92	0.00
RHOJ	-1.55	0.00	TMEM163	1.96	0.00
CRELD1	-1.88	0.00	CHRNA1	2.06	0.00
BIN1	-1.56	0.00	LOC653071	1.53	0.10
HSPH1	-3.11	0.00	TCFL5	1.52	0.10
CFLAR	-1.88	0.00	ANGPTL2	1.54	0.10
BIN1	-1.56	0.00	PHGDH	1.84	0.10
TUBB3	-1.73	0.00	NDST1	1.50	0.10
SLC2A3	-2.51	0.00	HLX	1.69	0.10
PLTP	-1.85	0.00	CENPM	1.53	0.10
DUSP5	-1.67	0.00	ECHDC2	1.53	0.10
ATP13A2	-1.69	0.00	SFRS5	1.62	0.10
CCDC102A	-1.59	0.00	TMEM14C	1.58	0.10
CPNE8	-1.75	0.00	KCNF1	1.52	0.10
TM7SF2	-1.54	0.00	GIMAP5	2.23	0.10
DNAJA1	-1.92	0.00	ABCA1	1.50	0.10
STOM	-1.55	0.00	IGFBP3	1.98	0.10
ADCY4	-1.95	0.00	CNTNAP3	1.74	0.10
CEBPD	-2.36	0.00	LOC387934	1.50	0.19
FCN3	-6.62	0.00	LOC653355	1.88	0.19
SP100	-1.50	0.00	FNDC5	2.68	0.19
TBXA2R	-1.77	0.00	ECHDC3	1.50	0.19
ADAM15	-2.08	0.00	CCNA1	2.52	0.19
MYCT1	-2.39	0.00	GMFG	1.61	0.19
C12orf34	-1.76	0.00	SNRK	1.65	0.19
INSIG1	-2.41	0.00	TXNRD1	1.60	0.19
LYPD5	-2.90	0.00	ADA	1.81	0.19
AKR1C4	-1.96	0.00	PRND	2.15	0.19

HSPA2	-2.42	0.00	DDX10	1.61	0.19
IFNAR1	-1.83	0.00	SLITRK4	1.59	0.19
MPZL2	-1.96	0.00	CCL15	2.71	0.23
LRRC8A	-1.69	0.00	NMT2	1.64	0.23
HCFC1R1	-1.50	0.00	STC2	1.93	0.23
PPP1R3F	-1.66	0.00	DACT3	1.91	0.23
HSP90B1	-2.10	0.00	CCND2	1.57	0.23
STARD10	-1.54	0.00	NMT2	2.03	0.23
TMEM189	-1.64	0.00	CCND2	3.78	0.39
TBC1D2	-1.88	0.00	CPA4	1.72	0.39
INTS3	-1.77	0.00	HOXB5	1.57	0.39
HEY2	-1.51	0.00	PHACTR2	1.50	0.59
OGT	-1.67	0.00	CLEC1B	1.88	0.59
ADAMTS6	-1.58	0.00	LYVE1	1.71	0.59
S100A4	-5.31	0.00			
GBGT1	-1.53	0.00			
PROCR	-1.59	0.00			
MRPL9	-1.59	0.00			
MPZL2	-2.25	0.00			
MEIS2	-1.66	0.00			
CPNE8	-1.67	0.00			
HTRA1	-1.55	0.00			
KLF11	-1.50	0.00			
SNTB2	-1.61	0.00			
COL17A1	-1.73	0.00			
ANXA6	-1.94	0.00			
SPCS3	-1.62	0.00			
FLJ20489	-1.81	0.00			
C8orf4	-2.40	0.00			
PALM	-1.77	0.00			
C21orf63	-1.54	0.00			
PRCP	-1.79	0.00			
LPCAT2	-1.51	0.00			
CXCR7	-3.40	0.00			
HIST1H2BK	-1.61	0.00			
AEBP1	-1.51	0.00			
ZNF589	-1.70	0.00			
CXCR7	-2.61	0.00			
HYAL1	-1.80	0.00			
TNFRSF25	-1.76	0.00			
ANGPTL4	-2.74	0.00			
LPHN2	-2.32	0.00			
CLIC3	-3.15	0.00			

GRRP1	-1.80	0.00
ADAM15	-1.99	0.00
DNASE1L1	-1.60	0.00
GSDMB	-1.55	0.00
MFAP2	-1.65	0.00
SERPINE2	-2.56	0.00
SIPA1	-1.59	0.00
IRF9	-1.51	0.00
C1QTNF1	-1.72	0.00
GPER	-3.06	0.00
LIX1L	-1.50	0.00
TRIMP1	-2.64	0.00
SRGN	-1.56	0.00
GLS	-3.20	0.00
UPP1	-1.52	0.00
FAM110A	-1.52	0.10
CHN1	-1.73	0.10
PDIA4	-1.75	0.10
C13orf33	-1.69	0.10
QPCT	-1.57	0.10
CYP1A1	-2.11	0.10
UBTD2	-1.54	0.10
GPRC5B	-1.51	0.10
EPHA4	-1.68	0.10
DNAJA4	-1.77	0.10
HIST1H3D	-1.56	0.10
PHF15	-1.55	0.10
CD14	-1.99	0.10
GRASP	-1.60	0.10
HSP90AA1	-1.83	0.10
IL32	-1.75	0.10
HSPA1B	-3.68	0.10
PMEPA1	-1.50	0.10
RYBP	-1.61	0.10
RUSC1	-1.59	0.10
HECW2	-2.25	0.10
HSP90AA1	-2.56	0.10
LAMC2	-1.67	0.10
BANP	-1.52	0.10
CALHM2	-1.83	0.10
ARMC7	-1.63	0.10
EFNB1	-1.51	0.10
ACAT2	-1.55	0.19

ATP1B1	-1.76	0.19
PDLIM4	-1.65	0.19
TFF3	-1.67	0.19
BCL9L	-1.51	0.19
HIST1H1C	-1.55	0.19
ZDHHC17	-1.63	0.19
HSPE1	-1.72	0.19
FILIP1L	-2.24	0.19
E2F7	-1.73	0.19
PPP1R14A	-1.93	0.19
IL32	-1.56	0.19
PTGS1	-1.56	0.19
HIST2H2AA3	-3.94	0.19
SQLE	-1.58	0.19
NTHL1	-1.75	0.19
FILIP1L	-2.90	0.19
LPAR5	-1.70	0.19
FILIP1L	-2.26	0.19
HSPA2	-1.94	0.19
HSPA1A	-4.08	0.19
MAP1B	-1.53	0.19
PLEK2	-2.09	0.19
CXCL2	-1.59	0.19
LRRC32	-1.71	0.19
FES	-1.66	0.19
CHORDC1	-1.50	0.19
OAS1	-1.88	0.19
TRIM47	-1.63	0.19
TMEM171	-1.66	0.19
CTSH	-1.51	0.19
FLJ11795	-1.90	0.19
C9orf3	-1.59	0.19
FAM70B	-1.53	0.23
FNDC4	-1.72	0.23
SC4MOL	-2.36	0.23
ITPKA	-1.70	0.23
VCAN	-1.92	0.23
DNAJB1	-1.64	0.23
LOC113386	-1.71	0.23
BST2	-1.60	0.23
BEX1	-3.30	0.23
CRELD2	-1.55	0.23
ITGA9	-1.56	0.23

RAB17	-2.72	0.23
SLC38A2	-2.24	0.23
SELE	-2.54	0.23
TMEM100	-2.63	0.23
KLF9	-1.82	0.23
SCD	-1.55	0.23
BANP	-1.66	0.23
CLDN15	-1.92	0.23
ISG20	-2.03	0.23
CYYR1	-1.57	0.23
CALCRL	-3.71	0.23
TUBA4A	-1.61	0.23
PLEKHB2	-1.63	0.23
HMGCR	-1.83	0.23
SRGN	-1.62	0.39
C12orf57	-1.52	0.39
H19	-1.78	0.39
LOC731895	-1.60	0.39
HIST2H2AC	-2.41	0.39
KCNJ2	-1.66	0.39
KAT2A	-1.60	0.39
AKR1C2	-2.59	0.39
IGFBP5	-8.63	0.39
LHX6	-1.56	0.39
PTPLB	-1.55	0.39
LOC650263	-1.60	0.39
PHTF1	-1.51	0.39
ANKRD55	-1.86	0.39
APLNR	-2.76	0.39
DNAJB11	-1.53	0.39
PALLD	-2.01	0.39
ARL4A	-1.50	0.39
P4HA1	-1.73	0.39
LOC346887	-2.55	0.39
SSH2	-1.53	0.39
ITM2A	-1.54	0.39
MMRN2	-1.80	0.39
C12orf48	-1.63	0.39
IGFBP5	-15.45	0.39
TMEM50B	-1.56	0.39
LOC88523	-1.90	0.39
PLEKHA1	-1.54	0.39
CNKSR3	-1.55	0.39

FTHL8	-1.53	0.39
ASS1	-1.88	0.59
SYNC1	-1.59	0.59
SLC20A1	-1.61	0.59
RHOJ	-1.58	0.59
ATP11C	-1.57	0.59
SC5DL	-1.62	0.59
PTHLH	-1.85	0.59
ATP11C	-1.64	0.59
FBXW7	-1.53	0.59
PTHLH	-1.83	0.59
PRSS35	-1.55	0.59
ANXA6	-1.67	0.59
DNAJB9	-1.57	0.59
CLDN1	-1.59	0.59
SMAD6	-1.64	0.59
CRIP1	-2.06	0.59
TCF15	-1.76	0.96
GPX3	-1.70	0.96
BUB3	-1.67	0.96
CRYAB	-2.55	0.96
FKBP4	-1.78	0.96
AHSA1	-1.63	0.96
ZBTB20	-1.61	0.96
FAM38B	-1.51	0.96
FGFR3	-1.60	0.96
BMPR2	-1.71	0.96
HMGCS1	-1.79	1.29
IFIT1	-1.69	1.29
CPXM2	-1.62	1.29
DKK2	-1.63	1.29
VIP	-1.67	2.27
CHD9	-1.53	2.27
KTN1	-1.50	2.27
ALDH3A1	-3.41	2.27
HMOX1	-2.62	2.27
EMCN	-1.63	3.25
GLCE	-1.55	3.25
ANKRD1	-1.53	4.27
NDUFS2	-2.13	5.90

APPENDIX D

TAQMAN ASSAYS FOR MESSENGER RNA AND MICRORNA VALIDATION

Table D.1 Taqman Probes for Messenger RNA and microRNA Validation

Assay Type	Gene Name	Assay ID
Slco2a1	Solute carrier organic anion transporter family, member 2A1	Hs00194554_m1
Igfbp5	Insulin-like growth factor-binding protein 5	Hs01052296_m1
Gdf3	Growth differentiation factor-3	Hs00220998_m1
Adamts1	ADAM metallopeptidase with thrombospondin type 1 motif, 1	Hs00199608_m1
Klf2	Kruppel-like factor 2	Hs00360439_g1
Klf4	Kruppel-like factor 4	Hs01034973_g1
Calcrl	Calcitonin receptor-like	Hs00907738_m1
Mycn	V-myc myelocytomatosis viral related oncogene, neuroblastoma derived	Hs00232074_m1
Nfkbia	Nuclear factor of κ light polypeptide gene enhancer in B-cells inhibitor, α	Hs00153283_m1
Nos3	Nitric oxide synthase 3	Hs00167166_m1
Id1	Inhibitor of DNA binding 1, dominant negative helix-loop-helix protein	Hs00704053_s1
Dhh	Desert hedgehog homolog (Drosophila)	Hs00368306_m1
Bcl3	B-cell CLL/lymphoma 3	Hs00180403_m1
Tlr4	Toll-like receptor 4	Hs01061963_m1
Shb	Src homology 2 domain containing adaptor protein B	Hs00182370_m1
Fstl1	Follistatin-like 1	Hs03986113_g1
Hdac1	Histone deacetylase 1	Hs02621185_s1
Atf3	Activating transcription factor 3	Hs00231069_m1
Asns	Asparagine synthetase	Hs00155888_m1
Thbs1	Thrombospondin 1	Hs00962908_m1
Prdm1	PR domain containing 1, with ZNF domain	Hs00153357_m1
Bmp4	Bone morphogenetic protein 4	Hs00370078_m1
Ctsk	Cathepsin K	Hs00166156_m1
Egr1	Early growth response 1	Hs00152928_m1
Ccnd2	Cyclin D2	Hs00922419_g1
Fosb	FBJ murine osteosarcoma viral oncogene homolog B	Hs00171851_m1
Sncaip	Synuclein, alpha interacting protein	Hs00193814_m1
Adm	Adrenomedullin	Hs00969450_g1

Assay Type	miRBase Accession	Assay ID
hsa-miR-486-5p	MIMAT0002177	001278
hsa-miR-1244	MIMAT0005896	002791
hsa-miR-483-3p	MIMAT0002173	002339

hsa-miR-486-3p	MIMAT0004762	002093
hsa-miR-139-3p	MIMAT0004552	002313
hsa-miR-923	MIMAT0005715	002153
hsa-miR-382	MIMAT0000737	000572
hsa-miR-433	MIMAT0001627	001028
hsa-miR-543	MIMAT0004954	002376
hsa-miR-485-3p	MIMAT0002176	001277
hsa-miR-1237	MIMAT0005592	002765
hsa-miR-549	MIMAT0003333	001511
hsa-miR-485-5p	MIMAT0002175	001036
hsa-miR-374a	MIMAT0000727	000563
hsa-miR-187	MIMAT0000262	001193
hsa-miR-217	MIMAT0000274	002337
hsa-miR-192	MIMAT0000222	000491
hsa-miR-370	MIMAT0000722	002275

APPENDIX E

SHEAR- AND SIDE-DEPENDENT MICRORNAS IN HAVECS

Table E.1: Shear-responsive microRNA Probes from Microarrays

Downregulated gene probes (FO/VL) (13)

miRNA Name	Fold Change	q-value (%)
hsa-miR-486-5p	-2.60	0.00
hsa-miR-483-3p	-2.15	7.29
hsa-miR-1244	-1.91	7.29
hsa-miR-139-3p	-1.86	7.29
hsa-miR-486-3p	-1.78	0.00
hsa-miR-382	-1.74	7.29
hsa-miR-923	-1.70	11.66
hsa-miR-543	-1.65	15.90
hsa-miR-1237	-1.63	15.90
hsa-miR-433	-1.63	7.29
hsa-miR-485-3p	-1.61	7.29
hsa-miR-549	-1.52	15.90
hsa-miR-485-5p	-1.50	15.90

Upregulated gene probes (FO/VL) (3)

miRNA Name	Fold Change	q-value (%)
hsa-miR-374a	1.51	15.90
hsa-miR-187	1.88	0.00
hsa-miR-217	1.92	15.90

Downregulated gene probes (VO/VL) (13)

miRNA Name	Fold Change	q-value (%)
hsa-miR-1290	-3.27	23.08
hsa-miR-486-5p	-1.93	0.00
hsa-miR-518e:9.1	-1.87	23.08
hsa-miR-548o	-1.79	23.08
hsa-miR-654-3p	-1.72	13.74
hsa-miR-486-3p	-1.70	5.56
hsa-miR-411	-1.69	23.08
hsa-miR-1244	-1.64	13.74
hsa-miR-1300	-1.61	23.08
hsa-miR-647	-1.57	23.08
hsa-miR-192	-1.57	10.38
hsa-miR-923	-1.52	23.08
hsa-miR-139-3p	-1.50	5.56

Upregulated gene probes (VO/VL) (2)

miRNA Name	Fold Change	q-value (%)
hsa-miR-217	1.52	0.00
hsa-miR-187	1.60	0.00

Downregulated gene probes (FO/FL) (4)

miRNA Name	Fold Change	q-value (%)

Upregulated gene probes (FO/FL) (2)

miRNA Name	Fold Change	q-value (%)

hsa-miR-486-5p	-2.67	0.00	hsa-miR-769-3p	1.58	0.00
hsa-miR-923	-1.80	0.00	hsa-miR-187	2.14	0.00
hsa-miR-1244	-1.64	5.08			
hsa-miR-486-3p	-1.64	5.08			

Downregulated gene probes (FO/VO) (2)

miRNA Name	Fold Change	q-value (%)
hsa-miR-485-3p	-1.58	0.00
hsa-miR-485-5p	-1.57	0.00

Upregulated gene probes (FO/VO) (0)

miRNA Name	Fold Change	q-value (%)

Downregulated gene probes (FL/VL) (1)

miRNA Name	Fold Change	q-value (%)
hsa-miR-370	-1.71	0.00

Upregulated gene probes (FL/VL) (0)

miRNA Name	Fold Change	q-value (%)

APPENDIX F

PREDICTIVE GENE TARGETS FOR SHEAR-SENSITIVE MICRORNAS

Table F.1: Predictive Gene Targets for Shear-sensitive microRNAs

miRNA	Predictive mRNA Target
hsa-miR-139-3p	*Fosb*
	Rnf41
hsa-miR-187	*Armc7*
	Cd276
	Cyyr1
	Dync1li2
	Ets1
	Flnc
	Ifnar1
	Lypd1
	Mbnl2
	Nfkbiz
	Pgm2l1
	Plod3
	Sema3f
	Snx27
	Ssh2
	Trib2
hsa-miR-192	*Acp1*
	Apln
	Asb1
	Atf3
	C10orf10
	Ccnd2
	Chrnb1
	Ctnnbip1
	Dynlt1
	Egr1
	Fam129a
	Fosb

	Hoxb5
	Mcm6
	Myo1d
	Nav1
	Ndst1
	Nmt2
	Nrip3
	Osbpl10
	Phactr2
	Phlda1
hsa-miR-486-5p	*Ak2*
	Als2cr4
	Camk2n1
	Ctdspl
	Efna1
	Mylk2
	Prnd
	Rnf41
hsa-miR-148a	*Abcc3*
	Abcc5
	Abi3
	Abi3bp
	Acsl5
	Adamts1
	Adamts6
	Ankrd55
	Anks1a
	Ano6
	Antxr2
	Ap1s2
	Aplnr
	Arhgap21
	Atxn7l1
	Bcl6b
	Bmpr2
	C12orf34
	C12orf48
	C1qtnf6
	Canx
	Cd68
	Cd276

Cdc25b
Cdh11
Cdkn2b
Cggbp1
Chd9
Clcn3
Cnst
Col6a3
Cpd
Creld1
Ctsl1
Cybrd1
Cyyr1
Dcbld2
Dkk2
Dusp1
Dusp3
E2f7
Eif4a2
Endod1
Entpd1
Epb49
Epha4
Ets1
Fam38b
Fbxo11
Fem1c
Flrt3
Fndc4
Furin
Glce
Golm1
Heca
Hecw2
Hey2
Hmox1
Hsp90aa1
Hsp90b1
Hspa12b
Id1
Igfbp5
Ikbkb
Insig1

Ints6
Itga3
Itga10
Itgb8
Itprip
Kat2a
Kiaa1522
Kif1b
Kitlg
Klf4
Klhl5
Ldb2
Ldlr
Lhx6
Lipg
Lphn2
Mafb
Map1b
Mobp
Mras
Mrpl9
Nktr
Npc1
Nqo1
Numb
Odz3
Ogt
Optn
Pea15
Pgm2l1
Phf15
Picalm
Plau
Plekhb2
Pmepa1
Pnpla6
Poxdl
Ppap2b
Pten
Ptgs1
Ptprb
Rab21
Rb1cc1

Rybp
Sertad2
Sh3pxd2a
Slc2a3
Slc38a2
Slc44a1
Slc5a3
Slfn11
Smad5
Sntb2
Snx27
Ssh2
Stard8
Sulf1
Svil
Sync
Tek
Tgfbr2
Tmbim1
Tmem123
Tmem217
Tmem184b
Tmem50b
Tns1
Tpp1
Trak1
Trib2
Ttyh3
Ubfd1
Ubn1
Vgll4
Zcchc24
Zdhhc6
Zdhhc17
Zfhx3
Zmiz2
Znf185
Znfx1

APPENDIX G

OVERREPRESENTED MICRORNA BINDING SEQUENCES IN HUMAN, SHEAR ARRAY

Diana Analysis: Overrepresented microRNA Binding Sites in Shear-sensitive Messenger RNA Dataset

Hexamer	miRNA	p value	Number of genes with hexamer
ACCTCT	hsa-let-7d	3.88E-02	173
ATGCTG	hsa-miR-103	6.36E-04	207
ATGCTG	hsa-miR-107	6.36E-04	207
ACAGGG	hsa-miR-10a	1.95E-03	172
CAGGGT	hsa-miR-10a	1.10E-02	166
ACAGGG	hsa-miR-10b	1.95E-03	172
CAGGGT	hsa-miR-10b	1.10E-02	166
CACTCC	hsa-miR-122	3.56E-02	161
GTGCCT	hsa-miR-124	4.51E-06	214
TGCCTT	hsa-miR-124	2.44E-02	232
ACCTGT	hsa-miR-125a-3p	1.47E-02	179
CAGGGA	hsa-miR-125a-5p	3.50E-02	202
CAGGGA	hsa-miR-125b	3.50E-02	202
CTGTGA	hsa-miR-128a	1.76E-02	213
CTGTGA	hsa-miR-128b	1.76E-02	213
GGGCTT	hsa-miR-129-3p	6.84E-03	162
AAGGGC	hsa-miR-129-3p	1.14E-02	140
AGGGCT	hsa-miR-129-3p	1.35E-02	177
TTGCAC	hsa-miR-130a	5.93E-03	148
TGCACT	hsa-miR-130a	3.42E-02	183
TTGCAC	hsa-miR-130b	5.93E-03	148
TGCACT	hsa-miR-130b	3.42E-02	183
GGACCA	hsa-miR-133a	2.95E-02	134
GGACCA	hsa-miR-133b	2.95E-02	134
AGTCAC	hsa-miR-134	3.28E-03	139
AAGCCA	hsa-miR-135a	1.09E-02	194
AAGCCA	hsa-miR-135b	1.09E-02	194
CCAGCT	hsa-miR-138	1.60E-03	232
ACCAGC	hsa-miR-138	4.17E-02	164
CACCAG	hsa-miR-138	4.98E-02	169
GTCTCC	hsa-miR-139-3p	3.35E-02	152
CTGTGG	hsa-miR-140-3p	2.48E-03	239

ATCTCA	hsa-miR-143	3.05E-02	156
CTGGAC	hsa-miR-145	2.58E-04	176
AGGGCA	hsa-miR-146b-3p	9.15E-04	177
ACAGGG	hsa-miR-146b-3p	1.95E-03	172
CAGGGC	hsa-miR-146b-3p	8.86E-03	190
CCACAC	hsa-miR-147	1.79E-02	161
GCACAC	hsa-miR-147b	2.13E-03	134
CCGCAC	hsa-miR-147b	1.01E-02	50
TGCACT	hsa-miR-148a	3.42E-02	183
TGCACT	hsa-miR-148b	3.42E-02	183
GAGCCA	hsa-miR-149	1.23E-03	194
GGGAGA	hsa-miR-150	1.58E-03	196
CTCCTC	hsa-miR-151-5p	1.67E-02	195
TGCACT	hsa-miR-152	3.42E-02	183
CTATGC	hsa-miR-153	2.56E-02	90
ATAACC	hsa-miR-154	5.17E-02	92
TGAATG	hsa-miR-181a	1.51E-02	192
TGAATG	hsa-miR-181b	1.51E-02	192
TGAATG	hsa-miR-181c	1.51E-02	192
TGAATG	hsa-miR-181d	1.51E-02	192
TGCCAA	hsa-miR-182	1.39E-04	183
TTGCCA	hsa-miR-182	9.19E-03	179
GCCAAA	hsa-miR-182	1.75E-02	155
TGCCAT	hsa-miR-183	3.46E-02	178
GTGCCA	hsa-miR-183	4.92E-02	159
CCGTCC	hsa-miR-184	2.09E-02	58
CTCTCC	hsa-miR-185	1.23E-03	217
TCTCCA	hsa-miR-185	4.21E-02	195
TCTTTG	hsa-miR-186	2.30E-02	226
TTCTTT	hsa-miR-186	4.40E-02	290
AGACAC	hsa-miR-187	5.14E-02	133
GTGGGA	hsa-miR-188-3p	6.00E-03	187
TGTGGG	hsa-miR-188-3p	9.32E-03	202
AAGGGA	hsa-miR-188-5p	2.51E-03	191
GGGATG	hsa-miR-188-5p	4.09E-02	149
GCCAGT	hsa-miR-193a-3p	5.46E-03	152
GGCCAG	hsa-miR-193a-3p	1.33E-02	195
GACCCA	hsa-miR-193a-5p	4.55E-03	138
GCCAGT	hsa-miR-193b	5.46E-03	152
GGCCAG	hsa-miR-193b	1.33E-02	195
TCTGGA	hsa-miR-198	1.35E-05	220
CTGGAC	hsa-miR-198	2.58E-04	176
TGGACC	hsa-miR-198	7.46E-03	132

TGCACA	hsa-miR-19a	4.77E-03	177
TTGCAC	hsa-miR-19a	5.93E-03	148
TGCACA	hsa-miR-19b	4.77E-03	177
TTGCAC	hsa-miR-19b	5.93E-03	148
ACCTCT	hsa-miR-202	3.88E-02	173
CATTTC	hsa-miR-203	5.04E-06	235
AAGGGA	hsa-miR-204	2.51E-03	191
AGGGAA	hsa-miR-204	1.83E-02	199
AAAGGG	hsa-miR-204	4.63E-02	173
GAAGGA	hsa-miR-205	4.37E-03	191
CGTCTT	hsa-miR-208	7.15E-03	58
CGTCTT	hsa-miR-208b	7.15E-03	58
GCACAG	hsa-miR-210	2.30E-02	168
AAGGGA	hsa-miR-211	2.51E-03	191
AGGGAA	hsa-miR-211	1.83E-02	199
AAAGGG	hsa-miR-211	4.63E-02	173
CTGCTG	hsa-miR-214	1.20E-02	251
CCTGCT	hsa-miR-214	3.70E-02	217
CAACTC	hsa-miR-219-1-3p	1.43E-02	112
GCAGCT	hsa-miR-22	2.21E-02	183
GGCAGC	hsa-miR-22	5.21E-02	170
CCTGTG	hsa-miR-220c	4.27E-04	242
CTGTGT	hsa-miR-220c	2.56E-03	249
CTGACA	hsa-miR-223	1.36E-02	158
GACTTG	hsa-miR-224	6.94E-05	165
TGACTT	hsa-miR-224	2.04E-02	190
GTGACT	hsa-miR-224	2.34E-02	152
GAGCCA	hsa-miR-24	1.23E-03	194
CTGAGC	hsa-miR-24	3.22E-02	184
GTGCAA	hsa-miR-25	2.46E-02	121
CTGTGA	hsa-miR-27a	1.76E-02	213
CTGTGA	hsa-miR-27b	1.76E-02	213
CTCCTT	hsa-miR-28-5p	6.33E-05	225
AGCTCC	hsa-miR-28-5p	1.35E-03	165
GCTCCT	hsa-miR-28-5p	3.85E-02	164
ACCCTC	hsa-miR-296-3p	1.57E-03	157
CAACCC	hsa-miR-296-3p	3.45E-03	119
AACCCT	hsa-miR-296-3p	8.17E-03	151
GGGGCC	hsa-miR-296-5p	2.06E-04	177
GGGCCC	hsa-miR-296-5p	5.54E-04	167
GGCCCT	hsa-miR-296-5p	4.69E-03	177
TTCTGC	hsa-miR-298	4.41E-03	207
CTTCTG	hsa-miR-298	4.53E-03	234

TGGTGC	hsa-miR-29a	5.69E-03	163
GGTGCT	hsa-miR-29a	7.32E-03	158
TGGTGC	hsa-miR-29b	5.69E-03	163
GGTGCT	hsa-miR-29b	7.32E-03	158
TGGTGC	hsa-miR-29c	5.69E-03	163
GGTGCT	hsa-miR-29c	7.32E-03	158
TTGCAC	hsa-miR-301a	5.93E-03	148
TGCACT	hsa-miR-301a	3.42E-02	183
TTGCAC	hsa-miR-301b	5.93E-03	148
TGCACT	hsa-miR-301b	3.42E-02	183
CACTTA	hsa-miR-302a	1.71E-02	133
CACTTA	hsa-miR-302b	1.71E-02	133
CACTTA	hsa-miR-302c	1.71E-02	133
CACTTA	hsa-miR-302d	1.71E-02	133
CTTGCC	hsa-miR-31	3.19E-02	159
GTGCAA	hsa-miR-32	2.46E-02	121
CCACCT	hsa-miR-323-5p	3.68E-03	212
GACCAC	hsa-miR-323-5p	8.11E-03	112
GGGGCA	hsa-miR-324-3p	2.10E-04	174
GGGCAG	hsa-miR-324-3p	2.55E-04	220
GGATGC	hsa-miR-324-5p	3.19E-02	115
GGGATG	hsa-miR-324-5p	4.09E-02	149
CCAGAG	hsa-miR-326	5.42E-05	226
CAGAGG	hsa-miR-326	2.44E-03	218
CCCAGA	hsa-miR-326	8.99E-03	210
GGCCAG	hsa-miR-328	1.33E-02	195
AGGGCC	hsa-miR-328	1.37E-02	159
GGGCCA	hsa-miR-328	1.76E-02	161
GTGTGT	hsa-miR-329	1.61E-02	196
GCTTTG	hsa-miR-330-3p	8.40E-03	196
CTTTGC	hsa-miR-330-3p	3.51E-02	183
CCAGAG	hsa-miR-330-5p	5.42E-05	226
CAGAGA	hsa-miR-330-5p	8.40E-03	210
CCCAGA	hsa-miR-330-5p	8.99E-03	210
AGGGGC	hsa-miR-331-3p	1.87E-05	176
CAGGGG	hsa-miR-331-3p	5.64E-04	182
CCAGGG	hsa-miR-331-3p	1.17E-03	211
ACCTAG	hsa-miR-331-5p	2.09E-02	96
ATGCTG	hsa-miR-338-3p	6.36E-04	207
TGCTGG	hsa-miR-338-3p	2.89E-03	231
GCTGGA	hsa-miR-338-3p	1.77E-02	202
ACAGGG	hsa-miR-339-5p	1.95E-03	172
GACAGG	hsa-miR-339-5p	2.87E-02	150

CAGGGA	hsa-miR-339-5p	3.50E-02	202
ATGCAC	hsa-miR-33a	1.58E-02	125
ATGCAC	hsa-miR-33b	1.58E-02	125
TGTGAG	hsa-miR-342-3p	1.36E-02	185
GTGTGA	hsa-miR-342-3p	1.52E-02	170
CACCCC	hsa-miR-342-5p	2.39E-04	190
ACCCCT	hsa-miR-342-5p	5.92E-04	164
GCACCC	hsa-miR-342-5p	6.02E-03	129
CTGCCA	hsa-miR-34a	2.28E-04	224
ACTGCC	hsa-miR-34a	6.82E-04	175
CACTGC	hsa-miR-34a	1.97E-02	205
ACTGCC	hsa-miR-34c-5p	6.82E-04	175
CTGCCT	hsa-miR-34c-5p	7.10E-04	272
CACTGC	hsa-miR-34c-5p	1.97E-02	205
CTGGGG	hsa-miR-361-3p	2.93E-05	242
TGGGGG	hsa-miR-361-3p	1.48E-02	200
GTGTGT	hsa-miR-362-3p	1.61E-02	196
AAGGAT	hsa-miR-362-5p	3.29E-02	150
GTGCAA	hsa-miR-363	2.46E-02	121
GGGCAT	hsa-miR-365	8.60E-03	134
GTGCAA	hsa-miR-367	2.46E-02	121
CGATCT	hsa-miR-369-5p	4.66E-02	37
CACTTC	hsa-miR-373	1.91E-04	165
TGTGTG	hsa-miR-377	1.28E-03	243
GTGTGA	hsa-miR-377	1.52E-02	170
CTGATC	hsa-miR-383	9.58E-03	114
CCCCTC	hsa-miR-423-5p	9.93E-04	204
CCCTCA	hsa-miR-423-5p	3.06E-02	177
CTGCTG	hsa-miR-424	1.20E-02	251
GTGTCA	hsa-miR-425	2.72E-02	140
GCAAGA	hsa-miR-431	1.32E-02	143
CTGCCA	hsa-miR-449a	2.28E-04	224
ACTGCC	hsa-miR-449a	6.82E-04	175
CACTGC	hsa-miR-449a	1.97E-02	205
ACTGCC	hsa-miR-449b	6.82E-04	175
CTGCCT	hsa-miR-449b	7.10E-04	272
CACTGC	hsa-miR-449b	1.97E-02	205
TCCCAA	hsa-miR-450b-3p	7.37E-03	179
GATCCC	hsa-miR-450b-3p	1.28E-02	96
TTGCAA	hsa-miR-450b-5p	5.02E-02	154
AAACAG	hsa-miR-452	2.59E-02	203
ACAACC	hsa-miR-453	2.91E-02	96
TTGCAC	hsa-miR-454	5.93E-03	148

TGCACT	hsa-miR-454	3.42E-02	183
GGACTG	hsa-miR-455-3p	5.94E-03	164
TGGACT	hsa-miR-455-3p	3.33E-02	162
GGAGTG	hsa-miR-483-3p	2.50E-02	162
CGTCTT	hsa-miR-483-5p	7.15E-03	58
GCCTGA	hsa-miR-484	7.12E-04	175
GAGCCT	hsa-miR-484	2.19E-02	163
GCCTCT	hsa-miR-485-5p	2.27E-03	200
AGCCTC	hsa-miR-485-5p	5.42E-03	202
TGCCCC	hsa-miR-486-3p	4.52E-04	195
CTGCCC	hsa-miR-486-3p	6.67E-04	239
CCTTTC	hsa-miR-488	1.08E-04	220
TGTCAC	hsa-miR-489	4.28E-02	160
CCATGG	hsa-miR-490-5p	7.17E-03	169
TCCCCA	hsa-miR-491-5p	7.35E-03	214
CCCACT	hsa-miR-491-5p	2.35E-02	173
CCCCAC	hsa-miR-491-5p	3.08E-02	190
AGGTCC	hsa-miR-492	3.01E-02	105
GACCTT	hsa-miR-493	5.08E-02	137
GTTTGT	hsa-miR-495	2.81E-02	203
CTGCTG	hsa-miR-497	1.20E-02	251
AAGGAT	hsa-miR-500	3.29E-02	150
AAGGAT	hsa-miR-501-5p	3.29E-02	150
GCAAGG	hsa-miR-502-5p	3.92E-04	138
AAGGAT	hsa-miR-502-5p	3.29E-02	150
CAGGGT	hsa-miR-504	1.10E-02	166
AGGGTC	hsa-miR-504	4.20E-02	122
GGGTCT	hsa-miR-504	5.35E-02	136
GTTGAC	hsa-miR-505	7.82E-03	94
GTGCCT	hsa-miR-506	4.51E-06	214
TGCCTT	hsa-miR-506	2.44E-02	232
GTGCAA	hsa-miR-507	2.46E-02	121
CTGGAG	hsa-miR-508-5p	5.25E-05	253
CTGAGT	hsa-miR-510	6.74E-05	191
AGACAC	hsa-miR-511	5.14E-02	133
CTGAGT	hsa-miR-512-5p	6.74E-05	191
GCTGAG	hsa-miR-512-5p	3.66E-03	212
CCTGTG	hsa-miR-513-5p	4.27E-04	242
CTGTGA	hsa-miR-513-5p	1.76E-02	213
GTGTCA	hsa-miR-514	2.72E-02	140
AGGCAC	hsa-miR-515-3p	6.22E-03	145
TGGAGA	hsa-miR-515-5p	1.98E-03	219
GGAGAA	hsa-miR-515-5p	8.35E-03	215

TTGGAG	hsa-miR-515-5p	3.35E-02	183
CTCCAG	hsa-miR-516b	2.56E-04	239
TGCACG	hsa-miR-517a	2.78E-02	55
ATGCAC	hsa-miR-517b	1.58E-02	125
TGCACG	hsa-miR-517b	2.78E-02	55
TGCACG	hsa-miR-517c	2.78E-02	55
CGCTTT	hsa-miR-518a-3p	3.07E-02	52
CTTTGC	hsa-miR-518a-5p	3.51E-02	183
GCTTTG	hsa-miR-518b	8.40E-03	196
CGCTTT	hsa-miR-518b	3.07E-02	52
GCTTTG	hsa-miR-518c	8.40E-03	196
CGCTTT	hsa-miR-518c	3.07E-02	52
GCTTTG	hsa-miR-518d-3p	8.40E-03	196
CGCTTT	hsa-miR-518d-3p	3.07E-02	52
CGCTTT	hsa-miR-518e	3.07E-02	52
AGCGCT	hsa-miR-518e	3.78E-02	45
CGCTTT	hsa-miR-518f	3.07E-02	52
TGCACT	hsa-miR-519a	3.42E-02	183
TGCACT	hsa-miR-519b-3p	3.42E-02	183
TGCACT	hsa-miR-519c-3p	3.42E-02	183
AGGCAC	hsa-miR-519e	6.22E-03	145
TCTGGA	hsa-miR-520a-5p	1.35E-05	220
CTGGAG	hsa-miR-520a-5p	5.25E-05	253
CTCTGG	hsa-miR-520a-5p	1.20E-04	224
TTGTAG	hsa-miR-520d-5p	3.32E-02	150
CGCCTT	hsa-miR-524-3p	1.52E-02	57
GCGCCT	hsa-miR-524-3p	2.31E-02	66
GCCTTC	hsa-miR-524-3p	4.15E-02	172
TTGTAG	hsa-miR-524-5p	3.32E-02	150
CGCCTT	hsa-miR-525-3p	1.52E-02	57
GCGCCT	hsa-miR-525-3p	2.31E-02	66
GCCTTC	hsa-miR-525-3p	4.15E-02	172
TCTGGA	hsa-miR-525-5p	1.35E-05	220
CTGGAG	hsa-miR-525-5p	5.25E-05	253
CTCTGG	hsa-miR-525-5p	1.20E-04	224
CTTTGC	hsa-miR-527	3.51E-02	183
GTGGGA	hsa-miR-532-3p	6.00E-03	187
GGCATG	hsa-miR-532-5p	1.06E-02	154
CCCACC	hsa-miR-541	5.89E-04	223
GCCCAC	hsa-miR-541	6.08E-03	155
CTGTCA	hsa-miR-542-3p	8.87E-03	190
TGTCAC	hsa-miR-542-3p	4.28E-02	160
ATCCCC	hsa-miR-542-5p	8.90E-04	130

TGCTGA	hsa-miR-545	1.72E-03	207
TTTGCT	hsa-miR-545	5.47E-02	221
GTTCTT	hsa-miR-548b-3p	5.89E-03	192
GGTTCT	hsa-miR-548b-3p	2.47E-02	141
TTTTTG	hsa-miR-548c-3p	3.01E-02	289
TTTTTG	hsa-miR-548d-3p	3.01E-02	289
AGGCAC	hsa-miR-550	6.22E-03	145
TGGGTC	hsa-miR-551a	8.89E-06	154
TGGGTC	hsa-miR-551b	8.89E-06	154
ACCTGT	hsa-miR-552	1.47E-02	179
CGTTTT	hsa-miR-553	4.77E-02	84
GGACTA	hsa-miR-554	3.57E-03	96
CTTACC	hsa-miR-555	1.75E-02	112
GTGCAA	hsa-miR-557	2.46E-02	121
CAGCTC	hsa-miR-558	6.20E-06	211
GCAGCT	hsa-miR-558	2.21E-02	183
GTGCCT	hsa-miR-564	4.51E-06	214
GCCAGC	hsa-miR-565	6.01E-03	167
CCAGCC	hsa-miR-565	6.78E-03	242
GCGCCC	hsa-miR-566	5.02E-02	57
CCAACT	hsa-miR-571	7.86E-03	133
CAACTC	hsa-miR-571	1.43E-02	112
CACTTC	hsa-miR-573	1.91E-04	165
TGAGCG	hsa-miR-574-3p	2.92E-03	53
AGCGTG	hsa-miR-574-3p	4.40E-02	58
CACACT	hsa-miR-574-5p	2.46E-02	156
CTGGCT	hsa-miR-575	1.12E-03	224
ACTGGC	hsa-miR-575	1.42E-02	141
CTCTTT	hsa-miR-583	4.92E-05	243
CCTCTT	hsa-miR-583	7.03E-04	219
TCTTTG	hsa-miR-583	2.30E-02	226
CCATAA	hsa-miR-584	4.33E-02	107
TACGCC	hsa-miR-585	2.62E-02	23
GTGGCC	hsa-miR-588	5.43E-02	158
GGTTCT	hsa-miR-589	2.47E-02	141
GAGACA	hsa-miR-593	4.47E-04	171
AGAGAC	hsa-miR-593	7.99E-04	177
CAGAGA	hsa-miR-593	8.40E-03	210
CACTTC	hsa-miR-595	1.91E-04	165
ACACTT	hsa-miR-595	3.66E-03	165
CACACT	hsa-miR-595	2.46E-02	156
AGGCTT	hsa-miR-596	5.21E-03	172
CTAGAC	hsa-miR-601	2.65E-02	78

TGTGTG	hsa-miR-603	1.28E-03	243
GTGTGT	hsa-miR-603	1.61E-02	196
CGCAGC	hsa-miR-604	5.45E-03	64
CACCCC	hsa-miR-608	2.39E-04	190
ACCCCT	hsa-miR-608	5.92E-04	164
CCACCC	hsa-miR-608	1.22E-03	209
CACCCT	hsa-miR-609	1.72E-02	175
ACACCC	hsa-miR-609	3.45E-02	122
GCCCAG	hsa-miR-612	3.63E-02	220
CCCAGC	hsa-miR-612	4.30E-02	241
GGACCC	hsa-miR-615-5p	4.30E-03	137
ACCCCC	hsa-miR-615-5p	2.81E-02	139
GACCCC	hsa-miR-615-5p	2.93E-02	130
AATGAC	hsa-miR-616	4.28E-02	136
TCCAGG	hsa-miR-619	1.04E-03	205
ATCTCC	hsa-miR-620	1.59E-02	138
TCTCCA	hsa-miR-620	4.21E-02	195
CAAGGG	hsa-miR-623	2.21E-03	150
AAGGGA	hsa-miR-623	2.51E-03	191
ACCTTG	hsa-miR-624	5.14E-03	165
CCTTGT	hsa-miR-624	1.52E-02	182
CTTGTG	hsa-miR-624	3.58E-02	171
TTCCCC	hsa-miR-625	1.94E-04	213
CCCCCT	hsa-miR-625	1.27E-03	176
TCCCCC	hsa-miR-625	1.38E-02	172
GACTCA	hsa-miR-627	3.48E-02	126
CAGCAT	hsa-miR-628-5p	4.84E-02	163
AGACAC	hsa-miR-632	5.14E-02	133
TGCTGG	hsa-miR-634	2.89E-03	231
CTGGTT	hsa-miR-634	3.83E-02	170
CCAAGT	hsa-miR-635	2.48E-02	160
CCCCAG	hsa-miR-637	1.14E-04	244
CCCCCA	hsa-miR-637	3.09E-02	199
CGATCC	hsa-miR-638	9.15E-03	28
GATCCC	hsa-miR-638	1.28E-02	96
ATCCCT	hsa-miR-638	4.36E-02	141
AGCGAT	hsa-miR-639	2.01E-02	43
GAGGGA	hsa-miR-642	1.10E-04	194
AGAGGG	hsa-miR-642	3.08E-04	184
AGGGAC	hsa-miR-642	3.72E-03	152
CCACAC	hsa-miR-644	1.79E-02	161
CACACT	hsa-miR-644	2.46E-02	156
AGCTGC	hsa-miR-646	3.30E-02	190

AGCCAC	hsa-miR-647	3.69E-05	197
CAGCCA	hsa-miR-647	5.26E-02	195
GCACAC	hsa-miR-648	2.13E-03	134
ACACTT	hsa-miR-648	3.66E-03	165
CACACT	hsa-miR-648	2.46E-02	156
CCTCCT	hsa-miR-650	3.31E-03	242
GCCTCC	hsa-miR-650	3.13E-02	207
CCCACC	hsa-miR-654-5p	5.89E-04	223
GCCCAC	hsa-miR-654-5p	6.08E-03	155
CCTGCC	hsa-miR-657	3.86E-05	264
AACCTG	hsa-miR-657	2.02E-02	170
AATGGG	hsa-miR-660	3.70E-02	147
ATGGGT	hsa-miR-660	3.88E-02	117
CCCAGG	hsa-miR-661	3.27E-03	252
GTGGGA	hsa-miR-662	6.00E-03	187
CCCCGC	hsa-miR-663	2.78E-02	90
TCCTGG	hsa-miR-665	1.14E-03	237
CTCCTG	hsa-miR-665	1.14E-02	239
CCTGGT	hsa-miR-665	4.45E-02	173
GGCTTC	hsa-miR-671-5p	5.58E-04	170
GCTTCC	hsa-miR-671-5p	2.57E-03	179
CTTCCT	hsa-miR-671-5p	2.70E-02	248
CCGCAC	hsa-miR-675	1.01E-02	50
CTTCCA	hsa-miR-7	9.18E-07	227
TCTTCC	hsa-miR-7	1.31E-02	217
CTCCTT	hsa-miR-708	6.33E-05	225
AGCTCC	hsa-miR-708	1.35E-03	165
GCTCCT	hsa-miR-708	3.85E-02	164
CCCCGC	hsa-miR-744	2.78E-02	90
CCCGCA	hsa-miR-744	4.16E-02	57
CAGAGC	hsa-miR-760	1.20E-05	221
AGAGCC	hsa-miR-760	2.45E-04	177
TCCTCC	hsa-miR-765	2.83E-04	221
CCTCCA	hsa-miR-765	7.13E-03	205
CTCCTC	hsa-miR-765	1.67E-02	195
CTGGAG	hsa-miR-766	5.25E-05	253
GCTGGA	hsa-miR-766	1.77E-02	202
GAGCAG	hsa-miR-767-3p	5.80E-03	195
AGCAGA	hsa-miR-767-3p	2.28E-02	195
TGGTGC	hsa-miR-767-5p	5.69E-03	163
CCTCCA	hsa-miR-768-5p	7.13E-03	205
GATCCC	hsa-miR-769-3p	1.28E-02	96
TTCCTG	hsa-miR-873	6.73E-04	256

TCCTGC	hsa-miR-873	2.13E-02	216
GGGCAG	hsa-miR-874	2.55E-04	220
AGGGCA	hsa-miR-874	9.15E-04	177
CAGGGC	hsa-miR-874	8.86E-03	190
TCCAGG	hsa-miR-875-3p	1.04E-03	205
TCCTCT	hsa-miR-877	1.75E-02	214
CTGCCT	hsa-miR-885-3p	7.10E-04	272
GCTGCC	hsa-miR-885-3p	5.07E-03	202
CACCCG	hsa-miR-886-3p	1.54E-03	72
CCAAGT	hsa-miR-890	2.48E-02	160
CGTTGC	hsa-miR-891a	9.23E-03	39
GCCAGT	hsa-miR-892b	5.46E-03	152
CCAAAG	hsa-miR-9	3.16E-02	191
GCTCCC	hsa-miR-920	5.48E-04	173
AGCTCC	hsa-miR-920	1.35E-03	165
CTCCCC	hsa-miR-920	2.67E-02	207
CTCACT	hsa-miR-921	1.88E-03	191
CTGCTG	hsa-miR-922	1.20E-02	251
GCTGAC	hsa-miR-923	1.33E-04	139
GTGCAA	hsa-miR-92a	2.46E-02	121
GTGCAA	hsa-miR-92b	2.46E-02	121
AGGGCA	hsa-miR-938	9.15E-04	177
TAAGGG	hsa-miR-938	3.62E-03	112
AAGGGC	hsa-miR-938	1.14E-02	140
GCTCCC	hsa-miR-939	5.48E-04	173
TCCCCA	hsa-miR-939	7.35E-03	214
CTCCCC	hsa-miR-939	2.67E-02	207
CCTGCC	hsa-miR-940	3.86E-05	264
CTGCCT	hsa-miR-940	7.10E-04	272
TGCCTT	hsa-miR-940	2.44E-02	232
GAGAAG	hsa-miR-942	2.25E-03	206
TGCCAA	hsa-miR-96	1.39E-04	183
GCCAAA	hsa-miR-96	1.75E-02	155
GTGCCA	hsa-miR-96	4.92E-02	159

APPENDIX H

FLUORESCENCE IN SITU HYBRIDIZATION PROTOCOLS

Adapted by Wakako Takabe from Obernosterer, et al.[71, 140]

Cryosection

Room temperature

- Formamide (SIGMA, F-9037) Allergenic, work in fume hood.
- 10xPBS (Ambion, AM9625)
- 20xSSC (Ambion, AM9763)
- Triethanolamine (Fluka, 90279)
- Blocking reagent (Roche, 109676)
- Acetic anhydride (Sigma, A-6404)

4℃

- Diethylpyrocarbonate (DEPC) (Sigma, D-5758) Carcinogenic, work in fume hood.
- Proteinase K (20mg/ml) (Amresco, E195-5ML)

-20℃

- 50x Denhardt's (Sigma, D-2532)
- Yeast tRNA (powder) (Sigma, R-6750)
- Salmon sperm DNA (Ambion, AM9680)

Not necessary to beRNase free:

Room temperature

- MilliQ
- Conc. HCl (Riedel, 30721) Corrosive. Work in fume hood.

- 1N Tris-HCl (pH=7.5) (Tris Base 60.57g, Conc HCl 33ml up to 500ml of milliQ)
- Tween20 (Sigma, P-7949)
- CHAPS (Sigma, C-5849)
- 5 M NaCl (29.22g/100ml milliQ)
- 10N NaOH

4℃

- Paraformaldehyde (PFA) (Sigma, P-6148) Allergenic, use gloves.
- Anti-digoxigenin POD antibody (Roche, 11207733910)

Equipment:

RNase Free:

- 1 1000ml Glass beakers: wiped with RNase Zap wipes
- 1 Glass and 1 plastic Slide holder: wiped with RNase Zap wipes
- 3 Glass Slide mailers: wiped with RNase Zap wipes
- Hybridization chamber: add 3MM paper soaked with 5xSSC/50% formamide to a 150mm dish.(4 slides/dish)

Not necessary to be RNase free:

- Hybridization oven. Check the real temperature by using thermometer. If our oven is set at 57℃, real temperature is 60℃.
- Humidifying chamber: add 3MM paper soaked in tap water to a 150mm dish. (4 slides/dish) or regular humidified chamber.

Reagent Setup:

DEPC-treated PBS (2L): Add 2 ml of DEPC to 2 liters of PBS and autoclave. DEPC is carcinogenic until autoclaved; use gloves and work in a fume hood.

DEPC-treated water (800ml): Add 0.8 ml of DEPC to 800 ml of milliQ and autoclave. DEPC is carcinogenic until autoclaved; use gloves and work in a fume hood.

4% PFA for fixation: Add 8 g PFA to 200 ml boiling PBS + 20 µl 10 N NaOH. Heat and shake until solved, chill on ice and store at 4℃. **Use within 3 days of preparation.** PFA is highly allergenic; use gloves and work in a fume hood.

Acetylation solution: Prepare 590 ml of DEPC-treated water in a 1000ml beaker during Step 3. Add 8 ml of triethanolamine and 1.05 ml conc. HCl (min. 37%). Mix gently with a magnetic stirrer. During the last wash step (in Step 3), add 1.5 ml acetic anhydride; wait until it has fully dissolved.

Hybridization solution (20ml): 10ml formamide (final concentration 50%), 5ml 20xSSC (5x), 2ml 50x Denhardt's (5x), 250 µl 20mg/ml yeast RNA (200µg/ml), 1ml 10mg/ml salmon sperm DNA (500µg/ml), 0.4 g Roche blocking reagents and 1.75 ml DEPC-treated water. **Can be stored for months at -20℃.**
Denature salmon sperm DNA at 96℃ for 5 min before adding to the hybridization solution.

Denaturating hybridization solution: Prepare as hybridization solution but add 500 µl of 10% CHAPS, 100 µl of 20% Tween and 1.15 ml (instead of 1.75ml of DEPC-treated

water. Use gloves and work in a fume hood to protect yourself from hazardous formamide and the hybridization solution from RNases.

5xSSC/50% formamide: 20 ml formamide, 10 ml 20xSSC and 10ml DEPC-treated water.

TN buffer (0.1 M Tris pH 7.5/0.15 M NaCl): 100ml of 1M Tris pH 7.5 and 30ml of 5M NaCl. Make up to 1L and then filter.

TN Blocking buffer: TN buffer + 0.5% Blocking Reagent (Roche).
To dissolve blocking reagent, warm up the solution at 55℃ for 30min. Bring to room temperature before use. Aliquot and store at -20℃.

TNT Wash buffer: TN buffer + 0.05% Tween 20

Experimental procedure:

<Day 1> **RNase-Free Conditions.**

1. Let slides dry at room temperature for 30 min.
2. Fix the dried slides in 4% fresh PFA for 10 min at room temperature.

   4% fresh PFA: Use within 3days.
3. Transfer the slides to slide holder in 1X PBS. Wash the slides 3 times for 3 min.
4. During final washing of Step 3, prepare "Acetylation solution".

   Acetylation solution: Prepare fresh before each use.
5. Transfer the slides to plastic slide holder. Put it in the "Acetylation solution".

Stretch parafilm over the beaker. Tape in place. Poke slide holder in parafilm so that slide holder in hanging in acetylation solution. Gently stir for 10min (dial 3 or 4 of the stirrer).

6. Transfer the slides to glass slide holder, and put it in 1X PBS for 5 min at room temperature without agitation.
7. Transfer the slides into a slide mailer containing 5µg/ml "Proteinase K solution" for 11 min (for 10um section).

   Proteinase K solution: 43.75ul of 20mg/ml ProK + 175ml of PBS.
8. Wash the slides 3 times for 3 min in 1X PBS at room temperature. During the washing steps, prepare the "Hybridization chamber".
9. Place the slides horizontally in the chamber and add 300ul of "Hybridization buffer" to each slide. Incubate slides at room temperature for 5h.
10. For each slide, prepare 100µl of "hybridization solution".

    Probes (25µM stock) 0.4µl / 500ul of "Denatured hybridization buffer" = 20nM.

    Denatured hybridization buffer:
11. Denature probes by heating (80℃ x 5min). Thereafter, quickly place them on ice.
12. Pipette the probe solution onto the tissues and apply glass coverslips.
13. Hybridize slides at 50-60℃ by hybridization oven.

    Usually, Tm – 20 to 22℃ should be fine (for example, miR712 Tm is 82℃. In this case, I did hybridization at 60℃). If you see highly background, you should try to increase the hybridization temperature at 1 or 2℃ or try to use less amount of probe concentration (20nM-60nM range is recommended from Exiqon). If you didn't see any signal from your probes, you can reduce the hybridization temperature or increase probe concentration by at least 60nM (60nM of scramble probe didn't have any signals by this procedure).

<Day 2> **RNase Free conditions are no longer required.**

14. Pre-warmed at 60℃: 40ml of 5x SSC solution and 175ml of 0.2x SSC solution
15. Soak the slides in 5x SSC and **carefully** remove coverslips.

This is one of the most important steps to avoid detachment sections.

16. Transfer the slides to glass slide holder. Put them into 0.2x SSC at 60℃ for 1h.
17. Incubate slides in TN buffer at room temperature for 10 min.
18. Prepare humidifying chamber (soak with DI water). Wipe around the tissue section with a kimwipe to remove excess liquid. Put 100μl of "TN Blocking buffer" on the tissue section at room temperature for 1h.
19. Wipe around the tissue section with a kimwipe to remove excess liquid. **After that, all steps mustbe done in dark!!**
20. Put 100μl of anti digoxigenin-HRP (Roche: anti-DIG-POD) diluted 1:100 in TN Blocking buffer on the tissue section. Put slides into "Humidified chamber" at 4℃ over night.

<Day 3> **Keep all steps in dark!!**

21. Wash the slides 3 times for 5 min in TNT Wash buffer at room temperature.
22. Wipe the slides around tissue section to remove excess liquid. Put 100μl of TSA-cy3 solution (1:50) on the tissue section for 3 to 10 min at room temperature.
    You have to optimize the condition!!
23. Wash the slides 2 times for 5 min in TNT Wash buffer at room temperature.
24. Wipe the slides around tissue section to remove excess liquid. Put 100μl of DAPI solution (1:2000 in TN buffer) on the tissue section for 8 min at room temperature.
25. Wash the slides 2 times for 5 min in TNT wash buffer at room temperature.
26. Rinse briefly in DI water and mount with DAKO solution.
27. Keep the slides at 4℃.

<Day4 >

28. Take photos by using fluorescence microscopy or confocal microscopy.

red: miR-cy3

blue(UV): DAPI

green: elastin lamina (auto fluorescence)

en face

RNase-free:

Room temperature

- Formamide (SIGMA, F-9037) Allergenic, work in fume hood.
- 10xPBS (Ambion, AM9625)
- 20xSSC (Ambion, AM9763)
- Triethanolamine (Fluka, 90279)
- Blocking reagent (Roche, 109676)
- Acetic anhydride (Sigma, A-6404)
- Tween20 (Sigma, P-7949)
- CHAPS (Sigma, C-5849)

4℃

- Diethylpyrocarbonate (DEPC) (Sigma, D-5758) Carcinogenic, work in fume hood.
- Proteinase K (20mg/ml) (Amresco, E195-5ML)

-20℃

- 50x Denhardt's solution (Sigma, D-2532)
- Yeast tRNA (powder) (Sigma, R-6750)
- Salmon sperm DNA (Ambion, AM9680)

Not necessary to be RNase-free:

Room temperature

- MilliQ water
- Conc. HCl (Riedel, 30721) Corrosive. Work in fume hood.
- 1N Tris-HCl (pH=7.5) (Tris Base 60.57g, Conc HCl 33ml up to 500ml of milliQ water)
- 5 M NaCl (29.22g/100ml milliQ water)
- 10N NaOH

4℃

- Paraformaldehyde (PFA) (Sigma, P-6148) Allergenic, use gloves.
- Anti-digoxigenin POD antibody (Roche, 11207733910)

Equipment:

RNase Free:

- 96well plate

Not necessary to be RNase free:

- Hybridization oven. Check the real temperature by using thermometer. If our oven is set at 57℃, real temperature is 60℃.

Reagent Setup:

DEPC-treated PBS: Add 0.1% of DEPC to 1xPBS, let sit overnight and autoclave. DEPC is carcinogenic until autoclaved; use gloves and work in a fume hood.

0.1% Active DEPC-PBS: 0.1% of DEPC in DEPC-treated PBS right before to use. Use gloves and work in a fume hood.

4% PFA for Fixation: Add 8 g PFA to 200 ml boiling PBS + 20 µl 10 N NaOH. Heat and shake until solved, chill on ice and store at 4℃. **Use within 3 days of preparation.** PFA is highly allergenic; use gloves and work in a fume hood.

Hybridization Solution (20ml): 10ml formamide (final concentration 50%), 5ml 20xSSC (5x), 2ml 50x Denhardt's solution (5x), 250 µl 20mg/ml yeast RNA (200µg/ml), 1ml 10mg/ml salmon sperm DNA (500µg/ml), 0.4 g Roche blocking reagents and 1.75 ml DEPC-treated water. **Can be stored for months at -20℃.**
Denature salmon sperm DNA at 96℃ for 5 min before adding to the hybridization solution.

Denaturating Hybridization Solution: Prepare as hybridization solution but add 500 µl of 10% CHAPS, 100 µl of 20% Tween and 1.15 ml (instead of 1.75ml of DEPC-treated water. Use gloves and work in a fume hood to protect yourself from hazardous formamide and the hybridization solution from RNases.

5xSSC/50% Formamide: 20 ml formamide, 10 ml 20xSSC and 10ml DEPC-treated water.

TN Buffer (0.1 M Tris pH 7.5/0.15 M NaCl): 100ml of 1M Tris pH 7.5 and 30ml of 5M NaCl. Make up to 1L and then filter.

TN Blocking Buffer: TN buffer + 0.5% Blocking Reagent (Roche).

To dissolve blocking reagent, warm solution at 55℃ for 30min before adding. Bring to room temperature before use. Aliquot and store at -20℃.

TNT Wash Buffer: TN buffer + 0.05% Tween 20

Experimental procedure:

<Day 1> **RNase-Free Conditions.**

29. Dissect mouse whole aorta (remove heart) after PFA perfusion.
30. Wash the aorta with PBS 2 times for 5 min.
31. Fix the aorta in 4% fresh PFA twice for 15 min each. Gently shake at room temperature during fixation

    4% fresh PFA: Use within 3days.
32. Wash the aorta with PBS 2 times for 10 min. Gently shake during fixation.
33. Cut the aorta in segments (for example, GC/LC/TA). Put them into 96well plate.
34. Wash the aorta with PBS 1 times for 10 min, shaking. Use "transfer pipette" to remove liquid.

To be careful not to touch pipette to tissue!! It will stick to pipette and damage the tissue.

35. Add 100ul of 0.1% active DEPC-PBS. Twice for 15min, shaking.

Work in a fume hood when put/remove liquid.

36. Wash with PBS 3 times for 5 min. Shake during wash.
37. Replace with100ul of 5ug/ml Proteinase K for 20 min. Shake during incubation.
38. Wash by PBS 3 times for 5 min, shaking.
39. Replace with 100ul of Hybridization Buffer for 2h. Shake during incubation.
40. For each well, prepare 100µl of "Hybridization solution".

    Hybridization solution: Probes (25µM stock) 0.8µl / 500ul of "Denatured hybridization buffer" = 40nM.

41. Denature probes by heating (80℃ x 5min). Thereafter, quickly place them on ice.
42. Pipette the probe solution in the wells.
43. Hybridize slides at 50-60℃ by hybridization oven.

Usually, hybridization temperature is should be set 20 to 22℃ less than Tm (for example, miR712 Tm is 82℃. In this case, I did hybridization at 60℃). If you see highly background, you should try to increase the hybridization temperature at 1 or 2℃ or try to use less amount of probe concentration (20nM-60nM range is recommended from Exiqon).

If you didn't see any signal from your probes, you can reduce the hybridization temperature or increase probe concentration by at least 60nM (60nM of scramble probe didn't have any signals by this procedure).

<Day 2> **RNase Free conditions are no longer required.**

44. Pre-warmed at 60℃: 5x SSC solution and 0.2x SSC solution
45. Replace with 100ul of 5x SSC in the well and replace it with 0.2xSSC.
46. Incubate the plate at 60℃ for 1h.
47. Incubate slides in TN buffer at room temperature twice for 10 min. Shake during incubation.
48. Remove TN buffer and add 100µl of "TN Blocking Buffer" in the well at room temperature for 1h. Shake during incubation.
49. **Keep this step in dark!!** Replace TN Blocking Buffer with 100µl of anti digoxigenin-HRP (Roche: anti-DIG-POD, diluted 1:100 in TN Blocking buffer) in the well. Keep the plate at 4℃ overnight.

<Day 3> **Keep all steps in dark!!**

50. Wash the wells 2 times for 10 min, shaking, in TNT Wash Buffer at room temperature.

51. Replace with 100μl of TSA-cy3 solution (1:50) on the tissue section for 3 to 10 min at room temperature with shake.

    You have to optimize the condition!!

52. Wash the slides 2 times for 10 min in TNT Wash buffer at room temperature. Shake during incubation.
53. Put 100μl of DAPI solution (1:2000 in TN buffer) on the tissue section for 10 min at room temperature with shake.
54. Wash the slides 2 times for 10 min in TNT wash buffer at room temperature.
55. Mount with DAKO solution under the microscopy.
56. Keep the slides at 4℃.
57. Take photos by using fluorescence confocal microscopy within the same day.

    red: miR-cy3

    blue(UV): DAPI

    green: elastin lamina (auto fluorescence)

APPENDIX I

LIST OF MICRORNAS EXPRESSED SIDE-SPECIFICALLY IN PORCINE AV ENDOTHELIUM

Side-specific microRNAs in Porcine AV Endothelium

Gene Name	Fold Change	q-value(%)
ggo-miR-199a_st	2.122027962	0
gga-miR-199_st	2.173988035	0
dre-miR-199_st	2.458473265	0
hsa-miR-181a_st	2.326768482	0
fru-miR-199_st	2.055957345	0
hsa-miR-199a-5p_st	2.061154999	0
mml-miR-199a-5p_st	1.974896436	0
sla-miR-199a_st	2.254336167	0
sla-miR-181a_st	1.99746792	0
mmu-miR-181a_st	2.659618528	0
xtr-miR-181a_st	2.143493437	0
tni-miR-199_st	2.735916121	0
ptr-miR-199a_st	2.745057432	0
rno-miR-199a-5p_st	2.032199447	0
mml-miR-199a_st	2.033437995	0
fru-miR-181a_st	1.870696263	0
mne-miR-199a_st	2.299408835	0
dre-miR-100_st	1.804606558	0
bta-miR-199a-5p_st	2.545981613	0
mdo-miR-181b_st	2.394053955	1.490638278
rno-miR-181a_st	1.997827933	1.490638278
cfa-miR-199_st	2.87447138	1.490638278
ptr-miR-181a_st	2.316335666	1.490638278
hsa-miR-214_st	1.854785474	1.490638278
ppa-miR-199a_st	2.291207309	1.490638278
lla-miR-181a_st	2.568861305	1.490638278
dre-miR-181a_st	1.74890792	1.490638278
gga-miR-181a_st	1.908520478	1.490638278
age-miR-100_st	1.64354239	1.490638278
bta-miR-181a_st	1.827608849	1.490638278

mmu-miR-199a-5p_st	3.492210848	1.490638278
rno-miR-181b_st	1.766611735	1.490638278
rno-miR-199a-3p_st	4.228381848	1.490638278
xtr-miR-199a_st	1.987012112	2.235957417
ggo-miR-100_st	1.810186906	2.235957417
mmu-miR-199b_st	3.23397382	2.235957417
mmu-miR-100_st	1.691903948	2.235957417
ggo-miR-130a_st	1.565110661	2.235957417
ggo-miR-181b_st	2.515420046	2.235957417
mne-miR-181a_st	1.895753868	2.235957417
ssc-miR-214_st	1.633428532	2.235957417
xtr-miR-199a-star_st	3.21541585	2.235957417
mml-miR-199a-3p_st	3.21410041	2.235957417
ppa-miR-100_st	1.653590112	2.235957417
mdo-miR-181c_st	1.951881768	2.235957417
hsa-miR-100_st	1.638841881	2.235957417
xtr-miR-181b_st	2.399651113	2.235957417
fru-miR-100_st	1.684783641	2.235957417
bta-miR-199a-3p_st	3.298447937	2.235957417
lla-miR-199a_st	2.06491825	2.235957417
lla-miR-100_st	1.627392973	2.235957417
bta-miR-181b_st	2.435168609	2.235957417
mml-miR-181a_st	1.649972142	2.235957417
ptr-miR-100_st	1.650609673	2.235957417
rno-miR-25_st	2.051565193	2.235957417
cfa-miR-181a_st	3.108918937	2.235957417
mdo-miR-100_st	1.888295216	2.235957417
mne-miR-127_st	1.846570913	2.235957417
gga-miR-181b_st	2.169131726	2.235957417
dre-miR-181c_st	2.254511705	2.235957417
ppa-miR-181a_st	2.325091781	2.235957417
dre-miR-199-star_st	3.230966965	2.235957417
dre-miR-25_st	1.607698638	2.235957417
hsa-miR-199b-3p_st	3.417698977	2.235957417
tni-miR-181a_st	1.825556095	2.235957417
hsa-miR-181b_st	2.146019224	2.235957417
ggo-miR-181a_st	1.832556484	2.851655836
mml-miR-150_st	1.541112662	2.851655836
tni-miR-100_st	1.564537603	2.851655836
lla-miR-181b_st	2.31963691	3.988464582
hsa-miR-708_st	1.901627054	3.988464582
mmu-miR-532-5p_st	1.690061798	3.988464582
xtr-miR-100_st	1.600960079	3.988464582

mdo-miR-214_st	1.702098664	3.988464582
mmu-miR-199a-3p_st	3.080342276	4.591165896
osa-miR809b_st	1.674776601	5.825257481
ppy-miR-199a_st	1.949026897	8.998365215
mne-miR-181b_st	1.573219165	8.998365215
rno-miR-100_st	1.488521094	8.998365215
mml-miR-181b_st	1.926562069	8.998365215
hsa-miR-150_st	2.029511713	8.998365215
hsa-miR-199a-3p_st	3.410530899	8.998365215
ggo-miR-214_st	1.780276507	8.998365215
mmu-miR-181d_st	1.782840534	9.955334214
ppa-miR-181b_st	2.712655173	9.955334214
mml-miR-25_st	2.295695029	11.8737049
cfa-miR-708_st	2.013370945	11.8737049
xtr-miR-25_st	2.198123329	12.71229722
ssc-miR-181b_st	2.338986714	12.71229722
cfa-miR-369_st	1.500068796	12.71229722
dre-miR-181b_st	1.879045064	13.75234024
ppy-miR-100_st	1.46731471	13.75234024
ssc-miR-181c_st	1.623301522	13.75234024
mml-miR-100_st	1.538016165	13.75234024
ppy-miR-181a_st	1.816016948	13.75234024
hsa-miR-455-3p_st	2.04663902	14.75731895
gga-miR-199-star_st	2.005085838	14.75731895
ame-miR-100_st	1.49954034	14.75731895
fru-miR-25_st	2.060147071	14.75731895
hsa-miR-618_st	1.513205229	14.75731895
rno-miR-214_st	1.608209473	14.75731895
ppa-miR-25_st	1.847027056	16.71540982
xtr-miR-130a_st	1.439070894	16.71540982
aga-miR-100_st	1.506975888	17.02767571
sla-miR-100_st	1.659381952	20.88299852
mdo-miR-181a_st	2.408092817	20.88299852
cfa-miR-543_st	1.40061101	20.95174913
hsa-miR-523-star_st	1.69790609	20.95174913
mmu-miR-708_st	1.675250688	20.95174913
mmu-miR-181c_st	1.715009617	20.95174913
tni-miR-181b_st	2.024126328	20.95174913
hsa-miR-223_st	1.532971986	20.95174913
osa-miR395s_st	1.430450261	28.28486133
mne-miR-214_st	1.849738505	28.28486133
mdo-miR-199b_st	1.405798675	28.28486133
ppt-miR166k_st	1.544284613	28.28486133

fru-miR-181b_st	1.778519345	28.28486133
ppy-miR-214_st	1.456885335	28.28486133
cfa-miR-25_st	2.219899966	28.28486133

APPENDIX J

TRANSFECTION PROTOCOL FOR PRE-MIRS AND LNA-ANTI-MIRS IN HAVECS

Note: This protocol may be scaled for dish size.

Number of Targets (conditions in 3x):	2

Step A:
for each of targets

Oligonucleotide - Precursor (20uM)	20	uL
OptiMEM	350	uL
TOTAL	370	uL

Put on ice.

Step B:

Oligofectamine	16	uL
OptiMEM	60	uL

Store at RT for 5-10min.

1. Add 30 uL of incubated B in each tube of A for a total of 400uL.
2. Allow for complexes to form for 15-20 min. at RT.
3. Meanwhile, rinse wells with OptiMEM 2x.
4. Add fresh OptiMEM to each well according to the following:

for 100nM	for 10nM	for 1nM	for 0.1nM
900uL	990uL	999uL	999uL

5. After complex formation, add A+B into each well according to the following:

for 100nM	for 10nM	for 1nM	for 0.1nM
100uL	10uL	1uL	1uL of diluted 1:10

Add 1uL of A+B to 9uL of OPTIMEM for the 0.1nM case.

6. After **4**-6 hours, add 30% Growth Media (for 40 wells, 4.5mL FBS into 16mL of 10% Growth Media.)
7. After 24 hours, change into shear media.
8. After 48 hours, collect samples.

APPENDIX K

MONOCYTE ADHESION PROTOCOL

Reagents: Warm all reagents in water bath before applying to cells

1. RPMI Media – No serum
2. RPMI Media – 10% FBS, L-glutamine
3. DMEM – Heparin, MNEAA, No Serum
4. mouse or human TNFα
5. HBSS with Calcium (sterile and non-sterile)
6. BCECF-AM fluorescent label (Molecular Probes): in -20C Freezer B
7. 4% Paraformaldehyde or Accustain
8. THP-1 cells and endothelial cells

Protocol:

1. Culture THP-1 monocyte cells in 15-20mL serum-containing RPMI media in T-75 culture flasks.
   a) See Culture Sheet attached. Usually 2 T75s will work for 15 10cm dishes. Will need 45 million monocytes for 15 10cm dishes.
2. For TNFα positive control:
   a) Wash confluent EC two times with serum-free EC base media.
   b) Add serum free-EC base media (1mL for 6 well, 6-10mL for 10cm dish) containing 40ng/mL TNF.
3. On the day of the assay, count THP-1 cells using the Coulter Counter or hemocytometer.
   a) Final labeled monocyte density required is $0.5x10^6$cells/mL. Determine number of monocytes needed for binding assay. (For 15 plates with 6mL each plate, need 90mL and 45 million monocytes.)
4. Place necessary cell suspension in a separate 50mL tube and added 10mL Serum-free RPMI media to wash slightly. These cells will be fluorescently labeled for the assay. Use the remainder of the cell suspension to split THP-1 cells for further culture.
5. Spin cells to be labeled in bench top centrifuge for 1.5 minutes at 2000rpm.
6. Aspirate media from the pellet and repeat washing/aspirating once more.
7. Resuspend monocyte pellet in base RPMI so that the concentration is $1x10^6$cells/mL monocytes/mL (for labeling purposes).
8. TURN OFF FLOW HOOD LIGHT.
9. Label THP-1 cells with BCECF-AM.
   a) Add 5uL/mL of BCECF-AM (Molecular Probes, 1mg/mL) to the THP-1 suspension (i.e. 35uL for a 7mL volume).
   b) Wrap the 50mL conical tube in foil to protect it from light.
   c) Incubate the monocytes and labeling agent at 37^0C for 30minutes with lid slightly ajar.

10. During monocyte labeling, treat ECs as relevant.
11. Remove media from ECs and, if necessary, reserve for Western blot.
12. Wash ECs three times with warmed HBSS (with Ca^{2+}).
13. Add HBSS (1mL/well for 6 well plate, 6mL for 10cm dish) and return to 37^{o}C.
14. Remove labeled-THP-1 cells from incubator and centrifuge for 1.5 minutes at 2000rpm.
15. Wash and centrifuge three times additional times with 10mL serum-free RPMI.
16. Resuspend THP-1 in applicable volume RPMI media. (For 15plates, 90mL.)
17. Remove HBSS from EC.
18. Add THP-1 suspension (1mL/well for 6 well plate, 6mL for 10cm dish) to MAEC and incubate at 37^{0}C for 30 minutes.
19. TURN OFF OVERHEAD ROOM LIGHT
20. Remove non-adherent THP-1 cells from EC by washing with HBSS.
    a) Pour warm, non-sterile HBSS very gently over plate surface using a 50mL conical tube. This will prevent uneven removal of monocytes.
    b) Repeat washes until no more floating cells are visible under the light microscope (3-5 washes).
21. Fix bound monocytes with 4% paraformaldehyde or Accustain for 5 minutes (1mL for 6well, 5mL for 10cm dish). Add non-sterile HBSS to prevent drying out of cells.
22. Visualize bound monocytes in 8 fields via fluorescent and bright field microscopy
    a) Draw a pie shaped grid on the bottom side of each well or dish. (Or just take pictures at the "numbers of the clock".)
    b) Visualize cells at a radius half way between the center and the outside edge of each well or dish.
    c) Average eight counts for each treatment group.
    d) Use 5X or 10X objective to acquire images with the fluorescent microscope.

APPENDIX L

ANNEXIN-V/PI STAINING FOR APOPTOSIS ANALYSIS AND PI STAINING FOR CELL CYCLE ANALYSIS

Supplies

- Treated Cells
- Media
- 1x Trypsin
- HBSS (Ca, Mg free)
- 1x PBS (ice cold)
- Annexin-V Binding Buffer 10x
- Annexin-V-APC
- 0.5M EDTA (pH=8.0; on WT's bench)
- EtOH
- Filtered MilliQ water
- 1mg/ml PI (in WT -20deg; powder on WT shelf in sliding fridge)
- 100mg/ml RNase solution (from Qiagen kit; on WT's bench)
- 0.5M Sodium Citrate (on WT's bench)
- FACS tube with cell strainer

Solutions for Annexin-V/PI Staining

- Annexin-V Binding Buffer (1x) – Dilute with DI water 1:10. Discard any unused solution at the end of the experiment.

Annexin-V/PI Staining Protocol

1. Prepare staurosporin media. Add 1:1000 (1uL for 1mL; 10uL for 10mL) and warm up water bath.
2. Treat 1 dish with apoptosis-inducing agent (1 µM staurosporin)
3. Harvest 1 dish of control cells. Divide in ½. Put ½ in water bath at 50degC for 30min.
4. Meanwhile, harvest cells (1000rpm, 5min) and wash with cold PBS at 4degC. Resuspend in 500uL cold PBS with EDTA. Transfer samples to microcentrifuge tubes (split in half: ½ for Annexin-V/PI and ½ for PI).
5. Pellet samples to be used for Annexin-V/PI staining. Add 500uL of cold 1x Annexin-V Binding Buffer to each centrifuge tube. Add 5uL of Annexin-V-APC to each tube.
6. Incubate in the dark at RT for 15min.
7. Pellet and resuspend in 500uL of cold 1x Annexin-V Binding Buffer at 4degC.
8. Add 15.5uL of PI (1mg/ml) to each tube for a final concentration of 30ug/mL.
9. Place tubes on ice.
10. Read on flow cytometer.

11. Reserve remaining samples for cell cycle analysis.

Solutions for PI Staining

- 1x PBS with 2mM EDTA- 0.5M EDTA 200uL + PBS 50mL
- 70% Ethanol – EtOH 35mL + filtered MilliQ water 15mL
- 2mg/ml RNase solution – 80uL of 100mg/ml RNaseA + 3920uL MilliQ water
- 40ug/ml PI solution with 3.8M Sodium Citrate – 160uL of 1mg/ml PI + 30.4uL of 0.5M Sodium Citrate + 3810uL PBS

PI Staining for Cell Cycle

1. Use ½ of the unused sample from above.
2. Spin down cells gently (max 1,500 rpm for 5min.)
3. Remove supernatant. Add 500uL 70% ice cold ethanol to fix. Incubate at 4degC for 10min.
4. Add 1mL cold PBS with EDTA to dilute. Spin down (~2,500 rpm for 5min).
5. Rinse with cold PBS with EDTA and pellet (~2,500 rpm for 5min).
6. Add 200uL of RNase solution and gently mix.
7. Add 200uL of PI solution and gently mix.
8. Incubate for 30-45min at RT.
9. Read on flow cytometer.

REFERENCES

1. Hsu SY, Hsieh IC, Chang SH, Wen MS, Hung KC. Aortic valve sclerosis is an echocardiographic indicator of significant coronary disease in patients undergoing diagnostic coronary angiography. *International Journal of Clinical Practice*. 2005;59:72-77
2. Mohler ER, Chawla MK, Chang AW, Vyavahare N, Levy RJ, Graham L, Gannon FH. Identification and characterization of calcifying valve cells from human and canine aortic valves. *Journal of Heart Valve Disease*. 1999;8:254-260
3. Otto CM, Lind BK, Kitzman DW, Gersh BJ, Siscovick DS, Cardiovascular Hlth S. Association of aortic-valve sclerosis with cardiovascular mortality and morbidity in the elderly. *N. Engl. J. Med.* 1999;341:142-147
4. Holliday CJ, Ankeny RF, Jo H, Nerem RM. Discovery of shear- and side-specific mrnas and mirnas in human aortic valvular endothelial cells. *American Journal of Physiology - Heart and Circulatory Physiology*. 2011
5. Butcher JT, Penrod AM, Garcia AJ, Nerem RM. Unique morphology and focal adhesion development of valvular endothelial cells in static and fluid flow environments. *Arterioscler. Thromb. Vasc. Biol.* 2004;24:1429-1434
6. Simmons CA, Grant GR, Manduchi E, Davies PF. Spatial heterogeneity of endothelial phenotypes correlates with side-specific vulnerability to calcification in normal porcine aortic valves. *Circ.Res.* 2005;96:792-799
7. Akat K, Borggrefe M, Kaden JJ. Aortic valve calcification: Basic science to clinical practice. *Heart*. 2009;95:616-623
8. Baxley WA. Aortic-valve disease. *Current Opinion in Cardiology*. 1994;9:152-157
9. Carabello BA, Paulus WJ. Aortic stenosis. *Lancet*. 2009;373:956-966
10. Mohler ER, Gannon F, Reynolds C, Zimmerman R, Keane MG, Kaplan FS. Bone formation and inflammation in cardiac valves. *Circulation*. 2001;103:1522-1528
11. Otto CM, Kuusisto J, Reichenbach DD, Gown AM, Obrien KD. Characterization of the early lesion of degenerative valvular aortic-stenosis - histological and immunohistochemical studies. *Circulation*. 1994;90:844-853
12. Butcher JT, Simmons CA, Warnock JN. Review - mechanobiology of the aortic heart valve. *Journal of Heart Valve Disease*. 2008;17:62-73
13. Scott M, Vesely I. Aortic-valve cusp microstructure - the role of elastin. *Annals of Thoracic Surgery*. 1995;60:S391-S394
14. Thiene G, Basso C. Pathology and pathogenesis of infective endocarditis in native heart valves. *Cardiovasc. Pathol.* 2006;15:256-263
15. Bonow RO, Carabello BA, Chatterjee K, de Leon AC, Faxon DP, Freed MD, Gaasch WH, Lytle BW, Nishimura RA, O'Gara PT, O'Rourke RA, Otto CM, Shah PM, Shanewise JS, Smith SC, Jacobs AK, Adams CD, Anderson JL, Antman EM, Fuster V, Halperin JL, Hiratzka LF, Hunt SA, Nishimura R, Page RL, Riegel B, Amer Col CardiologyAmer H. Acc/aha 2006 guidelines for the management of patients with valvular heart disease. *Circulation*. 2006;114:E84-E231
16. Nishimura RA. Aortic valve disease. *Circulation*. 2002;106:770-772
17. Lloyd-Jones D, Adams RJ, Brown TM, Carnethon M, Dai S, De Simone G, Ferguson TB, Ford E, Furie K, Gillespie C, Go A, Greenlund K, Haase N,

Hailpern S, Ho PM, Howard V, Kissela B, Kittner S, Lackland D, Lisabeth L, Marelli A, McDermott MM, Meigs J, Mozaffarian D, Mussolino M, Nichol G, Roger VL, Rosamond W, Sacco R, Sorlie P, Stafford R, Thom T, Wasserthiel-Smoller S, Wong ND, Wylie-Rosett J, Amer Heart Assoc Stat Comm S. Heart disease and stroke statistics-2010 update a report from the american heart association. *Circulation*. 2010;121:E46-E215

18. Roberts WC, Ko JM. Frequency by decades of unicuspid, bicuspid, and tricuspid aortic valves in adults having isolated aortic valve replacement for aortic stenosis, with or without associated aortic regurgitation. *Circulation*. 2005;111:920-925
19. Bosse Y, Mathieu P, Pibarot P. Genomics: The next step to elucidate the etiology of calcific aortic valve stenosis. *J. Am. Coll. Cardiol.* 2008;51:1327-1336
20. Obrien KD, Reichenbach DD, Marcovina SM, Kuusisto J, Alpers CE, Otto CM. Apolipoproteins b, (a), and e accumulate in the morphologically early lesion of 'degenerative' valvular aortic stenosis. *Arterioscler. Thromb. Vasc. Biol.* 1996;16:523-532
21. Jian B, Jones PL, Li QY, Mohler ER, Schoen FJ, Levy RJ. Matrix metalloproteinase-2 is associated with tenascin-c in calcific aortic stenosis. *Am. J. Pathol.* 2001;159:321-327
22. Jian B, Narula N, Li QY, Mohler ER, Levy RJ. Progression of aortic valve stenosis: Tgf-beta 1 is present in calcified aortic valve cusps and promotes aortic valve interstitial cell calcification via apoptosis. *Annals of Thoracic Surgery*. 2003;75:457-465
23. Helske S, Lindstedt KA, Laine M, Mayranpaa M, Werkkala K, Lommi J, Turto H, Kupari M, Kovanen PT. Induction of local angiotensin ii-producing systems in stenotic aortic valves. *J. Am. Coll. Cardiol.* 2004;44:1859-1866
24. Olsson M, Thyberg J, Nilsson J. Presence of oxidized low density lipoprotein in nonrheumatic stenotic aortic valves. *Arterioscler. Thromb. Vasc. Biol.* 1999;19:1218-1222
25. Rossebo AB, Pedersen TR, Allen C, Boman K, Chambers J, Egstrup K, Gerdts E, Gohlke-Barwolf C, Holme I, Kesaniemi VAY, Malbecq W, Nienaber C, Ray S, Skjaerpe T, Wachtell K, Willenheimer R. Design and baseline characteristics of the simvastatin and ezetimibe in aortic stenosis (seas) study. *Am. J. Cardiol.* 2007;99:970-973
26. Chan KL, Teo K, Dumesnil JG, Ni A, Tam J, Investigators A. Effect of lipid lowering with rosuvastatin on progression of aortic stenosis results of the aortic stenosis progression observation: Measuring effects of rosuvastatin (astronomer) trial. *Circulation*. 2010;121:306-U247
27. Novo G, Fazio G, Visconti C, Carita P, Maira E, Fattouch K, Novo S. Atherosclerosis, degenerative aortic stenosis and statins. *Curr. Drug Targets*. 2011;12:115-121
28. Kaden JJ, Dempfle CE, Grobholz R, Fischer CS, Vocke DC, Kilic R, Sarikoc A, Pinol R, Hagl S, Lang S, Brueckmann M, Borggrefe M. Inflammatory regulation of extracellular matrix remodeling in calcific aortic valve stenosis. *Cardiovasc. Pathol.* 2005;14:80-87
29. Kaden JJ, Dempfle CE, Grobholz R, Tran HT, Kilic R, Sarikoc A, Brueckmann M, Vahl C, Hagl S, Haase KK, Borggrefe M. Interleukin-1 beta promotes matrix

metalloproteinase expression and cell proliferation in calcific aortic valve stenosis. *Atherosclerosis*. 2003;170:205-211
30. O'Brien KD, Shavelle DM, Caulfield MT, McDonald TO, Olin-Lewis K, Otto CM, Probstfield JL. Association of angiotensin-converting enzyme with low-density lipoprotein in aortic valvular lesions and in human plasma. *Circulation*. 2002;106:2224-2230
31. Ankeny RF, Thourani VH, Weiss D, Vega JD, Taylor WR, Nerem RM, Jo H. Preferential activation of smad1/5/8 on the fibrosa endothelium in calcified human aortic valves - association with low bmp antagonists and smad6. *PLoS One*. 2011;6
32. Rajamannan NM, Subramaniam M, Rickard D, Stock SR, Donovan J, Springett M, Orszulak T, Fullerton DA, Tajik AJ, Bonow RO, Spelsberg T. Human aortic valve calcification is associated with an osteoblast phenotype. *Circulation*. 2003;107:2181-2184
33. Bosse Y, Miqdad A, Fournier D, Pepin A, Pibarot P, Mathieu P. Refining molecular pathways leading to calcific aortic valve stenosis by studying gene expression profile of normal and calcified stenotic human aortic valves. *Circ.-Cardiovasc. Genet.* 2009;2:489-U185
34. Ankeny RF. The role of bone morphogenic proteins in human aortic valvular endothelial cells. *Biomedical Engineering*. 2010;Ph.D.
35. Ku DN, Giddens DP, Zarins CK, Glagov S. Pulsatile flow and atherosclerosis in the human carotid bifurcation - positive correlation between plaque location and low and oscillating shear-stress. *Arteriosclerosis*. 1985;5:293-302
36. Sorescu GP, Song H, Tressel SL, Hwang J, Dikalov S, Smith DA, Boyd NL, Platt MO, Lassegue B, Griendling KK, Jo H. Bone morphogenic protein 4 produced in endothelial cells by oscillatory shear stress induces monocyte adhesion by stimulating reactive oxygen species production from a nox1-based nadph oxidase. *Circ.Res.* 2004;95:773-779
37. Sorescu GP, Sykes M, Weiss D, Platt MO, Saha A, Hwang J, Boyd N, Boo YC, Vega JD, Taylor WR, Jo H. Bone morphogenic protein 4 produced in endothelial cells by oscillatory shear stress stimulates an inflammatory response. *J. Biol. Chem.* 2003;278:31128-31135
38. Zarins CK, Giddens DP, Bharadvaj BK, Sottiurai VS, Mabon RF, Glagov S. Carotid bifurcation atherosclerosis quantitative correlation of plaque localization with flow velocity profiles and wall shear-stress. *Circ.Res.* 1983;53:502-514
39. Muller AM, Cronen C, Kupferwasser LI, Oelert H, Muller KM, Kirkpatrick CJ. Expression of endothelial cell adhesion molecules on heart valves: Up-regulation in degeneration as well as acute endocarditis. *J. Pathol.* 2000;191:54-60
40. Ghaisas NK, Foley JB, O'Briain DS, Crean P, Kelleher D, Walsh M. Adhesion molecules in nonrheumatic aortic valve disease: Endothelial expression, serum levels and effects of valve replacement. *J. Am. Coll. Cardiol.* 2000;36:2257-2262
41. Weinberg EJ, Mack PJ, Schoen FJ, Garcia-Cardena G, Mofrad MRK. Hemodynamic environments from opposing sides of human aortic valve leaflets evoke distinct endothelial phenotypes in vitro. *Cardiovascular Engineering*. 2010;10:5-11

42. Yap C, Saikrishnan N, Yoganathan A. Experimental measurement of dynamic fluid shear stress on the ventricular surface of the aortic valve leaflet. *Biomechanics and Modeling in Mechanobiology*. 2011:1-14
43. Yap CH, Saikrishnan N, Tamilselvan G, Yoganathan AP. Experimental technique of measuring dynamic fluid shear stress on the aortic surface of the aortic valve leaflet. *J. Biomech. Eng.-Trans. ASME*. 2011;133
44. Sucosky P, Balachandran K, Elhammali A, Jo H, Yoganathan AP. Altered shear stress stimulates upregulation of endothelial vcam-1 and icam-1 in a bmp-4-and tgf-beta 1-dependent pathway. *Arterioscler. Thromb. Vasc. Biol.* 2009;29:254-260
45. Papadaki M, Eskin SG. Effects of fluid shear stress on gene regulation of vascular cells. *Biotechnol. Prog.* 1997;13:209-221
46. Chien S. Effects of disturbed flow on endothelial cells. *Annals of Biomedical Engineering*. 2008;36:554-562
47. Ni C-W, Qiu, Haiwei, Rezvan, Amir, Kwon, Kihwan, Nam, Douglas, Son, Dong Ju, Visvader, Jane E., Jo, Hanjoong. Discovery of novel mechanosensitive genes in vivo using mouse carotid artery endothelium exposed to disturbed flow. *Blood*. 2010;116:E66-E73
48. Qin XM, Wang XH, Wang Y, Tang ZH, Cui QH, Xi JZ, Li YSJ, Chien S, Wang NP. Microrna-19a mediates the suppressive effect of laminar flow on cyclin d1 expression in human umbilical vein endothelial cells. *Proc. Natl. Acad. Sci. U. S. A.* 2010;107:3240-3244
49. Wang KC, Garmire LX, Young A, Nguyen P, Trinh A, Subramaniam S, Wang NP, Shyy JYJ, Li YS, Chien S. Role of microrna-23b in flow-regulation of rb phosphorylation and endothelial cell growth. *Proc. Natl. Acad. Sci. U. S. A.* 2010;107:3234-3239
50. Conway DE, Williams, Marcie R., Eskin, Suzanne G., McIntire, Larry V. Endothelial cell responses to atheroprone flow are driven by two separate flow components: Low time-average shear stress and fluid flow reversal. *Am. J. Physiol.-Heart Circul. Physiol.* 2010;298:H367-H374
51. Guo HL, Ingolia NT, Weissman JS, Bartel DP. Mammalian micrornas predominantly act to decrease target mrna levels. *Nature*. 2010;466:835-U866
52. Mirnezami AHF, Pickard K, Zhang L, Primrose JN, Packham G. Microrna: Key players in carcinogenesis and novel therapeutic targets. *Ejso*. 2009;35:339-347
53. Zhang CX. Microrna: Role in cardiovascular biology and disease. *Clin. Sci.* 2008;114:699-706
54. Liu N, Olson EN. Microrna regulatory networks in cardiovascular development. *Dev. Cell*. 2010;18:510-525
55. van Rooij E, Marshall WS, Olson EN. Toward microrna-based therapeutics for heart disease the sense in antisense. *Circ.Res.* 2008;103:919-928
56. Fang Y, Shi CZ, Manduchi E, Civelek M, Davies PF. Microrna-10a regulation of proinflammatory phenotype in athero-susceptible endothelium in vivo and in vitro. *Proc. Natl. Acad. Sci. U. S. A.* 2010;107:13450-13455
57. Nigam V, Hans H. Sievers, Brian C. Jansen, Holger A. Sier, Paul C. Simpson, Deepak Srivastava, Salah A. Mohamed. Altered microrna in bicuspid aortic valve: A comparison between stenotic and insufficient valves. *Journal of Heart Valve Disease*. 2010;19:459-465

58. Dimmeler S, Zeiher AM. Circulating micrornas: Novel biomarkers for cardiovascular diseases? *Eur. Heart J.* 2010;31:2705-2707
59. Mohler ER. Mechanisms of aortic valve calcification. *Am. J. Cardiol.* 2004;94:1396-1402
60. Booyse FM, Sedlak BJ, Rafelson ME. Culture of arterial endothelial cells - characterization and growth of bovine aortic cells. *Thrombosis Et Diathesis Haemorrhagica*. 1975;34:825-839
61. Jaffe EA NR, Becker CG, Minick CR. Culture of human endothelial cells derived from umbilical veins. Identification by morphologic and immunologic criteria. *J Clin Invest.* 1973;52:2745-2756
62. Garlanda C, Dejana E. Heterogeneity of endothelial cells - specific markers. *Arterioscler. Thromb. Vasc. Biol.* 1997;17:1193-1202
63. Farivar RS, Cohn LH, Soltesz EG, Mihaljevic T, Rawn JD, Byrne JG. Transcriptional profiling and growth kinetics of endothelium reveals differences between cells derived from porcine aorta versus aortic valve. *Eur. J. Cardio-Thorac. Surg.* 2003;24:527-534
64. Kumar S, West DC, Ager A. Heterogeneity in endothelial-cells from large vessels and microvessels. *Differentiation*. 1987;36:57-70
65. Paranya G, Vineberg S, Dvorin E, Kaushal S, Roth SJ, Rabkin E, Schoen FJ, Bischoff J. Aortic valve endothelial cells undergo transforming growth factor-beta-mediated and non-transforming growth factor-beta-mediated transdifferentiation in vitro. *Am. J. Pathol.* 2001;159:1335-1343
66. Young EWK, Wheeler AR, Simmons CA. Matrix-dependent adhesion of vascular and valvular endothelial cells in microfluidic channels. *Lab on a Chip*. 2007;7:1759-1766
67. Butcher JT, Nerem RM. Valvular endothelial cells regulate the phenotype of interstitial cells in co-culture: Effects of steady shear stress. *Tissue Engineering*. 2006;12:905-915
68. Butcher JT, Tressel S, Johnson T, Turner D, Sorescu G, Jo H, Nerem RM. Transcriptional profiles of valvular and vascular endothelial cells reveal phenotypic differences - influence of shear stress. *Arterioscler. Thromb. Vasc. Biol.* 2006;26:69-77
69. Mowbray AL, Kang DH, Rhee SG, Kang SW, Jo H. Laminar shear stress up-regulates peroxiredoxins (prx) in endothelial cells. *J. Biol. Chem.* 2008;283:1622-1627
70. Levesque MJ, Nerem RM. The elongation and orientation of cultured endothelial-cells in response to shear-stress. *J. Biomech. Eng.-Trans. ASME*. 1985;107:341-347
71. Ando H, Kubin T, Schaper W, Schaper J. Cardiac microvascular endothelial cells express alpha-smooth muscle actin and show low nosiii activity. *Am. J. Physiol.-Heart Circul. Physiol.* 1999;276:H1755-H1768
72. Medici D, Shore EM, Lounev VY, Kaplan FS, Kalluri R, Olsen BR. Conversion of vascular endothelial cells into multipotent stem-like cells. *Nat. Med.* 2010;16:1400-U1480

73. Ishisaki A, Hiyashi H, Li AJ, Imamura T. Human umbilical vein endothelium-derived cells retain potential to differentiate into smooth muscle-like cells. *J. Biol. Chem.* 2003;278:1303-1309
74. Ni C-W, Qiu H, Jo H. Microrna-663 upregulated by oscillatory shear stress plays a role in inflammatory response of endothelial cells. *American Journal of Physiology - Heart and Circulatory Physiology*. 2011;300:H1762-H1769
75. Mirochnik Y, Kwiatek A, Volpert OV. Thrombospondin and apoptosis: Molecular mechanisms and use for design of complementation treatments. *Curr. Drug Targets*. 2008;9:851-862
76. Li XX, Stark GR. Nf kappa b-dependent signaling pathways. *Exp. Hematol.* 2002;30:285-296
77. Padovani AMS, Molina MF, Mann KK. Inhibition of liver x receptor/retinoid x receptor-mediated transcription contributes to the proatherogenic effects of arsenic in macrophages in vitro. *Arterioscler. Thromb. Vasc. Biol.* 2010;30:1228-U1347
78. Salloum FN, Chau VQ, Hoke NN, Abbate A, Varma A, Ockaili RA, Toldo S, Kukreja RC. Phosphodiesterase-5 inhibitor, tadalafil, protects against myocardial ischemia/reperfusion through protein-kinase g-dependent generation of hydrogen sulfide. *Circulation*. 2009;120:S31-S36
79. Nikiforova MN, Tseng GC, Steward D, Diorio D, Nikiforov YE. Microrna expression profiling of thyroid tumors: Biological significance and diagnostic utility. *J. Clin. Endocrinol. Metab.* 2008;93:1600-1608
80. Moschos SA, Williams AE, Perry MM, Birrell MA, Belvisi MG, Lindsay MA. Expression profiling in vivo demonstrates rapid changes in lung microrna levels following lipopolysaccharide-induced inflammation but not in the anti-inflammatory action of glucocorticoids. *BMC Genomics*. 2007;8
81. Cheng AM, Byrom MW, Shelton J, Ford LP. Antisense inhibition of human mirnas and indications for an involvement of mirna in cell growth and apoptosis. *Nucleic Acids Res.* 2005;33:1290-1297
82. Navon R, Wang H, Steinfeld I, Tsalenko A, Ben-Dor A, Yakhini Z. Novel rank-based statistical methods reveal micrornas with differential expression in multiple cancer types. *PLoS One*. 2009;4
83. Zhang JL, Zhang F, Didelot X, Bruce KD, Cagampang FR, Vatish M, Hanson M, Lehnert H, Ceriello A, Byrne CD. Maternal high fat diet during pregnancy and lactation alters hepatic expression of insulin like growth factor-2 and key micrornas in the adult offspring. *BMC Genomics*. 2009;10
84. Song B, Wang Y, Kudo K, Gavin EJ, Xi YG, Ju JF. Mir-192 regulates dihydrofolate reductase and cellular proliferation through the p53-microrna circuit. *Clin. Cancer Res.* 2008;14:8080-8086
85. Georges SA, Biery MC, Kim SY, Schelter JM, Guo J, Chang AN, Jackson AL, Carleton MO, Linsley PS, Cleary MA, Chau BN. Coordinated regulation of cell cycle transcripts by p53-inducible micrornas, mir-192 and mir-215. *Cancer Res.* 2008;68:10105-10112
86. Schmitz KJ, Helwig J, Bertram S, Sheu SY, Suttorp AC, Seggewiß J, Willscher E, Walz MK, Worm K, Schmid KW. Differential expression of microrna-675,

microrna-139-3p and microrna-335 in benign and malignant adrenocortical tumours. *Journal of Clinical Pathology*. 2011;64:529-535
87. Lin MS, Chen WC, Huang JX, Gao HJ, Ye YL, Song ZY, Shen XY. Microrna expression profiles in human colorectal cancers with liver metastases. *Oncol. Rep.* 2011;25:739-747
88. Tombol Z, Eder K, Kovacs A, Szabo PM, Kulka J, Liko I, Zalatnai A, Racz G, Toth M, Patocs A, Falus A, Racz K, Igaz P. Microrna expression profiling in benign (sporadic and hereditary) and recurring adrenal pheochromocytomas. *Mod. Pathol.* 2010;23:1583-1595
89. Chen Y, Song YX, Wang ZN, Yue ZY, Xu HM, Xing CZ, Liu ZK. Altered expression of mir-148a and mir-152 in gastrointestinal cancers and its clinical significance. *J. Gastrointest. Surg.* 2010;14:1170-1179
90. Kushibiki T. Photodynamic therapy induces microrna-210 and-296 expression in hela cells. *J. Biophotonics*. 2010;3:368-372
91. Murata T, Takayama K, Katayama S, Urano T, Horie-Inoue K, Ikeda K, Takahashi S, Kawazu C, Hasegawa A, Ouchi Y, Homma Y, Hayashizaki Y, Inoue S. Mir-148a is an androgen-responsive microrna that promotes lncap prostate cell growth by repressing its target cand1 expression. *Prostate Cancer Prostatic Dis.* 2010;13:356-361
92. Liu XG, Zhan ZZ, Xu L, Ma F, Li D, Guo ZH, Li N, Cao XT. Microrna-148/152 impair innate response and antigen presentation of tlr-triggered dendritic cells by targeting camkii alpha. *Journal of Immunology*. 2010;185:7244-7251
93. Palmieri A, Pezzetti F, Brunelli G, Martinelli M, Lo Muzio L, Scarano A, Degidi M, Piattelli A, Carinci F. Peptide-15 changes mirna expression in osteoblast-like cells. *Implant Dent.* 2008;17:100-108
94. Gao J, Yang TT, Han JW, Yan K, Qiu XC, Zhou Y, Fan QY, Ma BA. Microrna expression during osteogenic differentiation of human multipotent mesenchymal stromal cells from bone marrow. *J. Cell. Biochem.* 2011;112:1844-1856
95. Tseng CW, Lin CC, Chen CN, Huang HC, Juan HF. Integrative network analysis reveals active micrornas and their functions in gastric cancer. *BMC Syst. Biol.* 2011;5
96. Guo SL, Peng Z, Yang X, Fan KJ, Ye H, Li ZH, Wang Y, Xu XL, Li J, Wang YL, Teng Y. Mir-148a promoted cell proliferation by targeting p27 in gastric cancer cells. *Int. J. Biol. Sci.* 2011;7:567-574
97. Lujambio A, Calin GA, Villanueva A, Ropero S, Sanchez-Cespedes M, Blanco D, Montuenga LM, Rossi S, Nicoloso MS, Faller WJ, Gallagher WM, Eccles SA, Croce CM, Esteller M. A microrna DNA methylation signature for human cancer metastasis. *Proc. Natl. Acad. Sci. U. S. A.* 2008;105:13556-13561
98. Pavicic W, Perkio E, Kaur S, Peltomaki P. Altered methylation at microrna-associated cpg islands in hereditary and sporadic carcinomas: A methylation-specific multiplex ligation-dependent probe amplification (ms-mlpa)-based approach. *Mol. Med.* 2011;17:726-735
99. Kalimutho M, Di Cecilia S, Blanco GD, Roviello F, Sileri P, Cretella M, Formosa A, Corso G, Marrelli D, Pallone F, Federici G, Bernardini S. Epigenetically silenced mir-34b/c as a novel faecal-based screening marker for colorectal cancer. *Br. J. Cancer*. 2011;104:1770-1778

100. Schwind S, Marcucci G, Maharry K, Radmacher MD, Mrozek K, Holland KB, Margeson D, Becker H, Whitman SP, Wu YZ, Metzeler KH, Powell BL, Kolitz JE, Carter TH, Moore JO, Baer MR, Carroll AJ, Caligiuri MA, Larson RA, Bloomfield CD. Baalc and erg expression levels are associated with outcome and distinct gene and microrna expression profiles in older patients with de novo cytogenetically normal acute myeloid leukemia: A cancer and leukemia group b study. *Blood*. 2010;116:5660-5669
101. Hanoun N, Delpu Y, Suriawinata AA, Bournet B, Bureau C, Selves J, Tsongalis GJ, Dufresne M, Buscail L, Cordelier P, Torrisani J. The silencing of microrna 148a production by DNA hypermethylation is an early event in pancreatic carcinogenesis. *Clin. Chem.* 2010;56:1107-1118
102. Braconi C, Huang NY, Patel T. Microrna-dependent regulation of DNA methyltransferase-1 and tumor suppressor gene expression by interleukin-6 in human malignant cholangiocytes. *Hepatology*. 2010;51:881-890
103. Ni CW, Qiu HW, Rezvan A, Kwon K, Nam D, Son DJ, Visvader JE, Jo H. Discovery of novel mechanosensitive genes in vivo using mouse carotid artery endothelium exposed to disturbed flow. *Blood*. 2010;116:E66-E73
104. Roth KaB, DG. *Enzyme-based fluorescence amplification for immunohistochemistry and in situ hybridization.* Boca Raton; 2005.
105. Feng Y, Cao JH, Li XY, Zhao SH. Inhibition of mir-214 expression represses proliferation and differentiation of c2c12 myoblasts. *Cell Biochemistry and Function*. 2011;29:378-383
106. Jindra PT, Bagley J, Godwin JG, Iacomini J. Costimulation-dependent expression of microrna-214 increases the ability of t cells to proliferate by targeting pten. *Journal of Immunology*. 2010;185:990-997
107. Penna E, Orso F, Cimino D, Tenaglia E, Lembo A, Quaglino E, Poliseno L, Haimovic A, Osella-Abate S, De Pitta C, Pinatel E, Stadler MB, Provero P, Bernengo MG, Osman I, Taverna D. Microrna-214 contributes to melanoma tumour progression through suppression of tfap2c. *Embo Journal*. 2011;30:1990-2007
108. Li LM, Hou DX, Guo YL, Yang JW, Liu YA, Zhang CY, Zen K. Role of microrna-214-targeting phosphatase and tensin homolog in advanced glycation end product-induced apoptosis delay in monocytes. *Journal of Immunology*. 2011;186:2552-2560
109. Yin G, Chen R, Alvero AB, Fu HH, Holmberg J, Glackin C, Rutherford T, Mor G. Twisting stemness, inflammation and proliferation of epithelial ovarian cancer cells through mir199a2/214. *Oncogene*. 2010;29:3545-3553
110. Chan LS, Yue PYK, Mak NK, Wong RNS. Role of microrna-214 in ginsenoside-rg1-induced angiogenesis. *European Journal of Pharmaceutical Sciences*. 2009;38:370-377
111. Duan ZF, Choy E, Harmon D, Liu XZ, Susa M, Mankin H, Hornicek F. Microrna-199a-3p is downregulated in human osteosarcoma and regulates cell proliferation and migration. *Molecular Cancer Therapeutics*. 2011;10:1337-1345
112. Song GA, Zeng HZ, Li JA, Xiao LF, He YZ, Tang YH, Li YR. Mir-199a regulates the tumor suppressor mitogen-activated protein kinase kinase kinase 11 in gastric cancer. *Biological & Pharmaceutical Bulletin*. 2010;33:1822-1827

113. Fornari F, Milazzo M, Chieco P, Negrini M, Calin GA, Grazi GL, Pollutri D, Croce CM, Bolondi L, Gramantieri L. Mir-199a-3p regulates mtor and c-met to influence the doxorubicin sensitivity of human hepatocarcinoma cells. *Cancer Res.* 2010;70:5184-5193
114. Lin EA, Kong L, Bai X-H, Luan Y, Liu C-j. Mir-199a*, a bone morphogenic protein 2-responsive microrna, regulates chondrogenesis via direct targeting to smad1. *J. Biol. Chem.* 2009;284:11326-11335
115. Lobert S, Jefferson B, Morris K. Regulation of beta-tubulin isotypes by micro-rna 100 in mcf7 breast cancer cells. *Cytoskeleton*. 2011;68:355-362
116. Shi W, Alajez NM, Bastianutto C, Hui ABY, Mocanu JD, Ito E, Busson P, Lo K-W, Ng R, Waldron J, O'Sullivan B, Liu F-F. Significance of plk1 regulation by mir-100 in human nasopharyngeal cancer. *International Journal of Cancer*. 2010;126:2036-2048
117. Grundmann S, Hans FP, Kinniry S, Heinke J, Helbing T, Bluhm F, Sluijter JPG, Hoefer I, Pasterkamp G, Bode C, Moser M. Microrna-100 regulates neovascularization by suppression of mammalian target of rapamycin in endothelial and vascular smooth muscle cells. *Circulation*. 2011;123:999-1009
118. Shi L, Cheng Z, Zhang J, Li R, Zhao P, Fu Z, You Y. Hsa-mir-181a and hsa-mir-181b function as tumor suppressors in human glioma cells. *Brain Research*. 2008;1236:185-193
119. Shin K-H, Bae SD, Hong HS, Kim RH, Kang MK, Park N-H. Mir-181a shows tumor suppressive effect against oral squamous cell carcinoma cells by downregulating k-ras. *Biochem. Biophys. Res. Commun.* 2011;404:896-902
120. Bhattacharya SD, Garrison J, Guo H, Mi Z, Markovic J, Kim VM, Kuo PC. Micro-rna-181a regulates osteopontin-dependent metastatic function in hepatocellular cancer cell lines. *Surgery*. 2010;148:291-297
121. Galluzzi L, Morselli E, Vitale I, Kepp O, Senovilla L, Criollo A, Servant N, Paccard C, Hupe P, Robert T, Ripoche H, Lazar V, Harel-Bellan A, Dessen P, Barillot E, Kroemer G. Mir-181a and mir-630 regulate cisplatin-induced cancer cell death. *Cancer Res.* 2010;70:1793-1803
122. Oliveras-Ferraros C, Cufi S, Vazquez-Martin A, Zenobia Torres-Garcia V, Del Barco S, Martin-Castillo B, Menendez JA. Micro(mi)rna expression profile of breast cancer epithelial cells treated with the anti-diabetic drug metformin induction of the tumor suppressor mirna let-7a and suppression of the tgf beta-induced oncomir mirna-181a. *Cell Cycle*. 2011;10:1144-1151
123. Cuesta R, Martinez-Sanchez A, Gebauer F. Mir-181a regulates cap-dependent translation of p27(kip1) mrna in myeloid cells. *Molecular and Cellular Biology*. 2009;29:2841-2851
124. Oh H-K, Tan AL-K, Das K, Ooi C-H, Deng N-T, Tan IB, Beillard E, Lee J, Ramnarayanan K, Rha S-Y, Palanisamy N, Voorhoeve PM, Tan P. Genomic loss of mir-486 regulates tumor progression and the olfm4 antiapoptotic factor in gastric cancer. *Clin. Cancer Res.* 2011;17:2657-2667
125. Olson E, Small E, Xin M. Inhibiting smooth muscle cell proliferation comprises contacting a smooth muscle cell with microrna (mir)-486 inhibitor and/or an agonist of mir-143 and/or mir-145.

126. Narducci MG, Arcelli D, Picchio MC, Lazzeri C, Pagani E, Sampogna F, Scala E, Fadda P, Cristofoletti C, Facchiano A, Frontani M, Monopoli A, Ferracin M, Negrini M, Lombardo GA, Caprini E, Russo G. Microrna profiling reveals that mir-21, mir486 and mir-214 are upregulated and involved in cell survival in sezary syndrome. *Cell Death & Disease*. 2011;2
127. Small EM, O'Rourke JR, Moresi V, Sutherland LB, McAnally J, Gerard RD, Richardson JA, Olson EN. Regulation of pi3-kinase/akt signaling by muscle-enriched microrna-486. *Proc. Natl. Acad. Sci. U. S. A.* 2010;107:4218-4223
128. Kato M, Zhang J, Wang M, Lanting L, Yuan H, Rossi JJ, Natarajan R. Microrna-192 in diabetic kidney glomeruli and its function in tgf-beta-induced collagen expression via inhibition of e-box repressors. *Proc. Natl. Acad. Sci. U. S. A.* 2007;104:3432-3437
129. Pichiorri F, Suh SS, Rocci A, De Luca L, Taccioli C, Santhanam R, Zhou WC, Benson DM, Hofmainster C, Alder H, Garofalo M, Di Leva G, Volinia S, Lin HJ, Perrotti D, Kuehl M, Aqeilan RI, Palumbo A, Croce CM. Downregulation of p53-inducible microrna s 192, 194, and 215 impairs the p53/mdm2 autoregulatory loop in multiple myeloma development. *Cancer Cell*. 2010;18:367-381
130. Boni V, Bitarte N, Cristobal I, Zarate R, Rodriguez J, Maiello E, Garcia-Foncillas J, Bandres E. Mir-192/mir-215 influence 5-fluorouracil resistance through cell cycle-mediated mechanisms complementary to its post-transcriptional thymidilate synthase regulation. *Molecular Cancer Therapeutics*. 2010;9:2265-2275
131. Braun CJ, Zhang X, Savelyeva I, Wolff S, Moll UM, Schepeler T, Orntoft TF, Andersen CL, Dobbelstein M. P53-responsive micrornas 192 and 215 are capable of inducing cell cycle arrest. *Cancer Res.* 2008;68:10094-10104
132. Feng SP, Cong SJ, Zhang X, Bao XC, Wang W, Li HP, Wang Z, Wang GX, Xu JZ, Du BW, Qu DZ, Xiong W, Yin MH, Ren XS, Wang FF, He JX, Zhang BL. Microrna-192 targeting retinoblastoma 1 inhibits cell proliferation and induces cell apoptosis in lung cancer cells. *Nucleic Acids Res.* 2011;39:6669-6678
133. Lee Y-B, Bantounas I, Lee D-Y, Phylactou L, Caldwell MA, Uney JB. Twist-1 regulates the mir-199a/214 cluster during development. *Nucleic Acids Res.* 2009;37:123-128
134. Abraham S, Knapp DW, Cheng L, Snyder PW, Mittal SK, Bangari DS, Kinch M, Wu L, Dhariwal J, Mohammed SI. Expression of epha2 and ephrin a-1 in carcinoma of the urinary bladder. *Clin. Cancer Res.* 2006;12:353-360
135. Frieden LA, Townsend TA, Vaught DB, Delaughter DM, Hwang Y, Barnett JV, Chen J. Regulation of heart valve morphogenesis by eph receptor ligand, ephrin-a1. *Dev. Dyn.* 2010;239:3226-3234
136. Bischoff J, Aikawa E. Progenitor cells confer plasticity to cardiac valve endothelium. *J. Cardiovasc. Transl. Res.*:1-10
137. Brown DR, Wong BS, Hafiz F, Clive C, Haswell SJ, Jones IM. Normal prion protein has an activity like that of superoxide dismutase (vol 344, pg 1, 1999). *Biochem. J.* 2000;345:767-767
138. Mirotsou M, Dzau VJ, Pratt RE, Weinberg EO. Physiological genomics of cardiac disease: Quantitative relationships between gene expression and left ventricular hypertrophy. *Physiol. Genomics*. 2006;27:86-94

139. Hjorthaug HS, Aasheim HC. Ephrin-a1 stimulates migration of cd8(+)ccr7(+) t lymphocytes. *European Journal of Immunology*. 2007;37:2326-2336
140. Obernosterer G, Martinez J, Alenius M. Locked nucleic acid-based in situ detection of microrna s in mouse tissue sections. *Nat. Protoc.* 2007;2:1508-1514
141. Nigam V, Srivastava D. Notch1 represses osteogenic pathways in aortic valve cells. *J. Mol. Cell. Cardiol.* 2009;47:828-834

VITA

CASEY J. HOLLIDAY

HOLLIDAY was born in Norfolk, Virginia. She attended Hickory High School in Chesapeake, Virginia, received a B.S. in Biomedical Engineering from the University of Virginia, Charlottesville, Virginia in 2006 before coming to Georgia Tech to pursue a doctorate in Biomedical Engineering. When she is not working on her research, Ms. Holliday enjoys spending time with her fiancé/husband, Randy and her dogs, Ralphie and Dakota.